

Co-funded by the



DISCO

Grant Agreement: **755443**

DELIVERABLE D1.15

2nd Annual Meeting Proceedings

Author(s)/Editor(s): **L.Z. Evins, A. Valls, L. Duro (SKB & Amphos 21)**

Date of issue of this report: **09/2019**

Report number of pages: **146 p**

Start date of project: **01/06/2017**

Duration: **48 Months**

| Project co-funded by the European Commission under the Euratom Research and Training Programme on Nuclear Energy within the Horizon 2020 Framework Programme | | |
|--|--|---|
| Dissemination Level | | |
| PU | Public | X |
| PP | Restricted to other programme participants (including the Commission Services) | |
| RE | Restricted to a group specified by the partners of the Disco project | |
| CO | Confidential, only for partners of the Disco project | |

Foreword

The present document is the proceedings of the First Annual Meeting of the EURATOM H2020 Collaborative Project DisCo (Modern Spent Fuel Dissolution and Chemistry in Failed Container Conditions). The electronic version of these proceedings is available on the webpage of the project (<https://disco-h2020.eu/>) The project started in June 2017 and will last for 48 months. DisCo is implemented by a consortium with 16 Beneficiaries, advised by the so-called End User Group (EUG). EUG consists of Waste Management Organisations in 7 countries (Belgium, Finland, France, Spain, Sweden, Switzerland, and the UK) as well as Regulatory Authorities in 5 countries (Belgium, Germany, Spain, Sweden, and Switzerland). The inclusion of Waste Management Organisations (WMOs) and Regulatory Authorities in this group ensures that the research conducted in the proposed project will be relevant and useful for the ultimate goal of safe radioactive waste disposal.

These proceedings document the progress of the project by means of work-package summaries and individual Scientific and Technical contributions. The key purpose is to ensure dissemination of knowledge and creating the required awareness of the project achievements.

The progress shown corresponds to the work conducted during the 2nd year of the project and presented at the 2nd Annual Meeting in Cologne (May 2019). All groups have started their research and good results are produced.

The main technical outcome of the meeting are the Scientific and Technical contributions (S+T) explaining the progress of the research conducted by each partner. The contributions have been reviewed and validated by, at least, two members of the End User Group.

The proceedings give an overview of the project, its organization and planned activities. The project website (<https://disco-h2020.eu/>) provides all this information in detail. The reader could also contact the project Coordinator or its team for more information.

The editors are grateful to all consortium members and everyone involved who contributes to the smooth development of the project. We want to give special thanks to (i) work-package leaders for providing the summaries of their corresponding work-package, (ii) partners for their comprehensive and significant contributions, and to (iii) all members of the EUG for their reviews, providing constructive, relevant and interesting comments. These efforts reflect their commitment and dedication to the project and contribute to a high quality of research performed within DisCo.

Contents

| | |
|--|------------|
| Foreword | i |
| Contents | ii |
| The Project | 1 |
| The 2nd Annual Meeting | 2 |
| WP Overview | 4 |
| WP1 Overview: Management, coordination and dissemination | 5 |
| WP3 Overview: Spent fuel dissolution experiments | 8 |
| WP4 Overview: Model material dissolution experiments..... | 10 |
| WP5 Overview: Chemical modelling..... | 12 |
| Extended Abstracts | 17 |
| SNF sample leaching and ⁷⁹ Se solution production | 18 |
| Status of leaching experiments performed with irradiated MOX fuel in bicarbonate water under reducing conditions at KIT-INE..... | 20 |
| High Burnup Spent Fuel dissolution under highly alkaline conditions..... | 29 |
| Aqueous leaching of ADOPT and standard UO ₂ spent nuclear fuel under H ₂ atmosphere | 33 |
| Chromium doped UO ₂ -based model systems: Synthesis and characterization of model materials for the study of the matrix corrosion of spent modern nuclear fuels..... | 41 |
| Dissolution experiments with Cr-(Pu) doped UO ₂ at FZJ and SCK·CEN: Preparatory tests with depleted and low alpha-doped UO ₂ at SCK·CEN..... | 49 |
| Influence of iron on the oxidative dissolution of a homogeneous U _{1-x} Pu _x O ₂ MOX fuel | 58 |
| Dissolution of alpha-doped UO ₂ with and without Cr in the presence of corroding Fe, in synthetic and natural groundwater..... | 63 |
| Production and characterisation of (U _{1-x} Th _x)O ₂ samples to model mixed-oxide fuel dissolution..... | 68 |
| Ongoing CIEMAT activities on fabrication and stability studies of doped UO ₂ in the frame of the DisCo project: sample characterization, experimental set-up and first results..... | 75 |
| Synthesis and characterisation of Cr-doped UO ₂ : A model material for modern nuclear fuel dissolution studies | 89 |
| Optical examination of wetted long-stored uranium dioxide fuel..... | 97 |
| Development of a matrix dissolution model for the prediction of activity release from used fuel in long term storage..... | 103 |
| Spent fuel alteration model integrating processes of different time scales - Validation | 112 |
| Modeling of the oxidative leaching of U _{0.73} Pu _{0.27} O ₂ in synthetic clay groundwater with metallic iron | 122 |
| Development and application of a solid solution model for Cr-doped UO ₂ fuel | 131 |
| EUG Feedback | 142 |

The Project

DisCo is a Collaborative Project funded by the European Commission under the Horizon 2020 Research and Training Programme of the European Atomic Energy Community (EURATOM) (H2020-NFRP-2016-2017-1), section B - Contribute to the Development of Solutions for the Management of Radioactive Waste. Topic NFRP 6: Addressing key priority R&I issues for the first-of-the-kind geological repositories.

DisCo is an acronym for “Modern Spent Fuel Dissolution and Chemistry in Failed Container Conditions.” It started on 1st June 2017 and it is planned to run for four years. The project is implemented by a consortium with 16 Beneficiaries.

The project is set up to answer the Euratom call of 2016-2017, which focused on high priority topics identified by the IGD- TP (Implementing Geological Disposal – Technology Platform: www.igdtp.eu/). One of these areas is the disposal of new and unconventional fuels. DisCo started as a response to the need to test the hypothesis that dopants in the UO₂ fuel matrix do not significantly affect the dissolution rate of the spent fuel in a repository environment. Dopants in the UO₂ fuel matrix here considered are Cr, or Cr+Al, and Gd. In addition, the behaviour of Mixed-Oxide fuel (MOX) which contains Pu in addition to the UO₂ matrix is also investigated, leading to the study of the effect of an analogous mixed Th-U oxide for comparison. The DisCo project uses three paths to study these issues which mainly define the objectives of the technical work-packages (WP): dissolution experiments with real spent fuel (WP3), dissolution experiments with model materials (WP4) and modelling of the chemical system expected in the failed waste container (WP5). An additional technical work-package (WP2) is devoted to the preparation and characterization of the samples to be used in the experiments planned in WP3 and WP4.

The central part of the scientific investigation in this project concerns how elements other than uranium (metal, lanthanide, actinide) in the oxide matrix affect its redox chemistry and solubility. Any impurity in a solid phase will affect the crystal lattice and atomic bonds, so that parameters such that the solubility of the solid can be affected. In addition, the electronic configuration on an atomic scale affects the average oxidation state of the uranium in the solid. Since these aspects are fundamental to the spent fuel dissolution process, it is necessary to test whether these changes affect measured dissolution rates.

This DisCo project also contributes to knowledge management, dissemination and communication, through the efforts made in WP1. The involvement of an End User Group (EUG) representing waste management organisations and national regulators, as well as an Associate Group (AG) consisting mainly but not exclusively by organisations from countries with less advanced programs (LAPs), is central to the successful knowledge transfer and management foreseen in DisCo. Efforts are focused on communication and dissemination activities such as webinars and training events.

The 2nd Annual Meeting

The second annual meeting of the DisCo project was held in Cologne (Germany), 27th – 29th May 2019. The meeting was hosted by JUELICH at the Cologne Marriott Hotel. There were 48 attendees including representatives of the partners, the End User Group (EUG) and some external organizations.

The meeting was scheduled in four blocks (see Figure 1): (i) individual talks where each partner presented the work conducted during the 2nd year of the project; (ii) separate WP sessions to discuss on the progress and organizing the work for the next year; (iii) work-package (WP) overviews summarizing the status of each WP and further steps; and (iv) webinar as part of the training activities within the project. A summary of the WP presentations given during the Coordination Team Presentation (WP1) and the technical WP overview session (WP3 to WP5) is presented in the following chapter. As WP2 work was integrated within WP3 and WP4 presentations, no separate summary is presented in the current proceedings.

|  Preliminary Agenda (27 th - 29 th May 2019)  | | |
|---|--|---|
| Monday 27 th May 2019 | Tuesday 28 th May 2019 | Wednesday 29 th May 2019 |
| 10:00 ExCom meeting <i>(restricted to ExCom members)</i> | 09:00 Individual talks (cont., 20'+10' each) CIEMAT / CEA / VTT | 8:30 Individual WP Session & EUG Meeting <i>(restricted to EUG members)</i> |
| 13:00 LUNCH | 10:30 Coffee break | 10:00 Coffee break |
| 14:00 Welcome & Coordination Team Presentation (WP1) | 11:00 Individual talks (cont., 20'+10' each) UCAM / USFD / NNL | 10:30 WP Overviews (15'+5') WP3 / WP4 / WP5 |
| 14:30 Individual talks (20'+10' each) JRC / KIT-INE / CTM | 12:30 LUNCH | 12:00 General Assembly (GA) |
| 16:00 Coffee break | 14:00 Individual talks (cont., 20'+10' each) A21 / Armines / PSI | 12:30 EUG feedback |
| 16:30 Individual talks (cont., 20'+10' each) Studsvik / JUELICH / SCK-CEN | 16:00 Webinar (1.5 h) | 13:00 End of the 2nd Annual Workshop |
| 18:00 End of the 1st Day | 19:30 WORKSHOP DINNER | --- |
| | | 15:00 ExCom meeting <i>(restricted to ExCom members)</i> |

Figure 1: General agenda of the 2nd Annual Meeting of DisCo.

In addition to the technical sessions, the meeting included the following sessions focused on the management and progress of the project.

- › ExCom meeting: the Coordination Team (CT), WP leaders and one member of the EUG discussed on the progress of the project, organizing future events (meetings, training...), identify deviations and providing/suggesting solutions.
- › EUG meeting was restricted only to member of the End User Group. As Waste Management Organizations and Regulators, they ensure that the research conducted remains within the scope initially set and it is relevant and useful for the ultimate goal of safe radioactive waste disposal. At the end of each meeting they are providing their advice on the project status to all Consortium Members. Their feedback is included in the present Proceedings, Section “*Summary of Feedback from the end User Group*”.

- The General Assembly is the forum where actions that must be approved by all partners take place. All decisions taken during that Assembly are compiled in the Meeting Minutes which are available at the project website.

One important goal of this meeting was the organization of the 2nd Webinar. The webinar was on “Factors Affecting the Dissolution of Spent Nuclear Fuel” and was given by Brady Hanson (PNNL). It was followed by all the DisCo attendees and by 19 persons connected online via the Webex platform. The webinar was recorded, and it is available under demand (instructions given at the project webpage).

The Coordination Team want to thank all DisCo participants and the host organization, the Research Center of Juelich, for a well-organized and productive meeting. We are looking forward the next meeting that will be held in April-May 2020 in Karlsruhe (Germany), hosted by the JRC-KA. This meeting will be organized in conjunction with the training workshop that will be also organized by JRC-KA.



Figure 2: Group photo of the 2nd DisCo Annual Meeting attendees.

WP Overview

WP1 Overview: Management, coordination and dissemination

Lena Z. Evins, SKB (SE)

The progress of the project is overseen and managed in Work Package 1, divided into two main tasks:

- 1) General management and coordination
- 2) Communication, dissemination and training

Task 1 involves maintaining all the general project management tasks including the financial and legal matters, while Task 2 involves setting up and maintaining all the communication tools used in the project, such as the webpage, meetings, webinars and other training events.

The following deliverables have been submitted during the second year of the project (June 2018-June 2019 (approx.)). All of them are available at the project website.

- D1.10 AM1 Proceedings
- D1.11 2nd Mobility grant announcement
- D1.12 Webinar 2
- D1.13 AM2 Minutes
- D1.14 Newsletter#3

During the second year, 4 milestones have been reached: The first dissolution tests have started, the 1st periodic report has been approved by the EC, the second annual meeting has been held, and failed fuel data has been delivered to work package 5 for use in modelling activities. One more milestone was expected to be reached (all samples prepared) but due to some delays this milestone is instead expected to be reached in the third year.

The 2nd annual meeting was held 27-29 May in Cologne, Germany. Overall, the project is following the work plan. Some delays have been encountered for some experiments, however, it is expected that data will still be able to be delivered to work package 5 next year, to be used in modelling.

The next annual meeting is planned to be held in Karlsruhe (Germany) in April or May 2019 (the exact date will be soon published at the project webpage). The meeting will be hosted by JRC and be held in conjunction with a group training event.

During the 2nd year, two individual training visits to JRC have been planned. These will both take place during the autumn of 2019.

The project has been presented at international fora during the year. First at the 8th IGD-TP Exchange Forum (Berlin, December 2018), and later at the Euradwaste '19 Conference (Pitesti, June 2019).

Legal and financial status

All EUG agreements have been signed this second year.

Preliminary reporting was performed to make sure all organisations were ready for official periodic reporting. This worked fine for most organisations and the second payment (part of the pre-financing) was distributed. Official reporting to the EU for the first 18 month period took place in December 2018 and January 2019. The EC responded with some requests for clarifications, but the issues were handled and the report was approved in April. The interim payment was sent and at the time of writing it is in the process of being transferred to the partners.

Communication actions

During the second year, the general communication tools have been keep updated. The webpage (<https://www.disco-h2020.eu/>) is continuously updated which contains a Twitter feed displaying all tweets tagged with #discoH2020. An example of the tweets displayed in the home page of the project webpage is shown in Figure 1. 21 tweets have been published using the project hashtag during the second year.

Modern Spent Fuel Dissolution and Chemistry in Failed Container Conditions

DISCO is a Collaborative Project funded by the European Commission under the Horizon 2020 Research and Training Programme of the European Atomic Energy Community (EURATOM) (H2020-NFRP-2016-2017-1), section B - Contribute to the Development of Solutions for the Management of Radioactive Waste. Topic NFRP 6: Addressing key priority R&I issues for the first-of-the-kind geological repositories. Funding scheme: RIA - Research and Innovation action. Project ID: 755443.

The project started on 1st of June 2017 and will last for 48 months. The project is implemented by a consortium with **16 Beneficiaries**. The consortium will be advised by a so-called **End User Group (EUG)**, consisting of Waste Management Organisations in 7 countries (**Belgium, Finland, France, Spain, Sweden, Switzerland, and the UK**) as well as regulatory authorities in 5 countries (**Belgium, Germany, Spain, Sweden, and Switzerland**). The inclusion of Waste Management Organisations (WMOs) as an EUG in the project ensures that the research conducted in the proposed project will be relevant and useful for the ultimate goal of safe radioactive waste disposal.

The total budget is 4.69 million Euros. The European Commission contributes with 3.99 million Euros to the project.

COUNTRIES INVOLVED IN DISCO

(n° of beneficiaries)

Twitter Feed:

- Lara Duro (@laraduro1)**: Thanks Liam. It is very nice to see how people evolve after these early research experiences. I'd like to see some more comments like yours. They'd help spreading the word to others possibly interested. Comments from #discoh2020 or other @EU_H2020 young researchers welcome! twitter.com/LiamAbrahamsen...
- Liam Abrahamsen-Mills (@LiamAbrahamsen)**: En respuesta a @laraduro1 It was a great introduction to research into rad in the environment. My work focussed on nat org matter & complexation (lab & models). Now work in related areas for the UK's national lab. Always tinkering with PHREEQC and recently GWS.
- Lena Z. Evins (@lenazevins)**: Feeling very pleased with the progress of our project! Thanks to all excellent and hard-working spent nuclear fuel researchers who are contributing! #discoh2020
- Rob Winsley (@winsley_rob)**: Productive couple of days at the 2nd annual meeting of the #discoh2020 project. I learnt a...

Figure 1: Home page of the DisCo project.

The LinkedIn Group, also active since September 2017, has now 34 members, representing most of the project participants and some project external members.

A third newsletter was distributed in July 2019 after the second Annual meeting. It contains a summary of the project status reported during the second annual meeting, and it is available in the project website

The second Webinar, featuring Dr Brady Hanson (PNNL, USA) dealt with Factors Affecting the Dissolution of Spent Nuclear Fuel and it was attended by the project meeting attendants as well as followed on-line by 19 people from 8 different countries and the European Commission.

The available Mobility Grant to attend the 2nd Annual Meeting was announced in December 2018. The members of the Associate Group from the countries with less advanced programs are first priority. There were 4 applications for the grant this year.

WP3 Overview: Spent fuel dissolution experiments

Volker Metz, KIT-INE (DE)

Introduction

The main goal of Work Package 3 of the H2020-project DisCo is to study experimentally the matrix dissolution of spent UO_x fuels containing dopants as well as MOX fuels under relevant disposal conditions. The research groups that contributed with experiments on dissolution of such irradiated UO_x and MOX fuels within WP3 are Fundacio CTM Centre Tecnologic – now Fundacio Eurecat (EURECAT) in conjunction with Universitat Politècnica de Catalunya (UPC), Joint Research Centre (JRC-KA), Karlsruher Institut für Technologie (KIT-INE) and Studsvik Nuclear AB (STUDSVIK).

All partners of WP3 dealt with spent nuclear fuel (SNF), which had been irradiated in light water nuclear reactors. Current experiments are performed and future experiments will be performed with two BWR UO_x fuels having a burnup of 57 and 59 $\text{MWd}\cdot\text{kg}_{\text{HM}}^{-1}$, with two PWR MOX fuels of 38 and 54 $\text{MWd}\cdot\text{kg}_{\text{HM}}^{-1}$ as well as two PWR UO_x fuels of 58 and 73 $\text{MWd}\cdot\text{kg}_{\text{HM}}^{-1}$ (average burnups). Cladded segments and fragments of these irradiated fuel samples were characterized to a certain extent and prepared for dissolution experiments in diluted NaCl solution with 1 to 2 mM NaHCO_3 (pH ~ 8, denoted as NaCl-BIC) and so-called “Young Cement Water with Calcium”, a diluted solution NaOH, $\text{Ca}(\text{OH})_2$ solution, containing 77 mM Na_2CO_3 and other minor constituents (pH ~ 13.5, denoted as YCWCa).

Initial results of the dissolution experiments with irradiated UO_x and MOX fuels performed by KIT-INE and STUDSVIK and strongly reducing conditions, as well as by EURECAT dissolution experiments with an irradiated UO_x fuel under oxidic conditions are presented in the Proceedings of the 2nd Annual Workshop. Since there were some delays concerning, for example, sample preparation of the fuel samples and the autoclaves to be used in the anoxic dissolution experiments of JRC-KA and EURECAT, start of some of their experiments is expected in the third year of the project.

Achievements

KIT-INE studied matrix dissolution and the Instant Release Fraction in two dissolution experiments with a cladded segment and fragments of an irradiated PWR MOX fuel (73 $\text{MWd}\cdot\text{kg}_{\text{HM}}^{-1}$). González-Robles et al. [1] present data on radionuclide release in the two experiments for 160 days of leaching in NaCl-BIC type solution under hydrogen overpressure. In both experiments a continuous release of the fission products ^{90}Sr and ^{137}Cs is seen. Concentrations of actinides in solution are constant since the beginning of the experiments except for uranium and neptunium.

STUDSVIK is contributing to WP3 of DisCo with two dissolution experiments on a standard BWR UO_x fuel (57 $\text{MWd}\cdot(\text{kg}_{\text{HM}})^{-1}$) and a Al-Cr-doped BWR UO_x fuel (59 $\text{MWd}\cdot\text{kg}_{\text{HM}}^{-1}$). Fragments of both SNF samples are exposed to a NaCl-BIC type solution under hydrogen overpressure. Initial results of the two dissolution experiments are reported by Barreiro-Fidalgo et al. [2]. In both autoclave experiments, U concentration decreased with time to a level slightly above the solubility of amorphous

UO₂. Low levels of Xe have been detected in the gas phase of both autoclaves, achieving cumulative release fractions between 3 - 5 % of the inventory. A ratio of 1:1 between fission gases to ¹²⁹I was found.

Within WP3 of DisCo, **EURECAT** in conjunction with **UPC** is contributing with dissolution experiments on a PWR UO_x fuel with a local burnup of 73 MWd·kg_{HM}⁻¹. Initial results of the experiment performed with a cladded segment in YCWCa type solution under oxidic conditions are presented by Iglesias et al. [3]. For comparison, results of a dissolution experiment with a similar SNF sample used in another project and leached NaCl-BIC type solution under oxidic conditions are shown, too.

JRC-KA is contributing to WP3 of DisCo with experimental studies of the long-term stability of an irradiated Cr₂O₃-doped UO_x fuel (58 MWd·kg_{HM}⁻¹) and a spent MOX fuel (54 MWd·kg_{HM}⁻¹) in NaCl-BIC type solution under hydrogen overpressure. Carbol et al. [4] reports on activities related to preparation of these experiments and severe technical problems to be solved. The onset of the dissolution experiments has been postponed to the second half of 2019 due to the technical problems.

Acknowledgement

The research leading to these results has received funding from the European Commission Horizon 2020 Research and Training Programme of the European Atomic Energy Community (EURATOM) (H2020-NFRP-2016-2017-1) under grant agreement n° 755443 (DisCo project).

References

- [1] González-Robles, E., Herm, M., Müller, N., Walschburger, A., Böttle, M., Geyer, F., Metz, V. (2019). Status of leaching experiments performed with irradiated MOX fuel in bicarbonate water under reducing conditions at KIT-INE. 2nd Annual Workshop Proceedings, H2020-project DisCo (*this document*).
- [2] Barreiro-Fidalgo, A., Roth, O., Puranen, A., Evins, L.Z., Spahiu, K. (2019). Aqueous leaching of ADOPT and standard UO₂ spent nuclear fuel under H₂ atmosphere. 2nd Annual Workshop Proceedings, H2020-project DisCo (*this document*).
- [3] Iglesias, L., Serrano-Purroy, D., Martínez-Torrents, A., Clarens, F., de Pablo, J., Casas, I. (2019). High Burnup Spent Fuel dissolution under highly alkaline conditions. 2nd Annual Workshop Proceedings, H2020-project DisCo (*this document*).
- [4] Carbol, P., Serrano-Purroy, D., Aldave de las Heras, L., Millet, S., Montagnier, G., Papaioannou, D., Pell Lorente, A., Rasmussen, G., Sandow, M., Van Winckel, S., Wegen, D.H. (2019). SNF sample leaching and ⁷⁹Se solution production. 2nd Annual Workshop Proceedings, H2020-project DisCo (*this document*).

WP4 Overview: Model material dissolution experiments

Dirk Bosbach, FZJ (DE)

The objectives of WP4 within the DisCo project are: (1) Understanding matrix corrosion of modern LWR fuels under deep geological repository relevant conditions, (2) Systematic corrosion studies on Cr-doped-UO₂-based and MOX model systems (prepared in WP2) complementary to SF corrosion studies in WP3.

A special focus will be on the long-term (> 1000 years) matrix corrosion by using alpha-doped model systems. The experimental programme is intended to overcome the inherent complexity of spent fuel corrosion and to identify the separate effects of microstructure, doping, reactive surface area in support of the spent fuel corrosion studies in WP3. The results will allow for improving the predictive capability of SF corrosion models and reduction of associated uncertainties.

Almost all activities are on track as planned and results from first dissolution experiments or test experiments are available (see also D4.1). Apparently, many bilateral interaction have been established within WP4 as well as with WP2 and WP5. A report on results from first dissolution experiments (D4.1) is due end of May and has been delivered by mid-June. This report will be updated later.

A dedicated (internal) of WP4 workshop is planned prior to the SF workshop in Ghent on November 13, 2019 in the Novotel, starting at 14:00 - 18:00.

A review paper will be published at the end of the project. However, all participants have planned to have individual publications first.

The contributions of the WP4 participants can be summarized as followed:

SCK·CEN contribution - Static dissolution experiments (incl. α -doped materials) at SCK·CEN; Autoclaves in Ar glove box, PEEK cell, Reducing/ anoxic conditions; development and optimization of the method with depleted UO₂ and low alpha doped UO₂; 1st series of experiments, in autoclaves with and without dithionite (2/2); 2nd series of experiments, in autoclaves with H₂ and Pd/Pt catalyst; 3rd series of experiments, in PE bottles, to optimize pre-washing/ pre-leaching/ annealing. In summary, the leaching method of SCK·CEN has been optimized.

FZJ contribution - UO₂ and Cr-doped UO₂ samples available and characterized; Dissolution experiments with 1 mM NaHCO₃ and H₂O₂; So far, similar dissolution rates have been observed for Cr-doped and undoped samples; Indication of surface passivation observed on etched sample surfaces

VTT contribution - Scoping experiments with at VTT available ²³³U alpha doped UO₂ fragments; Natural brackish OL-KR6 groundwater obtained and characterized; Experimental setup established; Leaching experiments not started yet.

CIEMAT contribution - UO_2 -0.06w/o Cr_2O_3 , UO_2 -0.05w/o Cr_2O_3 -0.02w/o Al_2O_3 and UO_2 -4.5w/o Gd_2O_3 ; Batch-type: Dissolution experiments started with 20 mM NaClO_4 under a $\text{N}_2/4.7\%\text{H}_2$ atmosphere; First results: No element release detected so far / no dissolution

USFD contribution - Pelletised UO_2 samples containing 0, 300, 600, 1200, 1800 and 2400 ppm Cr; synthetic ground water (1 mM NaHCO_3 + 19 mM NaCl) - (T 30°C and 60°C); Leaching experiments started; Element release data not available yet.

CEA contribution - ($\text{U}_{0.73}\text{Pu}_{0.27}$) O_2 unirradiated MOX; synthetic CO_x groundwater, Fe-foil, reducing, Ar/ CO_2 3000 ppm; results: significant effect of iron on the oxidative dissolution of this homogeneous MOX fuel. Uranium concentrations are less than $1 \mu\text{g}\cdot\text{L}^{-1}$ after seven months of leaching; Leaching experiment was stopped last week – sample characterization; the respective data will be available by the end of the year.

UCAM contribution - (U/Th) O_2 samples available (and characterized); 1 mM NaHCO_3 ; synthetic CO_x ; experimental setup and approach established; Stability of 0.1 M H_2O_2 over 14 d indicated.

WP5 Overview: Chemical modelling

Lara Duro, Olga Riba, Amphos 21 (ES)

Introduction

WP5 focuses on the development and application of chemical models describing the solid and aqueous phases.

The work package is divided in the following major tasks:

1. Thermodynamic equilibrium calculations, targeting (a) the effect of dopants in the dry matrix in terms of oxygen potential and (b) dissolution/precipitation reactions inside the water-saturated canister.
2. Matrix dissolution model, incorporating redox and electron transfer reactions involving matrix, separate phases (e.g. metallic fission products), radiolysis and hydrogen in the system.
3. MOX dissolution model, focusing on the interplay with Fe species released from iron-based canister materials.

Four partners are participating in this WP: Amphos 21 (ES), PSI (CH), NNL(UK) and Armines (FR). Task 1 is developed by Amphos 21, PSI and NNL; Task 2 is developed by Amphos 21 and NNL, and Task 3 is developed by Armines.

Achievements

At the end of the second year of the project, all the institutions have developed their models, which have been presented in 4 Scientific and technical contributions to the proceedings [1-4].

AMPHOS 21 has developed a 1D reactive transport model implemented in iCP [5] (interface COMSOL Multiphysics and PhreeqC) to assess the corrosion of Spent Fuel (SF), considered as homogeneous $\text{UO}_2(\text{am})$ doped with Pd. The model couples: i) the generation of water radiolysis species by alpha and beta radiation considering a complete radiolysis system, ii) the processes occurring in the SF surface: oxidative dissolution reactions of $\text{UO}_2(\text{am})$ and subsequent reduction of oxidized fuel, considering H_2 activation by Pd, and iii) corrosion of Fe(s) considering both oxic and anoxic conditions. Processes i) have been implemented in COMSOL and processes ii) and iii) have been implemented in PHREEQC using ThermoChimie v.9.0 database (<https://www.thermochimie-tdb.com/>) with the kinetic constants being calibrated with different sets of experimental data published in the open literature. The model yields a $\text{UO}_2(\text{am})$ dissolution rates similar to the values selected in safety assessments.

At present there are no experimental data available from the experiments performed in DisCo project. Because of that, data from the related literature and generated in the framework of other projects were used to validate the model. The calibration of the kinetic constants of the processes involved in the oxidative dissolution of $\text{UO}_2(\text{am})$ with the O_2 and $\cdot\text{OH}$ as oxidants and water or carbonate as ligands

has been done by comparison with the experimental data described in Cera et al. (2006) [6]. On the other hand, the corrosion process of metallic Fe(s) has been validated with experimental data generated in the frame of the REDUPP project [7]. Modelling results are, in general, in good agreement with the different sets of experimental data and also with 1D reactive transport models from the literature and yields a $\text{UO}_2(\text{am})$ dissolution rates similar to the values selected in safety assessments.

Future work

The third year of the project will be devoted to extend the present model by including: i) metallic Fe corrosion in 1D reactive model, ii) the SF as a porous medium; iii) porosity changes of the SF by precipitation of secondary phases within the SF and on the SF surface and iv) evaluate the possibility to consider the heterogeneity of the SF matrix to account for different concentrations of epsilon particles (Pd). Also, as stated in Task 1 of the DisCo proposal, a conceptual geochemical model will be developed that accounts for the impact of platinoid metal alloy particles (epsilon metals) on SF dissolution under highly reducing conditions and in the presence of hydrogen.

PSI has performed thermodynamic calculations in order to assess the influence of Cr-doping on the fuel oxygen potential. After reviewing the defect chemistry literature on Cr(III), U(V) and O(-II) substitutions, a ternary 3-sites solid solution model for Cr-doped hyperstoichiometric urania has been developed. The mixing parameters describing non-ideality were calibrated against published experimental data on Cr-solubility in UO_2 and oxygen potentials of hyperstoichiometric UO_{2+y} . The model was implemented in the chemical equilibrium code GEM-Selektor (<http://gems.web.psi.ch>) with the in-house database HERACLES (<https://www.psi.ch/heracles/>) applied both to non-doped and Cr-doped model UO_2 fuel compositions.

The results yield higher potentials compared to analogous calculations carried out assuming ideal solid solution behaviour. This was expected since an ideal solid solution binds more oxygen to the UO_{2+y} phase compared to the corresponding non-ideal phase. However, the effect on oxygen potential is minor, since both curves lie well within the field defined by oxygen potential measurements of LWR fuels.

In summary, the results of the calculations do not indicate any significant effect of Cr-doping on the fuel oxygen potential. Specifically, there is no indication that dose-relevant nuclides (e.g. ^{99}Tc , ^{93}Mo , ^{107}Pd or ^{126}Sn) would be oxidized and become more soluble upon contact with aqueous solution in a repository. Also, the calculated oxygen potentials exclude formation of highly hyperstoichiometric matrix, which would facilitate fuel dissolution.

Future work

In the next project year, we will expand the model by adding lanthanides, Pu and minor actinides as components to the Cr(III)- UO_{2+y} phase. Furthermore, solid solutions for metallic inclusions (ϵ -particles) and the oxide “grey” phase will be implemented. Finally, we will estimate the influence of oxidation at the internal cladding surface and of burnup progress.

Armines worked in a 2D reactive transport model to assess the alteration of $U_{0.73}Pu_{0.27}O_2$ under self α -radiolysis, considering H_2O_2 as the most important species regarding MOX dissolution. The model is implemented in HYTEC code dealing with diffusive transport of a reactive species coupled to chemistry and using CHESS as a geochemical code for thermodynamic equilibrium and kinetic controls. The study has brought some insights into the following two main objectives of the DisCo project:

- To assess whether novel types of fuel (MOX) behave like the conventional ones (UOX): overall consistency of the kinetic processes (H_2O_2 production and disproportionation, oxidative dissolution) obtained from leaching of the unirradiated homogeneous $U_{0.73}Pu_{0.27}O_2$ pellet in carbonate water has been proved. The plutonium content seems to make $U_{0.73}Pu_{0.27}O_2$ more resistant towards leaching than UO_2 .
- To enhance the understanding of spent fuel matrix dissolution under conditions representative of failed containers: the release of uranium in groundwater in the presence of metallic iron became very significantly lowered compared to carbonate water conditions. This is very similar to what have been obtained on alpha-doped UO_2 pellet. In the modeling, iron corrosion has been identified to be a key parameter because Fe(II) released in solution by the iron foil anoxic corrosion consumes H_2O_2 produced by alpha-radiolysis of water. The CHESS/HYTEC model developed as part of this work led to results in agreement with the preliminary solution analysis, but should be further validated by mass balance (dissolved, colloidal and sorbed fractions for U and Pu) as well as the observation and analysis of the solid phases at the end of the leaching tests.

The knowledge gained from such reactive transport modelling at laboratory scales can then serve as a basis for simulations at larger scales and duration to better assess and constrain the long-term evolution of a disposal cell of spent MOX fuel.

Future work

In the second half of the DisCo project, the reactive transport model will be applied to a disposal package and disposal cell developed on the basis of the present French vitrified waste concept. One single MOX assembly will be inserted in carbon steel overpack. The overpack will directly be placed in a carbon steel liner within the Cox host rock. For the sake of simplicity, the MOX complexity will be reduced to the unirradiated homogeneous solid solution; possibly extended to the heterogeneous microstructure of unirradiated heterogeneous MOX fuel. Several types of corrosion products of the steel container and, therefore, various concentration limits of dissolved Fe(II), could be considered in the modelling, i.e. corresponding to different corrosion product of steel (chukanovite, siderite, magnetite..)

NNL has successfully implemented in gPROMS¹ code the mixed potential model developed by Canadian and American national laboratories to simulate the corrosion of the fuel in storage ponds, characterised within WP2 and under representative repository conditions (anoxic), focusing on nominal UK granitic rock repository conditions. To model the matrix dissolution of uranium dioxide spent fuel, the following process have been identified as important:

¹ gPROMS is a modelling tool which allows complex plants and processes to be described in terms of a collection of algebraic and differential equations which are solved to predict the steady state and/or dynamic behaviour of the system being modelled. Commercially available at (<https://www.psenterprise.com/products/gproms/platform>).

- Oxidative dissolution
- Chemical dissolution
- Diffusion of species to and from the fuel surface
- Precipitation of solids on the fuel surface
- Aqueous reactions
- Radiolysis of water near the fuel surface
- The effects of noble metal particles

A detailed assessment of the methods used to model these phenomena in existing literature was undertaken by NNL to identify the most significant uncertainties in the input parameters and the most important assumptions and simplifications that affect the reliability of the model. Also, the differences associated with high pH environments, drawing on the experience gained from the deployment of high pH pond storage regimes at Sellafield. The existing model can be readily modified to consider experimental work undertaken as part of the DisCo programme. This would be a pragmatic way to quickly assess the importance of the uncertainties identified with the model and their impact on its predictive capabilities.

Future work

The priority for the 2019/20 FY must be to clarify the impact of existing assumptions, particularly in relation to changing environmental conditions and to subsequently improve understanding to underpin more reliable predictions.

References

- [1] Riba, O., Coene, E., Silva, O., Duro, L. (2019). Spent fuel alteration model integrating processes of different time scales - Validation. 2nd Annual Workshop Proceedings, H2020-project DisCo (*this document*).
- [2] Curti, E., Miron, G.D., Kulik D. (2019). Development and application of a solid solution model for Cr-doped UO₂ fuel. 2nd Annual Workshop Proceedings, H2020-project DisCo (*this document*).
- [3] De Windt, L., Kerleguer, V., Jégou, C., Goblet, P., Martin, C., Tocino, F. (2019). Modelling of the oxidative leaching of U_{1-x}Pu_xO₂ in synthetic groundwater with metallic iron. 2nd Annual Workshop Proceedings, H2020-project DisCo (*this document*).
- [4] Hughes, R.J., Goode, J.B, Hambley, D.I. (2019). Development of a matrix dissolution model for the prediction of activity release from used fuel in long term storage. 2nd Annual Workshop Proceedings, H2020-project DisCo (*this document*).
- [5] Nardi, A., Idiart, A., Trincherro, P., de Vries, L.M., Molinero, J. (2014). Interface COMSOL-PHREEQC (iCP), an efficient numerical framework for the solution of coupled multiphysics and geochemistry. *Computers & Geosciences*, 69, 10-21.
- [6] Cera, E., Bruno, J., Duro, L., Eriksen, T. (2006). Experimental determination and chemical modelling of radiolytic processes at the spent fuel/water interface. SKB Technical Report, TR 06-07.
- [7] Evins, L.Z., Juhola, P., Vähänen, M. (2014). REDUPP Final Report. POSIVA report 2014-12.1. 128 pp. <http://www.posiva.fi/files/3672/WR2014-12.1.pdf>.

Extended Abstracts

SNF sample leaching and ^{79}Se solution production

Carbol, P., Serrano-Purroy, D., Aldave de las Heras, L., Millet, S., Montagnier, G., Papaioannou, D., Pell Lorente, A., Rasmussen, G., Sandow, M., Van Winckel, S., Wegen, D.H.

EC-JRC (BE)

1 Introduction

JRC Karlsruhe contributes to the DisCo project in WP2 and WP3. The characterisation of the fuels selected for the leaching studies is made within WP2. In WP3, JRC-KA performs the studies of the long-term stability of irradiated Cr_2O_3 -doped UO_2 -fuel and spent MOX fuels in aqueous media under anoxic and reducing conditions. Not only leachates and solid after leaching, but also the gas phase will be analysed in order to obtain a more complete description of the redox conditions and of the processes affecting the evolution of the system.

The leachability of the long-lived β -emitters ^{79}Se from spent fuel requires a robust and sensitive analytical method. Analysis of ^{79}Se concentrations in the leachates of MOX and Cr_2O_3 -doped UO_2 fuel (within WP3) is foreseen to obtain realistic ^{79}Se release rates and thereby decrease the uncertainty of Se-release in the performance assessment of the repository. Therefore, JRC Karlsruhe will separate ^{79}Se from a High-Active Raffinate solution (HAR), purify it to the extent needed, and determine its ^{79}Se content. It will serve as a reference solution for ^{79}Se analyses and will be made available to interested DisCo-partners.

2 WP2: Characterisation of spent fuels

As has been reported in the 12-month and 18-month reports the two irradiated MOX samples (MOX-l and MOX-H) have been selected from the agreeing γ -scan and burn-up profiles. The samples were cut and are stored under Ar-atmosphere in under-pressure awaiting leaching experiments. The irradiated Cr-doped UO_2 fuel was cut according to the cutting plan presented in the DisCo 1st annual report. They are stored together with the MOX samples. Both types of fuel samples are scheduled for dissolution and inventory determination, but the dissolutions has been postponed, to the second half of 2019, due to renovation of dissolution cell Z105. The inventory determination will follow the fuel dissolution and a comparison of the calculated and actual inventory is scheduled.

3 WP3: Spent fuel dissolution experiments

As concluded in section WP2 above, the cut fuel samples are ready for leaching experiments. JRC-KA presented, during the 1st annual DisCo workshop, pressure leak rate results from the first assembled hot cell autoclave. Nevertheless, at the final leak rate test before introducing the autoclave into hot cell Z112 it was discovered that some of the used Titanium cutting rings from the company Swagelok were

cracked (Figure 1). As a consequence, the final safety acceptance protocol could not be signed, and the hot cell autoclave is not cleared for hot cell use.

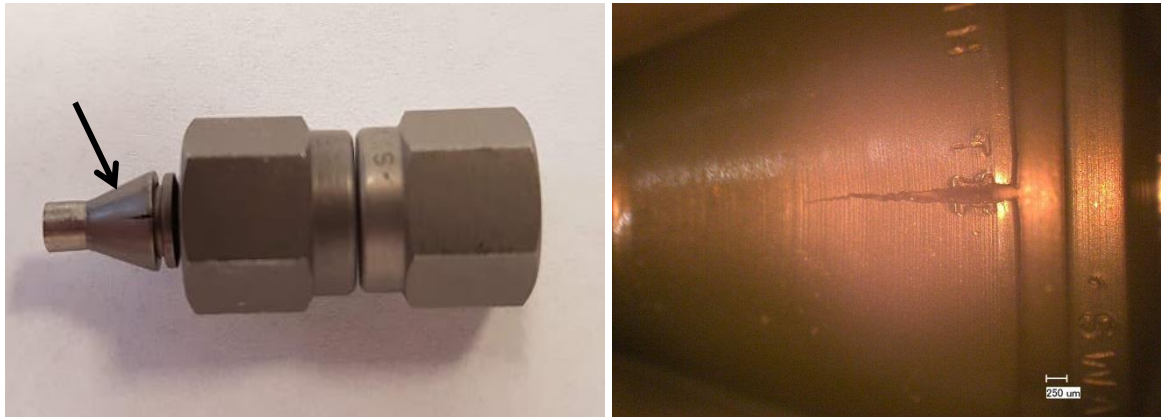


Figure 1: Titanium connection piece with a cutting ring crack at the position of the engraved Swagelok product number or batch.

Metallurgic investigation showed that the cracks are present where the cutting rings have engraved batch identification text. JRC-KA and Swagelok work intensively on a solution. In the 18-months progress report JRC-KA had planned to start the first leaching tests in the 1st quarter of 2019, but based on the present situation we will need to revise the time planning.

Selenium-79, with its half-life of 327,000 years, is a long-lived fission product. Validation of ⁷⁹Se inventory in spent fuel and concentrations in spent fuel leachates is practically missing due to absence of ⁷⁹Se standards. The consequence is that ⁷⁹Se must be handled very conservatively in the SNF repository performance assessment and turns-up, on long-time scales, as a radionuclide contributing significantly to radiological dose to man. As described in the last 18-months report two HAR solutions have been prepared for Se extraction. The biggest challenges analysing ⁷⁹Se and other Se-isotopes by Inductively Coupled Plasma – Mass Spectrometry (ICP-MS) are the isobaric interferences. The main isobaric interferences to expect on mass 79, are ⁶³Cu¹⁶O (from the Cu wire), ⁴⁰Ar³⁸Ar¹H (Ar being the plasma gas) and ⁷⁹Br (impurity in acids). Also, the other Se-isotopes suffer from isobaric interferences, mainly from Ar-dimer species. Tests using high-purity collision gas O₂ or NH₃ for Se analysis by Collision/Reaction Cell-ICP-MS (CRC-ICP-MS) were successful, but not for the full Se isotopic spectrum in one run. The Se isotopes that become interference-free depend on the collision gas used. Some other gases (high-purity CH₄ and CO₂) to be tested as collision gas have been ordered in January 2019 and safety checks are actually ongoing before being allowed to use them in the ICP-MS glove-box. Once the analytical procedure is established, the separation of Se from the HAR by reductive precipitation will be made. The recovery of the precipitated Se through dissolution from the Cu-wire will be followed by purification to the extent needed and ⁷⁹Se content determination.

Status of leaching experiments performed with irradiated MOX fuel in bicarbonate water under reducing conditions at KIT-INE

González-Robles, E., Herm, M., Müller, N., Walschburger, A., Böttle, M., Geyer, F., Metz, V.

KIT, Eggenstein-Leopoldshafen (DE)

Abstract

In this Scientific and Technical (S+T) contribution, results of leaching experiments performed with irradiated MOX fuel after 160 days of leaching in bicarbonate water under reducing conditions are shown. A continuous release of the fission products ^{90}Sr and ^{137}Cs is observed. Concentrations of actinides in solution are constant since the beginning of the experiments except for uranium and neptunium.

1 Introduction

Disposal in deep bedrock repositories is considered as the preferred option for the management of spent nuclear fuel (SNF) in many countries [1-3]. The aim is a permanent and safe disposal of this type of highly active waste so that it is isolated from the biosphere for an appropriate length of time. A multi-barrier system is interposed between the SNF and the environment considering the SNF matrix as the first technical barrier. In safety assessments for disposal of SNF in a deep underground repository, water access, consecutive failure of canisters and loss of integrity of fuel cladding is considered in the long-term. Assessing the performance of SNF in a potential geological disposal system requires the mechanistic understanding and quantification of the radionuclide release from SNF under reducing conditions of a breached container.

Up to now, many studies have been performed on dissolution of UO_2 fuels under oxidizing conditions and, in a lesser extent, studies on SNF dissolution under reducing conditions. Moreover, regarding the dissolution of irradiated mixed oxide (MOX) fuels, there is a lack of studies, especially, under reducing conditions.

Present studies performed at KIT-INE provide experimental data concerning the matrix dissolution of irradiated MOX fuel under reducing conditions. Moreover, the instant release fraction of safety relevant radionuclides are determined. For this purpose, two leaching experiments with spent MOX fuel (cladded pellet and fragments without cladding) are currently conducted in the shielded box-line of KIT-INE with periodical sampling campaigns of the gaseous and the aqueous phase. In this communication, results of radionuclides released into the aqueous phase up to 160 days of leaching are shown.

2. Materials and methods

3.1 Spent nuclear fuel characteristics

Irradiated fuel specimens were sampled from a MOX fuel rod that was irradiated in the pressurized water reactor of the Obrigheim nuclear power plant (KKO) in Germany. The irradiation was conducted in four cycles for a period of 1157 effective full power days with an average linear heat generation rate of 200 W/cm, achieving an average burn-up of $38 \text{ GWd} \cdot \text{t}_{\text{HM}}^{-1}$. The fuel rod was discharged in 1984, which implies a cooling time of 33 years before characterisation and cutting of the MOX samples. Initially, the fuel consisted of natural UO_2 enriched by 3.2% Pu and was fabricated following the optimised co-milling (OCOM) process.

3.2 Preparation of spent nuclear fuel samples

Two cladded pellets were dry cut from a segment of the MOX fuel rod using a low speed saw equipped with a diamond-wafering blade (Isomet 11-1180, Buehler Ltd.). Cutting was performed at the inter pellet gaps and, as a result, 10 mm length cladded pellets were obtained. The cladding tube of one pellet was mechanically removed and fuel fragments were obtained. The samples were weighed and length and diameter were measured before the start of the experiments. The characteristic values of the studied irradiated MOX specimens are reported in Table 1.

Table 1: Characteristic values of the studied irradiated MOX samples.

| Sample | Cladded pellet | Fragments |
|-------------------------------|-----------------|-----------------|
| Mass of fuel and cladding (g) | 7.85 ± 0.01 | – |
| Mass of fuel (g) | 6.85 ± 0.01 | 5.52 ± 0.01 |
| Length (mm) | 9.7 ± 0.1 | – |
| External diameter (mm) | 10.7 ± 0.1 | – |
| Internal diameter (mm) | 9.3 ± 0.1 | – |

Figure 1a and Figure 1b show both surfaces of the cladded specimen used in one of the two leaching experiments whereas Figure 1c shows the fuel fragments without cladding used in the other experiment.

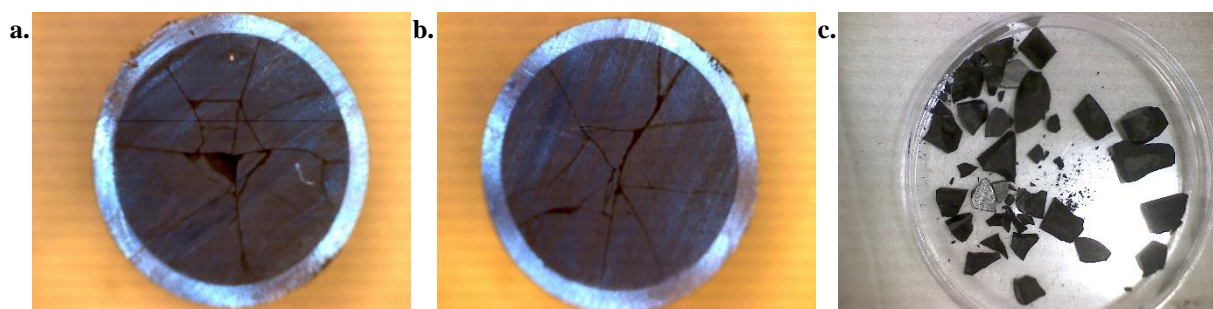


Figure 1: Cross sections of the selected cladded fuel sample used in one of the two leaching experiments are shown in *a)* and *b)* as well as fuel fragments used in the other leaching experiment are shown in *c)*.

3.3 Leaching experiments

The leaching experiments are performed in stainless steel autoclaves with Ti-liners under Ar/H₂ atmosphere. The starting date of each experiment is given in the following:

- Experiment with cladded pellet: 16/05/2018.
- Experiment with fragments: 23/05/2018.

As leachant bicarbonate water, containing 19 mM NaCl and 1 mM NaHCO₃ is used. The leachant was prepared in a glove box under Ar atmosphere, with ultrapure water purified with a Milli-Q academic apparatus (Millipore, 18.2 MΩ·cm, 22 ± 2°C, pore size 0.22 μm) and analytical grade chemicals (Merck GmbH).

After preparation and analysis of the leaching solution, the SNF corrosion experiments were started. As a first step, the cladded pellet was mounted in a titanium sample holder to ensure the contact of both pellet surfaces with the solution, and the fragments without cladding were placed in a quartz glass basket, see Figure 2.

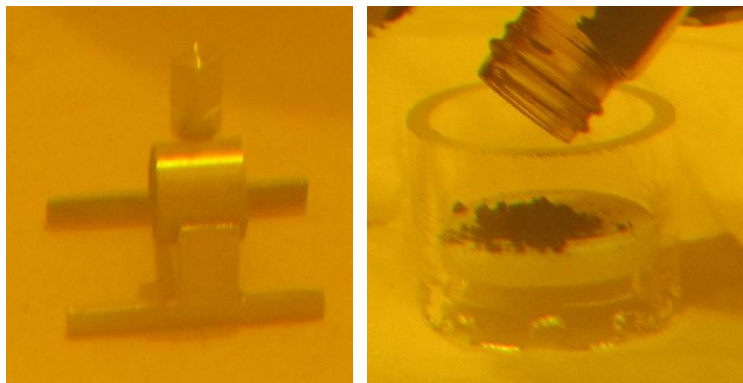


Figure 2: Spent MOX fuel pellet with cladding placed in Ti-sample holder is shown on the *left* picture and spent MOX fuel fragments in a quartz glass basket are shown on the *right* picture.

In a second step, once each of the SNF samples was placed inside its respective autoclave, the lid was closed and the autoclave was flushed with Ar, to remove residual air out of the autoclave and to avoid air intrusion. Afterwards, each autoclave was filled with 230 ± 5 mL of the leachant. Finally, the total gas pressure was adjusted to 40 bar using an Ar/H₂ gas mixture (with volume fractions of 92% of Ar and 8% of H₂; provided by Basi and Schöberl GmbH) to create strongly reducing conditions (H₂ partial pressure: 3.2 bar).

After one day of exposure, the first gaseous and liquid samples were taken and analysed. After this so-called washing step, the solution was completely exchanged, in order to reduce the amount of caesium in solution and a possibly present pre-oxidised layer on the sample surfaces. A volume of 230 ± 5 mL of fresh bicarbonate solution was used for replenishment, and the Ar/H₂ atmosphere was again restored, following the procedure previously described.

Throughout the leaching experiments, sampling campaigns of the gaseous phase (with a sampling aliquot of 50.0 ± 2.5 mL volume) and liquid phase (with a sampling aliquot of 10 ± 1 mL volume) are performed periodically. During each liquid sampling, the headspace of each autoclave is purged with Ar, and afterwards the initial pressure conditions described above were restored using the Ar/H₂ gas

mixture. Except for the first sampling (i.e. so-called washing step), the solution is not replenished after the samplings.

3.4 Analytical methods

Concentrations of actinides and technetium in aqueous solutions were determined using high-resolution inductively coupled plasma mass spectrometry (HR-ICP-MS) A sector field device (ELEMENT XR, ThermoFisher Scientific) was used to quantify ^{99}Tc , $^{235,238}\text{U}$, ^{237}Np , $^{239,240,242}\text{Pu}$, $^{241,243}\text{Am}$ and ^{244}Cm .

Liquid scintillation counting (LSC, Quantulus 1220, Wallac Oy, PerkinElmer) was used to quantify aqueous concentration of ^{90}Sr . Firstly, ^{90}Sr was extracted from the liquid sample aliquots by chromatography using a Sr-Resin crown ether (4,4'(5')-di-t-butylcyclohexano-18-crown-6). Then, solution aliquots were homogenized in Polyvials (HDPE, Zinsser Analytic) with LSC-Cocktail (Ultima Gold LLT, Perkin Elmer) for the measurements.

Aqueous concentrations of ^{134}Cs and ^{137}Cs were quantified using γ -spectroscopy. Measurements were performed by means of an extended range coaxial Ge detector (GX3018, Canberra Industries Inc.) with a relative efficiency of $\geq 30\%$. Energy and efficiency calibration of the detector was done using a certified multi-nuclide standard solution (Mixed Gamma 7600, Eckert & Ziegler Strahlen- und Medizintechnik AG). Data evaluation was performed using the Genie 2000 software (Canberra Industries Inc.). APEX screw-cap microcentrifuge tubes (2 mL, polypropylene, Alpha Laboratories Ltd.) were used as sample vessels during the measurements.

4 Results and discussion

Aqueous concentrations of fission products ^{90}Sr , ^{99}Tc , ^{129}I and ^{137}Cs as a function of leaching time are shown in Figure 3. After about 160 days of leaching, concentrations of ^{90}Sr and ^{137}Cs are still increasing. In the first two samplings, aqueous concentrations of ^{99}Tc and ^{129}I were below detection limit. Aqueous concentrations of the volatile fission products ^{129}I and ^{137}Cs are similar, and those of the matrix bound fission products ^{90}Sr and ^{99}Tc are similar, respectively.

Aqueous concentrations of the studied actinides are shown as a function of leaching time in Figure 4. Uranium concentrations increase in both experiments to about 10^{-7} M whereas the concentration of ^{237}Np decreases over time to below 10^{-10} M. Concentrations of other actinides in both experiments seem to be virtually constant since the first day of leaching.

The fraction of the radionuclide inventory released into the aqueous phase is calculated to compare the release behaviour of the different radionuclides and to assess the corrosion of the spent MOX fuel. The fraction of inventory of a radionuclide i released in the aqueous phase, $FIAP_i$, is given by Equation 1.

$$FIAP_i = \frac{m_{i,aq}}{m_{i,SNF}} = \frac{C_{(i,n)} \cdot V_{aq}}{m_{SNF} \cdot H_i} \quad \text{Eq. 1}$$

where $m_{i,aq}$ is the mass of radionuclide i in the aqueous phase (g), $m_{i,SNF}$ the mass of radionuclide i in the spent nuclear fuel sample (g), m_{SNF} is the mass of SNF sample used in the experiment (g), C_i is the concentration of element i in solution ($\text{g} \cdot \text{mL}^{-1}$), and V_{aq} is the volume of solution (mL). H_i corresponds

to the fraction of inventory for the radionuclide i ($g_i \cdot g_{SNF}^{-1}$) based on inventory calculations by means of the KORIGEN code.

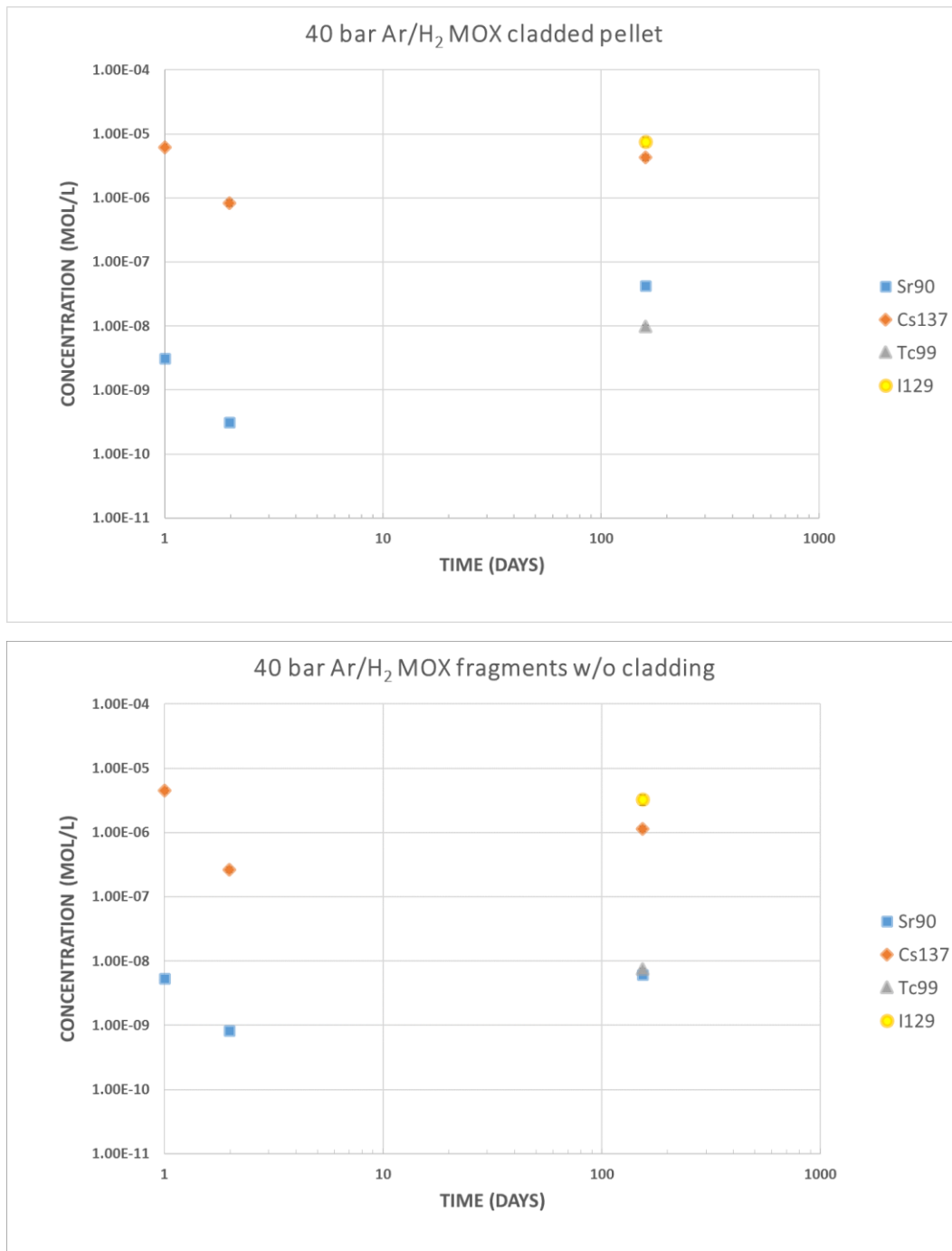


Figure 3: Aqueous concentrations of ^{90}Sr , ^{99}Tc , ^{129}I and ^{137}Cs as a function of leaching time in experiments performed with a cladded SNF pellet (*upper picture*) and SNF fragments (*lower picture*).

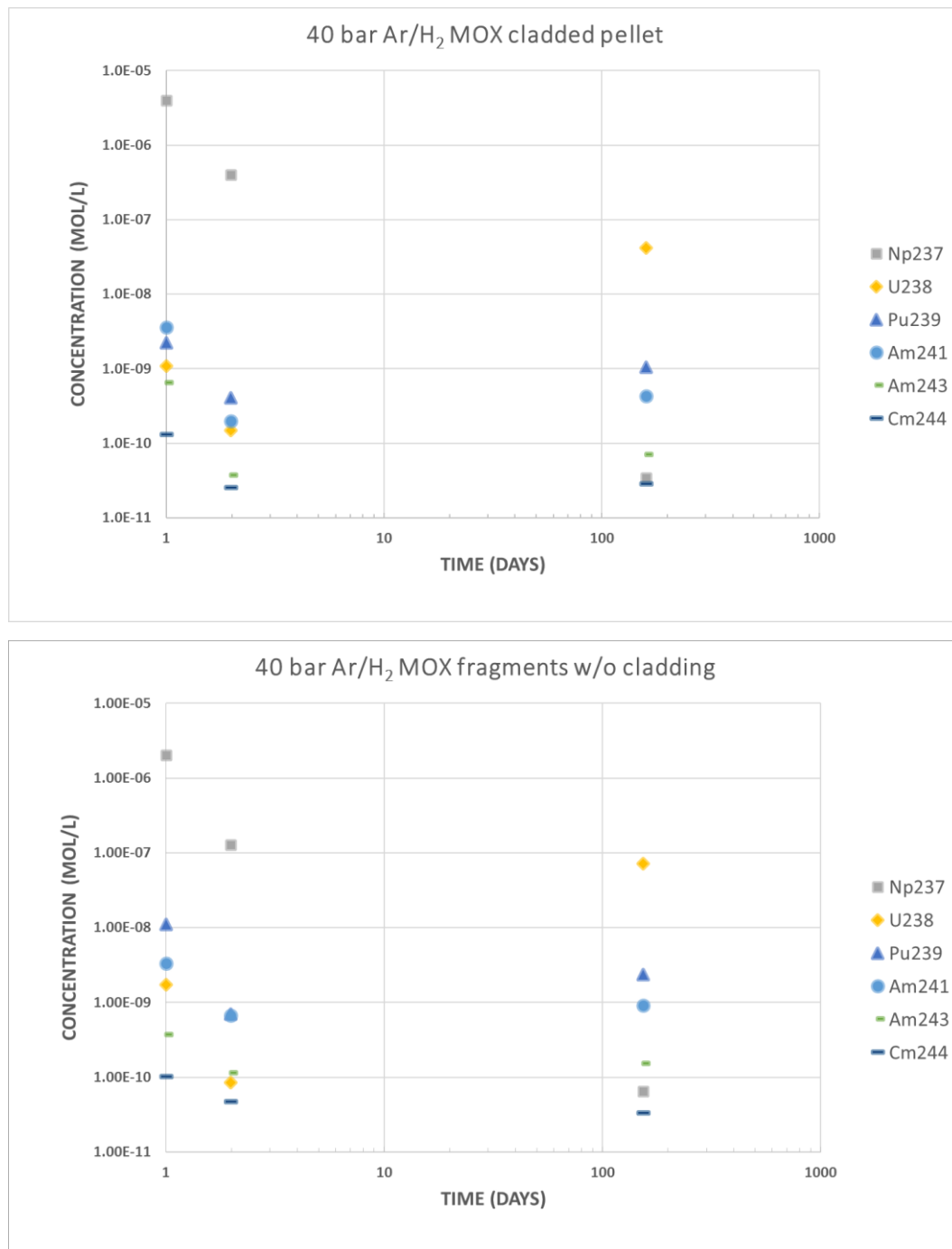


Figure 4: Aqueous concentrations of studied actinides as a function of leaching time in experiments performed with a cladded pellet (*upper* picture) and fragments (*lower* picture).

FIAP data is shown in Figure 5 and Figure 6 for fission products and actinides, respectively. Qualitatively, the temporal evolution of FIAP values of the studied fission products and actinides are similar to the evolution of the aqueous concentrations of the respective radionuclides. Quantitatively, it is obvious from the FIAP data that ^{129}I and ^{137}Cs release is significantly incongruent, i.e. two to four orders of magnitude higher than FIAP values of ^{90}Sr and ^{99}Tc , uranium and actinides. The considerable ^{129}I and ^{137}Cs release is related to a fast dissolving ^{129}I and ^{137}Cs fraction in the SNF samples. In contrast to other UO_2 matrix bound elements, ^{90}Sr is continuously released.

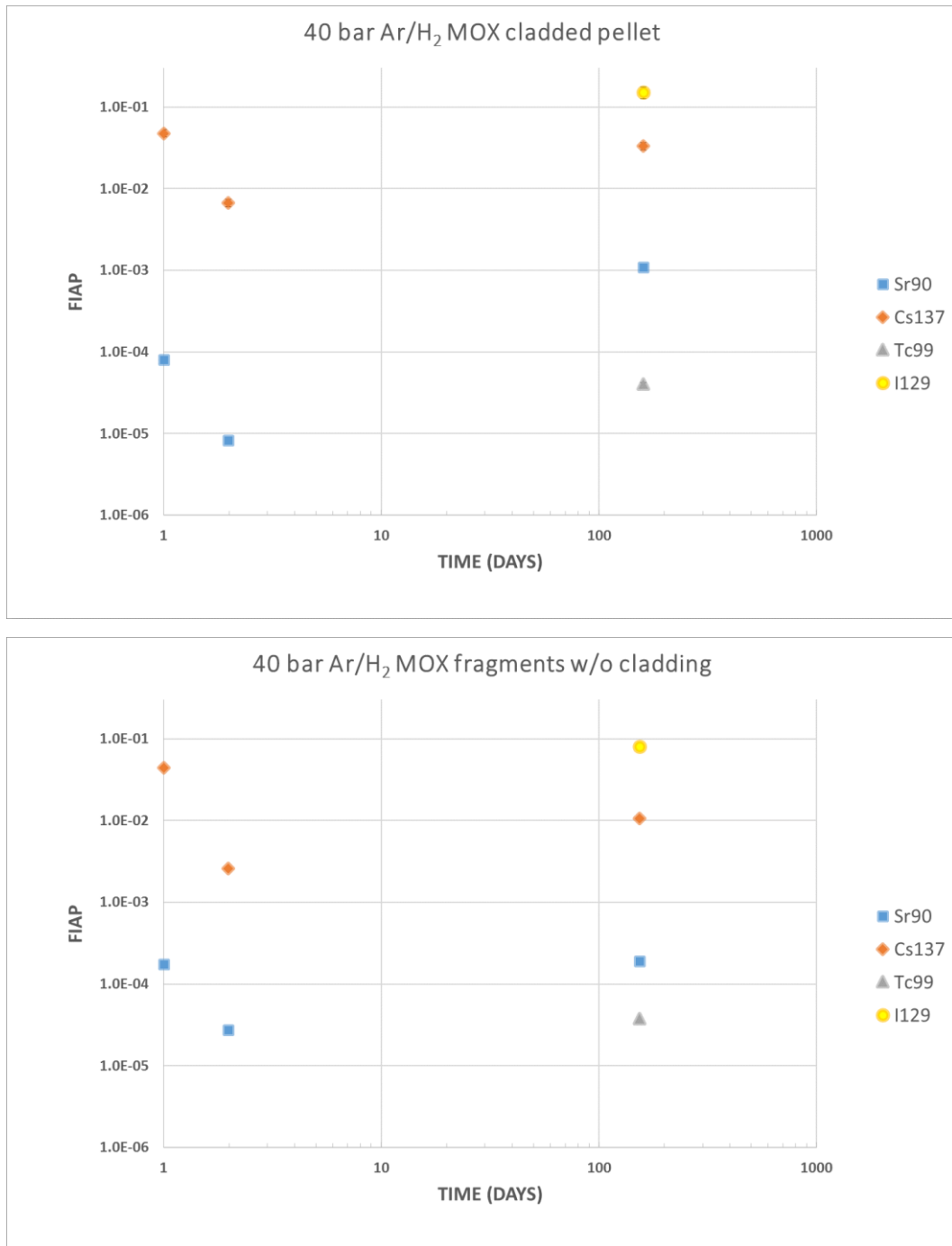


Figure 5: FIAP of ^{90}Sr , ^{99}Tc , ^{129}I and ^{137}Cs as a function of leaching time in experiments performed with a cladded pellet (*upper* picture) and fragments (*lower* picture).

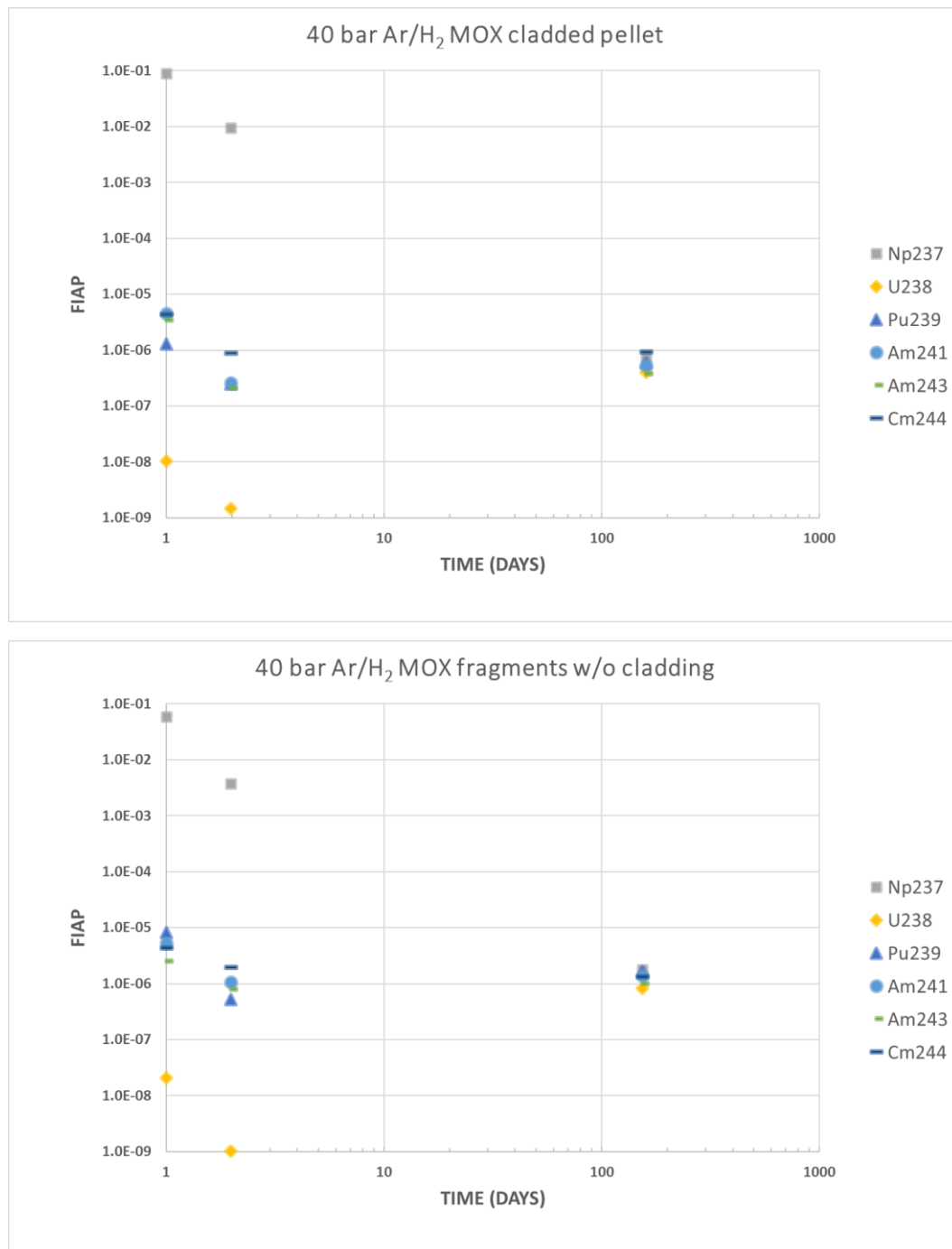


Figure 6: FIAP of various actinides as a function of leaching time in experiments performed with a cladded pellet (*upper picture*) and fragments (*lower picture*).

5 Summary and outlook

Two leaching experiments in autoclaves are currently performed using irradiated MOX fuel in bicarbonate water and hydrogen overpressure. Experiments will run until end of 2020. Three of eight sampling campaigns are completed including sampling of aqueous and gaseous phases. Analysis of the fourth sampling is currently ongoing.

Once, more results of radionuclide release into aqueous (and gaseous) phases become available a thorough discussion will be performed. Additionally, the data obtained in this study, using spent MOX fuel, will be compared to previous studies performed under similar conditions but with spent UO₂ fuel.

Acknowledgement

The research leading to these results has received funding from the European Commission Horizon 2020 Research and Training Programme of the European Atomic Energy Community (EURATOM) (H2020-NFRP-2016-2017-1) under grant agreement n° 755443 (DisCo project).

References

- [1] Ewing, R.C. (2015). Long-term storage of spent nuclear fuel. *Nature Materials*, 14, 252-257.
- [2] Bruno, J. and Ewing, R.C. (2006). Spent nuclear fuel. *Elements*, 2, 343-349.
- [3] Shoesmith, D.W. (2000). Fuel corrosion process under waste disposals. *Journal of Nuclear Materials*, 282, 1-31.

High Burnup Spent Fuel dissolution under highly alkaline conditions

Iglesias, L.^{1,2}, Serrano-Purroy, D.¹, Martínez-Torrents, A.², Clarens, F.², de Pablo, J.^{2,3}, Casas, I.³

1 Joint Research Center Karlsruhe (EU)

2 Eurecat (former Fundació CTM Centre Tecnològic) (ES)

3 UPC-Barcelona Tech, Department of Chemical Engineering (ES)

1 Introduction

The European Union's Horizon 2020 Framework Programme for Research and Innovation supports transnational research collaborations to improve our understanding of the Spent Nuclear Fuel (SNF) behaviour in repository conditions. Having knowledge about processes such as SNF leaching is mandatory to develop adequate concepts for deep geological disposal of highly radioactive waste. Although in the last years several Instant Release Fraction (IRF) and matrix corrosion studies have been made under different redox conditions and using several water compositions, there is still a lack of information regarding high burnup UO_2 samples in cementitious waters, both under oxidising and reducing conditions. The aim of Eurecat is to study the effect of water intrusion reaching high burnup UO_2 SNF deposited in a Deep Geological Repository (DGR) using representative repository conditions and water compositions as simplified cementitious water (BIC) and Young Cement Water with Ca (YCWCa). The YCWCa considers a previous contact with cement or concrete used in the construction of the DGR, having a higher pH with dissolved elements, such as Ca and Si (silicate anion).

Specifically, the scope is to analyse the behaviour of SNF in three different experiments: in contact with YCWCa in both oxidising and reducing conditions, and with BIC water in reducing conditions.

In this work, preliminary results of the experiment using YCWCa under oxidising conditions are shown. Results in reducing conditions are expected to be shown next year, after an unexpected delay of a number of months in the delivery of pieces for the autoclaves to the JRC Karlsruhe.

2 Experimental methods

A cladded fuel sample from a pressurized water reactor (PWR) SNF with a local burnup of $73 \text{ GWd}\cdot\text{tU}^{-1}$ was selected and cut through a pellet to obtain a segment without the interface between pellets. Further details about the sample, named 73YCWCa, are shown in Table 1.

Table 1: parameters of SNF cladged segment used in the described leaching experiment.

| Sample | 73YCWCa |
|--|------------------|
| Length (mm) | 2.9 ± 0.1 |
| Weight, only fuel (g) | 1.779 ± 0.05 |
| Diameter without cladding (mm) | 9.1 ± 0.1 |
| Surface area (mm ²) | 460 ± 10 |
| ²³⁵ U enrichment (weight%) | 3.95 |
| Grain size (μm) | 6.4 |
| Fission Gas Release (%) | 13.6 |
| Average Linear Power Density (W·cm ⁻¹) | 255 |

Based on the theoretical composition of the YCWCa solution, simulated cement water was prepared, whose composition is shown in Table 2.

Table 2: Theoretical composition in the synthetic YCWCa used for leaching experiment with 73YCWCa.

| Solution | pH | Na (mol·L ⁻¹) | Ca (mol·L ⁻¹) | Cl (mol·L ⁻¹) | Si (mol·L ⁻¹) | CO ₃ ²⁻ (mol·L ⁻¹) | OH ⁻ (mol·L ⁻¹) |
|----------|------|------------------------------|------------------------------|------------------------------|------------------------------|---|---|
| YCWCa | 13.4 | $4.6 \cdot 10^{-1}$ | $5.8 \cdot 10^{-4}$ | - | $2.7 \cdot 10^{-1}$ | $1.1 \cdot 10^{-3}$ | $2.5 \cdot 10^{-1}$ |

The methodology of the experiment followed a protocol reported in previous studies [1-3] and is schematically shown in Figure 1. The experiment was carried out under oxidising conditions in contact with air and at hot cell standard operation temperatures ($25 \pm 5^\circ\text{C}$). The cladged segment is submerged in a polyethylene bottle containing the leaching solution and stirred during a period of time. Then, the segment is transferred to another bottle containing fresh leaching solution (full replenishments). Therefore, the used waters are analysed, several aliquots were diluted in HNO₃ 1M or 1 wt.% tetramethylammonium hydroxide (TMAH), added to stabilise Iodine in solution, to be analysed by ICP-MS. The emptied bottles were refilled with HNO₃ 1 M and agitated during 7 days. This washing was done to recover any element that could have been adsorbed onto the plastic walls of the bottle during the leaching step. Finally, a sample of this HNO₃ rinsing solution was taken to be analysed by ICP-MS.

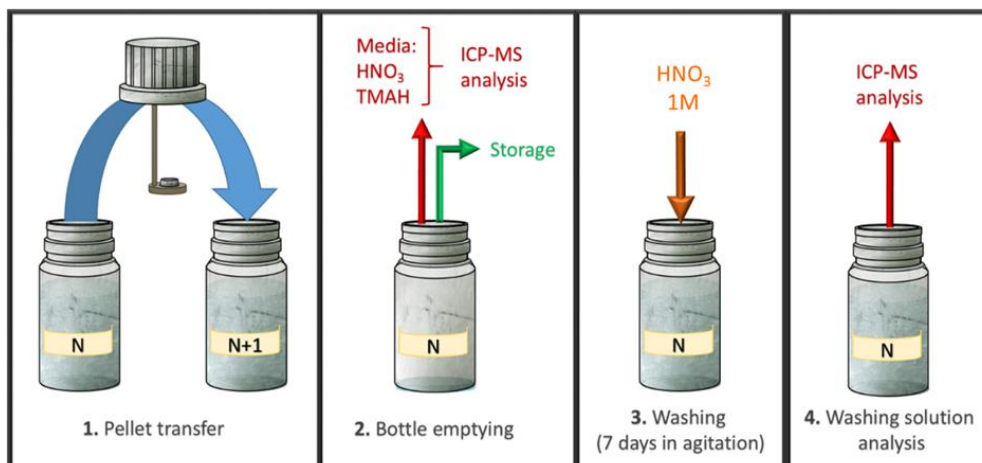


Figure 1: Solution sampling procedure.

3 Results and discussion

Preliminary results include 10 samples that have been analysed. Based on previous experience [1-3] some radionuclides (U, Rb, Sr, Mo, Tc, Cs, I) have been selected to be reported in Figure 2 and Table 3. Cumulative Fraction of Inventory in Aqueous Phase (CFIAP) results are shown in Figure 2. Iodine results are calculated after the analysis of TMAH samples, the others from the HNO₃ samples.

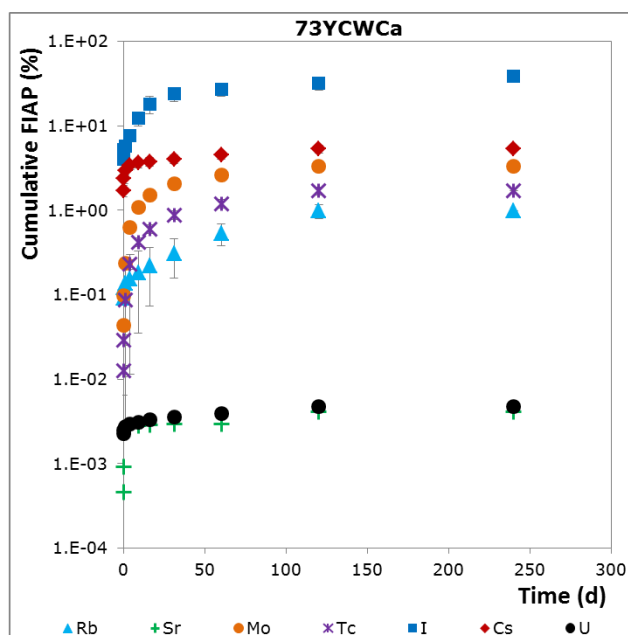


Figure 2: CFIAP (%) of the leaching experiment made with the 73YCWCa sample.

The trend is a faster release at the beginning and a slower dissolution after the first week. This could be partially explained by a faster dissolution of a uranium pre-oxidised phase in the surface of the pellet and a faster initial contribution coming from the gap and open voids in the case of the expected instant release radionuclides. Iodine, caesium, molybdenum, technetium and uranium present the highest CFIAP values. Sr has a different behaviour compared with the other elements, with a slower release, similar to the U, the matrix of the SNF.

The IRF, showed in Table 3, is calculated subtracting the CFIAP of the U to the CFIAP of the other elements.

Table 3: IRF results for 73YCWCa.

| IRF (%) | pH | Cs | I | Mo | Tc | Rb |
|---------|------|-----------|--------|-----------|-----------|-----------|
| 73YCWCa | 13.4 | 5.3 ± 0.6 | 39 ± 6 | 3.3 ± 0.3 | 1.7 ± 0.2 | 1.0 ± 0.2 |

A relevant RN release, faster than the matrix (U) can be observed for every studied element, excluding Sr, being its case different to previously reported results in simplified granitic waters [1-3]. On the one hand, technetium and molybdenum seem to have in this case more soluble phases than in precedent studies; on the other hand, strontium is less soluble. Planned speciation studies, as well as SEM examinations, will help for a complete understanding of the obtained results.

Acknowledgement

Special thanks to Stefaan van Winckel and Gert Rasmussen for the measurements by ICP-MS and their helpful recommendations in data evaluation. Daily work was supported by the Chemical Hot Cell technicians, Philippe Moisei, Komlan Anika and Caroline Diebold.

The authors would like to acknowledge ENRESA for underpinning this work and also to the European Commission for financially supporting the DisCo Project H2020 EURATOM ID: 755443.

References

- [1] González-Robles, E., Serrano-Purroy, D., Sureda, R., Casas, I., de Pablo, J. (2015). Dissolution experiments of commercial PWR (52 MWd/kgU) and BWR (53 MWd/kgU) spent nuclear fuel clad segments in bicarbonate water under oxidizing conditions. experimental determination of matrix and instant release fraction. *Journal of Nuclear Materials*, 465, 63-70.
- [2] Martínez-Torrents, A., Serrano-Purroy, D., Sureda, R., Casas, I., de Pablo, J. (2017). Instant release fraction corrosion studies of commercial UO₂ BWR spent nuclear fuel. *Journal of Nuclear Materials*, 488, 302-313.
- [3] Martínez-Torrents, A., Serrano-Purroy, D., Casas, I., De Pablo, J. (2017). Influence of the interpellet space to the instant release fraction determination of a commercial UO₂ Boiling water reactor spent nuclear fuel. *Journal of Nuclear Materials*, 499, 9-17.

Aqueous leaching of ADOPT and standard UO₂ spent nuclear fuel under H₂ atmosphere

Barreiro-Fidalgo, A.¹, Roth, O.¹, Puranen, A.¹, Evins, L.Z.², Spahiu, K.²

¹ Studsvik Nuclear AB, Nyköping (SE)

² SKB, Stockholm (SE)

Abstract

Within the EURATOM collaborative project “Modern Spent Fuel Dissolution and Chemistry in Failed Container Conditions – DisCo”, Studsvik is contributing with two experiments on different fuel types. The main objective of these investigations is to gather data on the dissolution behavior of a new type of fuel with additives (Advanced Doped Pellet Technology, ADOPT) under reducing conditions in presence of hydrogen. To compare the performance of the doped fuel with the standard UO₂ the samples are being leached in simplified groundwater under identical conditions in 2 autoclaves initially pressurized with 50 bar of H₂. Gaseous and liquid samples are being taken periodically and analysed to follow the leaching behavior. The U concentration decreased with time to a level of $1 - 2 \cdot 10^{-8}$ M, slightly above the solubility of amorphous UO₂. Low levels of Xe have been detected in the gas phase of both autoclaves, achieving cumulative release fractions between 3 - 5% of the inventory. A ratio of 1:1 between fission gases to ¹²⁹I was found. The release rate of most radionuclides is gradually transitioning to constant values. The preliminary data obtained supports the hypothesis that there is not major difference in leaching behavior between the two fuels.

1 Introduction

Within the EURATOM collaborative project “Modern Spent Fuel Dissolution and Chemistry in Failed Container Conditions – DisCo”, Studsvik is contributing with two experiments on different fuel types.

Improving reactor performance and reliability, reducing fuel cycle cost and the consequences of fuel failure are constant challenges for the nuclear industry. For this reason, in recent years new types of fuel have been developed. One example is the ADOPT fuel (Advanced Doped Pellet Technology) which consists of a UO₂-based fuel doped with small amounts of Cr₂O₃ and Al₂O₃. One of the main characteristics of this fuel is the enlarged grain size which results in lower Fission Gas Release (FGR) and increased density [1].

From the safety perspective of a deep geological repository for spent nuclear fuel (SNF), the new type of fuels must fulfil the acceptance criteria of low solubility under relevant repository conditions. Minor modifications on the UO₂ matrix resulting in property changes might affect the leaching behavior of the fuel. For this reason, it is important to gather new data on the dissolution behavior of a new type of fuel with additives under reducing conditions in presence of hydrogen. In this study, the behavior of the doped fuel (ADOPT) will be compared to the performance of standard UO₂ fuel under identical conditions.

The objective of this study is to gather data that will be used to support or refute the hypothesis that there is no significant difference in leaching behavior between the two fuels. In addition, thermodynamic and kinetic models will be developed in WP5 using the experimental data.

2 Experimental details

The experiments are being performed on fuel fragments without cladding. The selected fragments are the same samples leached in a previous EURATOM project, FIRST Nuclides, which were used to establish the instant release fraction and the matrix dissolution behavior under aerated conditions [2]. The fuels are listed in Table 1. The two fuels have very similar power histories, having been irradiated in the same assembly.

Table 1: Fuels selected for the experiments performed at Studsvik.

| Sample name | Reactor type | Fuel type | FGR (%) | Calculated BU (rod average) (MWd·kgU ⁻¹) |
|-------------|--------------|--------------------------------------|---------|--|
| 5A2 | BWR | Std. UO ₂ | 2.4 | 57.1 |
| C1 | BWR | ADOPT (Al/Cr doped UO ₂) | 1.4 | 59.1 |

The fuel fragments (2 g from each fuel type) were exposed to an initial leaching period (pre-wash) under aerated conditions in 200 mL 10:10 mM NaCl:NaHCO₃ solutions in the Hot Cell Laboratory at Studsvik. The main objective of this initial step is to wash away any pre-oxidized phases formed during air storage in cell by exposing them to relatively high NaHCO₃ concentrations. Figure 1a and Figure 1b show the collected fuel fragments and a leaching flask with the fuel immersed in the leaching solution.

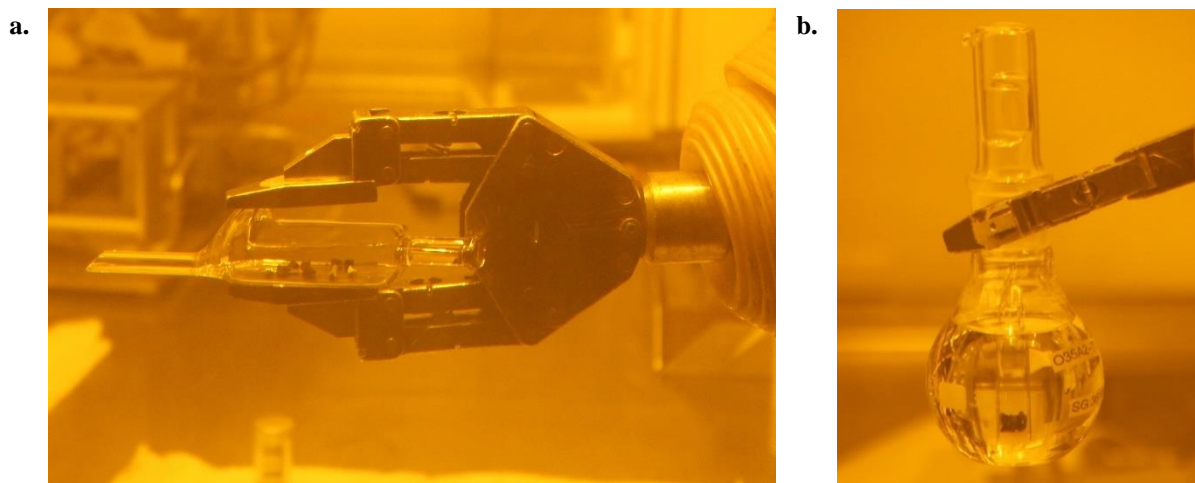


Figure 1: (a) One batch of fuel fragments and (b) leaching flask containing fuel samples.

The washing step was divided into a total of 5 contact periods as shown in Table 2. At the end of each contact period the glass baskets containing the fuel were transferred into a new flask containing fresh leaching solution.

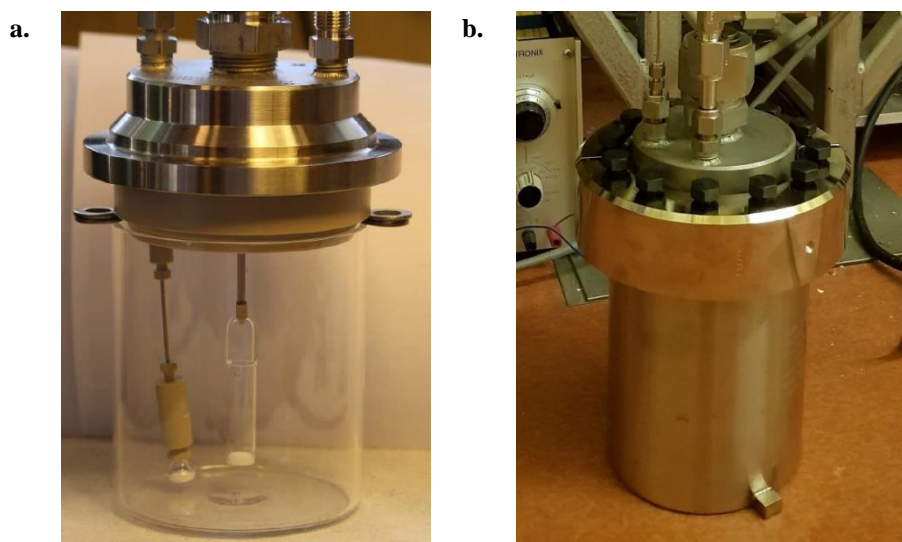
Table 2: Contact periods for the washing step.

| Contact period | Duration (days) | Cumulative duration (days) |
|----------------|-----------------|----------------------------|
| 1 | 1 | 1 |
| 2 | 5 | 6 |
| 3 | 8 | 14 |
| 4 | 20 | 54 |
| 5 | 71 | 105 |

Samples of the leaching solution were centrifuged for 1 h at 74,000 g at the end of each contact period to try to separate colloids from the solution.

Thereafter the samples were preserved in either 1% HNO₃ or 0.5% TMAH for analysis by Inductively Coupled Plasma Mass Spectrometry (ICP-MS) for masses 82 - 254 and ¹²⁹I respectively and gamma spectrometric analysis for ¹³⁷Cs determination. ¹¹⁵In and ²⁰⁹Bi are used as internal standards for the ICP-MS analysis.

After fulfillment of the criteria for a successful washing, both fuels were introduced in stainless-steel autoclaves with an inner quartz vessel that contains the leaching solution and PEEK internals. The sampling system consist of an internal PEEK line with a quartz filter (P4 10-16 μm pore size). The external line is made of stainless steel with two valves in series. Figure 2a and Figure 2b show an example of the internal and external parts of the autoclaves.

**Figure 2:** (a) Autoclave internals and (b) exterior of the autoclave.

Prior to assembling the autoclaves, the free internal volume was determined for gas phase calculations obtaining a value of 950 cm³. Leak tests were also performed by pressurizing the autoclaves with 50 bar of He and monitoring the pressure through 1 month. The pressure drop rate found was ~ 0.16 bar/month.

The autoclave vessels were filled with 680 mL of simplified groundwater, consisting of 10 mM NaCl and 2 mM NaHCO₃. Prior to loading, the autoclaves were sparged during 30 min with argon to minimize the air content. After loading the quartz baskets containing the fuel, the autoclaves were closed and sparged for another hour before the argon flow was stopped. Thereafter the autoclaves were pressurized up to the target pressure of 55 bar of H₂. No replenishment of gas due to pressure loss during the experiment is planned.

The concentration of fission products and actinides in the autoclave solution will be followed for ~ 2 years by 9 sampling points (liquid and gas sampling). The sample solutions are analysed in the same way as the solutions from the washing experiments. In addition, the composition of the gas phase is analysed by Gas-MS to detect air intrusion or release of fission gas from the fuel samples. The status of the planned sampling points is presented in Table 3.

Table 3: Autoclave sampling points. Samples already taken and analysed are marked with an “✓”.

| Sampling point | Leaching time (days) | Liquid sample | Gas sample |
|----------------|----------------------|---------------|------------|
| 1 | 0.1 | ✓ | x |
| 2 | 1 | ✓ | ✓ |
| 3 | 7 | ✓ | ✓ |
| 4 | 28 | ✓ | ✓ |
| 5 | 91 | ✓ | ✓ |
| 6 | 203 | ✓ | ✓ |
| 7 | 365 | June 2019 | June 2019 |
| 8 | 670 | April 2020 | April 2020 |
| 9 | 730 | June 2020 | June 2020 |

Each sample point is taken in triplicate. The first sample (A) is used to rinse the sampling system and it is not analysed. Samples B and C are centrifuged at 74,000 g during one hour and thereafter the supernatant is removed and preserved as described above for the pre-wash samples.

3 Preliminary results and discussion

It must be noted that the results presented are preliminary and therefore subjected to minor changes or adjustments.

3.1 Washing step

The uranium release rate is plotted against cumulative time in Figure 3. It can clearly be seen how the uranium release rate decreases markedly with washing time. After ~ 3 months both fuels exhibit considerably low and identical uranium release rates.

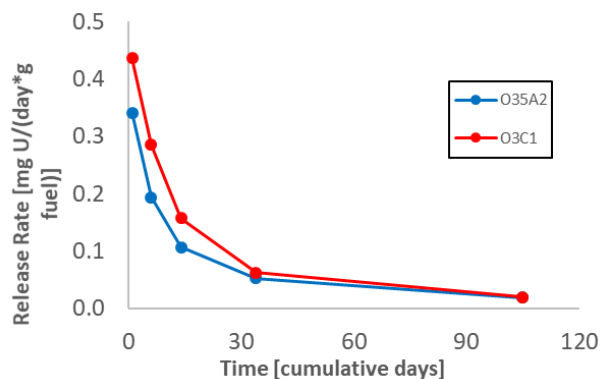


Figure 3: Uranium release rate as a function of time during the pre-wash. O35A2 corresponds to the std. UO_2 fuel and O3C1 to ADOPT.

3.2 Leaching under H_2 atmosphere

The initial pH and carbonate concentration were measured obtaining 8.2 and 2 mM, respectively.

3.2.1 Gas analysis

Table 4 and Table 5 summarize the evolution of the composition of the gas phase in the two autoclaves.

Table 4: Pressure and gas composition autoclave O35A2 (Std. UO_2).

| O35A2 | Gas | G1 | G2 | G3 | G4 | G5 |
|---------------------------|------------------|--------|--------|--------|--------|--------|
| (Std. UO_2) | Kr (%) | 0.000 | 0.000 | 0.000 | 0.000 | 0.000 |
| | Xe (%) | 0.000 | 0.000 | 0.001 | 0.001 | 0.002 |
| | H_2 (%) | 98.071 | 97.605 | 97.040 | 97.031 | 96.995 |
| | He (%) | 0.113 | 0.522 | 1.015 | 1.029 | 1.0584 |
| | N_2 (%) | 0.010 | 0.011 | 0.016 | 0.023 | 0.033 |
| | O_2 (%) | 0.006 | 0.006 | 0.006 | 0.007 | 0.007 |
| | Ar (%) | 1.800 | 1.856 | 1.920 | 1.909 | 1.904 |
| Autoclave Pressure | (bar) | 50.23 | 43.54 | 35.19 | 31.28 | 27.57 |
| Duration | (days) | 1 | 6 | 34 | 91 | 211 |

Table 5: Pressure and gas composition autoclave O3C1 (ADOPT).

| O3C1 | Gas | G1 | G2 | G3 | G4 | G5 |
|---------|------------------|--------|--------|--------|--------|--------|
| (ADOPT) | Kr (%) | 0.000 | 0.000 | 0.000 | 0.000 | 0.000 |
| | Xe (%) | 0.000 | 0.000 | 0.001 | 0.001 | 0.001 |
| | H_2 (%) | 98.901 | 98.228 | 98.695 | 97.562 | 97.435 |

| O3C1 | Gas | G1 | G2 | G3 | G4 | G5 |
|---------------------------|--------------------|-------|-------|-------|-------|-------|
| | He (%) | 0.056 | 0.274 | 0.724 | 0.847 | 0.934 |
| | N ₂ (%) | 0.010 | 0.011 | 0.014 | 0.017 | 0.023 |
| | O ₂ (%) | 0.006 | 0.006 | 0.006 | 0.006 | 0.008 |
| | Ar (%) | 1.027 | 1.481 | 1.560 | 1.567 | 1.598 |
| Autoclave Pressure | (bar) | 49.02 | 43.77 | 37.72 | 34.41 | 31.98 |
| Duration | (days) | 1 | 6 | 34 | 91 | 211 |

The Kr and Xe results are close or below the limit of quantification. However, from the first leaching month, the isotopic composition of Xe in the gas phase matches fairly well the Xe inventory in the fuel. This implies that fission gas is released to some extent from both samples. Preliminary calculations indicate that 5.0% of the Xe inventory is released for the standard UO₂ fuel and 3.8% for ADOPT.

Preliminary results of a number of radionuclides of interest from the aqueous phase of both autoclaves are summarized in Figure 4.

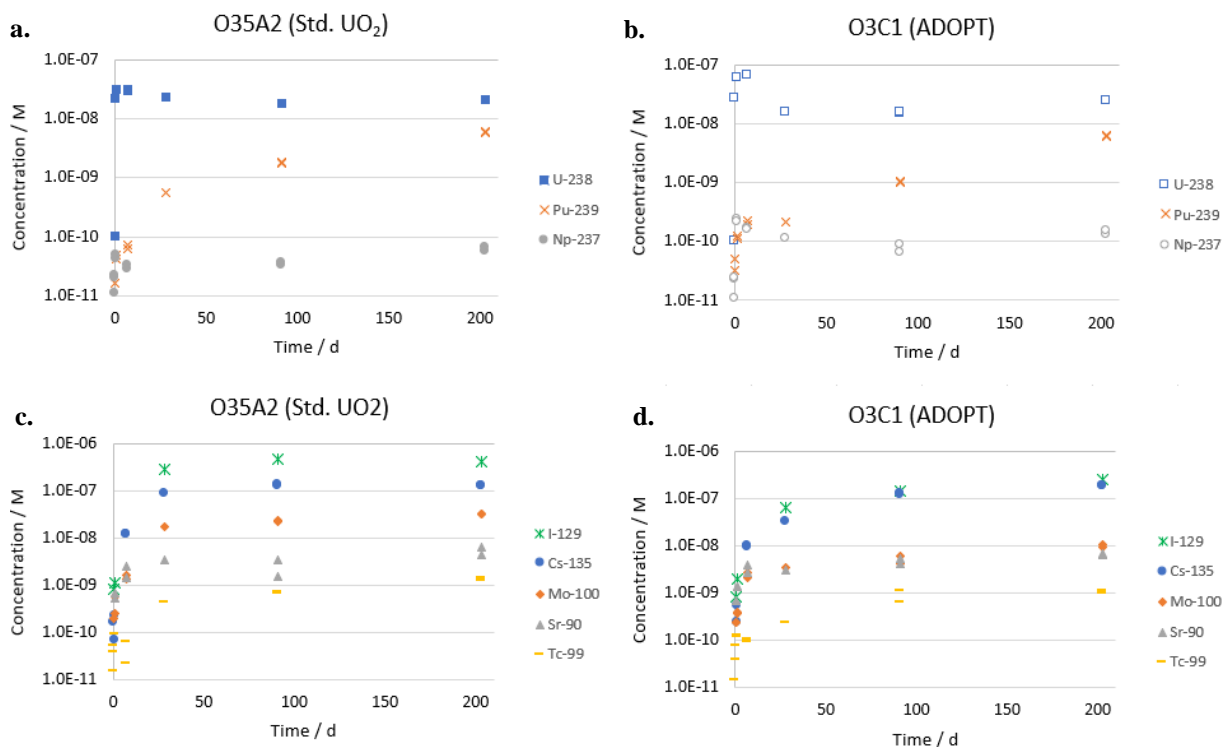


Figure 4: Autoclave concentrations of ²³⁸U, ²³⁹Pu and ²³⁷Np (a, b) and ¹²⁹I, ¹³⁵Cs, ¹⁰⁰Mo, ⁹⁰Sr and ⁹⁹Tc (c, d). The plots to the *left* belong to autoclave O35A2 (standard UO₂) and to the *right* to autoclave O3C1 (ADOPT).

As can be seen in Figure 4, the initial rise of ²³⁸U concentration in both autoclaves (due to dissolution of oxidized fuel layers as a result of air exposure during the transfer from the pre-wash to the autoclaves) is followed by a slow decrease attributable to reduction by H₂. For both autoclaves, the ²³⁸U concentration after 208 days seems to stabilize at 1 - 2 · 10⁻⁸ M, slightly higher than the solubility

for amorphous UO_2 ($2 - 5 \cdot 10^{-9}$ M) [3]. One possible explanation for this behavior is the formation of nanosized U-Si colloids within the autoclave leaching solution. Further analyses are being considered to elucidate this potential explanation. Relative low concentrations for Pu and Np are observed in both cases ($\sim 3 \cdot 10^{-10}$ for ^{137}Np and $\sim 6 \cdot 10^{-9}$ for ^{239}Pu), although one order of magnitude higher than values reported by a previous study on high burnup standard UO_2 fuel under hydrogen conditions [4].

Highly soluble nuclides such as ^{129}I and ^{137}Cs increased steadily during the first month reaching a relative constant level for the standard UO_2 fuel. The ADOPT specimen is also rapidly transiting to near-constant concentrations however an increasing trend is still observed. The major release of other elements of interest such as ^{100}Mo , ^{90}Sr and ^{99}Tc occurs within a few days, slowly approximating a constant value.

The largest difference between both fuels can be observed in the leaching behaviour of ^{129}I . The FIAP of an element (Fraction of Inventory in Aqueous Phase) is calculated by dividing the mass of the element present in the aqueous phase by the mass of the element in the spent nuclear fuel. After 6 months, the FIAP for ^{129}I for the standard UO_2 fuel is 6.7% while for ADOPT is 3.2%. This difference can be explained given the larger grain size in ADOPT fuel, decreasing fission gas diffusion through the fuel and therefore reducing the FGR and the release of volatile elements during reactor operation such as ^{129}I .

Furthermore, comparing the release of fission gases for standard UO_2 and ADOPT (Xe, 5.0% and 3.8% respectively) and ^{129}I (6.7% and 3.2%) a ratio of $\sim 1:1$ was observed for both autoclaves. This is in very good agreement with previous observations in a previous study by other authors [5].

At this point in the experiment, radionuclide concentrations are within the expected range when compared to previous leaching studies under hydrogen atmosphere [4, 6-8]. In addition, the overall doping effect on the leaching behaviour seem to be small.

4 Future work

As previously mentioned, the preliminary results presented so far support the hypothesis that there is no major difference in leaching behaviour between the two fuels. To further support this hypothesis, 3 additional sampling points (both liquid and gas) are planned in the next year and a half as summarized in Table 3.

Acknowledgement

The research leading to these results has received funding from the European Commission Horizon 2020 Research and Training Programme of the European Atomic Energy Community (EURATOM) (H2020-NFRP-2016-2017-1) under grant agreement n° 755443 (DisCo project).

References

- [1] Arborelius, J., Backman, K., Hallstadius, L., Limbaeck, M., Nilsson, J., Rebensdorff, B., Zhou, G., Kitano, K., Loeffstroem, R., Roennberg, G. (2006). Advanced doped UO_2 pellets in LWR applications. *Journal of Nuclear Science and Technology*, 43, 967-976.

-
- [2] Kienzler, B., Metz, V., Duro, L., Valls, A. (2014). Final (3rd) Annual Workshop Proceedings of the 7th EC FP CP FIRST-Nuclides project. KIT Scientific Report, 7716.
- [3] Guillaumont, R., Fanghänel, T., Neck, V., Fuger, J., Palmer, D.A., Grenthe, I., Rand, M.H. (2003). Update on the chemical thermodynamics of U, Np, Pu, Am and Tc. OECD NEA, Elsevier.
- [4] Puranen, A., Roth, O., Evins, L.Z., Spahiu, K. (2018). Aqueous leaching of high burnup UO₂ fuel under hydrogen conditions. MRS Advances, 3(19), 1013-1018.
- [5] González-Robles, E., Fuß, M., Bohnert, E., Müller, N., Herm, M., Metz, V., Kienzler, B. (2015). Study of the release of the fission gases (Xe and Kr) and the fission products (Cs and I) under anoxic conditions in bicarbonate water. MRS Proceedings, 1744, 35-41.
- [6] Fors, P., Carbol, P., Van Winkel, S., Spahiu, K. (2009). Corrosion of high burn-up structured UO₂ fuel in presence of dissolved H₂. Journal of Nuclear Materials, 394, 1-8.
- [7] Loida, A., Metz, V., Kienzler, B., Geckeis, H. (2005). Radionuclide release from high burnup spent fuel during corrosion in salt brine in the presence of hydrogen overpressure. Journal of Nuclear Materials, 346, 24-31.
- [8] Spahiu, K., Cui, D., Lundström, M. (2004). The reduction of U(VI) by near field hydrogen in the presence of UO₂(s). Radiochimica Acta, 92, 625-629.

Chromium doped UO₂-based model systems: Synthesis and characterization of model materials for the study of the matrix corrosion of spent modern nuclear fuels

Kegler, P., Klinkenberg, M., Bukaemskiy, A., Deissmann, G., Alekseev, E.V., Bosbach, D.

Forschungszentrum Jülich GmbH, Institute of Energy and Climate Research Nuclear Waste Management and Reactor Safety (IEK-6), Jülich, (DE)

Abstract

Studies on tailor-made UO₂-based model materials can provide additional insights into the behaviour of modern doped LWR-fuels under the post-closure conditions expected in a deep geological repository, complementary to dedicated dissolution experiments on spent nuclear fuels. Here, we describe the development and optimisation of the process steps for a wet-chemical route to produce Cr-doped UO₂ pellets with and without alpha dopants (²³⁸Pu), as well as pure UO₂ reference materials. The systematic investigation of various process parameters such as calcination temperature, pelletisation pressure and oxygen partial pressure was extended compared to the works described in the first AM proceedings. The challenges met during process development and optimisation and the effects of the process parameter variations on the materials properties are discussed. Moreover, first results of accelerated dissolution tests performed on Cr-doped and pure UO₂ materials using H₂O₂ to mimic radiolytic oxidation processes evoked from the alpha-irradiation of water in long-term disposal scenarios for spent nuclear fuel are presented. These experiments allow the determination of first initial dissolution rates for pure UO₂ reference as well as for Cr-doped pellets. In addition, an unknown effect of surface passivation of the pellets was determined.

1 Introduction

The efforts to improve fuel performance in nuclear power generation lead to an increased usage of a various new types of light-water reactor (LWR) fuels including Cr-, Al-, and Si-doped fuels [1-3]. While the improvement of in-reactor performance of these fuels has already been demonstrated, it is still uncertain, whether the corrosion/dissolution behaviour of such fuels in a deep geological repository is similar to conventional spent LWR-fuels. However, the chemical and structural complexity of spent nuclear fuels (SNF) and the associated high beta- and gamma radiation fields impede unravelling all the various concurring dissolution mechanisms from experiments with SNF. Thus, within the EU-DisCo project (www.disco-h2020.eu), experiments on irradiated doped fuels are complemented with dissolution studies using systematically produced and carefully characterised UO₂-based model materials to understand the effects of the addition of Cr- or Al-oxide into the fuel matrix on SNF dissolution behaviour under repository relevant conditions. These model materials comprise (i) UO₂ reference materials, and (ii) Cr-/Al-doped UO₂, both, with and without alpha-emitting nuclides such as ²³⁸Pu, to address the effects of alpha-radiolysis on the oxidative dissolution of aged SNF after recession of the beta/gamma radiation field in the long-term. Single-effect studies

on the dissolution behaviour of the model materials will provide complementary insights and supporting process understanding regarding the performance of modern doped fuels in the repository environment, which cannot be directly obtained from dissolution studies on SNF.

In this presentation, we provide an overview on (i) the development and optimisation of the synthesis route for the production of the UO₂ reference and Cr-doped UO₂ materials, and (ii) first results from accelerated dissolution experiments using pure and Cr-doped UO₂ pellets. In these experiments, H₂O₂ was used to mimic the radiolytic oxidation due to alpha-radiolysis that is relevant for SNF dissolution in the repository environment in the long-term. To provide insights into the effects of the material's microstructure on the dissolution behaviour (e.g. regarding the larger grain size in doped fuels and contributions from grain boundaries) as well as for comparability to SNF experiments, the model materials were produced in form of sintered pellets.

2 Development and optimisation of synthesis route

The following challenges had to be met during the optimisation of the synthesis process of the Cr-doped and undoped UO₂ reference pellets:

- i. the procedures had to be robust and easily reproducible in different laboratories (i.e. in Jülich and in Mol) with slightly different equipment,
- ii. in order to obtain a homogeneous distribution of Cr and, in particular, of ²³⁸Pu present only in trace amounts (< 50 ppm) in the pellets, a wet chemical synthesis was favoured,
- iii. milling/grinding steps should be avoided to minimise dust generation and carry-over of Pu, and
- iv. no lubricants such as Zn-stearate or sintering aids should be used during pelletising and sintering.

Moreover, all process steps, tested and optimised in Jülich without alpha-doping, had to be designed in a way to be accomplished also in a glove-box line at SCK·CEN in Mol, to produce ²³⁸Pu-doped pellets with similar characteristics.

Sample preparation techniques for UO₂ and Cr-doped UO₂ reference materials have been established at Jülich to optimize the future production of Cr and alpha-doped material at SCK·CEN. A method of wet-chemical synthesis was adopted to achieve a homogenous distribution of Cr as well as ²³⁸Pu. This method avoids a grinding step, and thus has been chosen in order to prevent potential contamination in the future steps of Pu-doped materials production (at SCK·CEN). The principal scheme of the two developed routes is presented in Figure 1.

As it can be seen from the Figure 1, chromium can be added at different stages of the synthesis process as Cr(NO₃)₃ solution to the starting solution (co-precipitation method) or as diluted Cr(NO₃)₃ solution to the UO₂ powder after the second step of thermal treatment (wet coating method). This plays an important role in the structure of the final pellets (e.g. regarding grain size, see Figure 3) and Cr distribution (in grains and/or on grain boundaries).

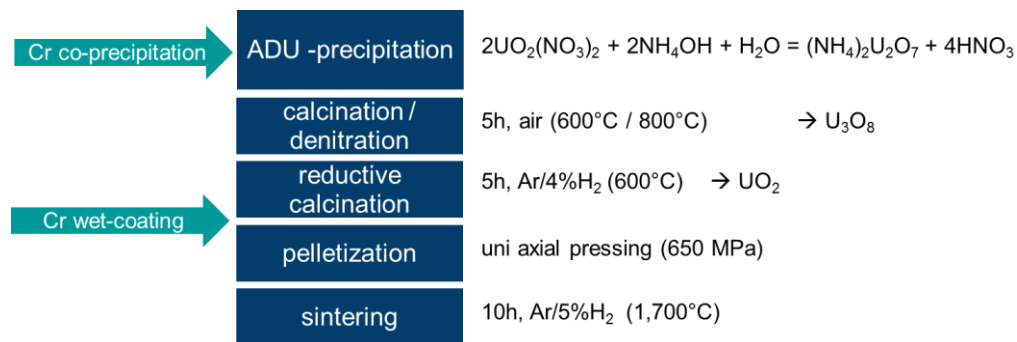


Figure 1: Simplified scheme of wet chemical synthetic route for pure and Cr-doped UO_2 .

A systematic study on the influence of the thermal treatment steps, the pressure used in the pelletising step as well as the oxygen potential ($-\Delta G^\circ = -RT \ln p\text{O}_2$) during the sintering step was performed; its results are presented in Figure 2. Optimum densities of the Cr-doped pellets (above 95 relative density) were achieved with a first calcination / denitration step at 600°C and a second reductive calcination step at 600°C, respectively. In order to achieve higher densities of the final pure UO_2 pellets the first calcination / denitration step under air atmosphere was performed at 800°C (Figure 1). We found that the optimal density of the sintered pellets can be achieved using a pressure of 650 MPa for the pelletisation step. The described synthesis routine was successfully transferred to and tested in the labs of SCK-CEN.

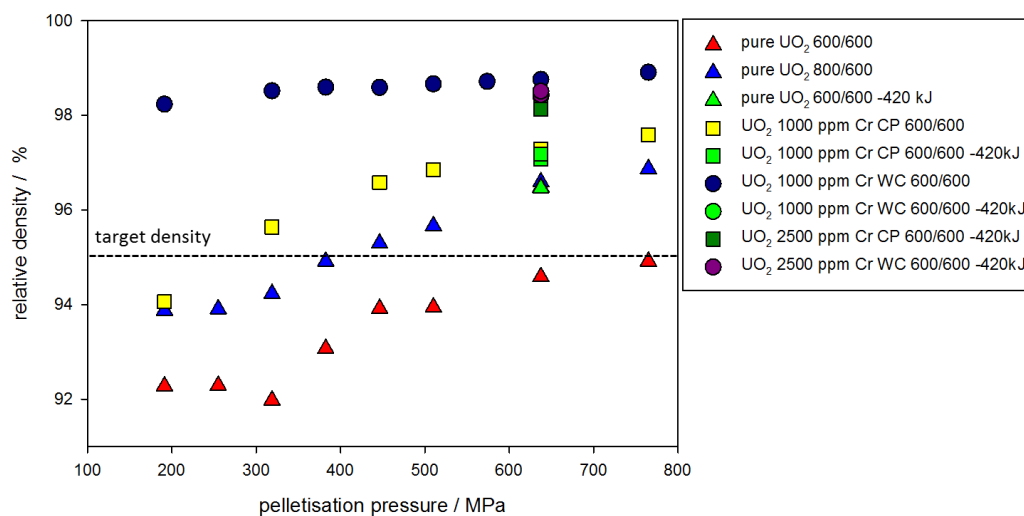


Figure 2: Density of sintered pellets in dependence on pelletisation pressure. The numbers behind the sample composition refer to the temperatures during the oxidative (first number) and reducing (second number) steps of thermal treatment, given in °C. 1000 and 2500 ppm represents the amount of Cr-doping. CP = co-precipitation method for Cr-doping, WC = wet coating method for Cr-doping. The sinter temperature of all pellets was 1700°C. Sinter atmosphere was Ar / 4% H₂ with an oxygen potential ($\Delta G^\circ = -RT \ln p\text{O}_2$) of $-510 \text{ kJ}\cdot\text{mol}^{-1} \text{ O}_2$ except samples marked with -420 kJ where an Ar / 4% H₂ + Ar / 1% O₂ atmosphere with an oxygen potential of $-420 \text{ kJ}\cdot\text{mol}^{-1} \text{ O}_2$ was used.

Cr-doping changes the microstructure of UO_2 pellets. The co-precipitation (i.e. addition of Cr in the first fabrication stage, cf. Figure 1) has a minor influence on grain size and speculatively most of the Cr is dissolved within the UO_2 grains. The wet-coating (i.e. Cr addition after stage 3, cf. Figure 1)

increases the materials' density and grain size (cf. Figure 3). In addition, large grains of a Cr-phase of up to 15 μm in diameter are visible in pores or on grain boundaries.

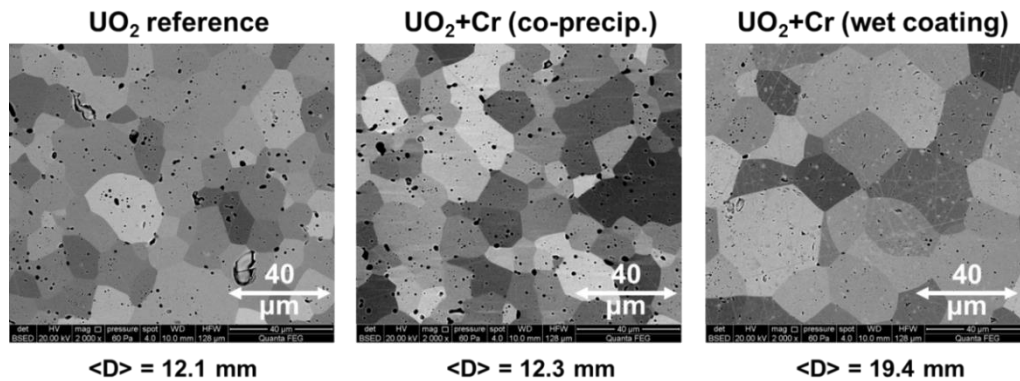


Figure 3: Microstructure of pure UO_2 and Cr-doped pellets depending on the doping method.

3 Accelerated dissolution experiments

First accelerated dissolution experiments with UO_2 model materials with and without Cr doping prepared in the form of sintered pellets were carried out in previously degassed bicarbonate solutions (NaHCO_3 , $10 \text{ mmol}\cdot\text{L}^{-1}$), using hydrogen peroxide (H_2O_2 , $2.25 \text{ mmol}\cdot\text{L}^{-1}$) to mimic the oxidative radiolytic dissolution of UO_2 . To achieve anoxic conditions the solutions were flushed with argon during the complete experimental run time. The experimental setup, developed at FZJ for these dissolution experiments and shown in Figure 4, was aimed in particular to:

- maintaining completely covered pellets with test solution throughout the whole dissolution experiments,
- allowing easy sampling of test solution and permanent flushing of the vessels with argon,
- providing light tight vessels to ensure constant conditions regarding H_2O_2 degradation during the experiments, and
- controlling the experiment temperature.

The setup allowed for the accomplishment of 11 dissolution experiments in parallel. The sample vessels were placed in a massive aluminium block equipped with a water conduit connected to a thermostat for temperature control. Plasticine gaskets were used to close the contact between the vessels and aluminium block and to ensure the light tightness of the vessels. In all experimental runs performed to date, 8 vessels were used for dissolution tests (Figure 4a, blue gaskets) with UO_2 based pellets, while 3 vessels were used as blanks to monitor the bulk degradation of H_2O_2 (Figure 4a, red gaskets).

Each single dissolution experiment was performed in an extensively washed and preleached (using 10 mM bicarbonate solution) 40 mL glass vessel with a layer of glass beads on the bottom (Figure 4b). Each sample vessel was closed using a septum punctured by a glass cannula serving as gas inlet and a cannula used as gas outlet and for sampling of the solution. These cannulae were only in contact with the solution during the sampling procedure. To achieve anoxic conditions the vessels were flushed constantly with argon during the experimental run time.



Figure 4: (a) Experimental setup of the dissolution experiments. (b) Schematic drawing of the experimental vessels for the accelerated dissolution experiments.

Figure 5 shows the typical evolution of the solution concentrations of U(VI) and H₂O₂ in the accelerated dissolution experiments with time. The evolution of the H₂O₂ concentration vs. time of blank experiments without pellets (Figure 5 a) demonstrates that the majority of the H₂O₂ is consumed by degradation on the surfaces inside of the vessel, and only a very minor part (< 1%) is used up by the oxidation of UO₂. For pure UO₂ pellets (Figure 5b) as well as Cr-doped UO₂ pellets (Figure 5c), the dissolution process is controlled by the concentration of H₂O₂ in solution, i.e. the dissolution (essentially) stops when all H₂O₂ is consumed. The U(VI) concentration in the solutions reached plateau levels that are clearly below the saturation limits of U(VI) phases, such as schoepite or studdite.

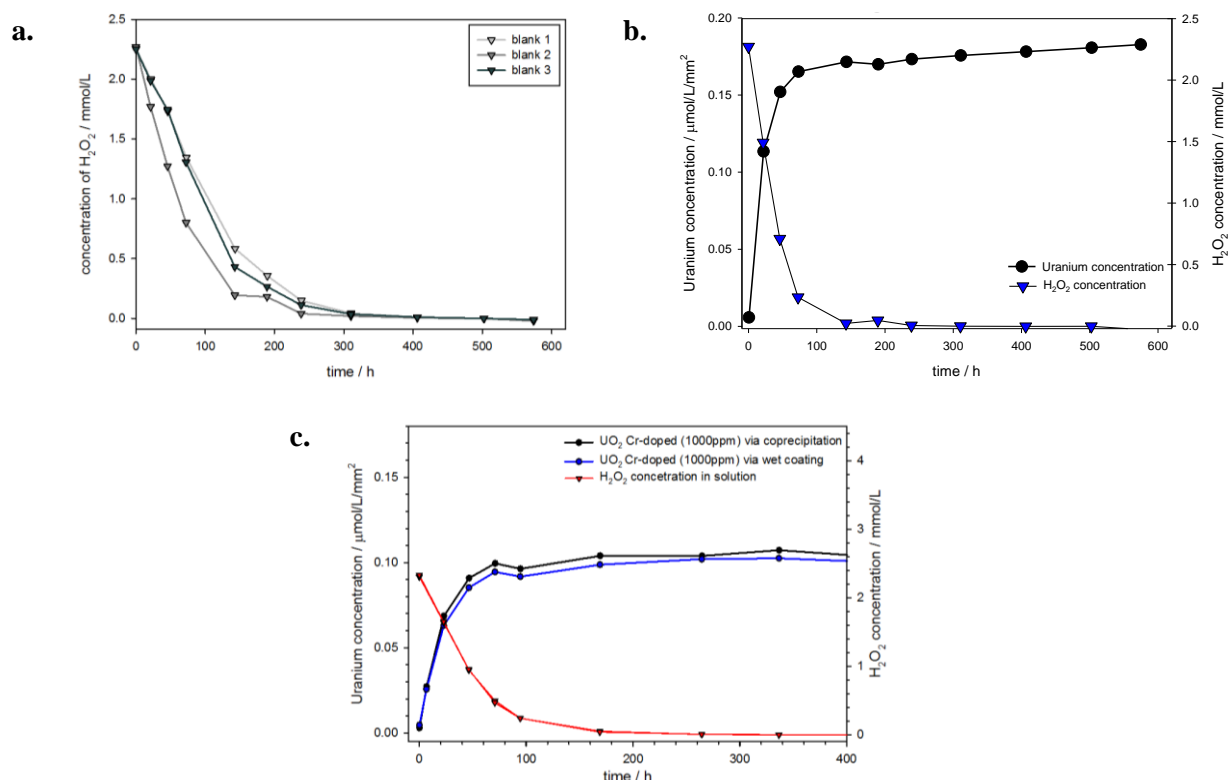


Figure 5: (a) Concentration of H₂O₂ in exemplary blank runs without UO₂ pellets. (b) Solution concentrations of U(VI) - normalised to the geometrical surface area of the pellet - and H₂O₂ vs. time for an experiment using a pure UO₂ pellet. (c) Solution concentrations of U(VI) - normalised to the geometrical surface area of the pellets - and H₂O₂ in two experiments using Cr-doped pellets prepared via co-precipitation, and wet coating, respectively vs. time.

The (initial) dissolution rates of the pellets were determined from the concentrations of dissolved U(VI) obtained within the first 24 hours of the experiments. Figure 6 depicts the data of a pure UO_2 reference pellet (95% relative density), a pellet Cr-doped by co-precipitation (97.5% relative density, 1000 ppm Cr) and a pellet doped by wet coating (98.8% relative density, 1000 ppm Cr). The initial dissolution rates were found to be $1.40 \cdot 10^{-6} \text{ mol} \cdot \text{m}^{-2} \cdot \text{s}^{-1}$ for the pure UO_2 reference pellet, $0.78 \cdot 10^{-6} \text{ mol} \cdot \text{m}^{-2} \cdot \text{s}^{-1}$ for the pellet doped via co-precipitation and $0.70 \cdot 10^{-6} \text{ mol} \cdot \text{m}^{-2} \cdot \text{s}$ for the Cr-doped pellet from the wet coating method, respectively. Taking into account the lower relative density of the pure UO_2 pellet and hence its higher reactive surface area, the initial dissolution rates for the shown pellets are rather similar, indicating that the Cr-doping has no significant effect on the oxidative dissolution rates of these UO_2 -based materials.

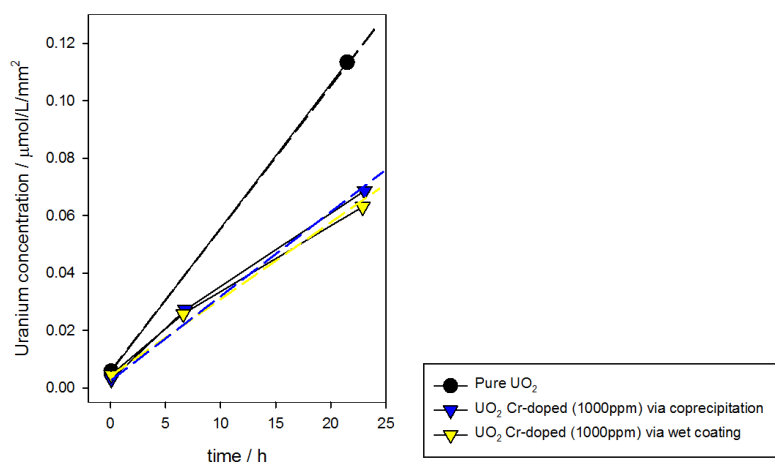


Figure 6: U(VI) concentrations in solution (normalised to the geometrical surface area of the pellets) during the first 24 hours of selected dissolution experiments, using a pure UO_2 reference (95% relative density, black circles) and two representative Cr-doped UO_2 samples produced by co-precipitation (97.5% relative density, blue triangles) and by wet coating (98.8% relative density, yellow triangles).

Repeated experiments with the same pure UO_2 pellets (after cleaning with bicarbonate solution) and following the procedure described above showed an unexpected decrease in the initial dissolution rates and lower plateau levels of the U(VI) concentration in solution from run to run, in spite of the same initial H_2O_2 concentration in solution (see Figure 7).

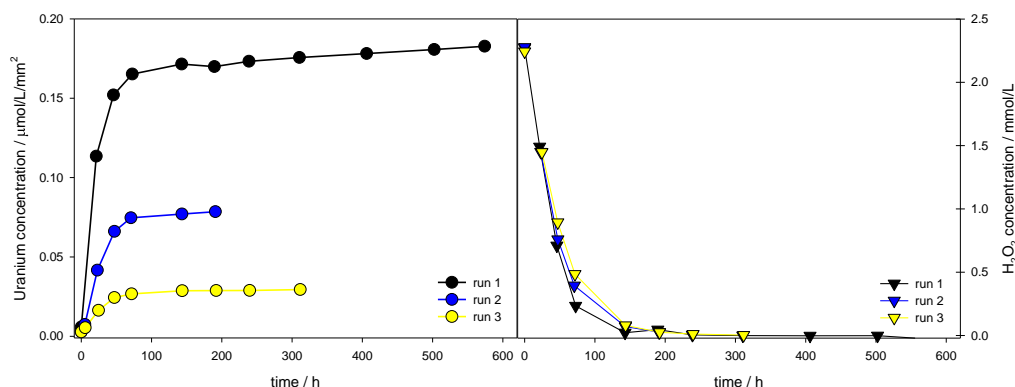


Figure 7: Concentration of uranium (left) and H_2O_2 in solution (right) in repeated experiments using a representative reference sample (i.e. pure UO_2) as function of time. Between each run the pellet and the complete experimental setup was extensively washed with NaHCO_3 solution.

A similar “passivation effect” of the pellet surface was also observed during dissolution experiments with Cr-doped pellets, when replenishing the leaching solution and adding additional H_2O_2 , after consumption of the initial oxidant (cf. Figure 8). Surprisingly, here the additional H_2O_2 had nearly no effect with respect to the further oxidative dissolution of the pellets, as indicated by the rather small increase in the U(VI) concentration in solution after the H_2O_2 addition. Again, it can be seen that the method of Cr-doping had no distinct effect on the dissolution behaviour of the doped UO_2 -materials.

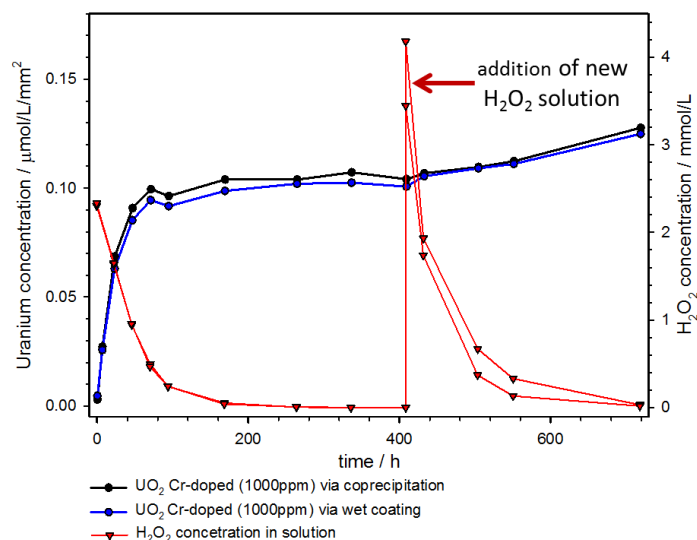


Figure 8: Concentrations of uranium and H_2O_2 in solution depending on run time for two representative Cr-doped UO_2 samples obtained by different doping methods.

To date SEM, XRD and Raman measurements on pellets after the dissolution experiments have been performed to unravel the reason for the surface “passivation” and the underlying mechanisms. First results suggest that the formation of a secondary phase or the remains of a hyperstoichiometric uraniumoxide on the surface of the pellets, which cannot be completely removed by the washing with bicarbonate solution, might be the cause of the observed dissolution behaviour.

4 Outlook

After the successful transfer of the developed synthesis route to SCK·CEN, the routines will be implemented in the glove box line to produce the ^{238}Pu doped pellets (with/without Cr-doping), which will be used in future dissolution experiments in autoclaves under reducing conditions. Additionally, careful chemical and structural analyses on real non-irradiated Cr-doped fuel (AREVA) will be carried out and compared to the materials synthesized at Juelich and at SCK·CEN. Further accelerated dissolution experiments will be performed at FZJ to understand the mechanisms of surface passivation of the pellets and to analyse the effects of different levels of Cr-doping, and grain sizes. This will, finally, give a more precise view on the mechanisms of dissolution of SNF in a deep geological repository.

Acknowledgement

The research leading to these results has received funding from the European Commission Horizon 2020 Research and Training Programme of the European Atomic Energy Community (EURATOM) (H2020-NFRP-2016-2017-1) under grant agreement n° 755443 (DisCo project).

References

- [1] Commissariat à l'énergie atomique (CEA) (2009) Nuclear fuels. A Nuclear Energy Division Monograph. Gif-sur-Yvette, 147 pp.
- [2] Arborelius, J., Backman, K., Hallstadius, L., Limbäck, M., Nilsson, J., Rebensdorff, B., Zhou, G., Kitano, K., Löfström, R., Rönnberg, G. (2006). Advanced doped UO₂ pellets in LWR applications. Journal of Nuclear Science & Technology, 43, 967-976.
- [3] Massih, A.R. (2014). Effects of additives on uranium dioxide fuel behavior. SSM report 2014:21, 62 pp.

Dissolution experiments with Cr-(Pu) doped UO₂ at FZJ and SCK·CEN: Preparatory tests with depleted and low alpha-doped UO₂ at SCK·CEN

Cachoir, C., Mennecart, T., Lemmens, K.

SCK·CEN, Belgium (BE)

Abstract

In order to understand the matrix dissolution of modern LWR fuels, Pu-Cr doped materials will be prepared, in addition to Cr doped materials, and will be exposed to two reference waters (young cementitious water at pH 13.5 and bicarbonate water at pH 8.5) in reducing/anoxic conditions, relevant for geological disposal. Here, we present results on the development and optimization of the method to impose effective reducing/anoxic conditions. These preparatory tests were performed with depleted and ²³³U-doped UO₂.

1 Introduction

The development of robust safety cases for geological disposal of spent fuel requires a solid understanding of its dissolution over very long-time scale (up to a million years). While the dissolution of standard spent fuel has reached a good level of comprehension, the development of modern LWR fuels (Cr/Al doped UO₂ or MOX fuels) raises the question whether these fuels will behave similarly to standard fuels in geological repository conditions. The EU-DisCo project aims at understanding the matrix dissolution of these modern LWR fuels, under deep geological repository relevant conditions. Experiments on irradiated fuels (WP3) are thus complemented with systematic dissolution studies (WP4) carried out with carefully prepared and characterized, simplified UO₂-based model materials, prepared in WP2. A special focus is given on the long-term (> 1000 years) matrix dissolution by using alpha doped UO₂. Therefore Pu-Cr doped materials, representative for 10,000 years old spent fuel, are prepared, next to Cr doped materials. These materials will be exposed to two reference ground waters (a highly alkaline cement water with pH 13.5 and carbonated NaCl solution with pH 8.5) to study the impact of the Cr doping on the dissolution behaviour. These tests will be done in reducing/anoxic media, as expected in geological disposal conditions. The first step in these experiments is the development of a test procedure to impose effective reducing/anoxic conditions without undesirable side-effects. This paper describes the current results of this method development study.

2 Experimental

Static dissolution experiments were performed with depleted UO₂ and low ²³³U-doped UO₂ pellets (1.45 MBq·g_{UO2}⁻¹), denominated as F7 pellets, either in Young Cementitious Water Light at pH 13.5 (YCWCa-L) or in bicarbonate solution at pH 8.5 (= the solution used also in the project First Nuclides, hence denominated as FIN solution), as defined in Table 1. All tests are performed in an Ar glove box with pO₂ below 10 ppm and P_{CO2} below the detection limits.

Three types of experiments were performed to impose reducing/anoxic conditions: in a first test series, the effect of dithionite and H₂ (without Pt/Pd catalyst) was tested. In a second type of experiment, the effect of a Pt/Pd catalyst on the effectiveness of H₂ was tested. In a third test series, the effect of the annealing and of an extra pre-leaching of the UO₂ pellet in KOH with iron strips was tested, to determine the best protocol to reduce or remove any oxidised surface material possibly present at the surface of the (depleted or F7) UO₂ pellet. The different series are detailed hereunder, and an overview is proposed in Table 2.

The first series of tests was carried out in autoclaves under Ar or H₂ atmosphere with and without addition of 10 ppm dithionite (Na₂S₂O₄) as reducing agent. One depleted UO₂ pellet (94% of theoretical density) was first annealed at 1000°C for 6 h under Ar/ 5% H₂ and heated again at 200°C for 2 h the day after before starting the leaching experiment to remove possible traces of overnight re-oxidation. The pellet was afterwards pre-leached in a 0.1 M KOH solution (pH 13) for 14 days with a total refreshing of the solution every 2 - 3 days. In the tests with dithionite, the dithionite was added to the solution 14 days before addition of the depleted UO₂ in order to let the system equilibrate.

In the second series of experiment, one experiment was performed with depleted UO₂ at pH 13.5 under H₂ in presence of Pt/Pd catalyst in order to scavenge the oxygen traces. The catalyst consists in a Pt-net electrochemically coated with Pd, this set-up has to be transferred to experiments with Cr-(Pu) doped UO₂ in the future. The catalyst is thus placed in the headspace of the autoclaves (gaseous phase) in order to avoid contact with water and consequently to avoid perturbation of the formation of oxygen through radiolysis. This experiment was combined with a pretreatment protocol, based on Ollila's procedure [1] in order to remove any surface material that may contain higher oxidation states of U. This pretreatment consists of three different stages lasting in total 3 weeks. First, the pellet is washed in 0.01 M NaCl during one week with a daily refreshing of the solution. Thereafter, the pellet is placed for one week in 0.01 M NaCl with an iron coupon (1.5 x 3 cm²) freshly cleaned with SiC paper. This step is repeated once after renewal of the NaCl solution and addition of a freshly cleaned iron coupon. Afterwards, the pellet is annealed for 8 hours at 1000°C in Ar / 5% H₂ and heated again at 200°C for 2 h before starting the leaching experiment. The pellet is first pre-leached in 0.001 M KOH (pH 11) for one week with a daily refreshing of the solution; no iron coupon is added. At the same time as the pre-leaching, the autoclave is pre-conditioned meaning that the leaching solution and the Pd catalyst are placed in the autoclaves under 5 bar H₂ for 1 week in order to remove all O₂ traces possibly present in the leaching solution.

In the third series of experiments, performed in poly-ethylene bottles, three routes (3rd series A, B and C in Table 2) were envisaged before leaching at pH 13.5 or pH 8.5. Each of these routes comprises the same pre-treatment as for the second series. The first route (3rd series A in Table 2) included no further treatment before the leach test was started. No annealing was considered. The second route (3rd series B in Table 2) comprised an annealing of the pellet before the pre-treatment. The annealing was performed for 8 hours at 1000°C in N₂/ 5% H₂ (the Ar / 5% H₂ mixture could not be used anymore because of safety reasons). The annealed pellets were heated again at 200°C for 2 h immediately before the pre-treatment, which was completed with a pre-leaching in 0.001 M KOH (pH 11) with or without iron coupon (1.5 x 3 cm²) and with a daily refreshing of the solution. Finally, the third route (3rd series C in Table 2) included an annealing of the pellet (the same protocol as for the 3rd series B), but this time after the pre-treatment, and the annealing was completed with a pre-leaching as for the 3rd series B, but always with iron coupons.

For all series of experiments, the unfiltered U concentrations were always measured while the ultrafiltered U concentrations (< 3.5 nm) were only determined in the (last) leaching step at pH 8.5 or pH 13.5. The latter concentrations correspond to the dissolved uranium. In addition, when iron was used in the different stage of the preparation, all coupons were rinsed with 1 M HNO₃ in order to estimate the amount of uranium sorbed on the iron surface. The U concentrations were measured by ICP-MS.

Table 1: Composition of the two reference leaching solutions.

| | mol·L ⁻¹ | Na | K | Ca | SO ₄ ²⁻ | CO ₃ ²⁻ | Cl ⁻ | pH |
|----------------|---------------------|----------------------|----------------------|----------------------|-------------------------------|-------------------------------|----------------------|------|
| YCWCa-L | | 1.3·10 ⁻¹ | 3.6·10 ⁻¹ | 3.8·10 ⁻⁴ | 2·10 ⁻³ | 3.7·10 ⁻⁴ | | 13.5 |
| FIN | | 1.9·10 ⁻² | | | | 1·10 ⁻³ | 1.9·10 ⁻² | 8.5 |

Table 2: Overview of the three series of experiments.

| series | Pellet | Annealing | Pre-treatment | Annealing | Pre-leaching | Leaching |
|--------------------------------|----------------------------------|-----------|--|-----------|--|---|
| 1st series | depl.UO ₂ | no | no | yes | 0.1 M KOH 2 weeks | with/without Na ₂ S ₂ O ₄ pH 13.5 and pH 8.5 in autoclaves under Ar or H ₂ atm. |
| 2nd series | depl.UO ₂ | no | 0.01 M NaCl 1 week + 0.01 M NaCl + Fe twice 1 week | yes | 0.001 M KOH 1 week | pH 13.5 in autoclaves with H ₂ atm. + Pt/Pd catalyst |
| 3rd series A | depl.UO ₂ or F7 | no | 0.01 M NaCl 1 week + 0.01 M NaCl + Fe twice 1 week | no | no | pH 13.5 and pH 8.5 in PE bottles |
| 3rd series B | depl.UO ₂ or F7 | yes | 0.01 M NaCl 1 week + 0.01 M NaCl + Fe twice 1 week | no | 0.001 M KOH with/without Fe 1 week | pH 13.5 and pH 8.5 in PE bottles |
| 3rd series C | depl.UO ₂ or F7 | no | 0.01 M NaCl 1 week + 0.01 M NaCl + Fe twice 1 week | yes | 0.001 M KOH + Fe 1 week | pH 13.5 and pH 8.5 in PE bottles |

Depl.UO₂= depleted UO₂; F7: ²³³U-doped UO₂ pellet with an alpha activity of 1.47 MBq·gUO₂⁻¹; PE= poly-ethylene; Fe = iron coupon

3 Results

Figure 1A and Figure 1B illustrate the ultrafiltered uranium concentration as function of time for the first type of experiments, with and without reducing agent ($\text{Na}_2\text{S}_2\text{O}_4 =$ dithionite) in bicarbonate water (pH 8.5) and in YCWCa-L water (pH 13.5), respectively. Most of the experiments lasted 180 days, except the experiments in bicarbonate water at pH 8.5 with H_2 atmosphere without reducing agent (series 'H₂ FIN'), stopped after 30 days.

At pH 8.5, the measured ultrafiltered U concentration stays mostly in the highest side of UO_2 solubility range of $3 \cdot 10^{-8}$ M [2], except at 180 days in Ar atmosphere with reducing agent (series 'Ar FIN + dithionite') in which the uranium concentration was higher and reached $2.7 \cdot 10^{-7}$ M. Up to 90 days, no clear complementary effect of H_2 is observed (Figure 1A) as the uranium concentrations in the tests with reducing agent dithionite and H_2 atmosphere are similar to those in the tests with only dithionite. The H_2 effect seems nevertheless more pronounced at longer term ('H₂ FIN + dithionite'). At 180 days, the [U] remains close to 10^{-9} M in presence of H_2 and dithionite, while it increases from 10^{-9} M to $2.7 \cdot 10^{-7}$ M in Ar with dithionite (Figure 1A).

At pH 13.5, higher U concentrations are observed compared to those at pH 8.5. A favorable effect of dithionite is observed with Ar (series 'Ar YCWCa-L + dithionite'). Although the measured U concentrations are within the UO_2 solubility range up to 90 days, the dithionite could not prevent a gradual increase of the U concentration from 10^{-9} to about 10^{-8} M with time. Tests at pH 13.5 with H_2 show very high uranium concentrations over the whole test duration, only slightly reduced by the dithionite. These results confirm the poor performance of $\text{H}_2(\text{g})$ to keep U in the tetravalent state in absence of a catalyst at alkaline pH, even if the dithionite slightly decreases the oxidative dissolution of UO_2 . At high pH, the dithionite would decompose, but the reaction products would still have a redox buffering effect [3]. Most of these measured U concentrations are either approaching the upper limit of the UO_2 solubility range or higher than the UO_2 solubility range, except in Ar with dithionite where the U concentration is $6 \cdot 10^{-9}$ M.

Based on the previous results, it appears that dithionite, even combined with H_2 atmosphere is not effective enough to keep the uranium concentration close to 10^{-9} M, especially at high pH. In order to have a better O_2 scavenging inside the autoclaves, a Pt/Pd catalyst in presence of H_2 atmosphere [4] was thus considered at pH 13.5. This other type of oxygen scavenger was coupled to a more thorough cleaning of the surface of the UO_2 pellet. This is the second type of experiment, as described in the section 'Experimental' (2nd series in Table 2).

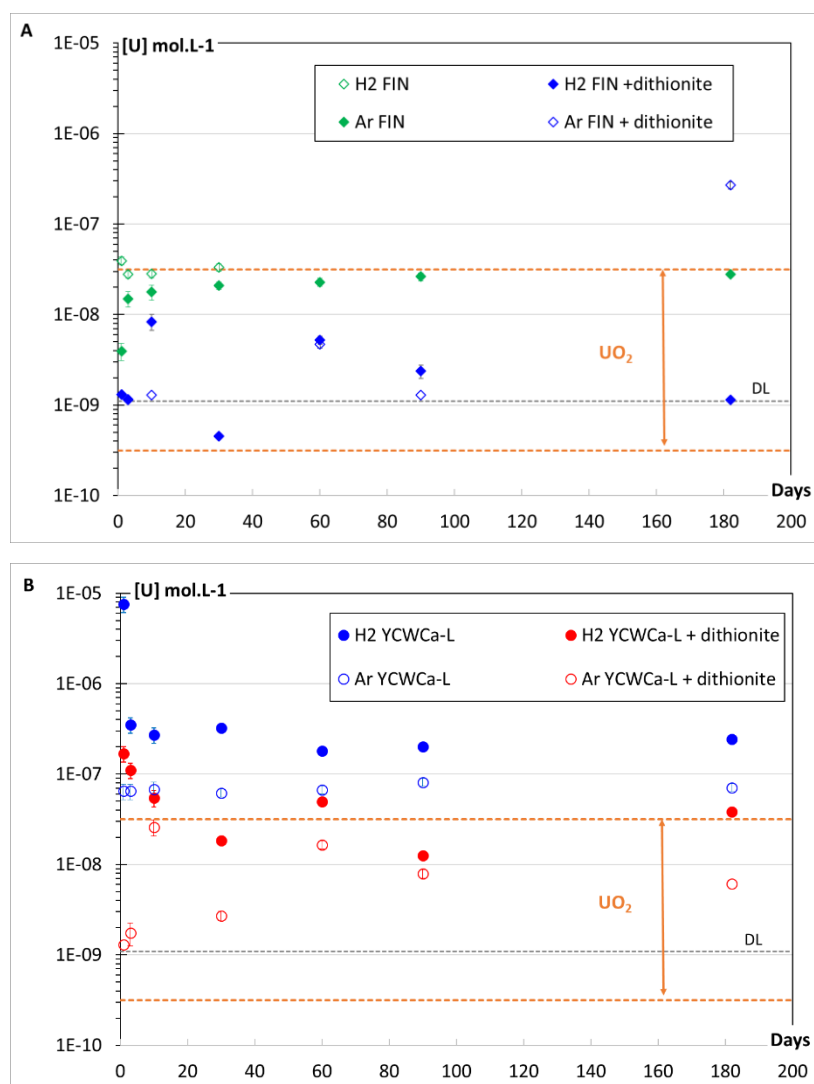


Figure 1: Results for the first test series. Ultrafiltered U concentration as function of time with depleted UO_2 pellet in autoclave experiments with and without 10 ppm dithionite ($\text{Na}_2\text{S}_2\text{O}_4$) under Ar and H_2 atmosphere at pH 8.5 in bicarbonate solution-FIN (A) and at pH 13.5 in young cementitious water (YCWCa-L) (B). The orange dashed lines represent the range of UO_2 solubility as stated in [2]. The grey dashed line is the detection limit (DL) of the ICP-MS in the experimental conditions.

Figure 2 shows the uranium concentration as function of time for the second type of experiment with depleted UO_2 pellet during the pre-treatment in 0.01 M NaCl, the pre-leaching phase in 0.001 M KOH and the leaching period in presence Pd/Pt catalyst at pH 13.5 in young cementitious water (YCWCa-L). During the pre-treatment step, the [U] in solution quickly decreased from $2.3 \cdot 10^{-9}$ M to below $5.1 \cdot 10^{-10}$ M, detection limit of the ICP-MS in our experimental conditions. After the annealing and during the pre-leaching in 0.001 M KOH at pH 11, the [U] increased to reach $9 \cdot 10^{-9}$ M, presumably as a result of the easier oxidation of uranium at higher pH. As soon as the leaching test starts at pH 13.5, we observed a second increase of U concentration reaching up to $8 \cdot 10^{-8}$ M after 10 days. After 30 days, the total U concentration reaches $1.4 \cdot 10^{-7}$ M (filled symbols in Figure 2) whereas the soluble U concentration is $3 \cdot 10^{-8}$ M (empty symbols in Figure 2), suggesting the formation of colloids. Although the Pt/Pd catalyst and the H_2 atmosphere are supposed to consume all O_2 traces in the system, the U concentrations of $3 - 8 \cdot 10^{-8}$ M at pH 13.5 are slightly higher than the UO_2

solubility range. These results are quite comparable to those obtained at pH 13.5 in experiments in H_2 atmosphere and reducing agent (Figure 1B). Before concluding that the Pt/Pd catalyst is not able to prevent UO_2 oxidation at pH 13.5, the experiment will be repeated at pH 13.5 and also tested at pH 8.5. A complementary set of experiments in autoclaves is currently ongoing.

The current experiment, nevertheless, tends to confirm that uranium is more easily oxidised at high pH (pre-leaching at pH 11 and leaching at pH 13.5) than at neutral pH (pre-treatment in 0.01 M NaCl), as already highlighted in Figure 1. Although the annealing between the pre-treatment and the pre-leaching steps should have avoided a (re)-oxidation of the pellet, the U concentration increases by a factor more than 10 during the pre-leaching stage. Besides a pH effect, two other hypotheses can be considered to explain the U behaviour: the combination of the annealing after the pre-treatment may have disturbed the structure of the material (see further the third series of tests), increasing the U release in the pre-leaching solution, or the presence of iron in the pre-leaching stage may be required to block the uranium oxidation.

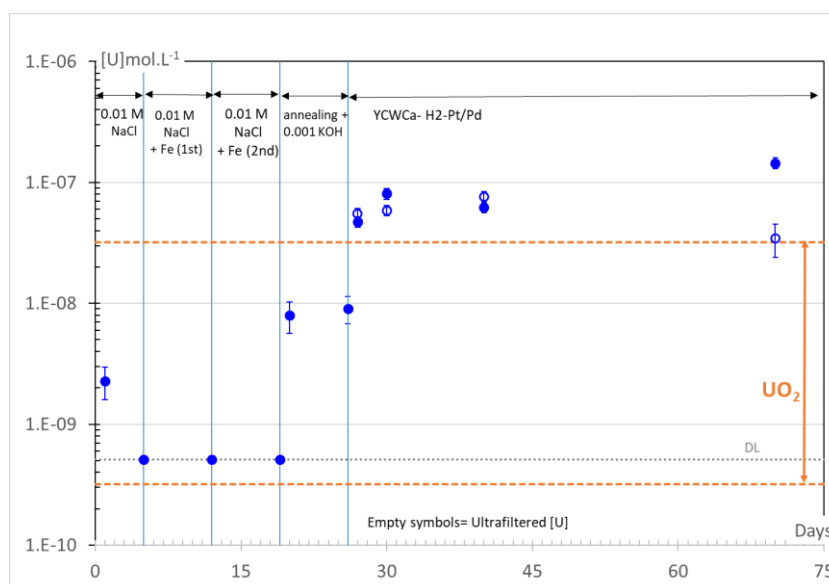


Figure 2: Results for the second test series. U concentration as function of time with depleted UO_2 pellet for the autoclave experiment with Pt/Pd catalyst under H_2 atmosphere at pH 13.5 in young cementitious water (YCWCa-L); filled symbols and empty symbols represent the unfiltered and the ultrafiltered U concentration, respectively. The orange dashed lines represent the range of UO_2 solubility as stated in [2]. The grey dashed line is the detection limit (DL) of the ICP-MS in the experimental conditions.

In order to assess these different hypotheses, a parametric study was performed in parallel by considering three different routes to pre-treat the pellet before the leaching experiments. This is the third type of experiment, as described in ‘Experimental’ section. The results of the three different routes are presented in Figure 3A, Figure 3B and Figure 3C, respectively, corresponding to the 3rd series A, B and C in Table 2.

Except when the annealing is performed between the pre-treatment and the pre-leaching stage (Figure 3C), most of the measured U concentrations are in the range of the UO_2 solubility (Figure 3), suggesting a perturbing effect of the annealing after the pre-treatment. Also, the annealing before the treatment did not improve the stability of the UO_2 , as shown by the increase of U concentration during the pre-treatment phase in Figure 3B, compared to the decrease of concentration observed in

Figure 3A and 3C when annealing is not done or done after the pre-treatment. Currently, we have no explanation for the observed adverse effect of the annealing, but it may be an effect of the annealing gas, which consisted of N₂ / 5% H₂, whereas in the past Ar / 5% H₂ was used. This will be investigated further.

The role of iron in our experiments is not yet fully understood. Does it reduce the amount of U(VI) in solution by sorption onto the iron strip, or does it prevent the U oxidation in the pre-treatment? At pH 11 in the pre-leaching step (in 0.001 M KOH), its role seems small as only a small decrease of U is observed (Figure 3B). Therefore, the presence of iron does not seem beneficial in our experiments.

The ultrafiltered concentrations are all very low ($1 \cdot 10^{-9}$ M or lower) in the leaching phase whatever the considered preparation (Figure 3, encircled data), and similar to the lowest concentrations in the autoclave experiments (with annealing and dithionite, Figure 1). So, this suggests that a simple pre-treatment with Fe is as good as annealing + dithionite and better than the test with Pt/Pd catalyst in H₂ atmosphere. However, as the leaching period of this series of tests is quite short (7 days), these experiments will be continued up to leaching durations comparable to those of the other series in order to confirm the results for longer duration.

The ultrafiltered U represents only a small part of the total U, most of which is colloidal (Figure 3). The amount of colloids is more important when annealing is performed between the pre-treatment and the pre-leaching stages (Figure 3C), confirming a disturbing effect of the annealing. However, the fact that the ultrafiltered concentrations are so low, is considered as an indication that there was little oxidation to U(VI) during the leaching.

Without annealing (Figure 3A) the total U concentrations are higher in bicarbonate water at pH 8.5 than in young cementitious water at pH 13.5 for depleted UO₂, but for the ultrafiltered U concentrations the opposite is observed. This is also observed for F7 doped pellet. The ultrafiltered concentrations are all close to 10^{-9} M, so the pH does not have a strong concentration increasing effect after a pre-treatment with Fe. The alpha activity of the F7 doped pellet causes slightly higher uranium concentrations in young cementitious water at pH 13.5, but less in bicarbonate solution at pH 8.5. This alpha effect is not observed for the two other routes of preparation (Figure 3B and Figure 3C), possibly masked by the disturbing effect of the annealing.

The fact that the slightly alpha-doped fuel F7 shows slightly higher concentrations than undoped UO₂, suggests that the alpha activity still caused some oxidation, although very little. The F7 has a very low alpha activity ($1.45 \text{ MBq} \cdot \text{g}^{-1}$), this is more than 10 times lower than spent fuel after 10,000 years, so it is likely that the tests with the 10,000 year Pu-Cr doped pellets planned for the DisCo project will show a well quantifiable increasing effect of the alpha activity, that can be compared with the results for Pu doped pellets without Cr. The main objective of the study is, indeed, to see if Cr doping leads to a different oxidation/dissolution behaviour (faster or slower).

The low concentrations also show that – although it was foreseen in the DisCo project – addition of reducing agents is not necessary to see the potential impact of the Cr doping. Addition of dithionite may even suppress the radiolytical oxidation, and thus mask the potential Cr effect on radiolytical oxidation. Addition of H₂ seems – with all information we have so far – not useful (Figure 1). New experiments in autoclaves (annealing before the pre-treatment and leaching in autoclaves with H₂ pressure in presence of Pt/Pd catalyst) will hopefully show ultrafiltered concentrations that are also around 10^{-9} M, and ideally no colloids.

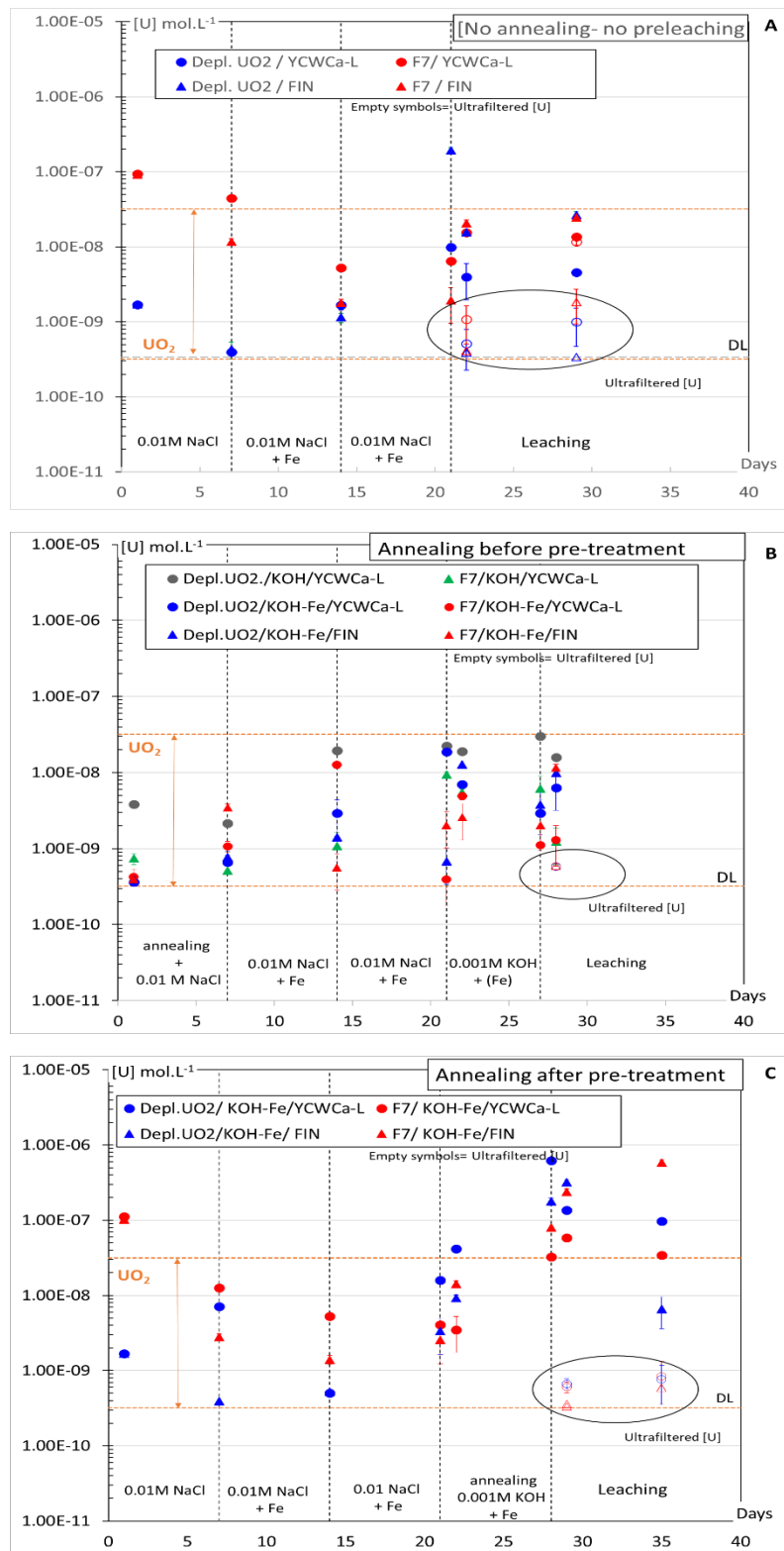


Figure 3: Results for the third test series. U concentration as function of time with depleted UO₂ and F7 pellet as function of annealing, pre-treatment in 0.01 M NaCl + (Fe) and pre-leaching in 0.001 M KOH + (Fe) of the pellet at pH 13.5 in young cementitious water (YCWCa-L) and at pH 8.5 in bicarbonate water (FIN). (A) experiments without annealing, no pre-leaching; (B) annealing before pre-treatment and pre-leaching; (C) annealing after pre-treatment and before pre-leaching. Filled symbols and empty symbols represent the unfiltered and the ultrafiltered U concentration, respectively. The orange dashed lines represent the range of UO₂ solubility as stated in [2]. DL corresponds to the detection limit of the ICP-MS in the experimental conditions.

4 Preliminary conclusions

Static leaching tests with depleted UO_2 and low alpha-doped UO_2 pellet were performed to optimize the method of the leaching experiments of Pu-(Cr) doped UO_2 in the frame of the DisCo project. This preliminary study shows that, although foreseen in the programme definition, the addition of reducing agent is not necessary to obtain uranium concentrations that are low enough to see a potential impact of Cr doping or of alpha doping. Bottle experiments demonstrated that a simple pre-treatment with Fe should be sufficient. New experiments in autoclaves (in H_2 atmosphere with Pt/Pd catalyst) are currently on-going to confirm these preliminary results.

Acknowledgements

The research leading to these results has received funding from the European Commission Horizon 2020 Research and Training Programme of the European Atomic Energy Community (EURATOM) (H2020-NFRP-2016-2017-1) under grant agreement n° 755443 (DisCo project).

This work is performed in close cooperation with, and with the partial financial support of ONDRAF/NIRAS, the Belgian Agency for Radioactive Waste and Fissile Materials, as part of the programme on geological disposal that is carried out by ONDRAF/NIRAS.

References

- [1] Ollila, K. (2008). Solubility of UO_2 in the high pH range in 0.01 to 0.1 M NaCl solution under reducing conditions. POSIVA Report, 2008-75.
- [2] Neck, V. and Kim, J.I. (2001). Solubility and hydrolysis of trivalent actinides. *Radiochimica Acta*, 89, 1-16.
- [3] Riba, O., Montoya, V., Grivé, M., Duro, L. (2012). Uranium solubility under alkaline conditions using different reducing agents. 4th Annual Workshop Proceedings of the RECOSY EU project. KIT Scientific Report, 7626.
- [4] Forsyth, R., Werme, L., Bruno, J. (1986). The corrosion of spent fuel in synthetic groundwater. *Journal of Nuclear Materials*, 138, 1-15.

Influence of iron on the oxidative dissolution of a homogeneous $U_{1-x}Pu_xO_2$ MOX fuel

Jégou, C.¹, Kerleguer, V.^{1,2}, De Windt, L.², Broudic, V.¹, Martin, C.³

¹ CEA/DEN/DE2D/SEVT/LMPA, Marcoule, Bagnols-sur-Cèze (FR)

² ARMINES/MINES ParisTech, Centre de Géosciences, Fontainebleau (FR)

³ Andra, Chatenay-Malabry (FR)

1 Context

Contrary to UOX fuel, little is known on the behavior of the heterogeneous Mimas MOX fuel in the presence of environmental materials including corrosion products from the containers. The microstructure observed on this type of MOX fuel has revealed the presence of two or three zones with different plutonium contents and microstructures arising from the fabrication process (dilution of a UO_2 and PuO_2 oxide blend in UO_2 powder) and from the origin of the UO_2 powder. Although the corrosion mechanisms are likely to be close to those of UOX fuel [1], it is still necessary to study the specific features of MOX fuels to better understand their behavior, in the eventuality of direct geological disposal.

The first studies on heterogeneous fuel pellet showed preferential dissolution of the UO_2 matrix compared to the Pu-enriched agglomerates [2]. In order to fully evaluate the behavioral analogy between UOX and MOX fuels and to provide data it is still necessary to perform targeted leaching experiments on various homogeneous materials with different Pu contents. Ultimately, these data should be available for each type of phase constituting the heterogeneous material and provide information for geochemical modeling (linked to the WP5 and the Chess-Hytec modeling task). The ongoing work, which is the subject of this progress report, is to address the leaching behavior of a homogeneous $(U,Pu)O_2$ compounds with high plutonium content (about 24 wt.%) in the presence of iron, a redox active species brought by the corrosion of the containers and being able to counteract the water radiolysis effects. Many data are available on UO_2 but relatively few on homogeneous compounds approaching the Pu enriched aggregates of a Mimas MOX fuel.

This summary focuses on the first three stages defined for the first two years of the Disco project: the initial characterization of the MOX fuel pellets, the precorrosion of an iron foil in a synthetic Callovo-Oxfordian (CO_x) water and the beginning of the leaching experiment of the MOX pellets at 25°C.

2 WP2-contribution

2.1 Initial characterizations of the $(U_{0.73}Pu_{0.27})O_2$ pellets before leaching (From Mid-2017 to January 2018)

Homogeneous $(U_{0.73}Pu_{0.27})O_2$ solid solution pellets (1 cm thickness and 5.4 mm diameter) were fabricated in 1985 at CEA Cadarache (COCA Process) and stored over 30 years at room temperature

under air in a hot-cell. The initial stoichiometry was O/M: 1.983 and the density was $10.421 \text{ g}\cdot\text{cm}^{-3}$. Table 1 shows the initial isotopic composition of the sample. The damage level of the sample due to the accumulation of alpha decays during the 30 years of storage was calculated as 0.58 dpa by considering each alpha decay event produces 1750 atomic displacements in UO_2 due to the recoil nucleus ($\sim 100 \text{ keV}$) and the alpha particle (5–6 MeV) [3]. After 30 years of storage period, one of the pellets was cut into $\sim 2 \text{ mm}$ thickness disks, which were then annealed at 1373 K for 6 h (heating and cooling rate $5 \text{ }^\circ\text{C}\cdot\text{min}^{-1}$) under Ar/H_2 4% atmosphere to repair the radiation damage and to adjust the stoichiometry of the sample. The pellets were characterized by EPMA, XRD and Raman spectroscopy to check the homogeneity of the plutonium distribution and to collect structural information.

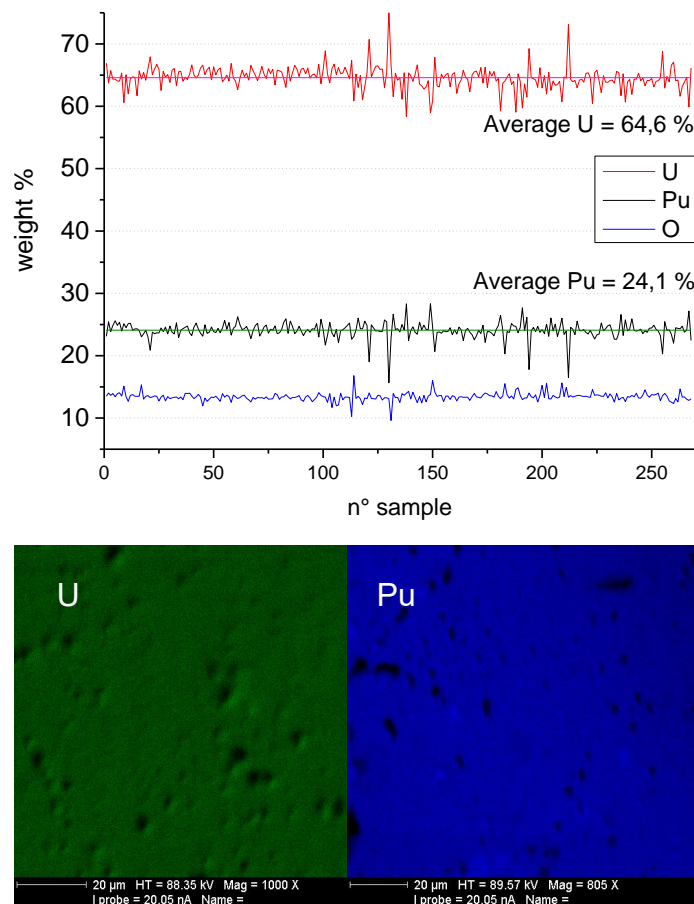


Figure 1: EPMA analysis of the sample (260 analysis points by steps of $35 \mu\text{m}$). Weight percentages in the oxide are consistent with stoichiometry $((\text{U}_{0.73}\text{Pu}_{0.27})\text{O}_2)$.

Table 1: Initial isotopic composition of the sample (November 1985) in weight.

| Isotopic Pu composition (%) | | | | | Isotopic U composition (%) | |
|-----------------------------|-----------------------------|-----------------------------|-----------------------------|-----------------------------|----------------------------|---------------------------|
| $^{238}\text{Pu}/\text{Pu}$ | $^{239}\text{Pu}/\text{Pu}$ | $^{240}\text{Pu}/\text{Pu}$ | $^{241}\text{Pu}/\text{Pu}$ | $^{242}\text{Pu}/\text{Pu}$ | $^{235}\text{U}/\text{U}$ | $^{238}\text{U}/\text{U}$ |
| 0.22 | 70.09 | 24.51 | 4.095 | 1.085 | 0.73 | 99.27 |

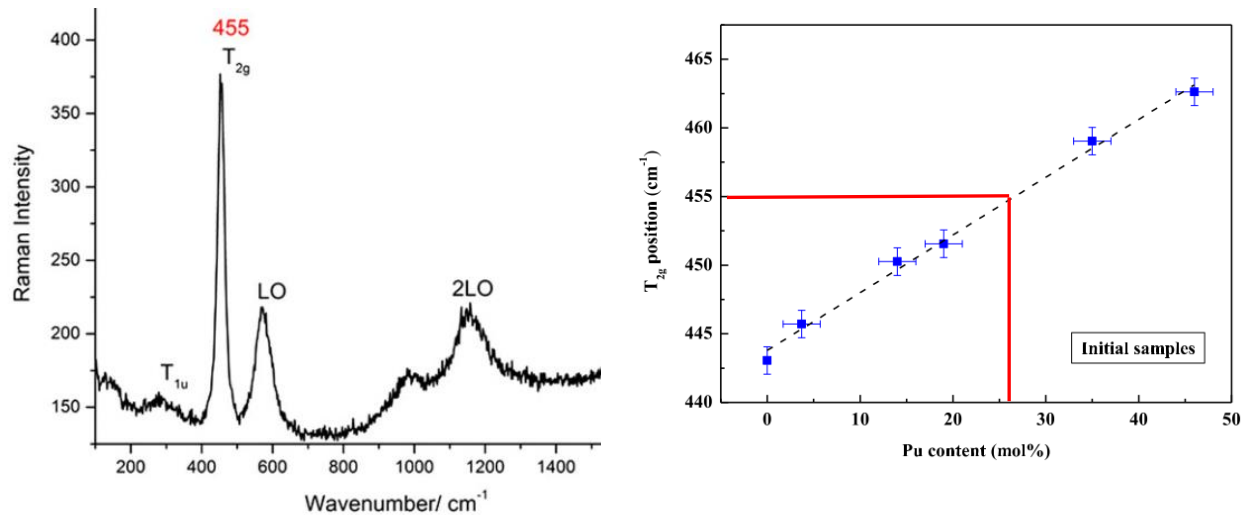


Figure 2: Raman analysis of the $((U_{0.73}Pu_{0.27})O_2)$ sample (left). The T_{2g} band position is fully consistent with the Pu content of the sample [4].

In parallel, the α and $\beta\gamma$ activities of the MOX fuel were recalculated at the date of the leaching experiment and the alpha, beta and gamma dose rate profiles determined from the surface of a pellet to the homogeneous solution. The α dose rate is 5 to 6 orders of magnitude higher than the β/γ dose rates and is therefore predominant [5].

3 WP 4 contribution

3.1 Precorrosion step of the iron foil (From November 2017 to January 2018)

Iron foils were placed in the autoclave to simulate container corrosion products and to move towards realistic reducing conditions in the absence of the fuel pellet. Such reducing conditions are expected in deep geological disposal [6]. Rolled 99.99% pure iron foils were purchased from Goodfellow. Their size was 2.5 cm by 2.5 cm for a thickness of 125 μm and a weight of around 0.64 g. One iron foil was used for the leaching experiment. Before being set up in the reactor, the foil was rinsed in ethanol and ultrasound-cleaned for 2 minutes.

The iron foil was first pre-corroded in 180 mL of synthetic COx water [6] for around 80-90 days in the absence of the MOX pellets. This first step was intended to ensure the presence of corrosion products on the iron foil surface, to obtain a solution chemistry containing Fe^{2+} ions not initially present in the synthetic COx water, and to have reducing conditions when the MOX pellets were introduced at a later date. The iron foil was slightly curved to enable maximum contact with water, and placed on the platform immediately under the pellet support (Figure 3). Once the leaching reactor had been closed, it was purged with a mixture Ar/CO₂ 3000 ppm for 2 h 30 min to stabilize the pH and carbonate content (pH = 7.2 and $[\text{HCO}_3^-] = 2.43 \cdot 10^{-3} \text{ mol} \cdot \text{L}^{-1}$) and then put under a pressure of 3.5 bars. The leaching solution was regularly sampled over time without adding any new fresh solution.

3.2 Long term leaching experiment with the homogeneous MOX fuel pellets (From Feb 2018 to June 2019)

After the iron pre-corrosion phase, the reactor was opened to add two MOX pellets with an alpha activity of $2.2 \cdot 10^9 \text{ Bq} \cdot \text{g}^{-1}$ (Figure 3), which were placed on a support above the iron foil. The reactor was then closed again, purged with a mixture of Ar/CO₂ 3000 ppm for 30 min, and returned to a pressure of 3.5 bars with the same gas mixture. Samples of the leaching solution were regularly collected over time. The first results indicate (Figure 4) a significant effect of iron on the oxidative dissolution of this homogeneous MOX fuel, the hydrogen having a minor effect taking into account the levels produced by the anoxic corrosion of iron. Uranium concentrations are less than $1 \mu\text{g} \cdot \text{L}^{-1}$ after seven months of leaching (Figure 4) in the presence of the iron foil and compatible with the formation of amorphous $\text{UO}_2 \cdot \text{H}_2\text{O}$.

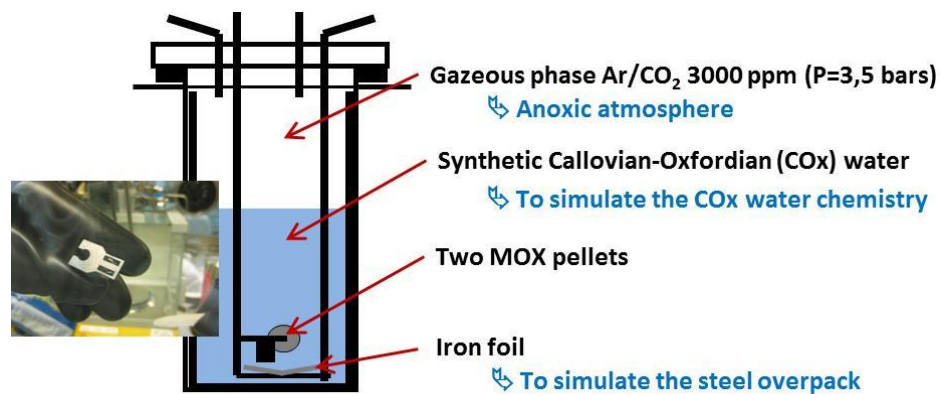


Figure 3: View of the experimental device. The entire leaching device is composed of titanium coated with a passivating oxide layer.

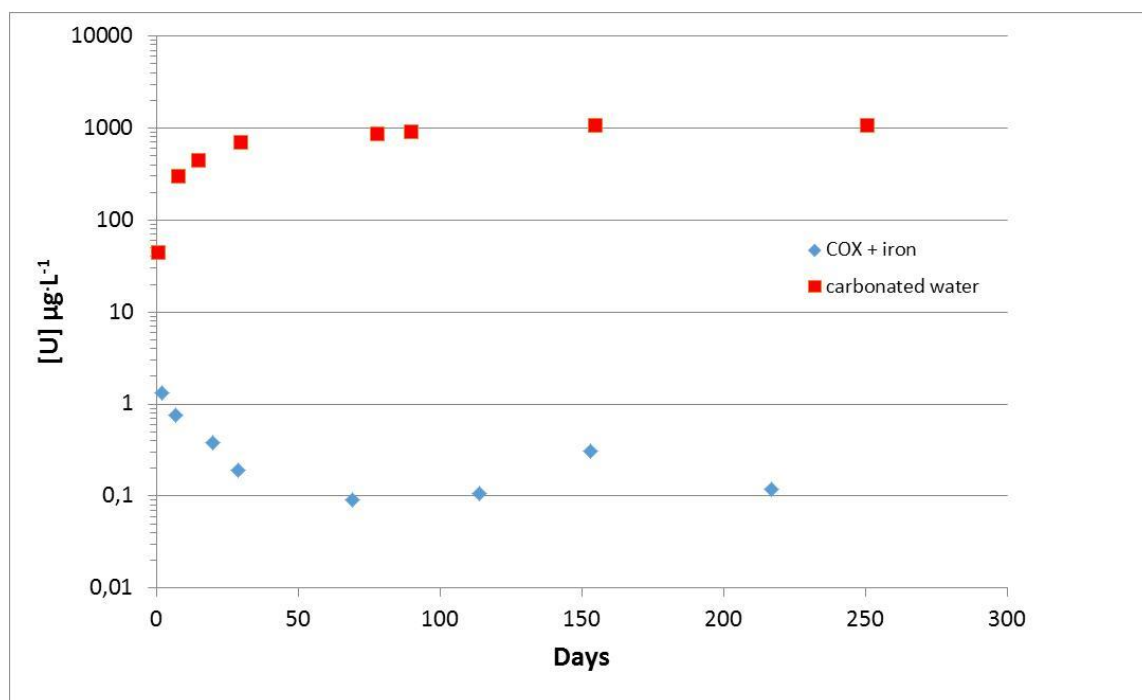


Figure 4: Evolution of the uranium concentrations as a function of time for the homogeneous MOX fuel. A reference experiment in a carbonated water and in the absence of an iron foil was added to quantify the oxidative dissolution under alpha radiolysis alone.

To conclude, the presence of iron inhibits the oxidizing dissolution of the homogeneous MOX fuel and leads to low uranium concentrations. These results are similar to those obtained on Pu-doped UO₂ or on heterogeneous Mimas MOX fuels [6]. The experiment will continue for about a year and all the surfaces (MOX, iron foil) will be characterized at the end of the experiment.

References

- [1] Ewing, R.C. (2015). Long-term storage of spent nuclear fuel. *Nature Materials*, 14, 252-257.
- [2] Odorowski, M., Jegou, C., De Windt, L., Broudic, V., Peugeot, S., Magnin, M., Tribet, M., Martin, C. (2016). Oxidative dissolution of unirradiated Mimas MOX fuel (U/Pu oxides) in carbonated water under oxidic and anoxic conditions. *Journal of Nuclear Materials*, 468, 17-25.
- [3] Staicu, D., Wiss, T., Rondinella, V.V., Hiermaut, J.P., Konings, R.J.M., Ronchi, C. (2010). Impact of auto-irradiation on the thermophysical properties of oxide nuclear reactor fuel. *Journal of Nuclear Materials*, 397, 8-18.
- [4] Elorrieta, J.M., Manar, D., Bonales, L.J., Vigier, J.F., Dieste, O., Naji, M., Belin, R.C., Baonza, V.G., Konings, R.J.M., Cobos, J. (2017). Raman study of the oxidation in (U,Pu)O₂ as a function of Pu content. *Journal of Nuclear Materials*, 495, 484-491.
- [5] Kerleguer, V., Jégou, C., De Windt, C., Broudic, V., Jouan, G., Miro, S., Tocino, F., Martin, C. (2019). The mechanisms of alteration of a homogeneous U_{0.73}Pu_{0.27}O₂ MOX fuel under alpha radiolysis of water. *Submitted to Journal of Nuclear Materials*.
- [6] Odorowski, M., Jegou, C., De Windt, L., Broudic, V., Jouan, G., Peugeot, S., Martin, C. (2017). Effect of metallic iron on the oxidative dissolution of UO₂ doped with a radioactive alpha emitter. *Geochimica et Cosmochimica Acta*, 219, 1-21.

Dissolution of alpha-doped UO₂ with and without Cr in the presence of corroding Fe, in synthetic and natural groundwater

Myllykylä, E.

VTT Technical Research Centre of Finland Ltd,
Espoo (FI)

The objective of this study is to investigate the effect of Cr-doping on the dissolution of α -doped UO₂ in conditions relevant to final disposal. The idea is to compare the results of these dissolution experiments to the ones conducted with real spent nuclear fuel in the DisCo project and also the ones conducted previously with similar simulant materials but in different reaction media and without Cr-doping. The aim is to understand the matrix dissolution of novel Cr-doped spent fuel in groundwater conditions.

The experiments are conducted in a glove box under anaerobic conditions under Ar atmosphere. The first experiments are conducted with ²³³U alpha doped UO₂ fragments, already used in previous EU project, REDUPP [2]. These materials are referred as “old” material herein and they are UO₂ materials with 5% or 10% ²³³U alpha doping, simulating the alpha dose of 10,000 years old and 3000 years old spent nuclear fuel, respectively. The new pellet materials (UO₂, Cr-doped UO₂, ²³⁸Pu-doped UO₂ and Cr/²³⁸Pu- doped UO₂) will be prepared and characterized by SCK·CEN in collaboration with Jülich. The doping level of ²³⁸Pu-doped UO₂ pellets, to be fabricated, will correspond to the alpha dose of ~ 10,000 years old nuclear fuel. These new materials are fabricated during 2019 and delivered to Finland at the latest in the beginning of 2020 for dissolution experiments.

The old samples have been stored under anaerobic glove box conditions for 4 years. However, the previous dissolution experiments had been carried under saline groundwater and thus, the samples required preparation before experiments by pre-leaching twice with bicarbonate solution before start of the actual experiments in natural groundwater. This removed salts possibly precipitated during the storage period.

In the previous EU project, REDUPP [1, 2], 3 different groundwaters selected from the Olkiluoto site, which is the planned site for disposal of spent nuclear fuel in Finland, were used (see Table 1). In the DisCo project the experiments with ²³³U-doped UO₂ are conducted only in brackish OL-KR6.

Table 1: Compositions for natural groundwaters used in REDUPP dissolution experiments [1]. Units are given in $\text{mmol}\cdot\text{L}^{-1}$ if not otherwise indicated.

| | Brackish water OL-KR6 | Saline water OL-KR5 | Fresh water ONK-PVA1 |
|---|--------------------------|------------------------|-------------------------|
| pH | 7.7 | 8.1 | 7.9 |
| Ammonium, NH_4 | 0.018 | < 0.001 | 0.026 |
| Bicarbonate, HCO_3 | 2.29 | 0.26 | 5.29 |
| Bromide, Br | 0.15 | 0.69 | 0.01 |
| Calcium, Ca | 12.73 | 43.66 | 1.32 |
| Chloride, Cl | 97.03 | 224.24 | 5.92 |
| Dissolved Inorganic Carbon | 2.00 | < 0.25 | 5.08 |
| Fluoride, F | - | 0.063 | 0.021 |
| Iron, Fe (total) | 0.0063 | 0.0036 | 0.0007 |
| Iron, Fe^{2+} | - | - | 0.0007 |
| Magnesium, Mg | 6.17 | 2.80 | 0.74 |
| Nitrate, NO_3 | <0.00032 | 0.00048 | < 0.0065 |
| Nitrite, NO_2 | <0.00022 | < 0.00022 | < 0.0043 |
| Nitrogen, N (total) | 0.03 | 0.086 | 0.041 |
| Non Purgeable Organic Carbon | 0.47 | 1.58 | 0.66 |
| Phosphate, PO_4 | - | - | 0.0032 |
| Potassium, K | 0.49 | 0.46 | 0.18 |
| Silicate, SiO_2 | 0.183 | 0.10 | 0.23 |
| Sodium, Na | 67.86 | 130.06 | 9.57 |
| Strontium, Sr | 0.068 | 0.19 | 0.0068 |
| Sulphate, SO_4 | 4.36 | 0.031 | 1.38 |
| Sulphide, S^{2-} | - | 0.062 | 0.004 |
| Sulphur, S (total) | 4.37 | 0.053 | 1.40 |
| Total dissolved solids (mg L^{-1}) | 6268 | 12880 | 981 |
| Carbonate alkalinity, HCl uptake | <0.05 | < 0.05 | < 0.05 |
| Total acidity, NaOH uptake | 0.15 | < 0.05 | 0.08 |
| Total alkalinity, HCl uptake | 2.3 | 0.27 | 5.3 |

There is a sampling and measurement station for KR6 groundwater (from depth 135 m to 137 m), where continuous measurements enable the sampling procedure (see Figure 1). The composition of natural water (OL-KR6) has shown slight temporal variation depending on the sampling year. The OL-KR6 groundwater was sampled and imported into the glove box in June 2018. The alkalinity and pH of the groundwater has been periodically measured under glove box conditions. Both pH and alkalinity showed slight increase during 300 days equilibration period in the glove box (see Figure 2).



Figure 1: Sampling station for OL-KR6 groundwater from dept of 135 m to 137 m. The station has continuous measuring devices for most critical parameters (e.g. pH, temperature, gases) and possibility for anoxic water sampling.

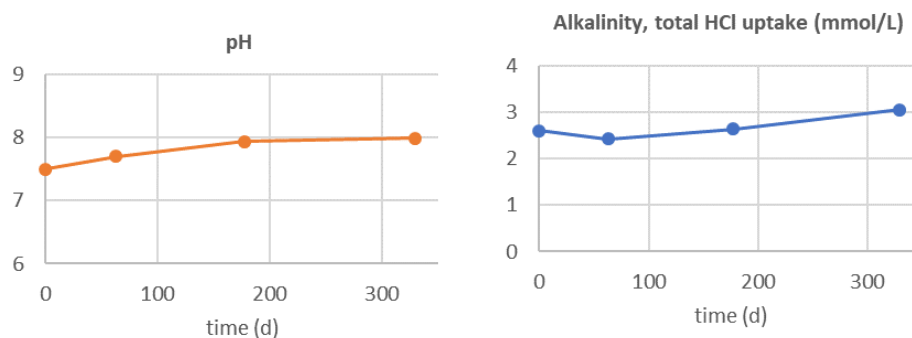


Figure 2: Evolution of pH and alkalinity of OL-KR6 ground water during 300 days period under glove box conditions.

1 L of the KR-6 groundwater was allowed to equilibrate with iron strips to sweep the natural uranium away from the groundwater before starting the actual dissolution experiments. The composition of OL-KR6 water was analysed in context of the sampling. The main components were analysed also after the U-sweep with iron strips, before the start of the dissolution tests to see the possible effects of sweep and balancing with atmosphere of Ar glove box. The experimental system for dissolution tests is described in Figure 3, showing the test vessel with an iron strip leaning to vessel wall, and UO_2 fragments placed into a saucer (zircaloy or glass saucer), which functions as a holder for the UO_2 fragments. Zircaloy is more relevant as it will also be present in final disposal system. In DisCo experiments zircaloy saucers are used in some experiments instead of glass ones to inspect if there is any influence from dissolved Si from glass saucer.

The initial composition of the ground waters is analysed and the concentration of essential elements; U, Cr, Fe and Zr followed by double focusing sector field ICP-MS during the dissolution experiment. Solution pH and Eh are also measured few times during the experiments. Duplicate experiments with and without UO_2 in the presence of Fe strip will be conducted to extract $\text{H}_2(\text{g})$, formed due to anoxic metal corrosion. These duplicate experiments will be performed in sealed vials from which the H_2 sampling is possible via a septum. In the end of the experiments, the metallic surfaces are going to be studied with microscopic methods (SEM, TEM) for identification of the formation of secondary minerals.

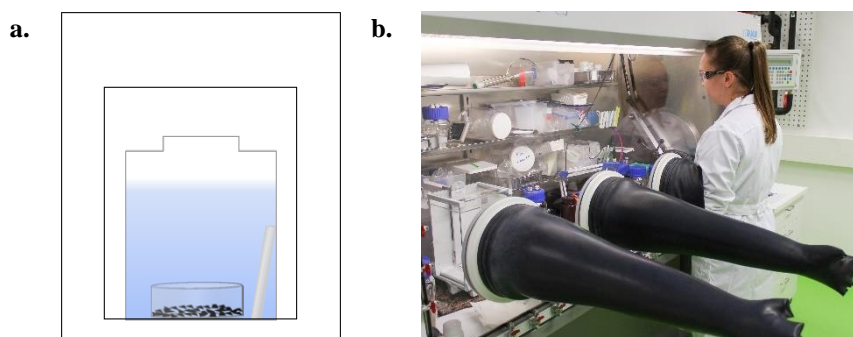


Figure 3: Schematic view of closed plastic vessel ($V = 60 \text{ mL}$) (a) in which the experiments will be conducted in the anaerobic glove box (b). UO_2 fragments are placed in the zircaloy or glass saucer and the iron strip is leaning on the vessel wall in experimental media.

The start of the experiments with ^{233}U -doped UO_2 was delayed due to the difficulties to precipitate the natural uranium from the OL-KR6 ground water on the surface of metallic iron. Sufficiently low uranium concentration was achieved in the end of June and the experiments with ^{233}U -doped fragments were launched in the beginning on July. Experiments have been sampled in 1h and 1, 4, 12 days but analyses are run only for the 1-hour and 1-day samples so far.

To enhance the analysis of low-level uranium concentrations, a sample introduction system APEX IR was installed prior to the experiments. The measured pulses increased 3 to 7 fold depending of the element in comparison to the analysis with traditional sample introduction system [3, 4]. Figure 4 shows the enhancements of counts on a detector with APEX IR sample introduction system in comparison with standard spray chamber with peltier cooling. The signal intensifying for uranium in leaching and groundwater samples was over 7 fold.

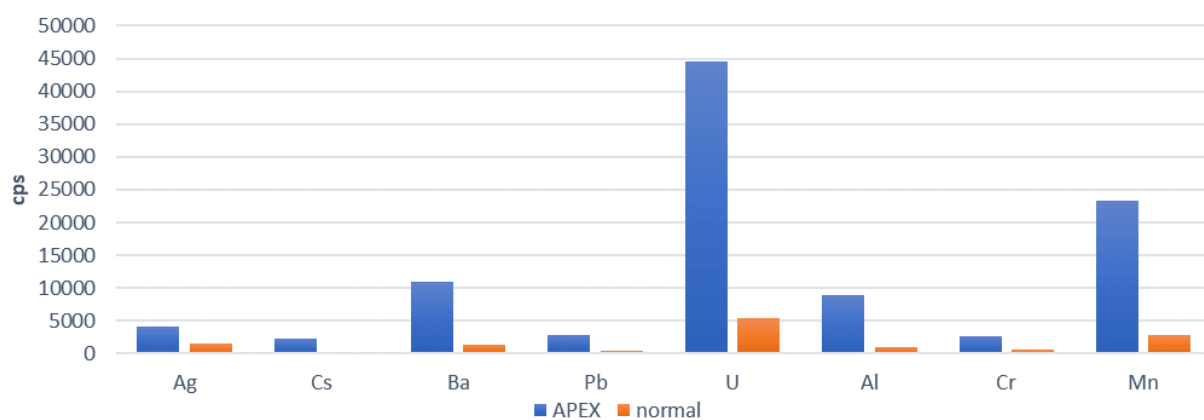


Figure 4: The enhancements of the measured pulses (cps = count per seconds) for selected elements with APEX IR sample introduction system in comparison to standard spray chamber with peltier cooling unit.

Experiments with the new UO_2 material fabricated in DisCo project will be conducted in a saline groundwater from the disposal depth (450 - 500 m). This water will be sampled from Olkiluoto during autumn 2019. Preparations to start the experiments as soon as possible after Cr doped materials arrive will be made during 2019. As a reference and to allow for comparability of results of other working groups within the DisCo project, the selected experimental series are also conducted in bicarbonate water (0.01 M NaCl + 2 mM NaHCO_3).

Acknowledgement

The research leading to these results has received funding from the European Commission Horizon 2020 Research and Training Programme of the European Atomic Energy Community (EURATOM) (H2020-NFRP-2016-2017-1) under grant agreement n° 755443 (DisCo project).

References

- [1] Evins, L.Z., Juhola, P., Vähänen, M. (2014). REDUPP Final Report (FP7, agreement no. 269903). POSIVA Working Report, 2014-12.
- [2] Ollila, K., Myllykylä, E., Tanhua-Tyrkkö, M., Lavonen, T. (2013). Dissolution rate of alpha-doped UO_2 in natural groundwater. *Journal of Nuclear Materials*, 442, 320-325.

- [3] Santos, J.S., Teixeira, L.S.G., dos Santos, W.N.L., Lemos, V.A., Godoy, J.M., Ferreira, S.L.C. (2010). Uranium determination using atomic spectrometric techniques: An overview. *Analytica Chimica Acta*, 674(2), 143-156.
- [4] Esaka, F., Magara, M., Lee, C.G., Sakurai, S., Usada, S., Shinohara, N. (2009). Comparison of ICP-MS and SIMS techniques for determining uranium isotope ratios in individual particles. *Talanta*, 78, 290-294.

Production and characterisation of $(U_{1-x}Th_x)O_2$ samples to model mixed-oxide fuel dissolution

Popel, A.J. and Farnan, I.

Department of Earth Sciences, University of
Cambridge, Cambridge (UK)

1 Introduction

The purpose of this preparation stage of the work was to obtain and characterise mixed oxide uranium-thorium samples. A simplified oxalic co-precipitation route was used based on a method reported by Altaş et al. [1] for making $(U_{1-x}Th_x)O_2$ samples. This $(U_{1-x}Th_x)O_2$ system was chosen to complement the CEA DisCo study involving the oxidative dissolution of $(U_{1-x}Pu_x)O_2$ in Callovo-Oxfordian clay water. This (U/Th) system serves as analogue model for the $(U_{1-x}Pu_x)O_2$ system to avoid sample handling limitations associated with Pu and to increase the techniques that can be applied to analyse the system and the number of experimental variables.

2 Preparation of samples

Before to work with radioactive materials (U and Th), a first practice oxalate precipitation was carried out using a non-radioactive surrogate – cerium (III) nitrate hexahydrate. One molar cerium nitrate solution was prepared by dissolving 2.5853 g of $Ce(NO_3)_3 \cdot 6H_2O$ salt in 5.8204 g of deionized water and cerium oxalate was precipitated by adding a 200% excess of 1 M oxalic acid solution prepared by dissolving 3.3755 g of $H_2C_2O_4 \cdot 2H_2O$ crystals in 26.793 g of deionized water. A white precipitate was collected on a filter paper. This non-radioactive surrogate synthesis was performed under open bench atmosphere to get trained with the oxalate precipitation step. The cerium oxalate precipitate obtained during this exercise was no further studied and was discarded.

Then, a stoichiometric 3:1 uranyl and thorium nitrate solution was prepared under air by dissolving 2.80 g of $UO_2(NO_3)_2 \cdot 6H_2O$ and 1.10 g of $Th(NO_3)_4 \cdot 6H_2O$ in 5.5909 g of deionised Milli-Q (18.2 M Ω ·cm) water to achieve a pellet target composition of $U_{0.75}Th_{0.25}O_2$. Since uranium was supplied in the form of a $UO_2(NO_3)_2 \cdot 6H_2O$ salt, where its oxidation state is +6, the key point in preparing $(U_{1-x}Th_x)O_2$ samples is to reduce $U^{6+}(aq)$ to $U^{4+}(aq)$ to ensure a congruent co-precipitation with $Th^{4+}(aq)$ on addition of oxalic acid, since $U^{4+}(aq)$ and $Th^{4+}(aq)$ have similar solubilities. For this reason, the prepared uranyl and thorium nitrate solution was transferred into an anoxic glove box and bubbled with a 5% H_2 /95% Ar gas mixture for 7.75 hours without and for 3.58 hours in the presence of a platinum catalyst [2]. The solution remained yellow in colour and no precipitation was observed. A 200% excess of 1 M oxalic acid solution was also prepared under ambient air by adding 4.025 g of $H_2C_2O_4$ to 44.693 g of deionised water and then the obtained solution was also deoxygenated inside the anoxic glove box by bubbling a 5% H_2 /95% Ar gas for 4.6 hours. A white precipitate formed and redissolved on shaking at the end of bubbling. Deionised water was also deoxygenated by bubbling a 5% H_2 /95% Ar gas for 4.73 hours to be later used for washing. The deoxygenated 1 M oxalic acid solution was added to the prepared U/Th nitrate solution to precipitate a mixed U/Th oxalate. The

solution remained yellow, indicating that some uranyl ions were still present in it. The finely divided solid obtained was filtered and thoroughly washed with the deoxygenated deionised water, then it was left over the weekend to dry on a filter paper in the glove box under anoxic conditions (Ar atmosphere, 0.1 ppm O₂), where the synthesis took place. Then, the yellowish precipitate was placed into a furnace attached to the Ar atmosphere glove box, where the synthesis took place, to be dried at 100°C (nominal – i.e. the temperature set on the furnace or 71°C on a thermocouple) for 3.25 hours. Then, the dried precipitate was decomposed by heating for 3 hours at 700°C nominal (526°C thermocouple). The decomposed solid was pressed (150 MPa) into three pellets of 5 mm diameter with a thickness of ~ 2 mm (rough estimates for the green pellets). These pellets were subsequently sintered at 1600°C for 1.33 hours and 0.67 hours at 1620 °C under Ar gas atmosphere. The flowsheet of the synthesis process is summarised in Figure 1. Three pellets have been produced and are shown in Figure 2 and their masses are presented in Table 1. Only the initial preparations of uranyl and thorium nitrate solution and oxalic acid solution were performed under air atmosphere, the subsequent entire synthesis of (U_{1-x}Th_x)O₂ samples was performed in a glove box under anoxic conditions (Ar atmosphere, 0.1 ppm O₂) to protect U⁴⁺ against oxidation, including deoxygenation of the solutions and deionised water, precipitate drying and decomposition, pelletisation and sintering processes. If it will become evident that the produced samples contain U⁶⁺, these samples can be annealed with a 5% H₂/ 95% Ar gas mixture to ensure complete reduction of U⁶⁺ to U⁴⁺.

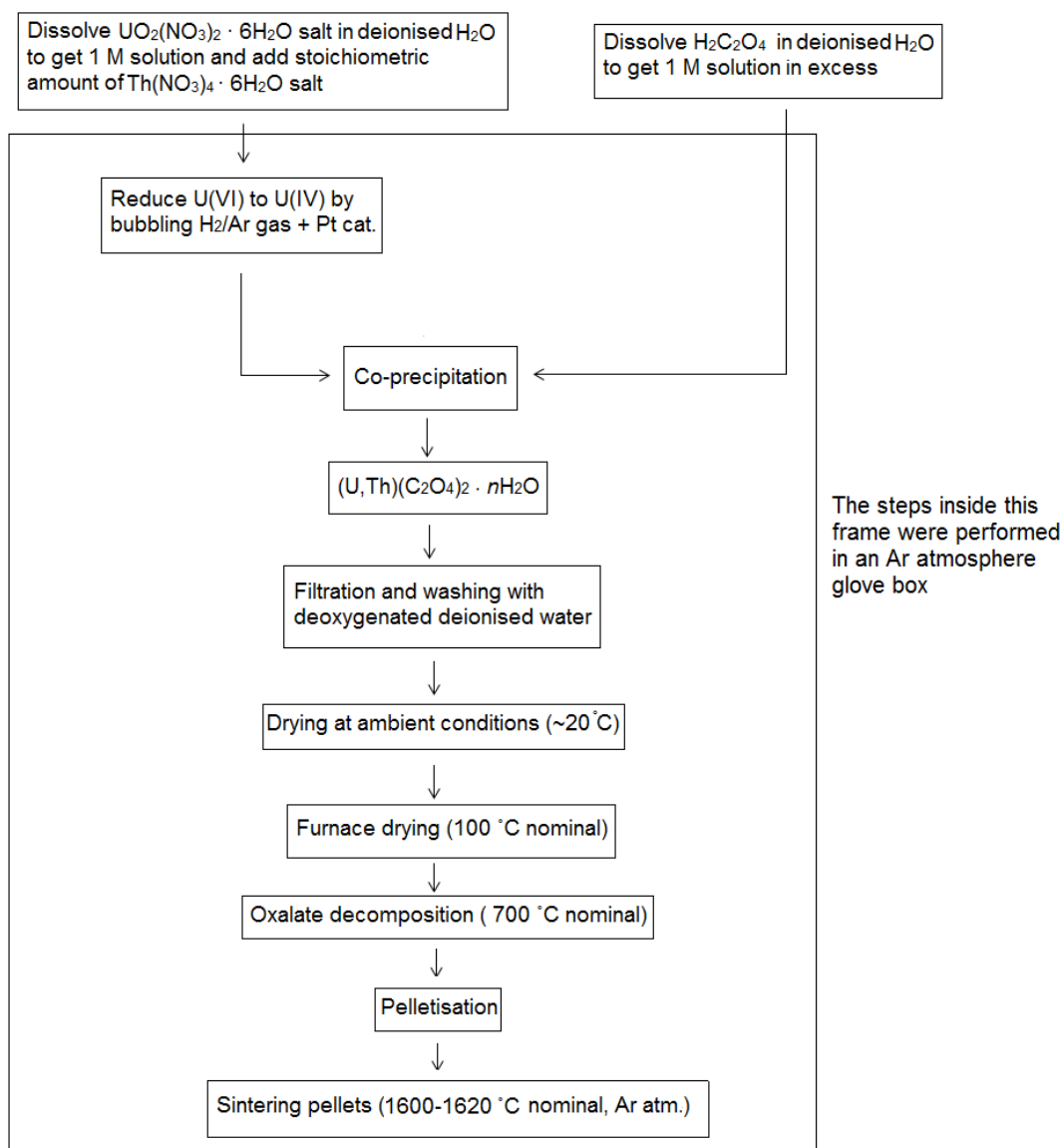


Figure 1: Flowsheet of the $(U_{1-x}Th_x)O_2$ synthesis process undertaken in an anoxic glove box (Ar, 0.1 ppm O_2). Nominal temperature refers to the temperature set on the furnace.



Figure 2: Photograph of three sintered pellets of U-Th mixed oxide handled in an anoxic glove box.

Table 1: Summary of the pellets produced.

| Pellet ID # | Pellet mass (g) |
|-------------|-----------------|
| B1-P1-S1 | 0.048 |
| B1-P1-S2 | 0.062 |
| B1-P1-S3 | 0.052 |

3 XRD study

One of the three produced pellets was characterized by XRD without crushing it (as-produced) to estimate its composition from Vegard's law:

$$a(\text{U}_{1-x}\text{Th}_x)\text{O}_2 = (1-x)a(\text{UO}_2) + xa(\text{ThO}_2), \quad \text{Eq. 1}$$

where a is the lattice parameter of the considered solid phase. The pellet can be used for further tests. It is generally accepted in the literature that the (U-Th)O₂ system follows Vegard's law rather well [3-5]. The lattice parameter of UO₂ was taken as 5.471 Å [6] and the lattice parameter of ThO₂ was taken as 5.598 Å [4]. It should be noted that there is quite a variation in the value of the lattice parameter for ThO₂ from 5.593 [7] Å to 5.598 Å [4], while the value of the lattice parameter for UO₂ is well accepted to be 5.471 Å [6]. This results in an error of ± 0.01 in estimating x in (U_{1-x}Th_x)O₂. The measured lattice parameter for the sintered pellet was 5.514 Å, yielding a pellet composition of U_{0.66}Th_{0.34}O₂ from Vegard's law. We are assuming that an incomplete reduction of U(VI) into U(IV) is the most plausible reason for the estimated value of uranium content to be lower than a target value of 75%.

XRD data were collected with a Bruker D8 Advance diffractometer in reflection geometry (Mo K α radiation, $\lambda_1 = 0.71073$ Å and $\lambda_2 = 0.71359$ Å, and a LynxEye XE-T position sensitive detector) over an angular range $15^\circ \leq 2\theta \leq 70^\circ$ ($\Delta 2\theta = 0.04^\circ$) for a total time of one hour. A full Rietveld refinement was carried out using the software Topas V6. The background was fitted with a 10 parameter Chebyshev function and the peak shape was modelled using a pseudo-Voigt function. Spherical harmonics were used to model preferred orientations. The structure of UO₂ (Fm-3m space group) was retrieved from the ICSD database (246851). No structural parameter other than the unit cell was allowed to vary in the refinement operation. A plot of the Rietveld refinement at convergence is shown in Figure 3. The background between 40° and 70° of 2θ arises from the glass sample holder. SEM and EDX analyses will be undertaken to examine the surface morphology of the sample and to confirm its chemical composition.

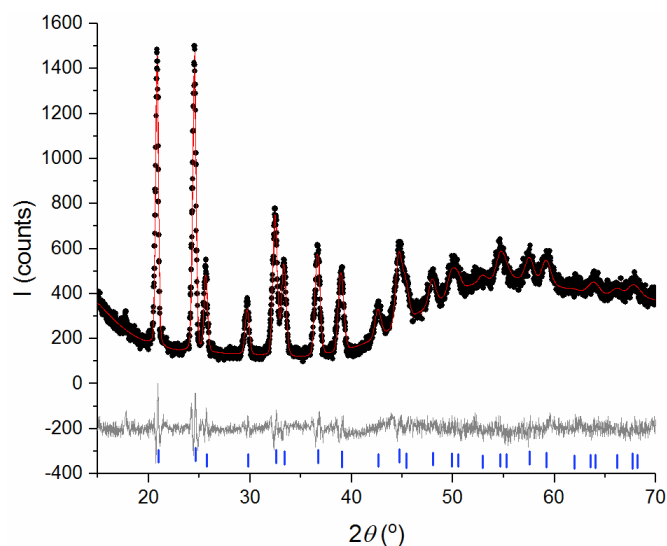


Figure 3: XRD spectrum (2θ with a Mo anode) of the as-produced $(U_{1-x}Th_x)O_2$ pellet. Rietveld refinement plot showing experimental (black dots), calculated (red line) and difference (grey line) patterns. Peak positions are indicated with blue markers. The background shape between 40° and 70° of 2θ arises from the glass sample holder.

4 Study of hydrogen peroxide stability

Preliminary control experiments on the stability of dissolved hydrogen peroxide (spontaneous disproportionation depending on pH) in synthetic COx (Callovo-Oxfordian) water and bicarbonate (1 mM HCO_3^-) solution have been performed. To perform this study, a stock solution with 0.1 mM ($3.4 \text{ mg}\cdot\text{L}^{-1}$) of H_2O_2 was prepared by mixing 6 w/v\% H_2O_2 solution with deionised water. Then, this stock solution was used to prepare 1 mM bicarbonate solution by adding the appropriate amount of $NaHCO_3$ and synthetic COx water by following the composition reported by Odorowski et al. [8]. It should be noted that there are some variations in the composition of COx water reported in the literature, for example [9]. The following chemicals were used to prepare synthetic COx water: $NaCl$, Na_2SO_4 , $NaHCO_3$, KCl , $CaSO_4\cdot 2H_2O$, $MgSO_4\cdot 7H_2O$, $SrCl_2\cdot 6H_2O$, $SiO_2\cdot 2H_2O$. The appropriate amounts of these reagents were weighed and dissolved in the stock solution of hydrogen peroxide. Then, three solutions containing 0.1 mM of H_2O_2 (COx water, bicarbonate water and the plain H_2O_2 stock solution) were deoxygenated by bubbling a $5\% H_2 / 95\% Ar$ gas mixture in a glove box with Ar atmosphere (0.1 ppm O_2) for 2 hours each (no noticeable decrease in H_2O_2 concentration was observed from this treatment) and transferred into another anoxic glove box with the same atmosphere to monitor hydrogen peroxide concentrations using semi-quantitative test strips Quantofix from Macherey-Nagel with the detection range from 0.5 to $25 \text{ mg}\cdot\text{L}^{-1}$ ($1.5\cdot 10^{-5}$ - $7.3\cdot 10^{-4} \text{ mol}\cdot\text{L}^{-1}$) (see Figure 4). Low density polyethylene (LDPE) vessels were used throughout the study to avoid any contact with silica (glass component) which is known to enhance H_2O_2 decomposition [10]. As can be seen from Table 2, for all three solutions only a slight decrease (disproportionation) in hydrogen peroxide concentration is expected over the foreseen 14 days oxidative dissolution experiments in the limit of the detection test applied.



Figure 4: Photograph of the semi-quantitative test strips kit used to monitor H_2O_2 concentration (for illustrative purpose only).

Table 2: Summary of the monitoring of H_2O_2 concentration.

| Number of days | Action taken | Concentration (mg/L) |
|----------------|--|---|
| 0 | 0.1 mM H_2O_2 stock solution prepared | no record |
| 1 | 1 mM bicarbonate and CO_x water solutions prepared based on the 0.1 mM H_2O_2 stock solution | between 5 and 2 for all three solutions |
| 2 | H_2O_2 concentration measured before bubbling H_2/Ar H_2O_2 concentration measured after bubbling H_2/Ar for 2 h through each solution and placing the solutions into another Ar atmosphere glove box | between 5 and 2 for all three solutions |
| 6 | H_2O_2 concentration measured in Ar atmosphere glove box | between 5 and 2 for all three solutions |
| 8 | H_2O_2 concentration measured in Ar atmosphere glove box | between 5 and 2 for all three solutions |
| 10 | H_2O_2 concentration measured in Ar atmosphere glove box | between 5 and 2 for all three solutions |
| 13 | H_2O_2 concentration measured in Ar atmosphere glove box | 2 for all three solutions |
| 24 | H_2O_2 concentration measured in Ar atmosphere glove box | 2 for all three solutions |

5 Summary

The first batch of $(\text{U}_{1-x}\text{Th}_x)\text{O}_2$ samples was produced and initially characterised. Most likely, incomplete reduction of U^{6+} to U^{4+} resulted in a lower content of U than targeted. The produced samples will be characterised by SEM and EDX techniques to get information on the surface microstructure and to verify the composition results from the XRD study and assess the distribution of U and Th (compositional homogeneity). It seems that the preparation route needs a slight adjustment to mimic the same stoichiometry composition as for the CEA MOX pellets. However, the pellets prepared are sufficiently similar to test the broad questions of mixed oxide fuel behaviour with respect to actinides with different redox properties. More pellets will be prepared to undertake dissolution tests with bicarbonate and CO_x water solutions spiked with H_2O_2 under anoxic conditions.

Acknowledgement

The research leading to these results has received funding from the European Commission Horizon 2020 Research and Training Programme of the European Atomic Energy Community (EURATOM) (H2020-NFRP-2016-2017-1) under grant agreement n° 755443 (DisCo project). Thanks are given to Giulio I. Lampronti for his help in conducting XRD study and data analysis.

References

- [1] Altaş, Y., Eral, M., Tel, H. (1997). Preparation of homogeneous $(\text{Th}_{0.8}\text{U}_{0.2})\text{O}_2$ pellets via coprecipitation of $(\text{Th,U})(\text{C}_2\text{O}_4)_2 \cdot n\text{H}_2\text{O}$ powders. *Journal of Nuclear Materials*, 249, 46-51.
- [2] Tamain, C., Arab Chapelet, B., Rivenet, M., Abraham, F., Caraballo, R., Grandjean, S. (2013). Crystal growth and first crystallographic characterization of mixed uranium(IV)-plutonium(III) oxalates. *Inorganic Chemistry*, 52, 4941-4949.
- [3] Balice, L., Bouëxière, D., Cologna, M., Cambriani, A., Vigier, J.-F., De Bona, E., Sorarù, G.D., Kübel, C., Walter, O., Popa, K. (2018). Nano and micro $\text{U}_{1-x}\text{Th}_x\text{O}_2$ solid solutions: From powders to pellets. *Journal of Nuclear Materials*, 498, 307-313.
- [4] Hubert, S., Purans, J., Heisbourg, G., Moisy, P., Dacheux, N. (2006). Local structure of actinide dioxide solid solutions $\text{Th}_{(1-x)}\text{U}_{(x)}\text{O}_2$ and $\text{Th}_{(1-x)}\text{Pu}_{(x)}\text{O}_2$. *Inorganic Chemistry*, 45, 3887-3894.
- [5] Kanno, M., Kokubo, S., Furuya, H. (1982). Preparation of thorium-uranium mixed oxide pellets. *Journal of Nuclear Science & Technology*, 19, 956-958.
- [6] Leinders, G., Cardinaels, T., Binnemans, K., Verwerft, M. (2015). Accurate lattice parameter measurements of stoichiometric uranium dioxide. *Journal of Nuclear Materials*, 459, 135-142.
- [7] Yang, J.H., Kang, K.W., Song, K.W., Lee, C.B., Jung, Y.H. (2017). Fabrication and thermal conductivity of $(\text{Th,U})\text{O}_2$ pellets. *Nuclear Technology*, 147, 113-119.
- [8] Odorowski, M., Jegou, C., De Windt, L., Broudic, V., Jouan, G., Peugeot, S., Martin, C. (2017). Effect of metallic iron on the oxidative dissolution of UO_2 doped with a radioactive alpha emitter in synthetic Callovian-Oxfordian groundwater. *Geochimica et Cosmochimica Acta*, 219, 1-21.
- [9] Beaucaire, C., Tertre, E., Ferrage, E., Grenut, B., Pronier, S., Madé, B. (2012). A thermodynamic model for the prediction of pore water composition of clayey rock at 25 and 80°C - Comparison with results from hydrothermal alteration experiments. *Chemical Geology*, 334, 62-76.
- [10] Hiroki, A. and LaVerne, J.A. (2005). Decomposition of hydrogen peroxide at water-ceramic oxide interfaces. *The Journal of Physical Chemistry B*, 109, 3364-3370.

Ongoing CIEMAT activities on fabrication and stability studies of doped UO₂ in the frame of the DisCo project: sample characterization, experimental set-up and first results

Cobos, J., Rodríguez-Villagra, N., Fernández, S., Gutierrez, L., Bonales, L.J., Durán, S., Anta, L.

Centro de Investigaciones Energéticas,
Medioambientales y Tecnológicas (CIEMAT),
Madrid (ES)

Abstract

This paper shows the current status of the experiments performed at CIEMAT within the WP2 and WP4 of the EURATOM H2020-NFRP-2016-2017-1 Collaborative Project, “Modern Spent Fuel Dissolution and Chemistry in Failed Container Conditions (DisCo)”. In this work, the fabrication of doped UO₂ fuel has been performed UO₂-0.02^{w/o} and 0.06^{w/o}Cr₂O₃, UO₂-0.05^{w/o}Cr₂O₃-0.02^{w/o}Al₂O₃ and UO₂-4.5^{w/o}Gd₂O₃. The aim of this investigation is to determine the effect of additives, the presence of H₂ and different types of aqueous solutions on UO₂ matrix stability, selected to represent groundwaters of varying complexities. The solid surface of the various fabricated samples is being characterized by X-Ray Diffraction (XRD), Raman spectroscopy and Scanning Electron Microscopy (SEM-EDX). The following sections describe, firstly the fabrication and characterisation for the various samples and then the leaching behaviour (thus far) of the samples (UO₂-0.06^{w/o}Cr₂O₃, UO₂-0.05^{w/o}Cr₂O₃-0.02^{w/o}Al₂O₃ and UO₂-4.5^{w/o}Gd₂O₃) under a granitic groundwater simulant (20 mM NaClO₄) and N₂/4.7% H₂ atmosphere with a total pressure of 8 ± 1 bar (pH₂ = 0.37 ± 1 bar). Other groundwaters will be studied later in the programme. Inductively Coupled Plasma Mass Spectrometry (ICP-MS) is used to quantify the uranium species released into the aqueous solution. After a cumulative contact time of 136 days that samples have been tested, the results obtained so far, showed that uranium concentration released into the aqueous phase was rather low (around 10⁻⁹ to 10⁻⁸ mol·L⁻¹). Besides, the dopants concentrations (Cr, Al, Gd) in solution were at comparable level than the own leachant (blank tests without solid) suggesting that little/no measurable fuel leaching had occurred.

1 Introduction

Safety assessment of irradiated/spent nuclear fuel disposal in a deep geological repository requires evidences (actual data to quantify and bound) radionuclides release after groundwater eventually gets into a breached container and contacts the fuel (i.e. conservatively assuming in PA exercises, an immediate failure of cladding). Within the EU DisCo project, the impact of additives (such as Cr, Cr/Al and Gd) is being investigated on the long term GDF (Geological Disposal Facility) leaching performance of traditional, UO₂ based fuels. In particular, we are looking at the impact of these dopants on the long-term matrix dissolution rate of the spent fuel (a key PA parameter) so called

advanced fuels, such as GAIA (Cr_2O_3 doped UO_2 fuel pellets, Framatome) [1, 2] and ADOPT (Cr_2O_3 and Al_2O_3 doped UO_2 fuel pellets, WESTINGHOUSE) [3].

Compared to UO_2 fuel, the advanced fuels GAIA and ADOPT have demonstrated that dopants provide enhanced safety against pellet-clad interaction failure (PCI), higher density, enlarged grain size, lower fission gas release (because pores appear precipitated inside grains) and higher creep rate (viscoplastic behaviour). The difference between GAIA or ADOPT and standard UO_2 in thermo-physical properties are almost negligible [1-4]. The question therefore remains as to whether or not these dopants impact upon the long term GDF leaching performance of these doped fuels when compared to more traditional UO_2 spent fuel.

The present contribution focuses on the dopants effect on UO_2 matrix leaching resistance through experiments in different representative aqueous systems. The aim of this work, performed in the context of WP2 and WP4 of the DisCo project, is to produce and characterize UO_2 pellets doped with UO_2 -0.06^w% Cr_2O_3 , UO_2 -0.05^w% Cr_2O_3 -0.02^w% Al_2O_3 and UO_2 -4.5^w% Gd_2O_3 , and to investigate experimentally the influence of $\text{H}_2(\text{g})$ on the matrix dissolution rate of doped UO_2 .

2 Materials and methods

2.1 WP2 – Model systems dissolution experiments: Powder preparation and characterization. Leachants composition

Starting materials description and fabrication data are available in [5]. Different techniques (Laser diffraction analyser, SEM, BET and XRD) were used for surface analysis techniques. The analyses have already been conducted, but at the time of producing this paper XRD and Raman spectra are still being interpreted.

The characterization of the Al_2O_3 powder revealed a coarse particle size and hydrated phases (Gibbsite) that would compromise the proportion of dopant added and the subsequent sintering. Therefore, heat treatment was carried out at 1100°C during 12 hours in order to achieve the phase α - Al_2O_3 [6]. SEM observations reveal that the powder microstructure consisted of semi-spherical and equiaxed grain and XRD analysis confirmed the absence of impurity phase, as it can be seen in Figure 1.

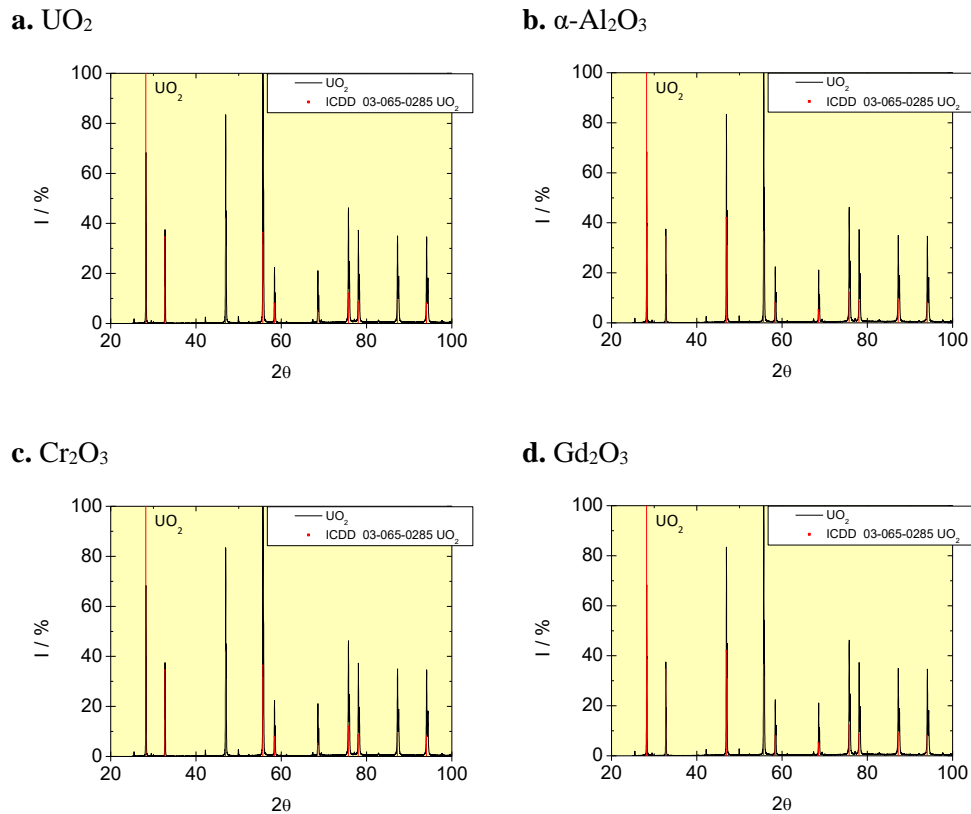


Figure 1: Powder SEM images and XRD pattern of initial powder of (a) UO₂, (b) α -Al₂O₃, (c) Cr₂O₃ and (d) Gd₂O₃.

The particle size distributions shown in Figure 2 are broad with an extended coil towards large particle sizes except in Cr₂O₃ powder, thus demonstrating that particles of UO₂, Al₂O₃ and Gd₂O₃ powders are agglomerated and the minor particle size of Cr₂O₃ fit with its narrow distribution. This fact confirms the need of a previous homogenizing mill stage to break the agglomerates and at the same time mix the different oxides. The methodology applied for fabrication of the fuel disk was classical uniaxial powder pressing and sintering [7]. The powders were mixed in the proportions using a mechanical mixing mill to ensure suitable homogenization. Pellet composition is: UO₂, UO₂ doped with 0.06^{w/o}Cr₂O₃, 0.05^{w/o}Cr₂O₃-0.02^{w/o}Al₂O₃, and 4.5^{w/o}Gd₂O₃.

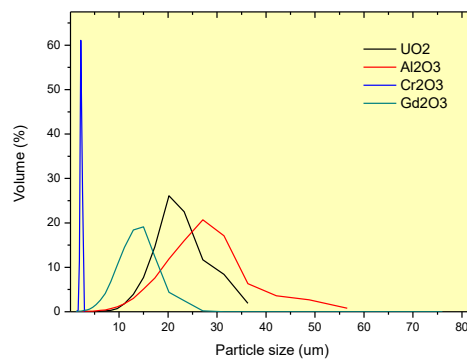


Figure 2.- Particle size distribution of starting material UO₂, Al₂O₃, Cr₂O₃, Gd₂O₃.

The final monoliths, were grinded and polished and thermally etched at 95% of the sintered temperature [8] to develop the surface/grain morphology. To confirm the final stoichiometry doped pellets characterization was carried out by XRD and Raman spectroscopy. SEM-EDX analyses were performed to identify the microstructure, porosity and grain size distribution calculated by the linear intercept method [9]. Specific surface area was determined by BET method [10] and the density was measured by both geometric and Archimedes methods. Three types of aqueous solutions were proposed in the project as leachants: non-complexing medium (20 mM NaClO₄) of low ionic strength, bicarbonate water (19 mM HCO₃⁻), and YCW (composition specified in Table 1).

Table 1. Aqueous media composition.

| Concentration (M) | NaClO ₄ 0.02 M | BC-1 | YCW-3 |
|-------------------|---------------------------|------------------------|------------------------|
| Na | $2.18 \cdot 10^{-2}$ | $2.1 \cdot 10^{-2}$ | $1.35 \cdot 10^{-1}$ |
| Mg | $2.07 \cdot 10^{-6}$ | $1.48 \cdot 10^{-6}$ | $2 \cdot 10^{-6}$ |
| Al | $3.61 \cdot 10^{-10}$ | $3.55 \cdot 10^{-9}$ | $5.0 \cdot 10^{-8}$ |
| K | $2.80 \cdot 10^{-4}$ | $1.40 \cdot 10^{-4}$ | $3.46 \cdot 10^{-1}$ |
| Ca | $2.89 \cdot 10^{-6}$ | $5.6 \cdot 10^{-6}$ | $7.8 \cdot 10^{-4}$ |
| Cr | $1.9 \cdot 10^{-9}$ | $4 \cdot 10^{-9}$ | $7 \cdot 10^{-8}$ |
| Mn | $7.0 \cdot 10^{-9}$ | $1.9 \cdot 10^{-8}$ | $1.6 \cdot 10^{-7}$ |
| Fe | $3.4 \cdot 10^{-8}$ | $9 \cdot 10^{-8}$ | $9.3 \cdot 10^{-7}$ |
| Co | $3.9 \cdot 10^{-10}$ | $1.43 \cdot 10^{-9}$ | $1.8 \cdot 10^{-9}$ |
| Ni | $< 1.7 \cdot 10^{-9}$ | $< 1.7 \cdot 10^{-9}$ | $< 1.7 \cdot 10^{-9}$ |
| Cu | $2.3 \cdot 10^{-9}$ | $1.2 \cdot 10^{-8}$ | $2.2 \cdot 10^{-7}$ |
| Cs | $1.9 \cdot 10^{-10}$ | $1.38 \cdot 10^{-9}$ | $1.7 \cdot 10^{-9}$ |
| Ba | $9.9 \cdot 10^{-9}$ | $1.8 \cdot 10^{-8}$ | $1.4 \cdot 10^{-7}$ |
| Ce | $7.1 \cdot 10^{-12}$ | $1 \cdot 10^{-10}$ | $< 7 \cdot 10^{-12}$ |
| Gd | $9 \cdot 10^{-12}$ | $8 \cdot 10^{-11}$ | $< 6 \cdot 10^{-12}$ |
| Pb | $5.7 \cdot 10^{-10}$ | $5.3 \cdot 10^{-9}$ | $4.0 \cdot 10^{-8}$ |
| Th | $< 4.3 \cdot 10^{-12}$ | $< 4.3 \cdot 10^{-12}$ | $< 4.3 \cdot 10^{-12}$ |
| U | $1.2 \cdot 10^{-10}$ | $3.6 \cdot 10^{-9}$ | $5.9 \cdot 10^{-9}$ |

Prior to preparation of the aqueous solutions, each chemical reagent was analysed by ICP-MS to quantify concentration trace elements. There is only a minor contribution in U concentration from potash, and all of them contained some unavoidable trace amounts of transition metals (iron and copper) around ppm. The leachant was prepared adjusting SCK-CEN methodology [11] according to composition defined in the project (two added steps out of glove box: the use of Milli-Q-water previously boiled to minimize the presence of CO₂, and bubbling with He or Ar during one hour

before being stored in a glove-box under Ar atmosphere for one month). Then it was filtered (by PVDF membrane with a pore size of 0.22 μm , except for high pH solution, that was used a PTFE membrane). The elemental composition, redox and pH were monitored ex-situ in the anoxic atmosphere glovebox. Details of element concentration of NaClO_4 , bicarbonate solution and YCW are shown in table 1. U concentration occurrence has been of around 10^{-10} M (NaClO_4), 10^{-9} M (BC) and ranged between 10^{-9} - 10^{-8} M (YCW). Fe concentration was around 10^{-8} - 10^{-7} M.

2.2 WP4 - Study of the spent fuel matrix dissolution behaviour under repository conditions

CIEMAT has made preparations and started the leach (doped UO_2) in the second semester of 2018. Static leaching experiments are being performed in stainless steel autoclaves with reaction vessels made of PEEK. Four valves in the lid allow for aqueous sampling, gas injection and extraction and in-situ temperature control (on the chance that high temperature experiments were required but not in the scope of DISCO project) [5]. Anoxic conditions are accomplished by the application of 8 ± 1 bar of a 4.7% H_2 - N_2 gas ($p_{\text{H}_2} = 0.37 \pm 1$ bar) within the autoclaves (Figure 3). Prior to use, unirradiated fuel disks of approximately 0.9 g were washed twice with 1 mM bicarbonate water and twice with pure MilliQ water (resistivity $r = 18.2 \text{ M}\Omega \cdot \text{cm}^{-1}$), mainly to remove U(VI) from the surface, and then the solid samples were stored in an Ar glove box. Aqueous phases from the cleaning process were sampled for further analysis by ICP-MS.



Figure 3: View of leaching experimental set up installed at CIEMAT in Ar glove box under 8 bar of 4.7% H_2 - N_2 .

A disk in presence of 300 mL 20 mM NaClO_4 solution was put into the autoclave. The experiments are being carried out in a glove-box at $22 \pm 3^\circ\text{C}$ under Ar atmosphere with p_{O_2} below 2 ppm. Thereafter, ~ 3.5 mL aliquots were taken at 0, 6, 14, 20, 27, 41, 54, 63, 76, 111 and 136 days. Additionally, blank tests containing only leaching solution were started under the same conditions in parallel experiments to check for possible cross-contamination. The aliquots were filtered using ~ 1.5 mL for microfiltration (0.22 μm) and ~ 1.5 mL for ultrafiltration (Amicon Ultra-4 3k Millipore 1 - 2 nm). The samples were conditioned with 10% HNO_3 solution. After each sampling the autoclave was refilled with N_2/H_2 mixture to reach 8 bar and the initial conditions were again established. In contrast, the aqueous solution was not renewed to replace the amount extracted during sampling. The pH is being measured at every sampling interval with a pH Glass Electrode (Metrohm) and pH-meter 905 Titrand (Metrohm). The pH electrode is calibrated with commercial pH buffer solutions (4, 7, 9).

Redox potential is being measured with an Ag/AgCl Combined Pt-ring Electrode (Metrohm). Soluble element concentrations leached U, Cr, Al and Gd among other low concentrated metals were measured by Inducted Coupled Plasma Mass Spectrometry ICP-MS (iCAP Qc Thermo Fisher Sci.). The limit of detection of ICP-MS is in the range of ppt ($\text{pg}\cdot\text{g}^{-1}$) and the limit of quantification in the ppb range ($\text{ng}\cdot\text{g}^{-1}$). Uncertainty of the elemental concentration measured by this technique is 10 to 15%.

3 Results

3.1 WP2 – Model systems dissolution experiments

The main purpose of this progress paper is to complete the documentation of the samples characterization in the first year of the project. The first year (i.e. 2017) has been used to prepare the solid samples (including some surface characterization) and leach tests. Detailed analyses from characterization data of UO_2 doped with 0.02 and 0.06^w% Cr_2O_3 , 0.05^w% Cr_2O_3 -0.02^w% Al_2O_3 , and 4.5^w% Gd_2O_3 pellets and leachant composition have been conducted in the second year (i.e. 2018). The characterisation of the doped samples was performed through XRD, Raman spectroscopy and SEM. Monoliths fabricated in WP2 are being used for dissolution experiments in WP4. In Figure 4a the microstructure revealed suitable sintered pellets with low porosity and 10 μm grain size.

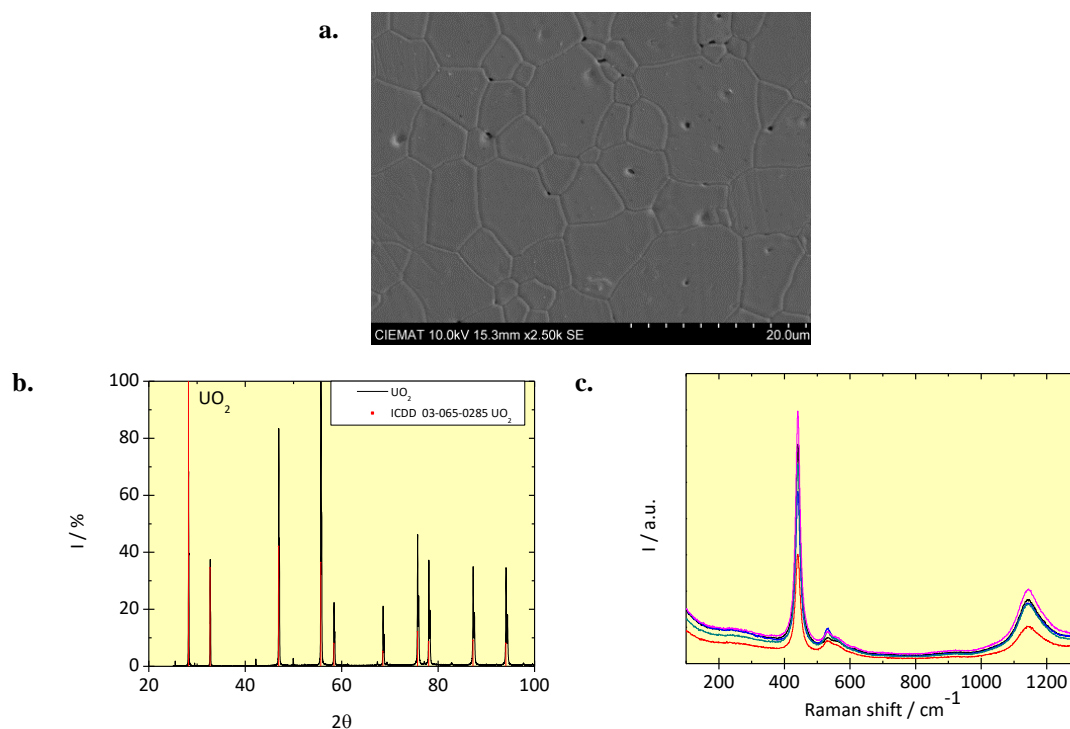


Figure 4: UO_2 pellet characterization by (a) Scanning electron Microscopy SEM, (b) XRD pattern and (c) RAMAN spectroscopy.

Figure 4b shows the X-ray diffractogram for the stoichiometric UO_2 structure, free of impurities and uranium hyper-oxides phases [12] with a measured lattice parameter of 0.547174 nm. On the other hand, Raman scattering of the pure UO_2 pellets (Figure 4c) shows the two fundamental vibrational stretches corresponding to $\text{UO}_{2.00}$, one at 445 cm^{-1} associated to the T_{2g} and ascribed to the symmetric

stretching mode which arises due to oxygen breathing vibrations around U(IV) in the fluorite structure, and the second band observed around 1150 cm^{-1} attributed to overtone (2L-O) of the first order L-O phonon (575 cm^{-1}) [13-15].

Figure 5a shows the XRD, for both, UO_2 and Cr_2O_3 pattern, and UO_2 doped with $0.02\text{ wt}\%$ and $0.06\text{ wt}\%$ with Cr_2O_3 . No isolated undoped phases ($\text{UO}_2/\text{Cr}_2\text{O}_3$) have been identified. Hence, from Figure 5b, it can be confirmed that the chromium has been completely dissolved into the UO_2 matrix. Besides, Figure 5b shows the Raman spectroscopy characterization, identifying pure stoichiometric UO_2 , shown as a single mode at 445 cm^{-1} and the band 1150 cm^{-1} attributed to overtone 2L-O as has been described in previous UO_2 characterization discussed above. Concerning the UO_2 doped samples, it can be seen that the higher the chromium concentration in the matrix is, the lower is the intensity of the peak at 450 cm^{-1} as well as the band at 1150 cm^{-1} , confirming the degradation of the fluorite structure due to doping. A remarkable additional feature is observed around 540 cm^{-1} not observed in UO_2 . Such a band has been described previously on RE^{III} -doped (Gd, Pu, Ce) UO_2 attributed to the creation of oxygen vacancies [16, 17]. The presence of such vacancies in UO_2 is attributed to a local phonon mode associated with O_v induced lattice distortion due to the need for charge compensation. This confirms that the dopants have been totally and homogeneously distributed into the UO_2 matrix [13-15].

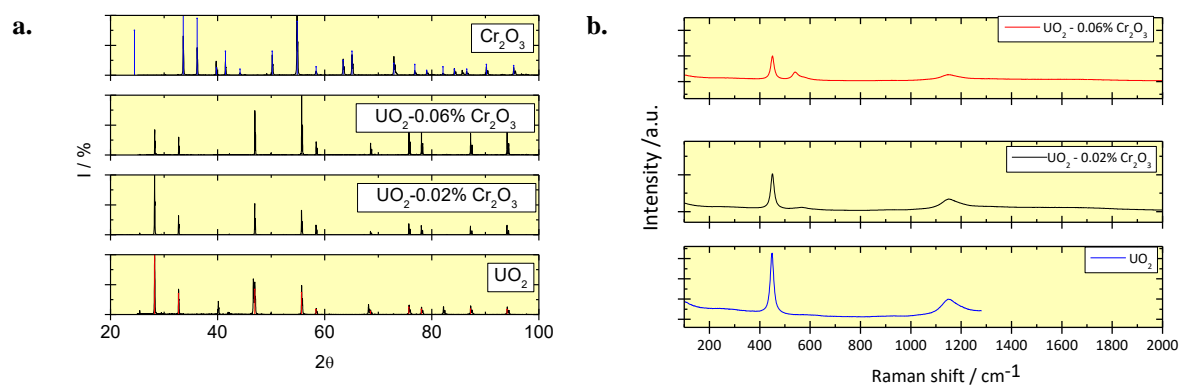


Figure 5: Characterization of $\text{UO}_2-x\text{Cr}_2\text{O}_3$; $x = 0.02$ & $0.06\text{ wt}\%$ pellets by (a) XRD and (b) RAMAN spectroscopy.

The XRD characterization of the pellets doped with $0.05\text{ wt}\%$ chromia and $0.02\text{ wt}\%$ alumina ($\text{UO}_2-0.05\text{ wt}\% \text{Cr}_2\text{O}_3-0.02\text{ wt}\% \text{Al}_2\text{O}_3$) (Figure 6a) shows a homogenous dissolution of the dopants into the UO_2 matrix without secondary phases can be observed. Figure 6b isolated in a plot illustrates the more intensive peak of the the $\text{UO}_2-0.05\text{ wt}\% \text{Cr}_2\text{O}_3-0.02\text{ wt}\% \text{Al}_2\text{O}_3$ samples, where it is shown that the tail shifted to the higher angle representing a lower lattice parameter. Therefore, this fact promotes a contraction of the UO_2 cubic lattice (Fm-3m) due to the substitution of the dopants in the UO_2 matrix. This effect is expected from the partial substitution of U(IV) ions by the much smaller Al(III) and Cr(III) ions. Regarding the Raman spectroscopy characterization of the pellet surfaces Figure 6c exhibits the typical spectra corresponding to a pure alpha Al_2O_3 phase with sharp bands at 1370 and 1397 cm^{-1} , indicating a well-defined crystal structure in this material. Concerning the Raman spectroscopy characterization, the same explanation as for the chromium doped sample can also be applied.

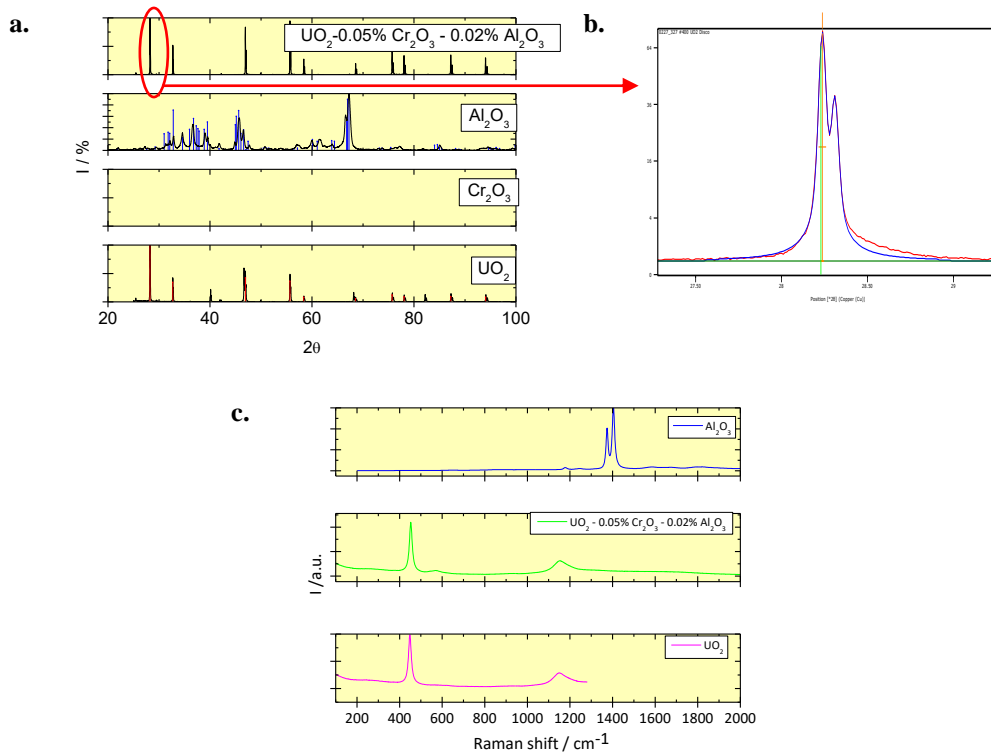


Figure 6: Surface Characterization of the UO_2 - $x\text{Cr}_2\text{O}_3$; $x = 0.02$ & 0.06 wt.% pellets (a) XRD pattern, (b) XRD (c) RAMAN spectroscopy.

Figure 7a shows the X-Ray diffractograms, of UO_2 , Gd_2O_3 and $(\text{U}_{0.96}\text{-Gd}_{0.04})\text{O}_2$ where any single peak of Gd_2O_3 has been identified. Gadolinium is dispersed in solid solution in the UO_2 lattice (not segregated), however, as in other works, three types of solid solutions with different gadolinium content has been identified with markedly different lattice parameters from 0.4% to 12% , nevertheless, the matrix presented an average of 4.5% . This seems to be in a good agreement with literature data due to higher concentration of Gd_2O_3 is precipitating in grain boundaries. Gadolinium is responsible for the grain size decrease and the porosity increase. Besides, the Raman spectroscopy characterization identifies pure stoichiometric UO_2 shown as a single mode at 445 cm^{-1} as has been described in previous pure UO_2 characterization above and the 1150 cm^{-1} attributed to overtone 2L-O .

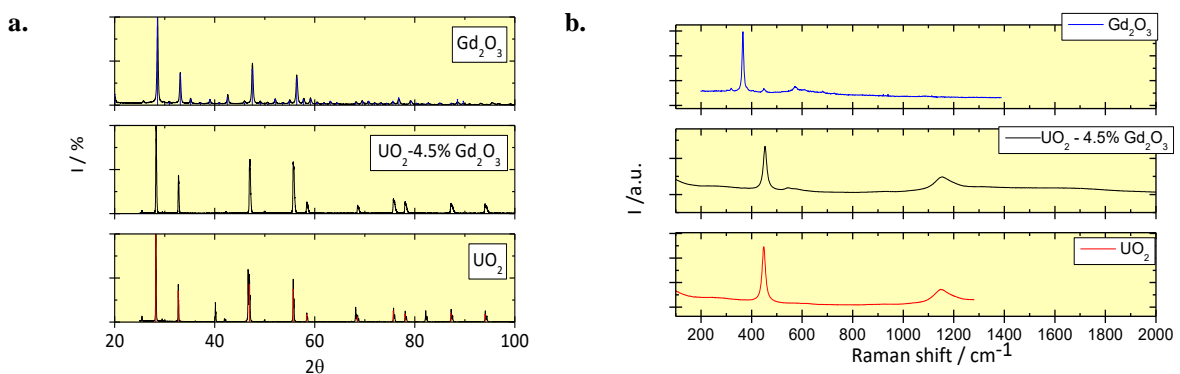


Figure 7: (a) XRD pattern, and (b) RAMAN spectroscopy of UO_2 - 4.5 wt% Gd_2O_3 pellets.

All the allowed modes could not be observed in Gd_2O_3 , except for the strongest mode at 360 cm^{-1} and some very weak peaks (318 , 448 and 572 cm^{-1}), because of the low intensity and poor signal to noise ratio for the other modes as has been reported by other authors [18]. Concerning the $(\text{U}_{0.96}\text{-Gd}_{0.04})\text{O}_2$ specimen the intensity of the peak at 450 cm^{-1} is considerably lower than observed on UO_2 , and the band at 1150 cm^{-1} is very weak confirming the degradation of the fluorite structure due to doping (Figure 7b). Like in the case of $\text{UO}_2\text{-xCr}_2\text{O}_3$, a remarkable additional feature is observed around 540 cm^{-1} not observed in UO_2 . The main characterization parameters of the fabricated materials are summarized in Table 2.

Table 2. Summary of the results obtained from the analysis of the UO_2 and doped UO_2 pellets.

| Sample (wt.%) | Lattice parameter (nm) | SSA (BET) ($\text{m}^2\cdot\text{g}^{-1}$) | Density ($\text{g}\cdot\text{cm}^{-3}$) |
|---|---|---|--|
| UO_2 | 0.547174 (6) | 0.36 ± 0.01 | 8.93 ± 0.07 |
| $\text{UO}_2\text{-0.02 Cr}_2\text{O}_3$ | 0.547108 (7) | 0.28 ± 0.01 | 9.80 ± 0.12 |
| $\text{UO}_2\text{-0.06 Cr}_2\text{O}_3$ | 0.547113 (7) | 0.63 ± 0.02 | 9.83 ± 0.07 |
| $\text{UO}_2\text{-4.5 Gd}_2\text{O}_3$ | Phase #1 0.54705(6) Phase #2 0.5463(2) Phase #3 0.5450(3) | 0.63 ± 0.01 | 9.81 ± 0.11 |
| $\text{UO}_2\text{-0.05 Cr}_2\text{O}_3 - 0.02\text{ Al}_2\text{O}_3$ | 0.547198 (5) | 0.25 ± 0.01 | 9.80 ± 0.43 |

In all the doped cases, the average grain size showed an increase except for UO_2 doped with Gd_2O_3 , which remained almost unchanged or even decreased for the three types of solid solutions with different Gd content found in the specimens, compared with undoped UO_2 . Figure 8 shows the surface morphology and the grain structure of UO_2 , $\text{UO}_2\text{-4.5}^w\text{Gd}_2\text{O}_3$, $\text{UO}_2\text{-0.05}^w\text{Cr}_2\text{O}_3\text{-0.02}^w\text{Al}_2\text{O}_3$ and $\text{UO}_2\text{-0.06}^w\text{Cr}_2\text{O}_3$ sintered pellets. Gd- UO_2 micrograph was acquired at higher magnification due to its low grain size. As expected, no precipitates or segregation have been observed in any of the characterized samples, meaning that dopants have been dissolved into the matrix.

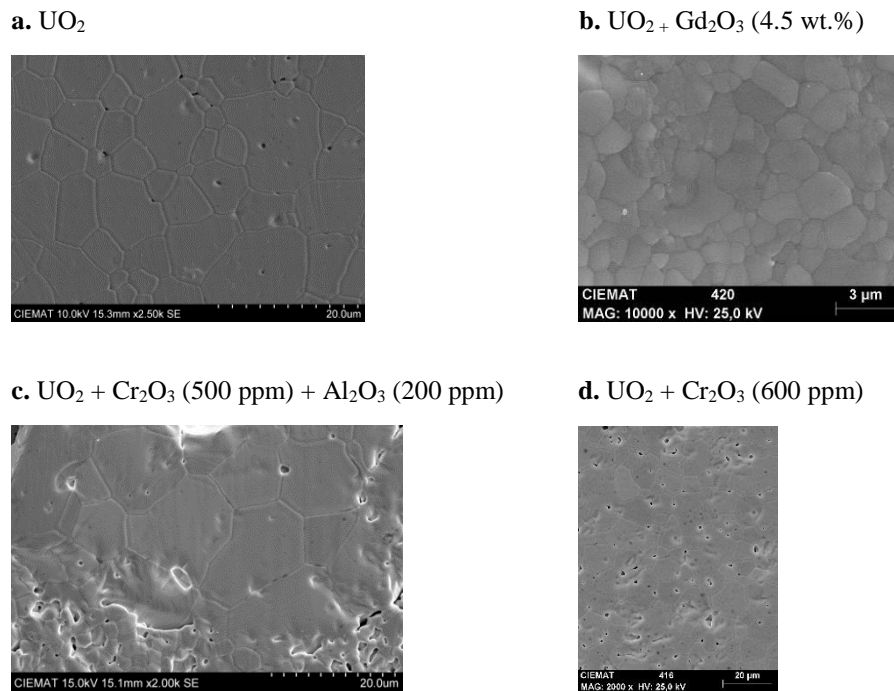


Figure 8: SEM micrographs showing the surface topography of (a) UO_2 , (b) $\text{UO}_2\text{-}4.5\text{wt}\% \text{Gd}_2\text{O}_3$ and (c) $(0.05\text{wt}\% \text{Cr}_2\text{O}_3\text{-}0.02\text{wt}\% \text{Al}_2\text{O}_3)$ (d) samples.

3.2 WP4 - Study of the spent fuel matrix dissolution behaviour under repository conditions

The initial stage of leach testing aimed to start the first leaching experiments under anoxic conditions using a synthetic groundwater without carbonates, 0.02 M NaClO_4 , carried out over a period of 136 days. The results of the aqueous solutions were obtained giving a concentration released after a cumulative contact time of 136 days of 10^{-9} M for U, indicating extremely low matrix dissolution. During the experiment pH measurements are carried out at each sampling time (Figure 9). The pH slightly increases from 7.9 to 8.4 - 9.3 up to 6 days and then decreases to 6.9 (blank test), 6.6 (Cr- UO_2), 7.2 (Cr/Al- UO_2) and 6.3 (Gd- UO_2) for contact times up to 136 days. The stability of pH values indicates a stable system in which little or no dissolution is taking place. The pe value decreases in all experiments below 0 (-0.19 blank, -0.31 Cr- UO_2 , -0.79 Cr/Al- UO_2 and -0.41 Gd- UO_2). A summary of the obtained results of leaching experiments in 0.02 M NaClO_4 is shown in Table 3 for each UO_2 doped sample performed in the DisCo project. The results of U, Cr, Al and Gd batch leaching experiments as a function of leaching time are shown in Figure 10a: $\text{UO}_2\text{-}0.06\text{wt}\% \text{Cr}_2\text{O}_3$; Figure 10b: U $\text{UO}_2\text{-}0.06\text{wt}\% \text{Cr}_2\text{O}_3$, b) $\text{UO}_2\text{-}0.05\text{wt}\% \text{Cr}_2\text{O}_3\text{-}0.02\text{wt}\% \text{Al}_2\text{O}_3$ and c) $\text{UO}_2\text{-}4.5\text{wt}\% \text{Gd}_2\text{O}_3$ in 0.02M NaClO_4 .

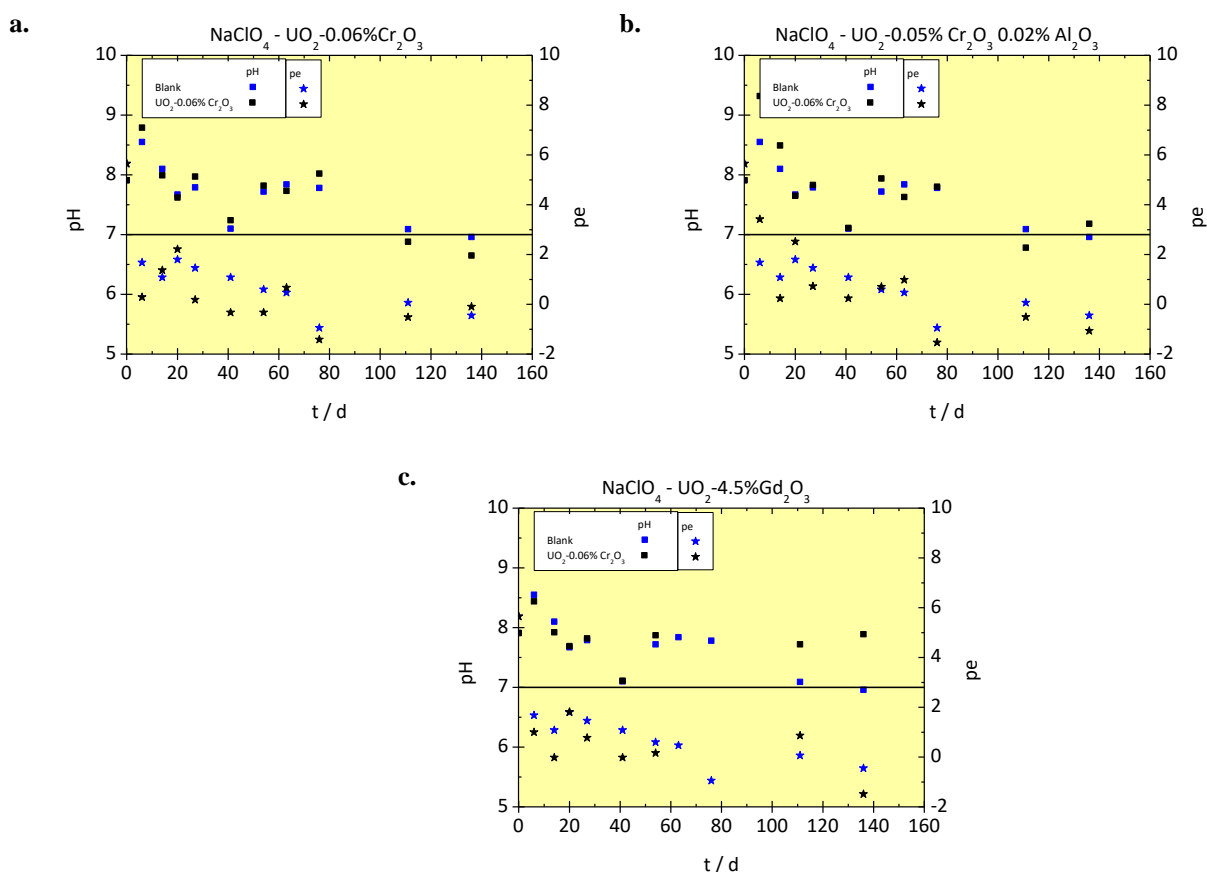


Figure 9: pH and pe measured of (a) $\text{UO}_2\text{-}0.06\% \text{Cr}_2\text{O}_3$, (b) $\text{UO}_2\text{-}0.05\% \text{Cr}_2\text{O}_3\text{-}0.02\% \text{Al}_2\text{O}_3$ and (c) $\text{UO}_2\text{-}4.5\% \text{Gd}_2\text{O}_3$.

Table 3. Experimental results (U, Cr, Al and Gd concentration in solution) measured during the UO_2 leaching experiments in 0.02 M NaClO_4 and $\text{pH}_2 = 0.37 \pm 1$ bar, in a glove-box (Ar) at $22 \pm 3^\circ\text{C}$ and $\text{pO}_2 < 2$ ppm.

| Concentration ($\text{mol}\cdot\text{L}^{-1}$) | [U]f | [U]u | [Cr]f | [Cr]u | [Al]f | [Al]u | [Gd]f | [Gd]u |
|---|-------------------------------|---------------------------|-------------------------------|-------------------------------|--------------------------------|----------------------------|------------------------------|----------------------------------|
| Blank | $(1 \pm 1) \cdot 10^{-9}$ | $(4 \pm 5) \cdot 10^{-9}$ | $(8 \pm 1) \cdot 10^{-9}$ | $(1 \pm 1) \cdot 10^{-8}$ | $(6 \pm 2) \cdot 10^{-10}$ | $(8 \pm 3) \cdot 10^{-10}$ | $(2 \pm 2) \cdot 10^{-11}$ | $(1.57 \pm 0.03) \cdot 10^{-11}$ |
| $\text{UO}_2\text{-}$ $0.06\% \text{Cr}_2\text{O}_3$ | $(1.7 \pm 0.6) \cdot 10^{-9}$ | $(1 \pm 2) \cdot 10^{-8}$ | $(7 \pm 3) \cdot 10^{-9}$ | $(9 \pm 1) \cdot 10^{-9}$ | $(4.9 \pm 0.9) \cdot 10^{-10}$ | $(8 \pm 5) \cdot 10^{-10}$ | $(3 \pm 8) \cdot 10^{-11}$ | $(5 \pm 3) \cdot 10^{-11}$ |
| $\text{UO}_2\text{-}$ $4.5\% \text{Gd}_2\text{O}_3$ | $(2 \pm 2) \cdot 10^{-9}$ | $(1 \pm 2) \cdot 10^{-9}$ | $(2 \pm 3) \cdot 10^{-8}$ | $(1.4 \pm 1.3) \cdot 10^{-8}$ | $(7 \pm 2) \cdot 10^{-10}$ | $(2 \pm 1) \cdot 10^{-9}$ | $(4 \pm 4) \cdot 10^{-9}$ | $(6 \pm 2) \cdot 10^{-10}$ |
| $\text{UO}_2\text{-}$ $0.05\% \text{Cr}_2\text{O}_3\text{-}$ $0.02\% \text{Al}_2\text{O}_3$ | $(2 \pm 1) \cdot 10^{-9}$ | $(6 \pm 5) \cdot 10^{-9}$ | $(4.8 \pm 0.4) \cdot 10^{-9}$ | $(7 \pm 3) \cdot 10^{-9}$ | $(8 \pm 6) \cdot 10^{-10}$ | $(1 \pm 1) \cdot 10^{-9}$ | $(0.9 \pm 2) \cdot 10^{-11}$ | $(3 \pm 4) \cdot 10^{-11}$ |

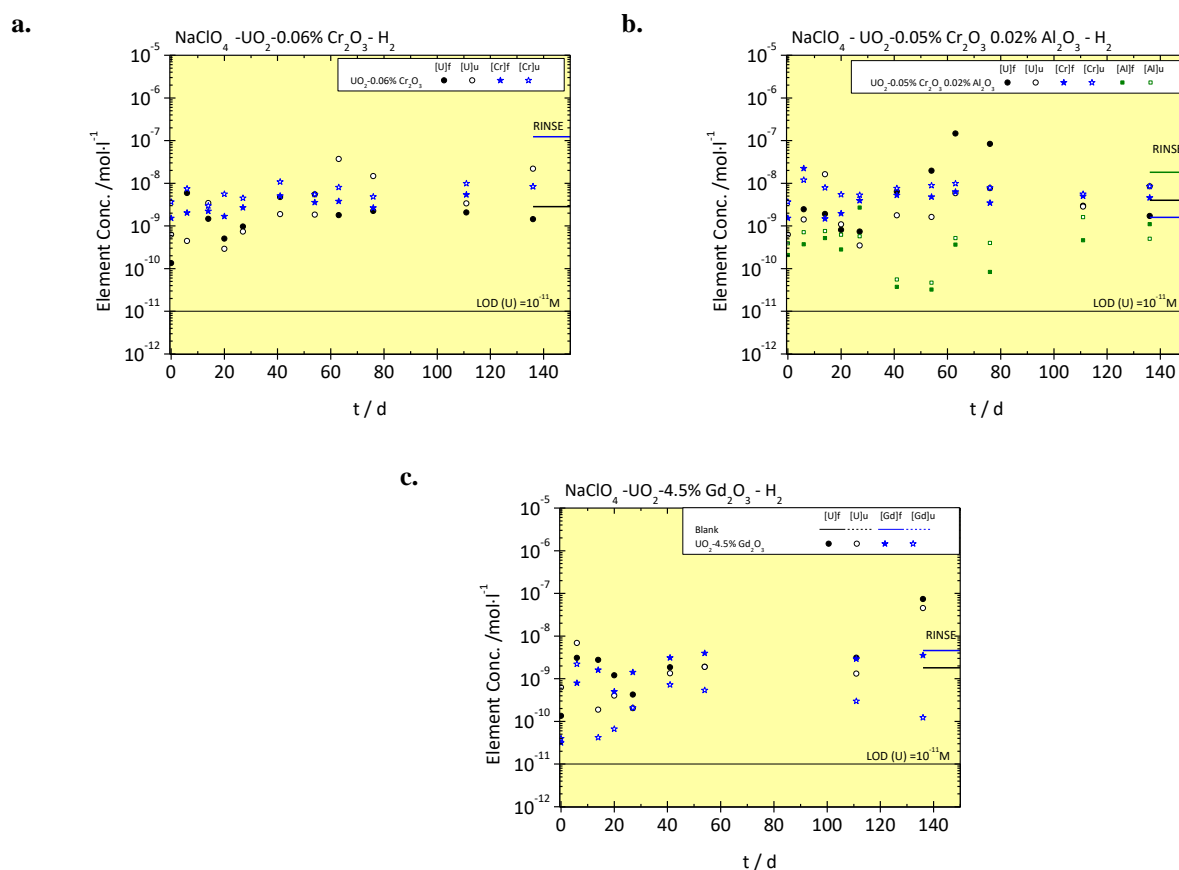


Figure 10: U and Cr concentration as a function of leaching time of (a) $\text{UO}_2\text{-}0.06\% \text{Cr}_2\text{O}_3$, (b) $\text{UO}_2\text{-}0.05\% \text{Cr}_2\text{O}_3\text{-}0.02\% \text{Al}_2\text{O}_3$ and (c) $\text{UO}_2\text{-}4.5\% \text{Gd}_2\text{O}_3$.

In the present study, for all types of samples, available data from U concentrations in NaClO_4 are around 10^{-9} to 10^{-8} mol·L⁻¹, which is consistent with the expected solubility range of $\text{UO}_2(\text{am})$ according to literature, of about 10^{-9} mol·L⁻¹ [6, 19, 20]. In order to demonstrate the expected absence of secondary phases formation, post leached samples will be characterized by XRD, SEM and Raman spectroscopy.

4 Conclusions and Future work

Advanced fuels ($\text{UO}_2\text{-}0.06\% \text{Cr}_2\text{O}_3$, $\text{UO}_2\text{-}0.05\% \text{Cr}_2\text{O}_3\text{-}0.02\% \text{Al}_2\text{O}_3$ and $\text{UO}_2\text{-}4.5\% \text{Gd}_2\text{O}_3$) were manufactured and the surface characterization of all the samples developed a quite consistent material. In all the pellets fabricated in this work the dopants are dissolved into the UO_2 matrix. Because the pellets fit with the requirements of the WP2-DisCo project, the materials have been used to study the influence of dopants on the dissolution of the spent fuel under deep geological disposal conditions. During the reporting period, three (plus blank test) leaching experiments have been performed in a time frame of 136 days to quantify the element release from doped UO_2 under 0.02 M NaClO_4 environment (inert electrolyte) and $\text{N}_2/4.7\% \text{H}_2$ overpressure. U in solution was close to the limit of quantification (10^{-9} - 10^{-8} M), indicating insignificant matrix dissolution effects. Among the elements measured by ICP-MS, Al, Cr, Mn, Fe, Co, Ni and Gd follow a very similar concentration evolution pattern to U.

During the reporting period, powdered solid samples have been prepared to chemically determine the inventory by acid dissolution and ICP-MS, chemical characterisation will be finalised and summarised in the next deliverable. The post-characterization of the solid samples will be completed. Future investigations will focus on a detail process understanding of leaching performance in other aqueous solutions, and tracking leachant evolution. It was decided for a better improvement of empirical conditions, no initial washing of the sample by aqueous solution in next experiments to avoid pre-leaching of the fuel sample and to suspend the sample with a platinum wire.

Acknowledgement

The research leading to these results has received funding from the European Commission Horizon 2020 Research and Training Programme of the European Atomic Energy Community (EURATOM) (H2020-NFRP-2016-2017-1) under grant agreement n° 755443 (DisCo project).

References

- [1] Thomas, G.A., D'Orio, J.S., Gentet, G., Louf, P.-H., Mindt, M. (2013). GAIA: AREVA's advanced PWR fuel design. LWR Fuel Performance Meeting. TopFuel, 201.
- [2] Gentet, G., Peucker, J., Gebhardt, C. (2015). post irradiation examinations of GAIA lead fuel assemblies. Top Fuel 2015 Conference Proceedings, A0198, 170-176.
- [3] Backman, K., Hallstadius, L., Roenberg, G. (2009). Westinghouse Advanced Doped Pellet - Characteristics and irradiation behaviour. INIS-XA--1074, International Atomic Energy Agency (IAEA).
- [4] Technical Exchange Meeting: EnCore® Accident Tolerant Fuel ADOPT Fuel Pellets. Closed Meeting with U.S. Nuclear Regulatory Commission on January 17, 2019 to Discuss Westinghouse Accident Tolerant Fuel Technology.
- [5] Rodríguez-Villagra, N., Fernández, S., Bonales, L.J., Gutiérrez, L., Elorrieta, J.M., Cobos, J. (2018). Manufacture and characterization of CIEMAT fuel samples used for leaching tests in the DisCo project. 1st Annual Meeting Proceedings of the DisCo Project. Deliverable D1.10, 39-44.
- [6] Yajima, T., Kawamura, Y., Ueta, S. (1994). Uranium(IV) solubility and hydrolysis constants under reduced conditions. MRS Proceedings, 353, 1137-1142.
- [7] Fernandez, S., Nieto, M.I., Cobos, J., Moreno, R. (2016). CeO₂ pellet fabrication as spent fuel matrix analogue. Journal of the European Ceramic Society, 36(14), 3505-3512.
- [8] Clinton, D.J. (1987). A guide to polishing and etching of technical and engineering ceramics. The Institute of Ceramics.
- [9] ISO 643:2012. Micrographic determination of the apparent grain size.
- [10] Brunauer, S., Emmett, P.H., Teller, E. (1938). Adsorption of gases in multimolecular layers. Journal of the American Chemical Society, 60(2), 309-319.
- [11] Wang, L. (2009). Near-field chemistry of a HLW/SF repository in boom clay – scoping calculations relevant to the supercontainer design. SCK-CEN Report, CEN-ER-17.
- [12] Clausen, K., Hayes, W., Macdonald, J.E., Schnabel, P., Hutchings, M.T., Kjems, J.K. (1983). Neutron scattering investigation of disorder in UO₂ and ThO₂ at high temperatures. High Temp. High Pressures, 15(4), 383-390.

- [13] Elorrieta, J.M., Bonales, L.J., Fernández, S., Rodríguez-Villagra, N., Gutiérrez-Nebot, L., Baonza, V.G., Cobos, J. (2018). Pre- and post-oxidation Raman analysis of (U,Ce)O₂ oxides. *Journal of Nuclear Materials*, 508, 116-122
- [14] Marlow, P.G., Russell, J.P., Hardy, J.R. (1966). Raman scattering in uranium dioxide. *The Philosophical Magazine: A Journal of Theoretical Experimental and Applied Physics*, 14(128), 409-410.
- [15] Livneh, T. and Sterer, E. (2006). Effect of pressure on the resonant multiphonon Raman scattering in UO₂. *Physical Review B: covering condensed matter and materials physics*, 73(8), 085118-085119.
- [16] Elorrieta, J.M., Manara, D., Bonales, L.J., Vigier, J.F., Dieste, O., Naji, M., Belin, R.C., Baonza, V.G., Konings, R.J.M., Cobos, J. (2017). Raman study of the oxidation in (U, Pu)O₂ as a function of Pu content. *Journal of Nuclear Materials*, 495, 484-491.
- [17] Razdana, M. and Shoesmith, D. (2014). Influence of trivalent-dopants on the structural and electrochemical properties of uranium dioxide (UO₂). *Journal of the Electrochemical Society*, 161(3), H105-H113.
- [18] Banerji, A., Grover, V., Sathe, V., Deb, S.K., Tyagi, A.K. (2009). CeO₂Gd₂O₃ system: Unraveling of microscopic features by Raman spectroscopy. *Solid State Communications*, 149(39-40), 1689-1692.
- [19] Rai, D., Felmy, A.R., Ryan, J.L. (1990). Uranium(IV) hydrolysis constants and solubility product of UO₂.cntdot.xH₂O(am). *Inorganic Chemistry*, 29(2), 260-264.
- [20] Rai, D., Yui, M., Moore, D.A. (2003). Solubility and solubility product at 22°C of UO₂(c) precipitated from aqueous U(IV) solutions. *Journal of Solution Chemistry*, 32(1), 1-17.

Synthesis and characterisation of Cr-doped UO₂: A model material for modern nuclear fuel dissolution studies

Cordara, T., Smith, H., Mohun, R., Stennett, M. C., Hyatt, N.C., Corkhill, C. L.

Immobilisation Science Laboratory, Department of
Materials Science and Engineering, The University
of Sheffield, Sheffield (UK)

Abstract

Model Cr-doped UO₂ materials were prepared by a series of synthesis routes. The most promising for use in further dissolution studies and for consolidation by hot isostatic pressing was determined to be *via* a nitrate precipitation route. Analysis of Cr-doped UO₂ by X-ray Diffraction, Raman Spectroscopy and X-ray Absorption Spectroscopy showed distinct Cr-incorporation behaviours based on the concentration of Cr-dopant. At Cr contents of < 600 ppm, it was found that Cr was incorporated in UO₂ lattice in a reduced form, possibly as Cr-clusters, and between 600 - 1200 ppm incorporation was as a higher valence state, close to Cr³⁺, into the UO₂ lattice. At concentrations of > 1200 ppm Cr, it was found that the solubility limit of Cr within the UO₂ lattice was exceeded, and the grain size reduced dramatically. The influence of Cr-dopant concentration on properties including grain size and density was found to be highly dependent on the Cr-incorporation mechanism. These results are in contradiction with previous studies of these materials, which assume that Cr enters the UO₂ structure as Cr³⁺ only. Thus, this work gives further insight to the structure of modern fuels as a function of dopant concentration, which is essential to underpin the dissolution mechanism. Details of preliminary experiments to ascertain dissolution behaviour, as a function of Cr-content are described.

1 Introduction

One solution to enhancing the life-time of UO₂ fuel within a nuclear reactor is to improve the fuel microstructure by promoting the growth of larger grains and promoting the fission product diffusion to the grain boundaries during fission [1]. This is achieved by doping UO₂ with additives; the most extensively applied are Cr₂O₃ [2-7], Al₂O₃ [3, 8-10] and a mixture of Cr₂O₃-Al₂O₃ [7, 11, 12]. Despite being used in reactors across Europe, the influence of Cr- and Al-oxide additions on the U coordination and local structure is not well understood; preliminary studies show that even small additions of these elements may significantly alter the defect chemistry and uranium stoichiometry [13]. Recent studies [14, 15] have shown that small alterations in defect chemistry and uranium stoichiometry can strongly influence the rate at which fluorite-type materials corrode; this is an important consideration for both long-term storage of spent nuclear fuel, and for its geological disposal where interactions of the fuel with groundwater will eventually lead to corrosion. In comparison to traditional UO₂ fuel, these new doped-fuels are poorly understood, which may prove problematic for storage and disposal regulators.

As such, the aim of this work is to synthesise simplified UO₂ materials with additions of Cr₂O₃ to understand how the addition of this dopant influences: i) the grain size and density of the fuel, ii) the

chemical coordination of the Cr in the UO_2 matrix, and iii) the kinetics and mechanisms of oxidative dissolution. In this contribution, we describe the synthesis and characterisation of Cr_2O_3 -doped UO_2 , in addition to future plans for dissolution studies. In literature the preparation of the modern fuel is not fully detailed by the nuclear companies, this is why in this work several dopant amounts and different synthesis routes were used to prepare samples.

2 Sample preparation and characterisation

2.1 Sample preparation

Uranium dioxide materials doped with Cr_2O_3 were prepared by four synthesis routes: (i) a dry synthesis method where UO_2 powder was mixed with varying amounts of Cr_2O_3 powder; two wet synthesis routes using (ii) oxalic precipitation and (iii) nitrate precipitation, and finally, (iv) synthesis by hot isostatic pressing of materials produced in synthesis route (iii).

Oxalic precipitation was achieved by mixing uranium (IV) chloride with chromium (III) chloride in solution. An excess of oxalic acid solution was added, and the precipitate was formed instantaneously to obtain a uranium (IV)/chromium (III) oxalate hexahydrate precursor. The nitrates precipitation method uses a mixture of uranium (VI) nitrate hexahydrate solution with a solution of chromium (III) nitrate nonahydrate. An excess of concentrated ammonium hydroxide solution was slowly added allowing the precipitation of a uranium (VI)/chromium (III) nitrates precursor. Precipitate obtained by both wet synthesis routes were filtered, washed and dried. Synthesised precursors were heat treated for 4 h at 750°C under reducing atmosphere ($\text{N}_2 / 5\% \text{H}_2$) to allow conversion to oxide. Dense pellets of uranium dioxide doped with different concentrations of chromium, synthesised via the three different routes, were then milled and sintered. Sintering was performed for 8 hours at 1700°C under a reducing atmosphere ($\text{N}_2 / 5\% \text{H}_2$).

2.2 Characterisation

The stoichiometry of samples was determined by Inductively Coupled Plasma- Optical Emission Spectroscopy (ICP-OES) analysis of the supernatant collected during the wet synthesis washing step and after full dissolution of an aliquot of the powder in aqua regia. The morphology and the grain size of UO_2 oxides doped with additives were characterised by Scanning Electron Microscopy (SEM). Back Scattered Electron (BSE) images were recorded using a Hitachi TM3030 SEM operating with an accelerating voltage of 15 kV. X-ray Diffraction (XRD) analyses were performed using a Bruker D2 Phase diffractometer utilizing a $\text{Cu K}\alpha$ source. Measurements were taken from 10° to $100^\circ 2\theta$ with a step size of 0.02° and 2 s counting time per step.

The densification rate was determined by geometric measurements. Raman measurements were performed using a Renishaw In via Reflex confocal spectrometer equipped with a Leica DM2500 microscope, using a 514 nm (green) argon excitation laser with $1800 \text{ lines}\cdot\text{mm}^{-1}$ grating acquiring a spectral acquisition between 200 and 750 cm^{-1} . The chromium oxidation state and co-ordination was determined by Cr K-edge (5989 eV) XANES at Beamline B18 of the Diamond Light Source (UK). Data were acquired in fluorescence mode and samples were measured alongside Cr standards of well-defined oxidation state and co-ordination environment.

3 Results

3.1 Synthesis route selection

Comparison of the morphology of Cr-doped UO_2 prepared via the (i), (ii) and (iii) synthesis routes showed that the highest density and grain size was obtained using the dry synthesis route (Figure 1). However, due to the difficulty in accurately weighing small amounts of Cr_2O_3 , the Cr content was far from intended and it was not possible to obtain the desired stoichiometry. The wet precipitation routes were highly effective in obtaining the correct Cr-content, although the oxalic precipitation route produced materials that did not change their grain size or density as a function of Cr-dopant concentration (data not shown). For this reason, the nitrates precipitation method was selected as the most appropriate to prepare samples for further analysis and synthesis (e.g. by hot isostatic pressing); all of the following results detailed were obtained on samples prepared via this synthesis route.

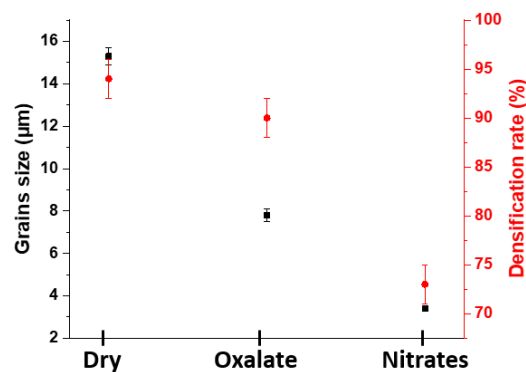


Figure 1: Evolution of the grain size (■) and the density (●) of UO_2 doped with 1500 ppm Cr as a function of synthesis route.

3.2 Cr-doped UO_2 characterisation

The evolution of the grain size and the density of Cr-doped UO_2 , as a function of dopant concentration (0 to 5000 ppm) is presented in Figure 2. An increase of the grain size and the density was observed between 0 and 300 ppm Cr. Above 300 ppm, the grain size decreased but remained fairly constant between 600 ppm and 2500 ppm. Above this concentration, the grain growth was significantly limited and, at 5000 ppm, the grain size was comparable to UO_2 with no Cr-dopant.

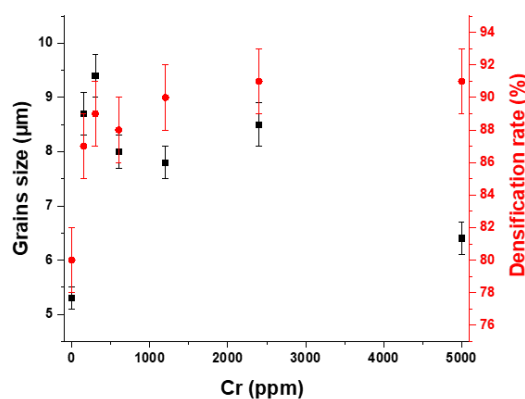


Figure 2: Evolution of the grain size (■) and the density (●) as a function of Cr-dopant concentration in UO_2 .

X-Ray Diffraction patterns confirmed that the samples prepared *via* the nitrate precipitation route crystallised in the fluorite structure (space group $Fm\bar{3}m$), characteristic of UO_2 (Figure 3a). Supplementary peaks linked to the presence of Cr were not observed, indicating incorporation of Cr in the UO_2 fluorite structure. The peak positions were observed to alter as a function of Cr-content, as highlighted in Figure 3b. At 150 and 300 ppm of Cr, the (111) peak was shifted to the left when compared with UO_2 , corresponding to an increase of the UO_2 lattice parameter. With Cr contents of > 600 ppm, the (111) peak was generally observed to shift to the right, indicating a decrease of the lattice parameter. The decrease of the lattice parameter during the incorporation of a trivalent element in a dioxide solid solution to create a IV/III system has already been reported [17, 18]. The radius of the Cr^{3+} ion (0.615 Å) is smaller than that of U^{4+} (1.03 Å) so that when the U^{4+} ion is substituted by Cr^{3+} , a decrease of the lattice parameter of UO_2 should be expected. The modification in the lattice parameter evolution observed between 300 and 600 ppm Cr might be explained by the incorporation of Cr in a different valence state.

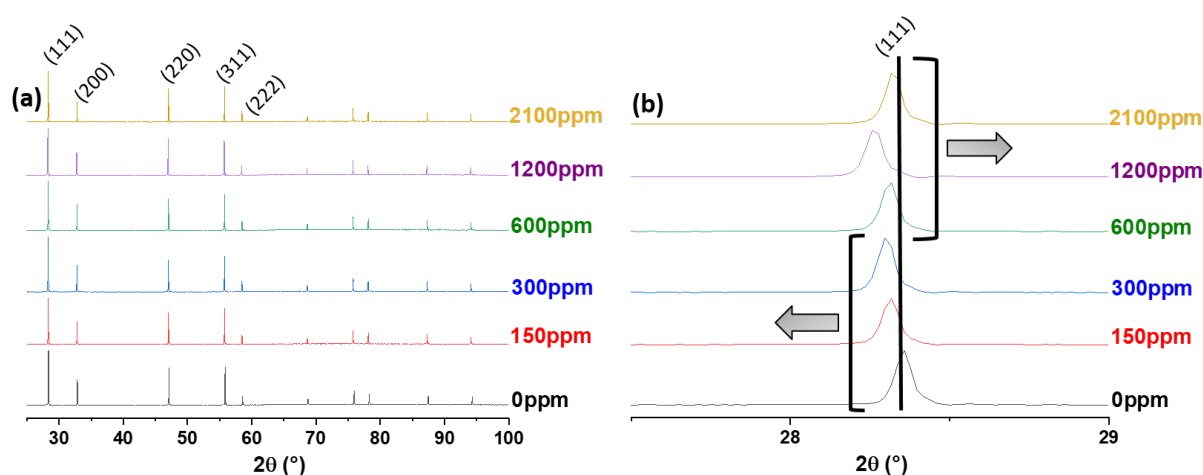


Figure 3: XRD patterns recorded for Cr-doped UO_2 from (a) 20° to 100° 2θ , and (b) focus on the (111) peak.

Raman spectroscopy, focusing on the region between 300 to 750 cm^{-1} , which contains a peak at 445 cm^{-1} relating to the symmetric T_{2g} vibration mode for UO_2 [19, 20], showed that, as Cr content was increased a second peak was observed at 575 cm^{-1} (Figure 4a). The incorporation of Cr^{3+} in UO_2 as substitute of U^{4+} ion creates structural defects, such as oxygen vacancies, oxygen interstitials, and changes in cubic cell symmetry. In Figure 4b, area and height ratios between the T_{2g} and the LO bands can be described as a defect ratio. When the Cr content is lower than 600 ppm the slope in Figure 4b is high which shows that there is a strong increase in the quantity of defects. Between 600 ppm and 1200 ppm of Cr, the slope seems to decrease, which would indicate a smaller rate of increase in the amount of defects compared with Cr contents lower than 600 ppm.

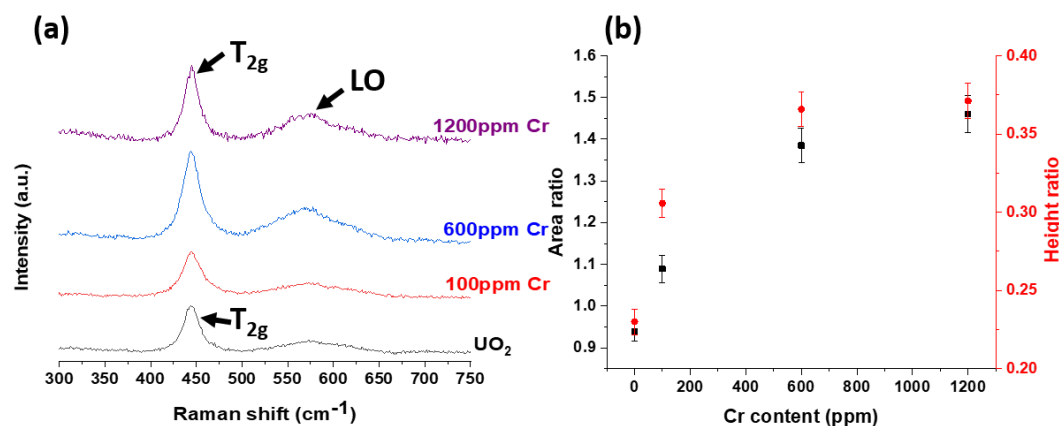


Figure 4: Raman spectroscopy patterns of Cr-doped UO₂ (a) at four Cr concentrations, and (b) showing the area (■) and height ratio (●) between T_{2g} and LO band (obtained from (a)) as a function of Cr-dopant content.

The oxidation state and local co-ordination of Cr in Cr-doped UO₂ samples were measured by X-ray Absorption Spectroscopy. The Cr-K edge X-ray Absorption Near Edge (XANES) spectra for UO₂ doped with between 300 and 2400 ppm of Cr is compared with Cr⁰ and Cr³⁺ standards in Figure 5. Preliminary analysis of these data by linear combination fitting to Cr⁰ and Cr³⁺ standards show that the coordination environment of Cr changes with increasing dopant concentration, with concentrations of < 600 ppm Cr containing more Cr⁰-like environments and those containing > 600 ppm Cr containing more Cr³⁺-like environments. Data pertaining to the full EXAFS region were collected and are currently under analysis to determine the coordination environment and nearest neighbours of Cr in UO₂ as a function of concentration.

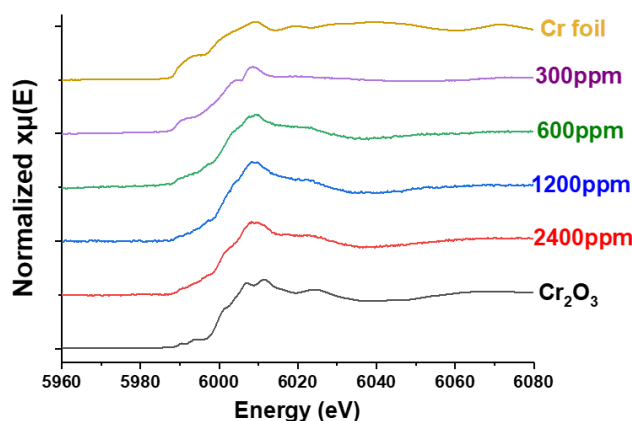


Figure 5: Cr K-edge XANES spectra of Cr-doped UO₂ at Cr concentrations from 300 to 2400 ppm and two standards Cr foil (Cr⁰) and Cr₂O₃ (Cr³⁺).

3.3 Discussion

All characterisations described above highlight a change in the behaviour of Cr when it is incorporated to the UO₂ matrix, dependent on the amount of Cr added, as summarised in Figure 6. These trends are described, and justified, herein.

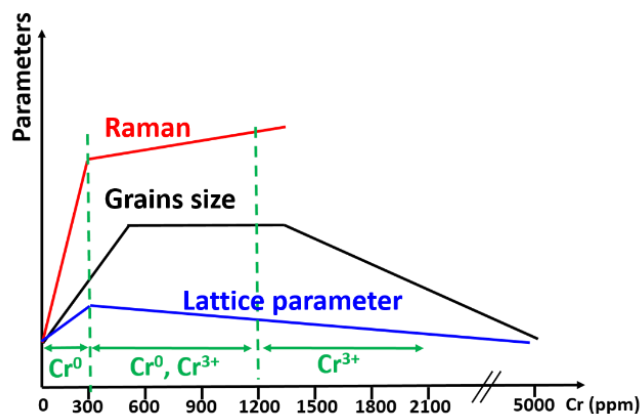


Figure 6: Schematic summary of the different characterizations performed.

Below 600 ppm of Cr, the XANES measurements showed that Cr was present in UO_2 as reduced Cr (possibly as Cr^0 , Cr^{1+} or Cr^{2+} ongoing analysis of EXAFS region will be used to support this assignment). Because reduced Cr has a larger radius (e.g. Cr^0 , 1.29 Å) than that of U^{4+} (1.03 Å), an expansion in the UO_2 lattice was observed in XRD patterns (Figure 3). Furthermore, the incorporation of chromium reduced form in the UO_2 lattice will create oxygen vacancies which can also explain the increase of the lattice size. Raman spectroscopy showed that at Cr concentrations of < 600 ppm, there was a rapid increase in the presence of structural defects, which may be due to interferences on the U-O bond induced by the presence of reduced Cr on U interstitial sites. This rapid increase in the presence of structural defects can also be explain by the presence of the oxygen vacancies induced by the incorporation of a chromium reduced in the UO_2 lattice. Many studies of Cr-doped UO_2 have reported that Cr is incorporated into UO_2 as Cr^{3+} [2, 5-6, 21-23], however, the present results are in agreement with Cooper et al. [24], who performed *ab initio* defect calculations for Cr-doped UO_2 , allowing the dopant to change charge state. They found that in their modelled Cr-doped UO_2 , significant quantities of Cr were present at the uranium interstitial site, as Cr^{1+} . It should be noted that the availability of hyper-stoichiometric defects in UO_2 is highly dependent on the $p\text{O}_2$ of the sintering atmosphere, therefore, the resulting Cr incorporation mechanism is anticipated to change with $p\text{O}_2$ [22], which may explain the differences between the present work and that reported in the literature.

As the Cr content was increased above 600 ppm, the XANES data (Figure 5) indicate a change in Cr oxidation state to higher valence (similar to Cr^{3+}). This is supported by XRD data, which show a decrease in the lattice parameter relative to samples doped with 150 and 300 ppm Cr. As discussed previously, such behaviour would arise from the incorporation of a dopant with smaller ionic radius than U^{4+} , such as Cr^{3+} . Because the structural defect concentration, as determined by Raman Spectroscopy, was observed to grow more slowly than for Cr concentrations of < 600 ppm, we hypothesise that once the U interstitial sites become completely occupied by reduced Cr clusters, the addition of further Cr results in the formation of oxygen vacancies, commensurate with the incorporation of Cr^{3+} within the UO_2 matrix as a solid solution. Further work is required to confirm this hypothesis.

There was an increase in the grain size of Cr-doped UO_2 from 0 to 300 ppm of Cr and, between 600 ppm and 1200 ppm Cr, the grain size remained constant (within error). Between 1200 and

2100 ppm of Cr, the grain size decreased. At 2100 ppm Cr, Cr₂O₃ agglomerates were observed in SEM / EDX analysis (data not shown), which limit grain growth. Therefore, the limit of solubility of the chromium in uranium dioxide, seems to be between 1200 and 2100 ppm of chromium. This is broadly in agreement with published values of Cr solubility within the UO₂ matrix, of 700 - 1000 ppm Cr (e.g. [22] and references therein).

3.4 Further work: Dissolution of Cr-doped UO₂

The dissolution rate and behaviour of Cr₂O₃-doped UO₂ prepared by the nitrate and Hot Isostatic Pressing (HIP) routes is underway. Pelletised UO₂ samples containing 0, 300, 600, 1200, 1800 and 2400 ppm Cr were placed in 60 mL Teflon vessels. Each vessel was filled with 50 mL of a synthetic ground water (1 mM NaHCO₃ + 19 mM NaCl). Duplicate samples, plus blanks, were placed in an oven at 30°C and 60°C. Periodic sampling, for a minimum of 28 days, will be performed and solutions analysed by Inductively Coupled Plasma-Mass Spectroscopy (ICP-MS).

Acknowledgements

The research leading to these results has received funding from the European Commission Horizon 2020 Research and Training Programme of the European Atomic Energy Community (EURATOM) (H2020-NFRP-2016-2017-1) under grant agreement n° 755443 (DisCo project).

References

- [1] Lindback, J.E. (2003). Advanced fuel pellet materials and designs for water cooled reactors. IAEA TECDOC-1416, 101-110.
- [2] Bourgeois, L., Dehaut, P., Lemaignan, C., Hammou, A. (2001). Factors governing microstructure development of Cr₂O₃-doped UO₂ during sintering. *Journal of Nuclear Materials*, 297, 313-326.
- [3] Kashibe, S. and Une, K. (1998). Effect of additives Cr₂O₃, Al₂O₃, SiO₂, MgO on diffusional release of ¹³³Xe from UO₂ fuels. *Journal of Nuclear Materials*, 254(2-3), 234-242.
- [4] Killeen, J.C. (1980). Fission gas release and swelling in UO₂ doped with Cr₂O₃. *Journal of Nuclear Materials*, 88, 177-184.
- [5] Leenaers, A., De Tollenaere, L., Delafoy, C., Van den Berghe, S. (2003). On the solubility of chromium sesquioxide in uranium dioxide fuel. *Journal of Nuclear Materials*, 317, 62-68.
- [6] Cardinaels, T., Govers, K., Vos, B., Van Den Berghe, S., Verwerft, M., De Tollenaere, L., Maier, G., Delafoy, C. (2012). Chromia doped UO₂ fuel: Investigation of the lattice parameter. *Journal of Nuclear Materials*, 424, 252-260.
- [7] Arborelius, J., Backman, K., Hallstadius, L., Limbaeck, M., Nilsson, J., Rebensdorff, B., Zhou, G., Kitano, K., Loefstroem, R., Roenberg, G. (2006). Advanced doped UO₂ pellets in LWR applications. *Journal of Nuclear Science and Technology*, 43, 967-976.
- [8] Kim, D. (2007). Effect of sintering on the grain growth of an Al-doped UO₂ pellet. *Proceedings of the Transactions of the Korean Nuclear Society Spring Meeting*.
- [9] Kim, D. (2006). Effect of small amounts of aluminium doping on the grain growth of a UO₂ pellet. *Proceedings of the Transactions of the Korean Nuclear Society Spring Meeting*.

- [10] Costa, D.R. (2017). Thermal stability test of UO₂-doped pellet manufactured at INB. International Nuclear Atlantic Conference - INAC 2017.
- [11] Backman, K., Hallstadius, L., Rönnberg, G. (2010). Westinghouse advanced doped pellet - Characteristics and irradiation behaviour. IAEA-TECDOC-1654.
- [12] Cooper, M.W.D., Gregg, D.J., Zhang, Y., Thorogood, G.J., Lumpkin, G.R., Grimes, R.W., Middleburgh, S.C. (2013). Formation of (Cr,Al)UO₄ from doped UO₂ and its influence on partition of soluble fission products. *Journal of Nuclear Materials*, 443, 236-241.
- [13] He, H., Qin, Z., Shoesmith, D.W. (2010). Characterizing the relationship between hyperstoichiometry, defect structure and local corrosion kinetics of uranium dioxide. *Electrochimica Acta*, 56, 53-60.
- [14] Corkhill, C.L., Bailey, D.J., Tocino, F.Y., Stennett, M.C., Miller, J.A., Provis, J.L., Travis, K.P., Hyatt, N.C. (2016). Role of microstructure and surface defects on the dissolution kinetics of CeO₂, a UO₂ fuel analogue. *ACS Applied Materials & Interfaces*, 8, 10562-10571.
- [15] Cordara, T., Szenknect, S., Claparede, L., Podor, R., Mesbah, A., Lavalette, C., Dacheux, N. (2017). Kinetics of dissolution of UO₂ in nitric acid solutions: A multiparametric study of the non-catalysed reaction. *Journal of Nuclear Materials*, 496, 251-264.
- [16] Bellière, V., Joorst, G., Stephan, O., De Groot, F.M.F., Weckhuysen, B.M. (2006). Phase segregation in cerium - Lanthanum solid solutions. *The Journal of Physical Chemistry B*, 110(20), 9984-9990.
- [17] Horlait, D., Claparède, L., Clavier, N., Szenknect, S., Dacheux, N., Ravaux, J., Podor, R. (2011). Stability and structural evolution of Ce^{IV}_{1-x}Ln^{III}_xO_{2-x/2} solid solutions: A coupled μ -Raman/XRD approach. *Inorganic Chemistry*, 50(15), 7150-7161.
- [18] Sung, J., Kil, W., Hee, C. (2004). The crystal structure of ionic conductor La_xCe_{1-x}O_{2-x/2}. *Journal of the European Ceramic Society*, 24(6), 1291-1294.
- [19] Desgranges, L., Baldinozzi, G., Rousseau, G., Nièpce, J.C., Calvarin, G. (2009). Neutron diffraction study of the in situ oxidation of UO₂. *Inorganic Chemistry*, 48, 7585-7592.
- [20] Böhler, R., Quaini, A., Capriotti, L., Çakır, P., Beneš, O., Boboridis, K., Guiot, A., Luzzi, L., Konings, R.J.M., Manara, D. (2014). The solidification behaviour of the UO₂ - ThO₂ system in a laser heating study. *Journal of Alloys and Compounds*, 616, 5-13.
- [21] Kuri, Z., Mieszczyński, C., Martin, M., Bertsch, J., Borca, C.N., Delafoy, C., Simioni, E. (2014). Local atomic structure of chromium-bearing precipitates in chromia doped uranium dioxide investigated by combined micro-beam X-ray diffraction and absorption spectroscopy. *Journal of Nuclear Materials*, 449, 158-167.
- [22] Riglet-Martial, Ch., Martin, Ph., Testemale, S., Sabithier-Devals, C., Carlot, G., Matheron, P., Iltis, X., Pasquet, U., Valot, C., Delafoy, C., Largenton, R. (2014). Thermodynamics of chromium in UO₂ fuel: A solubility model. *Journal of Nuclear Materials*, 447, 63-72.
- [23] Peres, V., Favergeon, L., Andrieu, M., Palussière, J.C., Balland, J., Delafoy, C., Pijolat, M. (2012). High temperature chromium volatilisation from Cr₂O₃ powder and Cr₂O₃-doped UO₂ pellets in reducing atmospheres. *Journal of Nuclear Materials*, 423, 93-101.
- [24] Cooper, M.W.D., Stanek, C.R., Andersson, D.A. (2018). The role of dopant charge state on defect chemistry and grain growth of doped UO₂. *Acta Materialia*, 150, 403-413.

Optical examination of wetted long-stored uranium dioxide fuel

Goode, J. and Hambley, D.

National Nuclear Laboratory (NNL), Central
Laboratory, Sellafield (UK)

1 Introduction

In 2013 a number of cans of fuel from the UK's experimental Windscale Advanced Gas-Cooled Reactor (WAGR) were recovered from storage for repackaging. All cans were found to have filled with water and modelling indicates that the cans would have been flooded for in excess of 40 years. After repackaging the majority of fuel was returned to pond storage however a number of fuel sections from two different cans were retained for examination because they would provide evidence of the long-term effects of water storage on uranium dioxide fuel. As part of the DisCo project NNL have committed to carry out optical and electron microscopy on some of these fuel sections

2 Fuel identification

Records indicated that the retained fuel was from cans containing the remains of pins that underwent post irradiation examination (PIE) in the 1960's. Records also suggested that the burnup of these pins varied from 5 - 20 GWd·teU⁻¹ and had different geometries, since WAGR was an experimental reactor used to trial different fuel designs. Despite having a somewhat lower burnup than current fuel, the highest burn-up section of the recovered fuel (20 GWd teU⁻¹) fuel was felt to be the most valuable. This fuel is also geometrically similar to modern LWR fuel (~ 10 mm diameter). It was also considered to be worthwhile to examine a section of fuel which was geometrically similar to modern CAGR (Civil Advanced Gas-cooled Reactor) fuel (~ 15 mm diameter with a hollow bore) even though it was of lower burn-up.

Interrogation of the original PIE records indicated that the high burn fuel recovered came from stringer 4 of irradiation experiment 221B (IE 221B/4). Unfortunately, the can also contained sections of fuel pin from stringer 2 of the same irradiation experiment which contained identical fuel pins but were removed with a burnup of only ~ 5 GWd·teU⁻¹. It was therefore necessary to carry out gamma spectroscopy to identify the high burnup pins.

For completeness all 18 of the recovered fuel sections underwent spot gamma spectroscopy (Figure 1) and a low power visual examination. In order to identify the pin section most likely to have been wetted, the higher burn-up fuel sections underwent axial gamma scans to reveal any indications of caesium loss due to water leaching (Figure 2). From the axial gamma scan of high burnup (HBU) pin section B206/41/C11 (C11) it was possible to see evidence of apparent caesium leaching at the wetted ends, the presence of a Sintox pellet and some clearly defined pellet-pellet interfaces (PPI). The axial gamma scan of hollow pin B206/41/C5 (C5) showed no variation of gamma intensity most likely because the bore had allowed water access along the entire length of the fuel sections and almost equal

leaching along the pin length. PPI's were not discernible in this pin although the anti-stacking grooves (ASG) are evident. Pin C11 had only one ASG however since the groove was in the Sintox pellet it is not apparent.

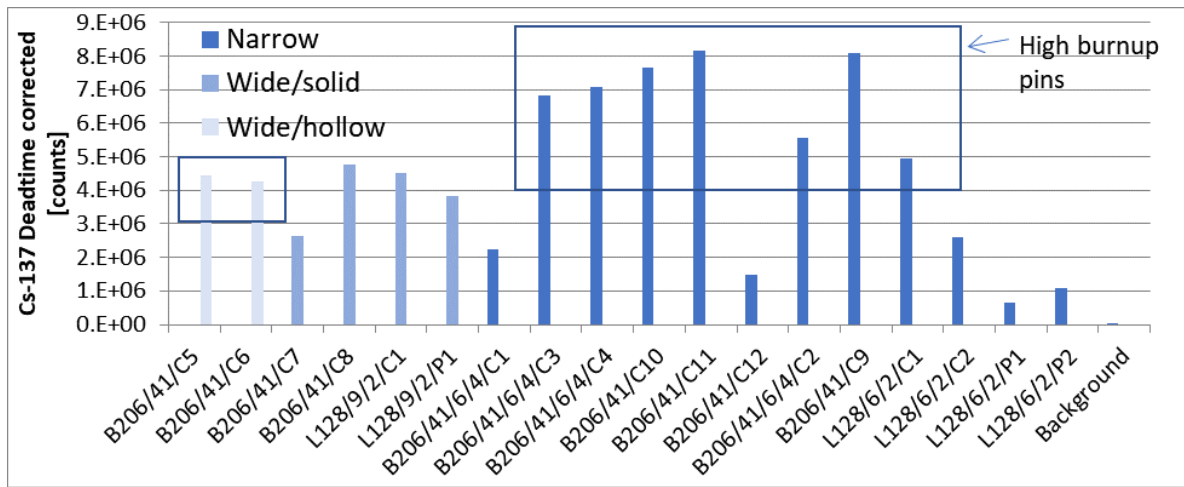


Figure 1: Spot gamma spectroscopy of fuel pins recovered from extended pond storage.

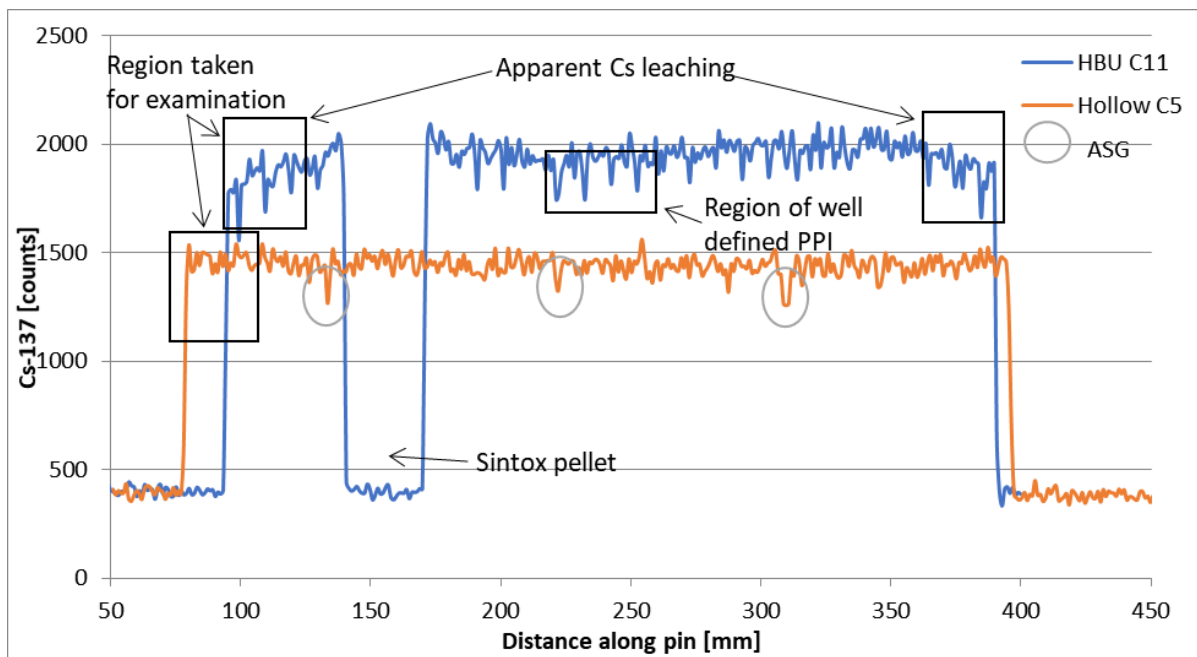


Figure 2: Axial gamma scans of the two sections examined showing some well defined pellet-pellet interfaces (PPI), anti stacking grooves (ASG), caesium leaching and the regions selected for examination.

Images of the two sections examined are shown in Figure 3 and Figure 4 below.

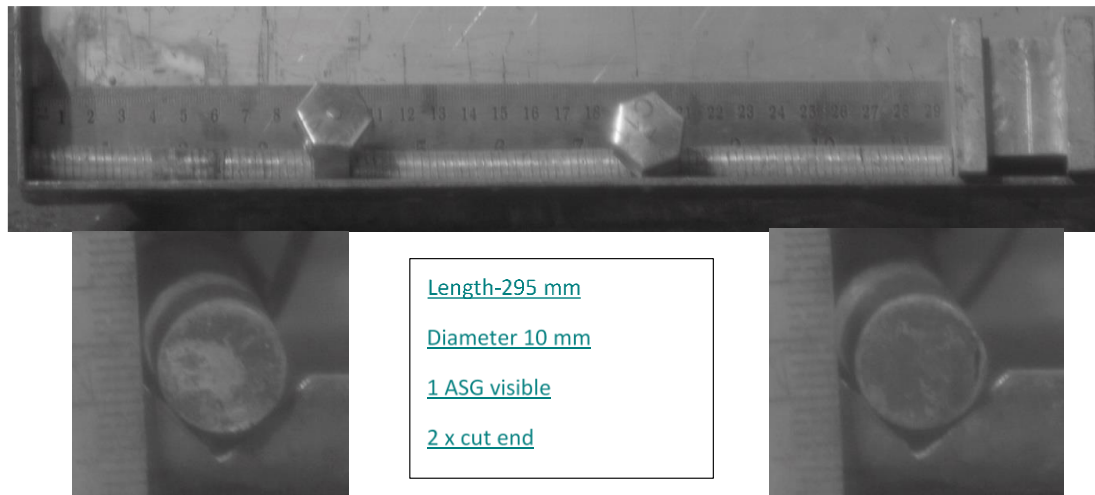


Figure 3. High burnup pin C11.

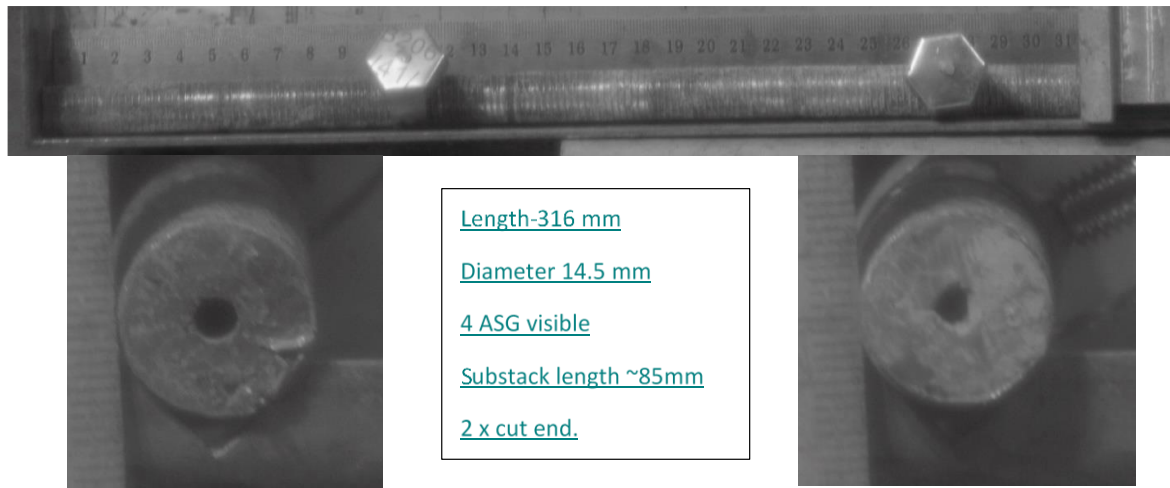


Figure 4. Hollow pin C5.

3 Optical Examination

The regions of pins C11 and C5 mounted for optical examination are shown in Figure 2. These sections were mounted in resin and the examined by light microscopy in the as polished state (AP), after a fuel etch in a mixture of sulphuric acid and hydrogen peroxide and after a cladding etch in oxalic acid.

Figure 5 shows the wetted and non-wetted ends of the section cut from high burnup pin C11 in the AP state and following a fuel etch. There is no evidence of increased oxidation at the wetted compared to the non-wetted end. The same results were obtained for hollow pin C5 which is shown in Figure 6. None of the samples showed any evidence of the microstructural features often seen when higher oxides (U_3O_7/U_3O_8) are present¹. There was a small amount of interlinked intergranular porosity around the PPI/pellet bore of the hollow pin C5 (Figure 7) however this was not deemed to be significant compared to the overall results.

¹ While higher oxides cannot be seen directly with light microscopy previous work has shown that after etching, microstructural features are evident which have after EDX/WDX have been found to be higher oxides.

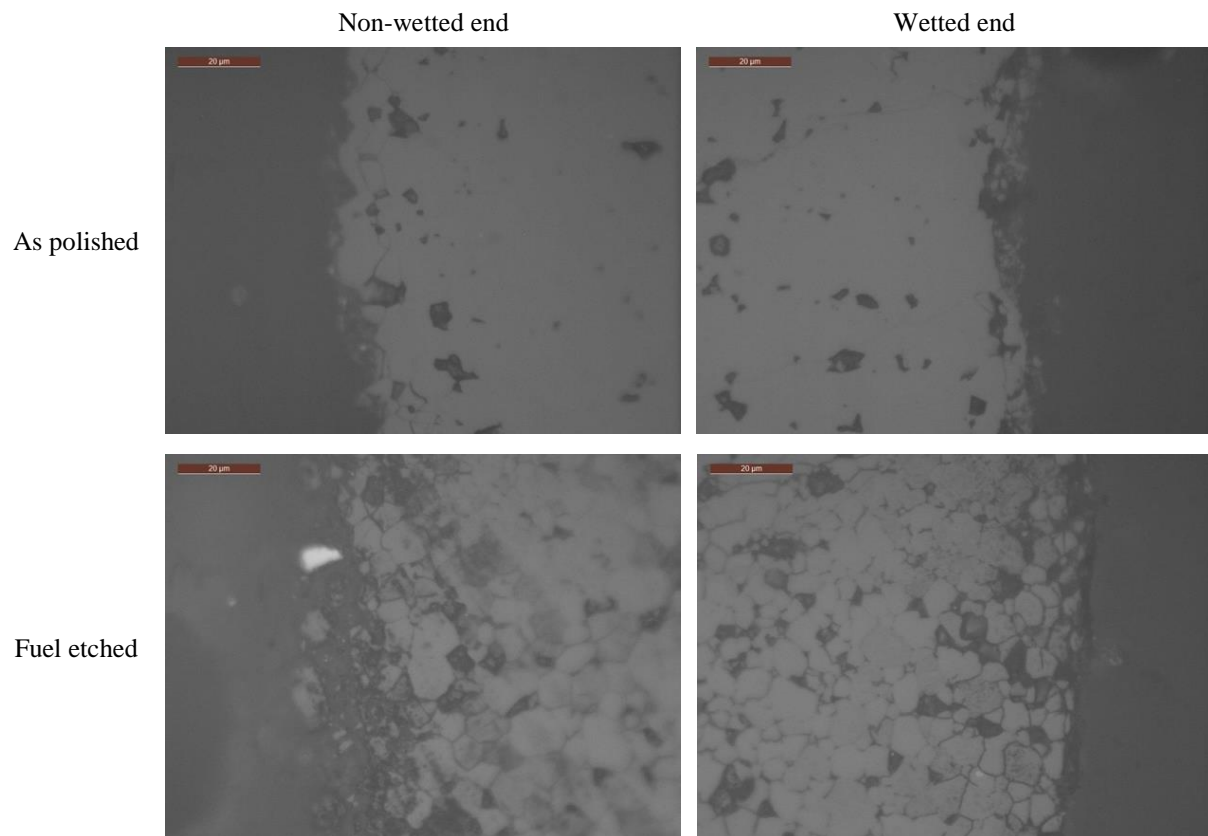


Figure 5: Non wetted and wetted ends of solid pellet pin C11 (element burnup of $27.1 \text{ GWd} \cdot \text{teU}^{-1}$).

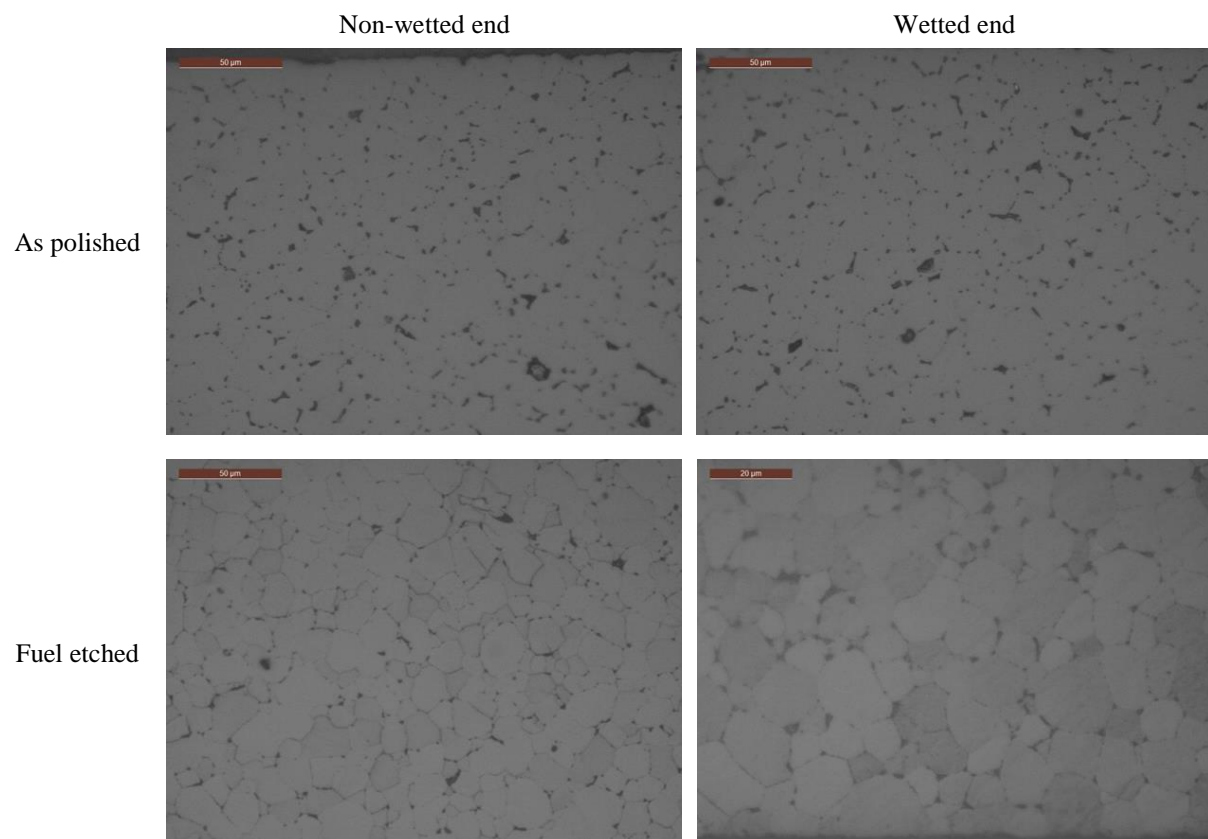


Figure 6: Non-wetted and wetted ends of hollow pin C5 (element burnup of $8.9 \text{ GWd} \cdot \text{teU}^{-1}$).

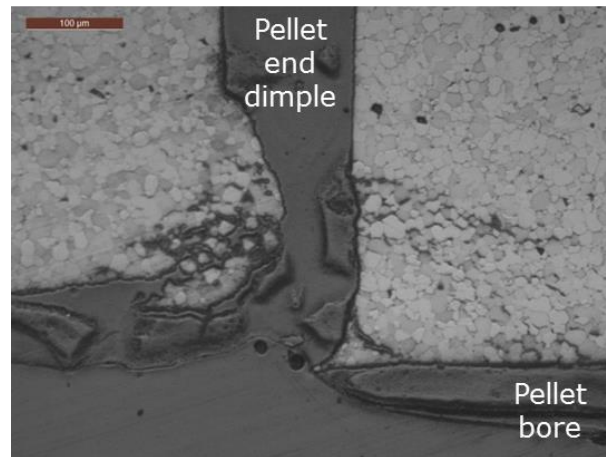


Figure 7: Interlinked intergranular porosity in hollow pin C5.

Figure 8 shows images of the fuel microstructure now and in the 1960's during the original PIE. There is no evidence of significantly increased oxidation or degradation.

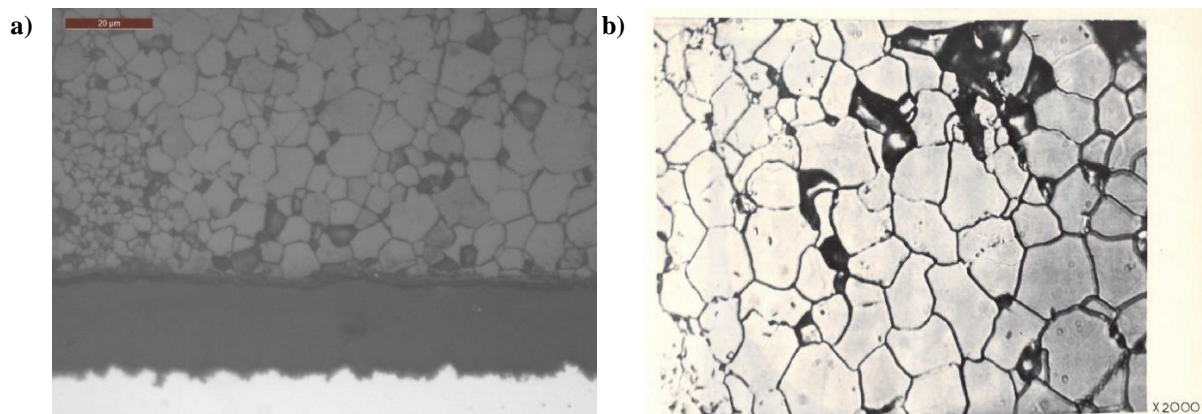


Figure 8: Fuel microstructure from solid fuel pin C11 (a) recent examination and (b) historic examination [1].

The cladding appeared as expected based on the irradiation conditions and appeared to have changed little compared to images taken during the original PIE in the 1960's (Figure 9).

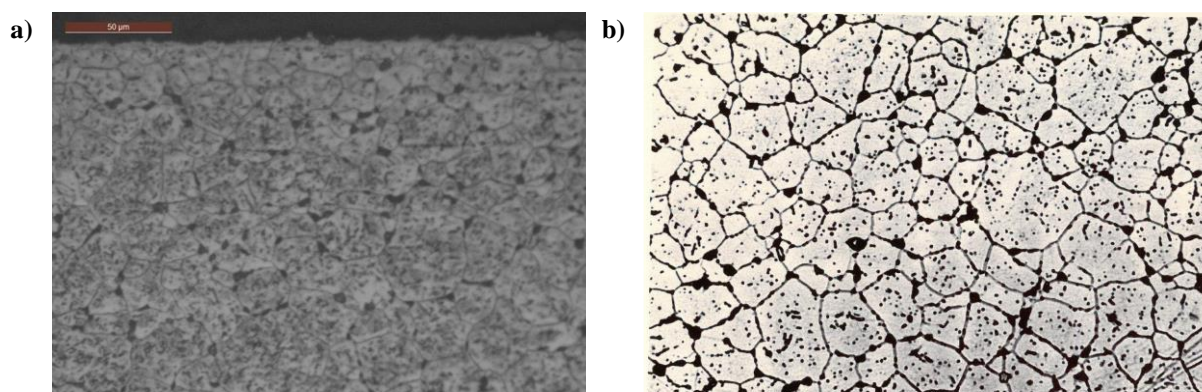


Figure 9: Cladding from high burnup pin C11 (a) recent examination and (b) historic examination [1].

It was however noted that the oxide layer was almost entirely absent, being seen in only one small region on HBU pin C11 while a typical oxide layer is present on hollow pin C5 (Figure 10).

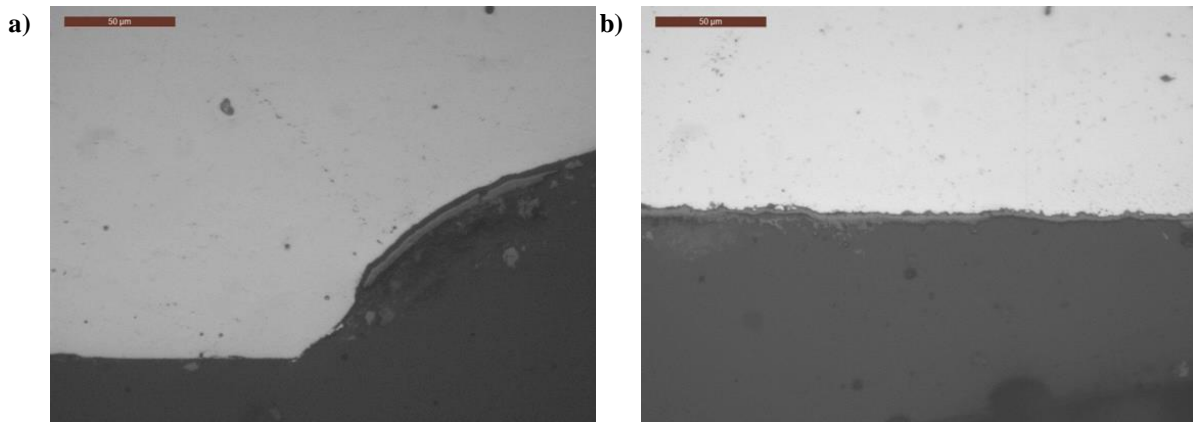


Figure 10: The one region of cladding oxide remaining solid pin C11 (a) and the normal oxide observed on hollow pin C5 (b).

4 Conclusions

Light optical microscopy of uranium dioxide fuel which is known to have been wetted for in excess of 40 years shows no evidence of degradation as a result of contact with water with both wetted and non-wetted sections appearing to be much the same. Comparison of images collected today, with those collected in the 1960's shows no significant difference despite there being an apparent loss of caesium from some sections.

5 Further Work

Small “matchstick” sections of fuel have been prepared from the adjoining regions of the pins seen in here. These will be examined by secondary electron microscopy/wavelength dispersive X-ray spectroscopy and Raman microscopy at a later date to confirm the absence of higher oxides.

Acknowledgement

The research leading to these results has received funding from the European Commission Horizon 2020 Research and Training Programme of the European Atomic Energy Community (EURATOM) (H2020-NFRP-2016-2017-1) under grant agreement n° 755443 (DisCo project).

References

- [1] Nairn, J.S., Skinner, J., Bradshaw, K.A. (1970). Post-irradiation examination of Windscale AGR fuel elements. Progress Report No. 42. UKAEA.

Development of a matrix dissolution model for the prediction of activity release from used fuel in long term storage

Hughes, R.J., Goode, J.B, Hambley, D.I.

National Nuclear Laboratory (NNL), Central
Laboratory, Sellafield (UK)

1 Introduction

Understanding activity releases caused by fuel matrix dissolution will be important in underpinning the safety cases for long term storage and disposal of spent fuels. An appropriate mechanistic model will enable the extrapolation of data generated by short term tests to longer timescales and to look for potential deviations in behaviour arising from changes in the local environment. In a disposal context this can be used to account for evolution of the repository environment and in pond storage it could be used to identify the characteristics of different containment failure modes and to understand what environmental conditions could result in a significant increase in fuel dissolution and activity release.

Over the past two years NNL has been developing a fuel dissolution model suitable for such tasks. The work funded under the EU DisCo programme is focussed on understanding the sources of uncertainties in the model and to examine the application of the models, which were developed for near neutral systems (pH 6-9) to higher pH environments (11-13) relevant to high pH pond storage regimes at Sellafield and potentially for early containment failure in repository.

2 Model development

In the 2017/18 financial year a literature review of matrix dissolution modelling approaches was undertaken. Mixed-potential modelling is mechanistic in nature and should allow the simulation of a range of conditions and scenarios when provided with sufficient input data. These include long-term storage of used fuel in a geological disposal facility as well as interim pond storage of fuels prior to final disposal. This review concluded that developing an electrochemical mixed potential model based on previous work by Canadian and American national laboratories [1-5] was the optimal approach for implementation in gPROMS process modelling framework used by NNL for advanced simulations.

Consideration was also given to options for interfacing such a model with the geochemical modelling code PHREEQ-C as a means of leveraging well established thermodynamic datasets for use in this application. However, prior experience within NNL showed that interfacing of PHREEQ-C with gPROMS in this particular application would likely prove untenable. This is because the runtime of the model would be significantly impacted by the communication between the packages. When looking to model over timescales of 1000's of years, model efficiency is of paramount importance.

During the 2018/19 financial year, a mixed potential model has been successfully implemented to model the dissolution of the fuel matrix of uranium dioxide ceramic fuel when exposed to water and

the congruent release of radionuclides as the fuel matrix dissolves. It does not attempt to address the separate release of radionuclides segregated from the fuel matrix, which are known to be released rapidly from the fuel surface on first contact with water. These rapid releases, known as the instant release fraction, require a different approach and are outside the scope of this activity. In annular fuel there can be a significant axial migration of volatile fission products released from the fuel whilst in reactor and treatment of this inventory is also outside the scope of this activity.

To model the matrix dissolution of uranium dioxide spent fuel using electrochemical approaches, the following have been identified as important [1-4]:

- Oxidative dissolution
- Chemical dissolution¹
- Diffusion of species to and from the fuel surface
- Precipitation of solids on the fuel surface
- Aqueous reactions (including the effects of iron and dissolved ground water species)
- Radiolysis of water near the fuel surface
- The effects of noble metal particles

A detailed assessment of the methods used to model these phenomena in existing literature was undertaken to identify the most significant uncertainties in the input parameters and the most important assumptions and simplifications that affect the reliability of the model.

3 Model comparison and discussion

The results of the NNL model were compared with previous literature models [3, 4] for identical conditions for the purposes of verifying the code implementation. In general, the overall agreement could be said to be good. These comparisons are made in figures from Figure 1 to Figure 6², for previous literature model runs of types A, B and C.

Model runs, type A:

- No H₂ or Fe present
- No noble metal particles present
- No precipitate present and no precipitation/dissolution reactions
- A boundary condition of constant bulk concentrations
- Varying hydroxide concentration
- A fixed temperature and carbonate concentration

¹ For completeness, although this is not anticipated to be significant in repository environments.

² Some of the graphs shown in figures 1-6 show experimental results which the original authors compared to their models. However, the conditions in which these experimental results were obtained is not clear from the available papers. Hence no comment is passed on these results.

Three cases of this type were run:

1. 25°C with no carbonate present (black lines in Figure 1 and Figure 2)
2. 25°C with 0.1 M Carbonate present (blue lines in Figure 1 and Figure 2)
3. 50°C with no carbonate present (brown line in Figure 1)

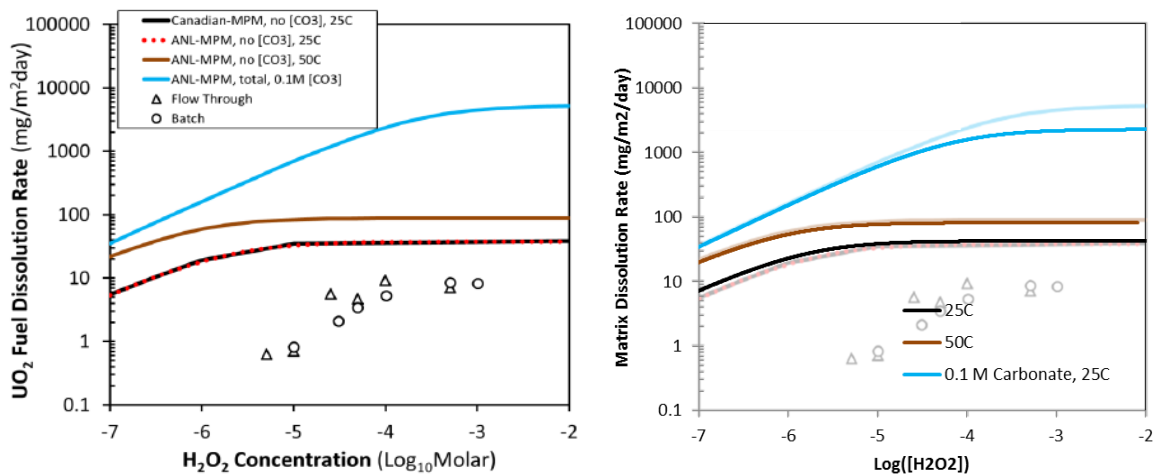


Figure 1: Comparison of dissolution rate predicted in literature (*left*) vs. NNL model (*right*) [3] - Model type A.

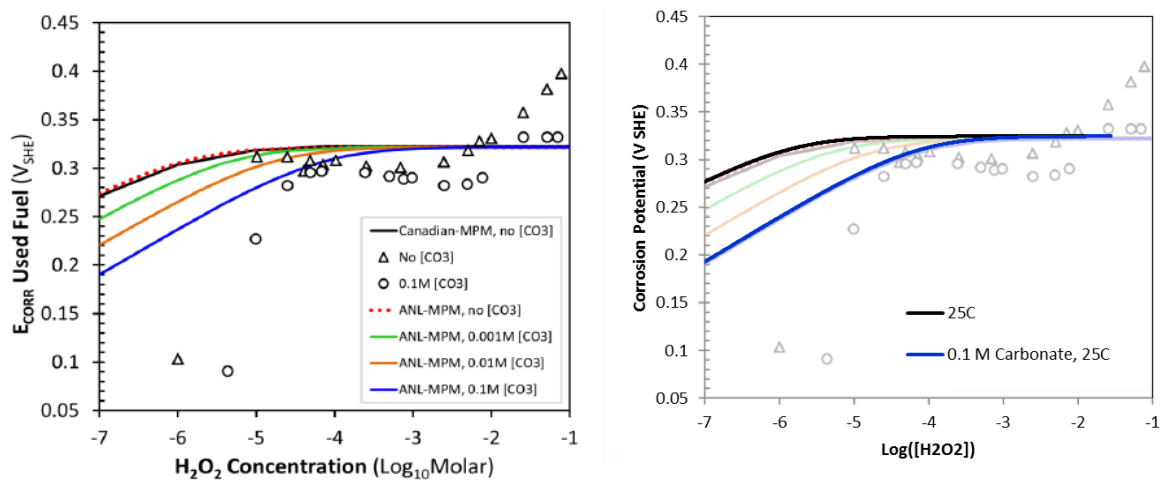


Figure 2: Comparison of corrosion potential predicted in literature (*left*) vs. NNL model (*right*) [3] - Model type A.

Model runs, type B:

- No H₂ or Fe present
- No noble metal particles present
- No precipitate present and no precipitation/dissolution reactions
- A boundary condition of constant bulk concentrations
- Varying carbonate concentration
- A fixed hydroxide concentration ($1 \cdot 10^{-7}$ M) and temperature

Three cases of this type were run:

1. 25°C (light blue line in Figure 3)
2. 50°C (dark blue line in Figure 3)
3. 50°C, but only including oxidative dissolution caused by the presence of carbonate (red line in Figure 3)

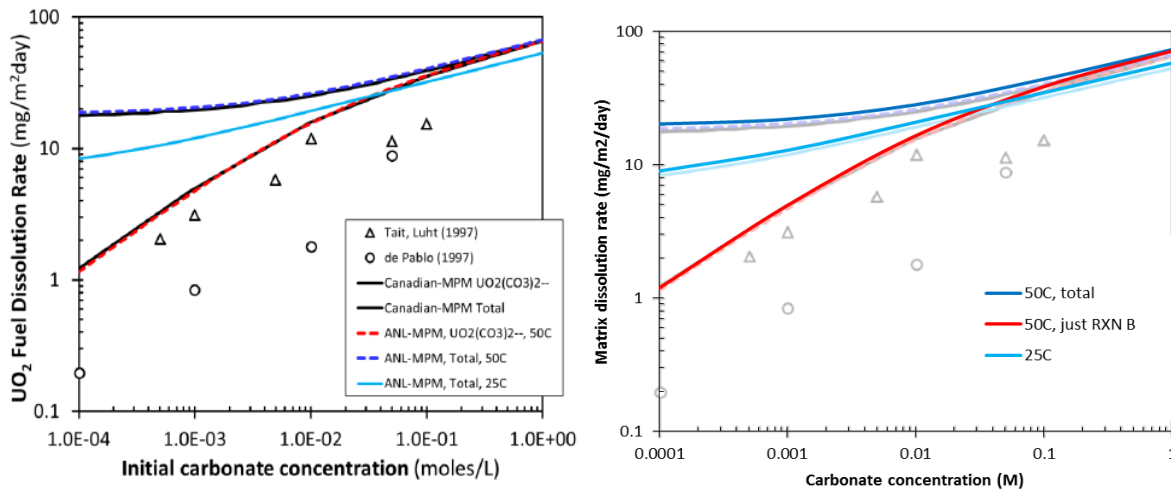


Figure 3: Comparison of dissolution rate predicted in literature (*left*) vs. NNL model (*right*) [3] - Model type B.

Model runs, type C:

- No iron or carbonate is present
- The bulk boundary condition for all non-uranium species is a constant concentration condition
- The bulk boundary condition of uranium species is a zero flux condition.
- Oxygen is present at $1 \cdot 10^{-9}$ M at the bulk boundary
- Precipitation and dissolution are allowed to occur
- A constant alpha dose rate of $0.1 \text{ Gy} \cdot \text{s}^{-1}$ is used and H₂O₂ G-value constant at $1.021 \cdot 10^{-4} \text{ mol} \cdot \text{m}^{-3} \cdot \text{Gy}^{-1}$
- Surface coverage of noble metal particles of 1%

Five cases of this type were run, each spanning a 10,000 years time frame and using a constant H₂ concentration varying between $1 \cdot 10^{-4}$ - $1 \cdot 10^{-1}$ M and a case with 0 M H₂³.

³ The NNL model had to be modified for these runs to *include* an error in the original radiolysis model proposed by the American authors. Hence while these results match well, they are erroneous and are only used to compare the NNL model to the literature. The NNL model can be returned to its original state to produce correct results instead.

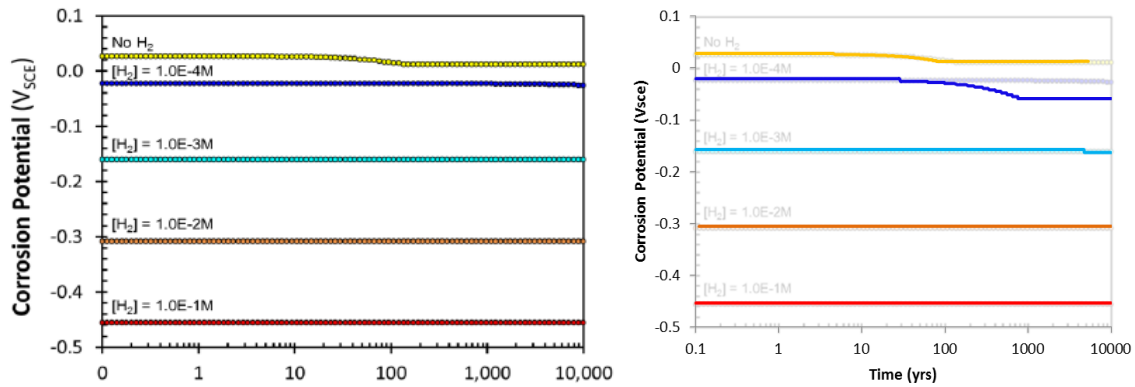


Figure 4: Comparison of corrosion potential predicted in literature (*left*) vs. NNL model (*right*) [4] - Model type C.

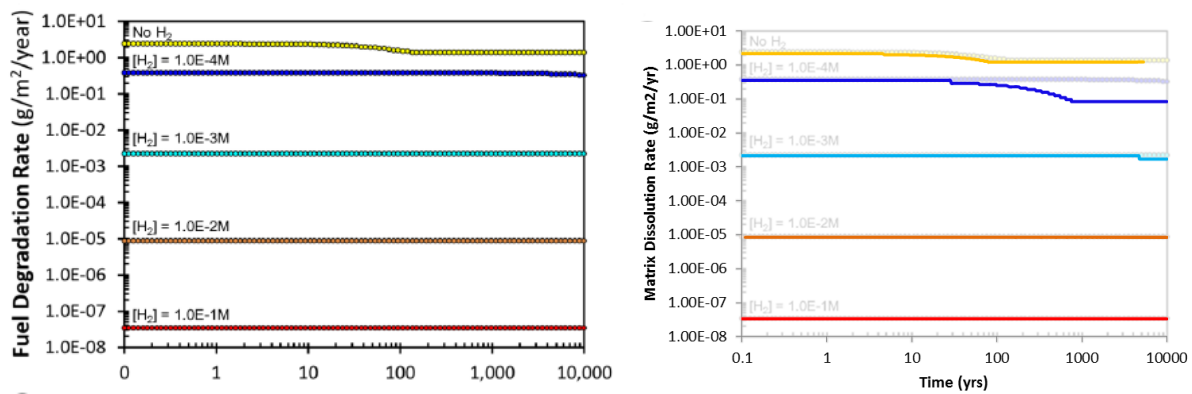


Figure 5: Comparison of dissolution rate predicted in literature (*left*) vs. NNL model (*right*) [4] - Model type C.

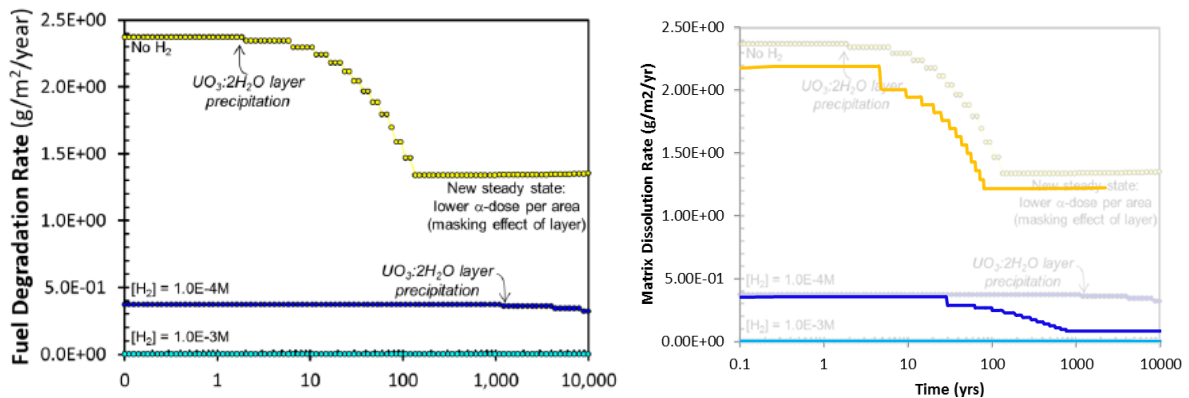


Figure 6: Comparison of dissolution rate predicted in literature (*left*) vs. NNL model (*right*) [4] - Model type C.

It can be seen from Figure 1, Figure 4, Figure 5 and Figure 6 that there is some disagreement between the model and previous literature models. For Figure 1, it is thought that there is some error in the calculation of the matrix dissolution rate in the original model for the case with carbonate present. This is because the corrosion potential predictions of the two models match well. A simple calculation whereby this corrosion potential is put into the matrix dissolution equations stated in the original author's paper [3] agrees with the NNL model. The disagreements between the NNL model and literature models in Figure 5 and Figure 6 are similarly offset with respect to matrix dissolution rate

(exemplified by Figure 6), yet remain well matched for corrosion potential. This is thought to be due to a similar error in the original models.

For Figure 4 to Figure 6, there is a clear offset in timings for when the matrix dissolution rates and corrosion potentials begin to decrease. In these runs, these reductions are caused by precipitation of uranium solids onto the surface of the fuel⁴. Thus, the NNL model predicts precipitation occurs earlier than the literature models. There are a number of potential reasons for this:

- The original paper [4] does not state its assumed saturation concentration for UO_2^{2+} . It could be that they have a much higher value for this, delaying precipitation.
- Similarly, the precipitation kinetics used are not stated, so they may use much slower precipitation kinetics
- The bulk boundary conditions were not entirely clear from the original paper [4]. The boundary conditions used were the only sensible ones considered which produced similar results to the original paper – however it is possible that the authors used subtly different conditions.

It is worth noting also that throughout the literature papers used for comparison [3, 4], there were numerous errors including unit errors and fundamental theory errors which had to be corrected or accounted for in the NNL model runs to make them match the literature models. It is easily possible that the cause of the discrepancies seen is a simple error in the original models that it is not possible to identify from the available reports.

4 Model uncertainties identified

A number of key uncertainties have been identified which warrant further investigation, particularly when considering application of the existing models to conditions other than those for which they were originally developed, e.g. at higher pH conditions. Without a careful review of these factors, the final model may fail to provide useful predictive results.

Key amongst the uncertainties is the historic treatment of electrochemical phenomena in literature models. These models utilise fixed values for the equilibrium potentials of electrochemical half-reactions on the fuel surface which are independent of conditions. Generally, equilibrium potentials in systems such as these are treated using the Nernst equation, which accounts for changes in surface concentrations and the effects of temperature on equilibrium potentials. Neglecting this could have a significant impact on the results of the model as the rate of corrosion is highly dependent on equilibrium potentials.

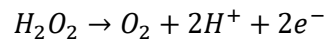
$$E_{redox} = E_{redox}^0 - \frac{RT}{\epsilon_{redox}F} \ln\{S_{Redox}\}$$

Equation 1: Nernst equation.

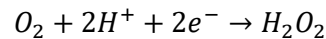
⁴ with the final plateau occurring when the precipitate layer extends further from the fuel surface than the range of alpha radiolysis.

Where E_{redox} is the equilibrium potential, E_{redox}^0 is the equilibrium potential at standard conditions, ϵ_{redox} is the number of electrons in the redox reaction, S_{redox} is the reaction quotient, T is temperature, R is the gas constant and F is Faraday's constant.

An additional concern is the assumption of irreversibility of surface reactions. Equation 2 shows the oxidation reaction for hydrogen peroxide on the fuel surface which is currently used in the model. This will proceed if the equilibrium potential of the half-reaction is less than the overall corrosion potential at the fuel surface. However, in the event that the corrosion potential is lower than the equilibrium potential the reverse reaction occurs. In the literature models reviewed, it is assumed that only the oxidation reaction can occur and indeed all half-reactions modelled have an assumed direction.

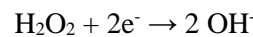


Equation 2: Oxidation reaction consuming hydrogen peroxide on fuel surface.



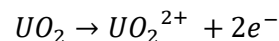
Equation 3: Reduction reaction producing hydrogen peroxide at fuel surface.

In some instances, this may not be a significant problem. For instance, within the electrochemical model, there is an alternative reduction reaction that would be activated instead of Equation 3 (Equation 4, [2]) when the corrosion potential drops sufficiently.



Additionally, Hiroki and LaVerne 2005 [6] identified that the catalytic decomposition of peroxide involves radical formation, so even electrochemical models are only approximate representations of the fundamental chemistry and in some cases the additional complexity associated with including of all reverse reactions may not be warranted.

However, examining the existing literature, the predicted corrosion potentials are often lower than the equilibrium potentials for uranium dissolution oxidation half-reactions (Equation 4 and Equation 5) which determine the matrix dissolution rate.



Equation 4: Oxidation reaction for matrix dissolution without carbonate.



Equation 5: Oxidation reaction for matrix dissolution in the presence of carbonate

In this event oxidative dissolution of the uranium dioxide matrix should cease entirely, however the literature continues to predict oxidative dissolution in such instances. In part this is likely to be because data does not currently exist to model the reverse reactions – however this still results in uncertainties in the applicability of model outputs.

Further to these concerns there are also a number of other uncertainties which have become apparent in the development of the model, including:

- The applicability of the parameters used in the model away from pH 9.
- The applicability of the reaction schemes used away from pH 9.
- The simplicity of the radiolysis model used and uncertainty in the important species created by radiolysis – especially for beta and gamma radiation.
- The treatment of available surface area for oxidative dissolution and the evolution of this over time.
- The potential for electronic resistance between noble metal particles and the fuel surface.
- The treatment of precipitation, both in its kinetics and in the locations at which it occurs.
- The potential for passivation effects, currently ignored in the model.
- A lack of a validated temperature dependency model for the majority of processes in the system.

In the light of the above assessments and the extent of gaps in fundamental data needed to reliably extend the range of applicability of the model, numerical sensitivity analysis is not considered to be a priority. Instead the model will be benchmarked against real world conditions and observations described in NNL WP2 (*previous contribution*).

5 Conclusion

Existing literature models have been replicated by NNL as part of the EU DisCo project and the capability to produce predictions of fuel matrix dissolution rates has been developed. However, in the process of writing these models a wide range of uncertainties have been identified. The priority for the 2019/20 FY must be to clarify the impact of existing assumptions, particularly in relation to changing environmental conditions and to subsequently improve understanding to underpin more reliable predictions.

The existing model can be readily modified to consider experimental work undertaken as part of the DisCo programme. This would be a pragmatic way to quickly assess the importance of the uncertainties identified with the model and their impact on its predictive capabilities.

A report setting out the model description, results and uncertainties in much more detail will be made available at a later date. This makes clearer the issues identified with previous literature models and the structure of the NNL model.

Acknowledgement

The research leading to these results has received funding from the European Commission Horizon 2020 Research and Training Programme of the European Atomic Energy Community (EURATOM) (H2020-NFRP-2016-2017-1) under grant agreement n° 755443 (DisCo project).

References

- [1] King, F. and Kolar, M. (1999). mathematical implementation of the mixed-potential model of fuel dissolution model version MPM-V1.0. Ontario Hydro Report, 06819-REP-01200-10005 R00.
- [2] King, F. and Kolar, M. (2003). The mixed-potential model for UO₂ dissolution MPM versions V1.3 and V1.4. Ontario Hydro Report, 06819-REP-01200-10104 R00.
- [3] Sassani, D., Colón, C., Weck, P., Jerden Jr., J., Frey, K., Cruse, T.E.W., Buck, E., Wittman, R., Skomurski, F., Cantrell, K., McNamara, B., Soderquist, C. (2012). Integration of EBS models with generic disposal system models. FCRD-UFD-2012-000277, SAND2012-7762P.
- [4] Sassani, D., Colón, C., Weck, P., Jerden Jr., J., Frey, K., Cruse, T.E.W., Buck, E., Wittman, R. (2013). Used fuel degradation: Experimental and modeling report. US DOE, FCRD-UFD-2013-000404, SAND2013- 9077P.
- [5] Wang, Y., Matteo, E., Rutqvist, J., Davis, J., Zheng, L., Houseworth, J., Birkholzer, J., Dittrich, T., Gable, C.W., Karra, S., Makedonska, N., Chu, S., Harp, D., Painter, S.L., Reimus, P., Perry, F., Zhao, P., Begg, J., Zavarin, M., Tumey, S.J., Dai, Z., Kersting, A.B., Jerden, J., Frey, K., Copple, J.M., Ebert, W. (2014). Used fuel disposal in crystalline rocks: Status and FY14 Progress. US DOE, FCRD-UFD-2014-000060, SAND2014-17992R.
- [6] Hiroki, A. and Laverne, J.A. (2005). Decomposition of hydrogen peroxide at water-ceramic oxide interfaces. *Journal of Physical Chemistry B*, 109(8), 3364-70.

Spent fuel alteration model integrating processes of different time scales - Validation

Riba, O., Coene, E., Silva, O., Duro, L.

Amphos 21, Barcelona (ES)

Abstract

A 1D reactive transport model has been implemented in iCP (interface COMSOL Multiphysics and PhreeqC) to assess the corrosion of Spent Fuel (SF), considered as homogeneous $\text{UO}_2(\text{am})$ doped with Pd. The model couples: i) the generation of water radiolysis species by alpha and beta radiation considering a complete radiolysis system, ii) the processes occurring in the SF surface: oxidative dissolution reactions of $\text{UO}_2(\text{am})$ and subsequent reduction of oxidized fuel, considering H_2 activation by Pd, and iii) corrosion of Fe(s) considering both oxic and anoxic conditions. Processes i) have been implemented in COMSOL and processes ii) and iii) have been implemented in PHREEQC with their kinetic constants being calibrated with different sets of experimental data published in the open literature. The model yields a $\text{UO}_2(\text{am})$ dissolution rates similar to the values selected in safety assessments.

1 Introduction and objectives

The safety assessment of deep geological disposal of used nuclear fuel requires a fundamental understanding of the processes controlling fuel corrosion and the release of radionuclides into the geosphere.

In the last years, source-term models describing spent fuel (SF) dissolution have been improved by incorporating new processes that were not considered in classical quantitative approaches. The late advances include the work of Wu et al. (2012, 2014a,b) [1-3], Jerden et al. (2015) [4] and Odorowski et al. (2015) [5], who developed reactive transport models based on the calculation of the corrosion potential at the surface of the fuel.

Improved models implemented in software such as COMSOL [1-3], MATLAB [4], and HYTEC [5] have allowed to include the most relevant processes of the system by introducing some simplifications. These simplifications were mainly applied to the chemistry of the system and to the radiolytic scheme, for instance, considering only the production of H_2O_2 and H_2 instead of the complete radiolysis scheme. Radiolysis and chemical complexation/dissolution reactions occur at very different time scales, often with rates differing by more than 6 orders of magnitude. Uranium (the main element of the fuel) and the iron of the steel-container and metallic insert have a complex chemistry. This complexity and the difference in time scales represent an important modelling challenge and these are the main reasons for adopting simplifications.

The objectives of Amphos 21 in the DisCo European project are:

- *Task 1.* To develop a conceptual geochemical model that accounts for the impact of platinum metal alloy particles (epsilon metals) on SF dissolution under highly reducing conditions and in the presence of hydrogen. Under these conditions, in finely divided form and well dispersed into the UO_2 matrix, and if the partial pressure of hydrogen (p_{H_2}) is high enough, elements of the platinum group (Tc, Ru, Rh, Pd, Ir, Pt, ...) are expected to behave as catalyst and to reduce U(VI) into U(IV).
- *Task 2.* Assessment of the behaviour of the fuel under the conditions developed inside the canister, as discussed with experimentalists. This includes a discussion on the effect that different types of metallic dopants (Cr_2O_3 , Al_2O_3 , Gd_2O_3) can have on the SF response to the environment conditions.

During the first two years of the project, the main work has been to assess the behaviour of SF by developing a 1D reactive transport model with coupled radiolysis and chemistry. This model was implemented in the reactive transport tool iCP [6] (interface coupling COMSOL Multiphysics [7] and PhreeqC [8]).

2 Modelling approach

A practical method to couple water radiolysis, aqueous chemistry and solute transport was developed to simulate the dissolution of SF inside a failed waste container. The integration of the different physico-chemical processes into iCP is achieved by a two-way coupling approach, as shown in the Figure 1.

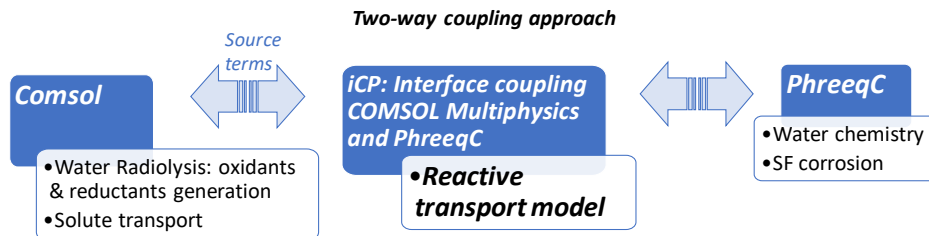


Figure 1: Integrating in iCP different processes involved in the SF alteration.

The coupled processes included in the model are described below.

2.1 Generation of oxidants and reductants by water radiolysis with alpha/beta radiation

The present work considers the formation of radiolytic species and recombination of radiolysis products in the physico-chemical and chemical stage [9]. Water radiolysis by alpha and beta radiation are considered according to the treatment performed in Cera et al. (2006) [10] and considering the radiolytic scheme and yields of primary products from Kelm and Bohnert (2004) [11] and Eriksen et al. (2008) [12] (see Appendix A of this contribution).

Apart from the water radiolysis scheme, two more processes were implemented in COMSOL with a set of ordinary differential equations (ODE): the generation of $\cdot\text{OH}$ by decomposition reaction of H_2O_2 on the $\text{UO}_2 \cdot 2\text{H}_2\text{O}$ surface and the generation of $\text{H}\cdot$ by activation of H_2 on the Pd surface. The kinetic constant used in the model for these two processes correspond to the values reported in Clarens et al. (2005) [15] and Trummer et al. (2008) [16], respectively.

The generation of the above described products, calculated with an ODE solver, were coupled with the solute transport equation (Eq. 1) through a source term.

2.2 Transport of dissolved species

In theory, mineral precipitation can occur from the water that is in contact with the fuel surface. The fuel may be also considered as a porous media. For that reason, the model considers that aqueous species are transported by diffusion according to the following equation:

$$\phi \frac{\partial c_i}{\partial t} + \nabla(-D_e \nabla c_i) = S_i + \sum_j R_{ij} \quad \text{Eq. 1}$$

where ϕ [-] is the porosity, c_i [mol·kg_w⁻¹] the aqueous concentration of species i , D_e [m²·s⁻¹] the effective diffusion coefficient, S_i [mol·kg_w⁻¹·s⁻¹] the source term of species i and R_{ij} the reaction term between species i and j . In the current state of the model, SF is considered only as a surface, not as a porous medium. Therefore, the porosity is 1 and the effective diffusion coefficient is 10⁻⁹ m²·s⁻¹.

The chemical reaction terms S_i and R_{ij} , on the other hand, are calculated in PhreeqC as explained below (note that the radiolysis calculated in Comsol also contributes to the source term of this equation).

2.3 Corrosion of the SF surface

The solid phase considered as SF matrix is the amorphous UO₂ with the formulation: UO₂·2H₂O. The following kinetic reactions are implemented in PhreeqC:

- a) Oxidation of UO₂·2H₂O to UO₃(s) by ·OH
- b) Oxidation of UO₂·2H₂O to UO₃(s) by O₂
- c) Dissolution of UO₃(s) by H₂O
- d) Dissolution of UO₃(s) by CO₃²⁻
- e) Non-oxidative dissolution of UO₂·2H₂O
- f) Reduction of UO₃(s) to UO₂·2H₂O by H·
- g) Corrosion of Fe(s) to Fe⁺² by O₂ and H₂O

The thermodynamic database used in the modelling is ThermoChimie version 9b0 [14].

3 Calibration of the kinetic constants

At present there are no experimental data available from the experiments performed in DisCo project. Because of that, data from the related literature and generated in the framework of other projects were used to calibrate the model.

Validation of the kinetic constants of the processes (a), (b), (c), (d) and (f), occurring on the SF matrix, have been performed by comparison with the experimental data described by Cera et al. (2006) [10]. The kinetic value corresponding to the non-oxidative dissolution (process (e)) was taken from Bruno et al. (1991) [17]. For process (g) the experimental data generated in REDUPP European project [18]

on UO_2 dissolution in natural groundwater in the presence of corroding metallic iron strip have been used.

The dissolution experiments of SF fragments reported in Cera et al. (2006) [10], and also used in the MICADO project [19], were set up in closed ampoules to keep the gases produced by radiolysis (O_2 and H_2). This experimental design allows us to determine the values of the kinetic constants in the rate expressions corresponding to the processes a), b), c), d) and f), occurring in the SF surface by adjusting the model to the experimental datasets. The calibration process started with arbitrary values for the kinetic constants and they were progressively adjusted considering the experimental H_2O_2 , O_2 , H_2 and U concentrations. In a first step, the oxidative dissolution process was considered and the kinetic constants involved in this process were adjusted. Afterwards the reduction of $\text{UO}_3(\text{s})$ by H- (process f) was included and its corresponding kinetic constant was calibrated.

The modelling results together with the experimental concentrations of O_2 , H_2 , H_2O_2 are shown in Figure 2a. The [U] (M) obtained by Cera et al. (2006) [10] in their 2 mM NaCl and in 10 mM $\text{NaHCO}_3 + 2$ mM NaCl leaching solutions¹ is shown in Figure 2b.

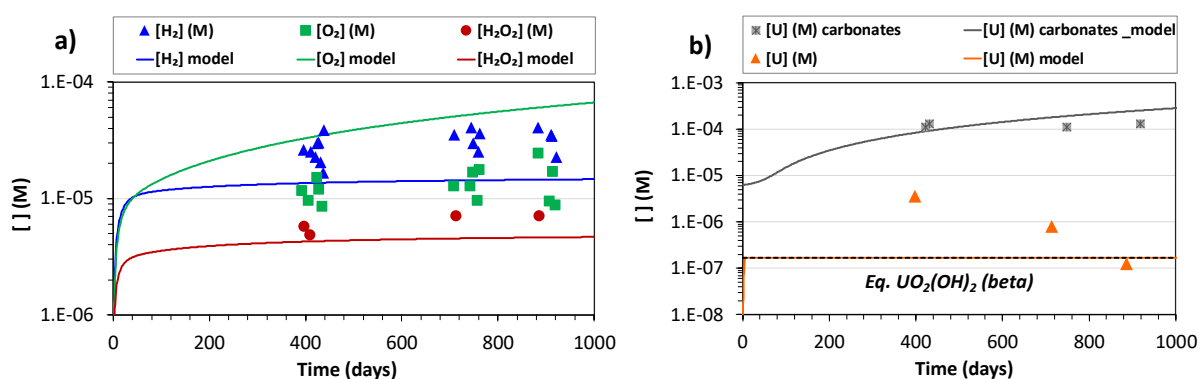


Figure 2: (a) Concentrations of H_2 , O_2 and H_2O_2 as a function of time obtained experimentally (symbols) and through the present modelling (lines); (b) concentration of U obtained experimentally by Cera et al. (2006) [10] (symbols) and by the present modelling exercise (lines). The dashed line represents the U concentration in equilibrium with schoepite ($\text{UO}_2(\text{OH})_2(\text{beta})$).

As shown in Figure 2a, the model is well adjusted to the experimental $[\text{H}_2\text{O}_2]$. There is only a difference of less than half order of magnitude between the modelled $[\text{H}_2]$ and $[\text{O}_2]$ and the corresponding experimental data. It is worth noting that the linear dependency of $[\text{O}_2]$ with time obtained with the simulations does not follow the trend observed in the experimental data. Different tests during the calibration exercise indicated that this linear increase in the modelled $[\text{O}_2]$ is due to the radiolytic system. As a principle, it has been preferred not to adjust the kinetic constants of the water radiolysis reactions. As shown in Figure 2b, uranium concentration in equilibrium with schoepite ($\text{UO}_2(\text{OH})_2(\text{beta})$) has been considered to model the experiments without carbonate.

The corrosion process of metallic Fe(s) has been validated with experimental data generated in the frame of the REDUPP project [18]. Dissolution experiments of UO_2 α -doped with 10 at.% of ^{233}U ($31.4 \text{ MBq}\cdot\text{g}^{-1}$) and $\text{SA/V} = 12.5 \text{ m}^{-1}$ in the presence of Fe(s) were considered. The initial water composition corresponds to the fresh water of REDUPP experiments. However, to simplify the model

¹ It has to be noted that the compositions of the leaching solutions agreed amongst the experimenters in the frame of the DisCo project are not the same than these used by Cera et al. (2006) [10].

only the following species were included as input data: Na^+ , Ca^{2+} , Fe^{2+} , Cl^- , HCO_3^- and SO_4^{2-} . In accordance with the experimental set up, the initial water pH and Eh were set at 8.7 and -0.39 V, respectively. Both calcite and any iron phases included in the ThermoChimie database version 9b0 were allowed to precipitate if they reached oversaturation. Two sets of experimental uranium concentration in solution were used for the validation: i) total [U] (M) determined in solution and ii) calculated [U] (M) considering the isotopic composition and corresponding to uranium in solution caused by UO_2 oxidation without reprecipitation.

The experimental data shown in Figure 3 is the [U] corresponding to the oxidative dissolution process for the experiments with UO_2 α -doped, 10 at.% of ^{233}U and $\text{SA/V} = 12.5 \text{ m}^{-1}$. The calculated uranium concentration resulting from the kinetic oxidation of $\text{UO}_2(\text{s})$ by O_2 and $\cdot\text{OH}$ and subsequent dissolution with H_2O and carbonate (processes from a) to d)) (solid line in Figure 3) is in good agreement with the experimental data at reaction time higher than 30 days. However, the model shows a rapid increase of [U] during the first 10 days, and this pattern is not seen in the experimental data. This initial sharp increase of [U] is attributed to rapid generation of $[\text{O}_2]$ by water radiolysis and subsequent oxidative dissolution of $\text{UO}_2 \cdot 2\text{H}_2\text{O}$ (the high concentration of O_2 by water radiolysis is also observed in the adjustment of kinetic constants of processes occurring in the SF surface, see Figure 2a). The dashed line shown in Figure 3 corresponds to the total uranium in solution calculated with the model. It corresponds to the equilibrium concentration of uranium with the amorphous UO_2 phase ($[\text{U}] = 3.15 \cdot 10^{-9} \text{ M}$) [14]. This concentration is significantly higher than the concentration experimentally determined for other types of groundwater reported in [18] under the same experimental conditions. The experimental uranium concentrations that are below this value are attributed to reprecipitation of UO_2 crystalline phase [18].

Iron corrosion with H_2O and O_2 has been included in the model (process g). The kinetic constant for iron oxidation in anoxic conditions was set to $6.6 \mu\text{m} \cdot \text{y}^{-1}$ in accordance with the literature under reducing conditions [20, 21]. The kinetic constant for iron oxidation with O_2 was adjusted to experimental data. The adjusted kinetic constant corresponds to a rate value of $20 \mu\text{m} \cdot \text{y}^{-1}$, which is in accordance with the values found in the literature for iron corrosion in oxidizing conditions [20].

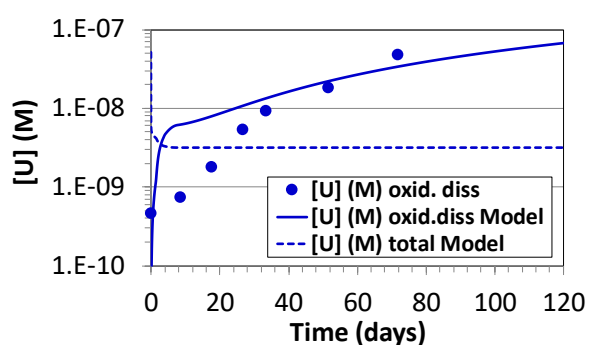


Figure 3: Symbols represent the experimental data from the REDUPP final report [18] of UO_2 α -doped with 10 at.% of ^{233}U ; $\text{SA/V} 12.5 \text{ m}^{-1}$, in the presence of metallic $\text{Fe}(\text{s})$ strip. Lines represent the modelling results of total uranium in solution (dashed line) and calculated uranium corresponding to the oxidative dissolution of UO_2 without reprecipitation (solid line).

4 Results: 1D reactive transport model

Once the kinetic constants have been calibrated, a 1D reactive transport model was implemented considering a homogeneous SF solid surface (UO₂ containing 1 at.% of Pd, as representative element of the epsilon particles, behaving as catalyst of the reduction reactions involving H₂). A sketch of the model domain is shown in Figure 4. With the aim to compare the present modelling results with the simulations from Wu et al. (2014a) [3], the same conditions in terms of dose rate were considered. A uniform alpha dose rate of $2.86 \cdot 10^{-2} \text{ Gy} \cdot \text{s}^{-1}$ affecting the first 13 μm in water adjacent to the SF surface was assumed. This is consistent with an area enclosed equal to a non-uniform exponential distribution of dose rate affecting 35 μm in water adjacent to the SF surface [1]. The model also includes a diffusion layer of 1 mm thickness and a single effective diffusion coefficient (D_e) for all the species taken equal to their diffusion coefficient in pure water, with a typical value equal to $10^{-9} \text{ m}^2 \cdot \text{s}^{-1}$, in accordance with the present development state of the model (SF is considered only as a surface and not as a porous medium). The left boundary is located at the SF surface. Because of that, this boundary is considered closed to solute transport. The right boundary allows for out-diffusion. The prescribed concentration for all solutes at this boundary is zero.

As depicted in Figure 4, the model considers three sub-domains: SF non-porous surface zone (1 μm), α -radiation zone in the water very close to the SF surface (13 μm) and a diffusion zone (1 mm). Note that production and recombination reactions of the species generated by α -water radiolysis occurs also in the SF surface zone and the diffusion is also considered in the SF non-porous surface zone and in the α -radiation zone.

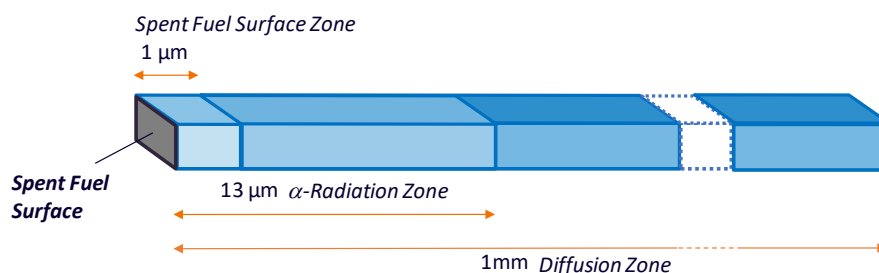


Figure 4: System domain considered in the preliminary 1D calculations.

The model results of [H₂O₂], [O₂(aq)], [H₂(aq)] and [U] evolution with the distance from the SF surface at 0.1 years are shown in Figure 5a. The calculated concentrations of the species generated by water radiolysis ([H₂O₂], [O₂(aq)], [H₂(aq)], [H·], [·OH], [e⁻], [HO₂·], [O·], [O₂·], [HO₂⁻] and [O₂⁻]) indicate that these species reached steady state very rapidly (in 4 hours). However, the concentration of uranium progressively increases, reaching a quasi-steady state concentration of [U] $\sim 10^{-9} \text{ M}$, after 36.5 days (Figure 5b).

The obtained results are comparable with the concentrations simulated in Wu et al. (2014b) [3] under the same alpha dose rate and radiation range in water. The concentrations [H₂(aq)], [H₂O₂] and [U] are very similar in both models and [O₂(aq)] almost two orders of magnitude greater in the present model than in [3]. This difference is attributed to the different radiolytic scheme and the different reaction rates or processes considered in the SF matrix by each model.

The model discussed in the present manuscript not only includes the complete radiolysis system and the surface reactions on the SF matrix and metallic Fe(s) but also permits the future inclusion of other chemical processes to account for the complex system of SF, steel-container and water chemistry. Therefore, it represents a step forward towards the development of a model that accomplishes with the modelling needs to assess the performance and the safety of a deep geological repository for spent nuclear fuel.

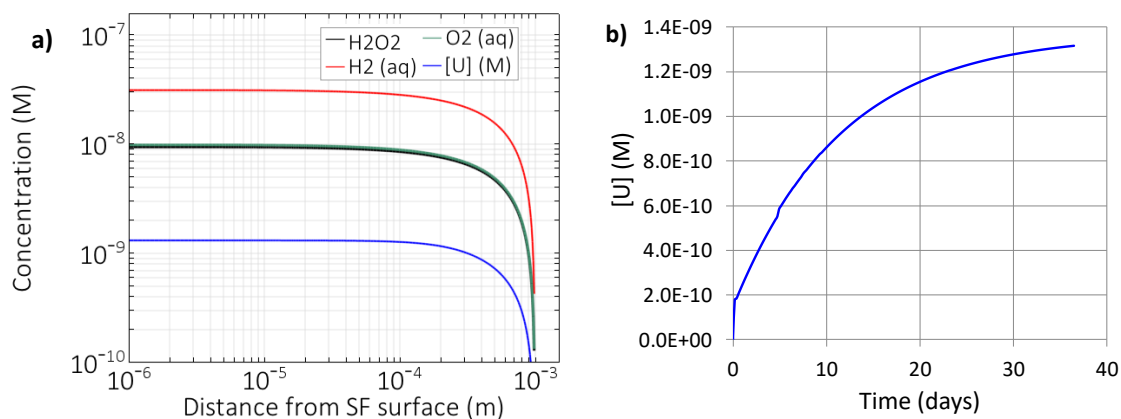


Figure 5: (a) Simulated [H₂O₂], [O₂(aq)], [H₂(aq)] and [U] profiles after 0.1 years; (b) temporal evolution of [U] (M) a distance of 10^{-5} m from the SF surface.

The UO₂(am) dissolution rate determined from the present model is close to the value considered in safety assessments when the inhibiting (protecting) effect of H₂ on the long-term dissolution of SF matrix is taken into account (10^{-7} y⁻¹) [22-27].

5 Conclusions and future work

During the second year of the project, a reactive transport model that couples water radiolysis, aqueous chemistry, surface reactions on both SF matrix and metallic Fe(s), and solute transport was implemented in iCP. This model was used to simulate the dissolution of SF inside a failed waste container. As the experimental data in the DisCo project are not available yet, the processes integrated in the present model have been validated with adequate experimental data from the literature. Modelling results are, in general, in good agreement with the different sets of experimental data and also with 1D reactive transport models from the literature [3].

The present work means a significant progress with respect to the first year given that: a) the complete set of radiolysis reactions has been coupled with the surface reactions and the aqueous chemistry (after the first year of the project the species generated by radiolysis were calculated separately with Chemsimul code and introduced in iCP as source terms) and b) iron corrosion, which were not implemented during the first year of the project [28], was included in the current model. This will allow to consider the dynamics of the canister corrosion.

The third year of the project will be devoted to extend the present model by including: i) metallic Fe corrosion in 1D reactive model, ii) the SF as a porous medium; iii) porosity changes of the SF by precipitation of secondary phases within the SF and on the SF surface and iv) evaluate the possibility to consider the heterogeneity of the SF matrix to account for different concentrations of epsilon

particles (Pd). Also, as stated in Task 1 of the DisCo proposal, a conceptual geochemical model will be developed that accounts for the impact of platinoid metal alloy particles (epsilon metals) on SF dissolution under highly reducing conditions and in the presence of hydrogen.

Acknowledgement

The research leading to these results has received funding from the European Commission Horizon 2020 Research and Training Programme of the European Atomic Energy Community (EURATOM) (H2020-NFRP-2016-2017-1) under grant agreement n° 755443 (DisCo project).

References

- [1] Wu, L., Beaugard, Y., Qin, Z., Rohani, S., Shoesmith, D.W. (2012). A model for the influence of steel corrosion products on nuclear fuel corrosion under permanent disposal conditions. *Corrosion Science*, 61, 83-91.
- [2] Wu, L., Liu, N., Qin, Z., Shoesmith, D.W. (2014a). Modeling the radiolytic corrosion of fractured nuclear fuel under permanent disposal conditions. *Journal of The Electrochemical Society*, 161(8), E3259-E3266.
- [3] Wu, L., Qin, Z., Shoesmith, D.W. (2014b). An improved model for the corrosion of used nuclear fuel inside a failed waste container under permanent disposal conditions. *Corrosion Science*, 84, 85-95.
- [4] Jerden, J.L., Frey, K., Ebert, W. (2015). A multiphase interfacial model for the dissolution of spent nuclear fuel. *Journal of Nuclear Materials*, 462, 135-146.
- [5] Odorowski, M. (2015). Etude de l'altération de la matrice (U,Pu)O₂ du combustible irradié en conditions de stockage géologique: Approche expérimentale et modélisation géochimique. Doctoral Thesis.
- [6] Nardi, A., Idiart, A., Trincherro, P., de Vries, L.M., Molinero, J. (2014). Interface COMSOL-PHREEQC (iCP), an efficient numerical framework for the solution of coupled multiphysics and geochemistry. *Computers & Geosciences*, 69, 10-21.
- [7] COMSOL Multiphysics, <https://www.comsol.com/>.
- [8] Parkhurst, D.L. and Appelo, C.A.J. (2013). Description of input and examples for PHREEQC version 3—A computer program for speciation, batch-reaction, one-dimensional transport, and inverse geochemical calculations. U.S. Geological Survey Techniques and Methods, book 6, chap. A43, 497 p.
- [9] Tian, Z., Jiang, S.B., Jia, X. (2017). Accelerated Monte Carlo simulation on the chemical stage in water radiolysis using GPU. *Physics in Medicine & Biology*, 62(8), 3081.
- [10] Cera, E., Bruno, J., Duro, L., Eriksen, T. (2006). Experimental determination and chemical modelling of radiolytic processes at the spent fuel/water interface. SKB Technical Report, TR 06-07.
- [11] Kelm, M. and Bohnert, E. (2004). A kinetic model for the radiolysis of chloride brine, its sensitivity against model parameters and a comparison with experiments. FZKA 6977, Forschungszentrum Karlsruhe.
- [12] Eriksen, T.E., Jonsson, M., Merino, J. (2008). Modelling of time resolved and long contact time dissolution studies of spent nuclear fuel in 10 mM carbonate solution—a comparison between two different models and experimental data. *Journal of Nuclear Materials*, 375(3), 331-339.
- [13] Christensen, H., Sunder, S., Shoesmith, D.W. (1994). Oxidation of nuclear fuel (UO₂) by the products of water radiolysis: development of a kinetic model. *Journal of alloys and compounds*, 213, 93-99.
- [14] ThermoChimie Database version 9b0. Andra thermodynamic database for performance assessment. <https://www.thermochimie-tdb.com/pages/version.php>.

- [15] Clarens, F., De Pablo, J., Casas, I., Gimenez, J., Rovira, M., Merino, J., Martinez-Esparza, A. (2005). The oxidative dissolution of unirradiated UO_2 by hydrogen peroxide as a function of pH. *Journal of Nuclear Materials*, 345(2-3), 225-231.
- [16] Trummer, M., Nilsson, S., Jonsson, M. (2008). On the effects of fission product noble metal inclusions on the kinetics of radiation induced dissolution of spent nuclear fuel. *Journal of Nuclear Materials*, 378(1), 55-59.
- [17] Bruno, J., Casas, I., Puigdomènech, I. (1991). The kinetics of dissolution of UO_2 under reducing conditions and the influence of an oxidized surface layer (UO_{2+x}): Application of a continuous flow-through reactor. *Geochimica et Cosmochimica Acta*, 55(3), 647-658.
- [18] Evins, L.Z., Juhola, P., Vähänen, M. (2014). REDUPP Final Report. POSIVA Report, 2014-12.1. 128 pp.
- [19] Bruno, J., Merino, J., Tamayo, A., Ferry, C., Quiñones, J., Iglesias, E., Rodriguez-Villagra, N., Nieto, J.M., Martínez-Esparza, A., Loida, A., Metz, V., Jonsson, M., Ekeröth, E., Grambow, B. (2005). MICADO project EURATOM specific programme for research and training on nuclear energy. Final D3.1 Deliverable: Application of models to selected datasets, NUWASTE-2005/6-3.2.1.1-2.
- [20] Féron, D., Crusset, D., Gras, J.M. (2008). Corrosion issues in nuclear waste disposal. *Journal of Nuclear Materials*, 379(1-3), 16-23.
- [21] ANDRA (2005). Andra Dossier 2005 Argile: Évaluation de la faisabilité du stockage géologique en formation argileuse. Document de synthèse. Andra, Paris.
- [22] Martínez-Esparza, A., Cuñado, M.A., Gago, J.A., Quiñones, J., Iglesias, E., Cobos, J., González de la Huebra, A., Cera, E., Merino, J., Bruno, J., de Pablo, J., Casas, I., Clarens, F., Giménez, J. (2005). Development of a Matrix Alteration Model (MAM). ENRESA Report, PT-01-2005.
- [23] SKB (2010). Data report for safety assessment SR-Site. SKB Technical Report, TR-10-52.
- [24] POSIVA (2013). Safety case for the disposal of spent nuclear fuel at Olkiluoto - Models and data for the repository system 2012. POSIVA Report, 2013-01.
- [25] Johnson, L. (2014). A model for radionuclide release from spent UO_2 and MOX fuel. Nagra Working Report, NAB 13-37.
- [26] NWMO (2015). Technical program for long-term management of Canada's used nuclear fuel – Annual Report 2014. NWMO Technical Report, TR-2015-01.
- [27] JAEA (2015). Preliminary assessment of geological disposal system for spent fuel in Japan - First progress report on direct disposal. JAEA-Research, 2015-016.
- [28] Riba, O., Coene, E., Silva, O., Duro, L. (2018). Integrated spent fuel alteration model. Method and first results. Deliverable D1.10: 1st Annual Meeting Proceedings of the DisCo project, 61-65.

Appendix A

Kinetic reaction scheme² for water radiolysis [11]

| Reactions | $M^{-1}\cdot s^{-1}$ or s^{-1} | Reactions | $M^{-1}\cdot s^{-1}$ or s^{-1} |
|---|----------------------------------|---|----------------------------------|
| $H_2O \rightarrow H^+ + OH^-$ | $k = 2.60E-05$ | $H + O_2^- \rightarrow HO_2^-$ | $k = 2.00E+10$ |
| $H^+ + OH^- \rightarrow H_2O$ | $k = 1.43E+11$ | $H + HO_2 \rightarrow H_2O_2$ | $k = 8.50E+09$ |
| $H_2O_2 \rightarrow H^+ + HO_2^-$ | $k = 3.56E-02$ | $H + H_2O_2 \rightarrow H_2O + OH$ | $k = 4.20E+07$ |
| $H^+ + HO_2^- \rightarrow H_2O_2$ | $k = 2.00E+10$ | $H + O_2 \rightarrow HO_2$ | $k = 2.10E+10$ |
| $E^- + H_2O \rightarrow H + OH^-$ | $k = 1.90E+01$ | $HO_2 + HO_2 \rightarrow H_2O_2 + O_2$ | $k = 8.40E+05$ |
| $H + OH^- \rightarrow E^- + H_2O$ | $k = 2.20E+07$ | $HO_2 + O_2^- \rightarrow O_2 + HO_2^-$ | $k = 9.60E+07$ |
| $OH + OH^- \rightarrow H_2O + O^-$ | $k = 1.30E+10$ | $OH + O^- \rightarrow HO_2^-$ | $k = 1.80E+10$ |
| $O^- + H_2O \rightarrow OH + OH^-$ | $k = 1.80E+06$ | $O + O \rightarrow O_2$ | $k = 1.00E+09$ |
| $HO_2 \rightarrow H + O_2^-$ | $k = 8.00E+05$ | $H_2O_2 \rightarrow H_2O + O$ | $k = 3.80E-04$ |
| $H + O_2^- \rightarrow HO_2$ | $k = 5.00E+10$ | | |
| $E^- + H^+ \rightarrow H$ | $k = 2.30E+10$ | | |
| $E^- + E^- \rightarrow H_2 + OH^- + OH^-$ | $k = 5.50E+09$ | | |
| $E^- + H \rightarrow H_2 + OH^-$ | $k = 2.50E+10$ | | |
| $E^- + O_2^- \rightarrow HO_2^- + OH^-$ | $k = 1.30E+10$ | | |
| $E^- + HO_2 \rightarrow HO_2^-$ | $k = 2.00E+10$ | | |
| $E^- + H_2O_2 \rightarrow OH + OH^-$ | $k = 1.10E+10$ | | |
| $E^- + O_2 \rightarrow O_2^-$ | $k = 1.90E+10$ | | |
| $E^- + HO_2^- \rightarrow O^- + OH^-$ | $k = 3.50E+09$ | | |
| $OH + OH \rightarrow H_2O_2$ | $k = 5.50E+09$ | | |
| $OH + E^- \rightarrow OH^-$ | $k = 3.00E+10$ | | |
| $OH + H \rightarrow H_2O$ | $k = 9.70E+09$ | | |
| $OH + HO_2 \rightarrow H_2O + O_2$ | $k = 6.60E+09$ | | |
| $OH + O_2^- \rightarrow O_2 + OH^-$ | $k = 1.00E+10$ | | |
| $OH + H_2O_2 \rightarrow HO_2 + H_2O$ | $k = 2.70E+07$ | | |
| $OH + H_2 \rightarrow H + H_2O$ | $k = 3.40E+07$ | | |
| $OH + HO_2^- \rightarrow HO_2 + OH^-$ | $k = 7.50E+09$ | | |
| $H + H \rightarrow H_2$ | $k = 7.80E+09$ | | |

Yields of primary products ($mol\cdot L^{-1} \times 10^7$) formed on radiolysis of water

| Species | Alpha [11] | Beta [12] |
|-------------|------------|-----------|
| $G(H_2O_2)$ | = 0.98 | = 0.74 |
| $G(HO_2)$ | = 0.22 | = 0.00 |
| $G(H_2)$ | = 1.30 | = 0.45 |
| $G(H)$ | = 0.21 | = 0.60 |
| $G(E^-)$ | = 0.06 | = 2.80 |
| $G(OH)$ | = 0.25 | = 2.80 |
| $G(OH^-)$ | = 0.00 | = 0.00 |
| $G(H^+)$ | = 0.06 | = 2.80 |
| $G(H_2O)$ | = -2.65 | = -4.30 |

² The kinetic constant for the decomposition reaction of H_2O_2 : $H_2O_2 \rightarrow O + H_2O$ is $k = 1 \cdot 10^{-3} s^{-1}$ [11, 13]. As described in Christensen et al. (1994) [13] this rate constant value was set as arbitrary. In the present work, it has been adjusted with the experimental data from Cera et al. (2006) [10] to $3.8 \cdot 10^{-4} s^{-1}$.

Modeling of the oxidative leaching of $U_{0.73}Pu_{0.27}O_2$ in synthetic clay groundwater with metallic iron

De Windt, L.¹, Kerleguer, V.^{1,2}, Jégou, C.², Goblet, P.¹, Martin, C.³, Tocino, F.⁴

¹ ARMINES/MINES ParisTech, Centre de Géosciences, Fontainebleau (FR)

² CEA/DEN/DE2D/SEVT/LMPA, Marcoule, Bagnol sur Cèze (FR)

³ Andra, Châtenay-Malabry (FR)

⁴ EDF R&D, Moret-sur-Loing (FR)

1 Context and objectives

The direct disposal of irradiated fuels in deep geological repositories is a major societal issue for several countries. The French National Radioactive Waste Management Agency (Andra) has selected a Callovo-Oxfordian (COx) clay formation for the deep repository of radioactive waste. The alpha activity of spent fuel may locally disrupt the reducing conditions by inducing alpha radiolysis of the surrounding water, and thus producing oxidizing species like hydrogen peroxide (H_2O_2). MOX (mixed plutonium and uranium oxide) fuels are currently used in several European nuclear reactors. The dissolution rate of the spent fuel matrix is a critical issue because actinides and fission products are entrapped in the UO_2 matrix. It will be responsible for the long-term radionuclide releases beyond the instant release fraction (IRF).

The activity of the MOX could be higher but the resistance of Pu-enriched agglomerates specifically found in MOX fuels is expected to play a beneficial role [1]. Their results indicated a very fast dissolution of the UO_2 grains, likely due to the high alpha-activity induced by the surrounding plutonium agglomerates. On the contrary, the plutonium agglomerates were not altered over the leaching. For the present sub-task of WP5, homogeneous MOX pellets (24 wt.% Pu, $U_{0.73}Pu_{0.27}O_2$) were considered to better investigate the effect of plutonium (content and repartition) on the dissolution resistance and mechanisms.

Furthermore, there has been an increasing focus on ensuring that data and models are capable of supporting the long-term performance assessment of geological repositories [2]. This means that spent nuclear fuel experiments must be done under repository-like conditions and using materials representative of those expected in the repository. In this context, it is well known that the presence of redox active species like hydrogen in the environmental water may scavenge the radiolytic dissolution of spent-fuel (e.g. [3]). Whether iron may also counteract the water radiolysis effects has been studied more recently (e.g. [4, 5]). In particular, there is a need to understand the behaviour of the spent fuel in truly reducing conditions imposed by the corrosion of the metallic iron containers encapsulating the waste.

2 Modelling codes and database

CHESS is a stand-alone geochemical code identical to the geochemical module of reactive transport code HYTEC [6]. CHESS simulates the chemistry of complex aqueous systems, including minerals, organics, colloids and gases. Thermodynamic equilibrium and kinetic controls can be both considered in CHESS. The diffusive transport of a reactive species i is coupled to chemistry in HYTEC according to the following equation:

$$\frac{\partial \omega c_i}{\partial t} = \nabla \cdot (D_e(\omega) \nabla c_i) - \frac{\partial \omega \bar{c}_i}{\partial t} \quad \text{Eq. 1}$$

D_e is the effective diffusion coefficient, ω is the porosity, c_i and \bar{c}_i are the mobile and immobile concentrations of a species i per unit volume of solution, respectively. The fixed or solid fraction is evaluated by the chemical calculations done with chemical module (identical to CHESS but fully integrated to HYTEC), whereas the aqueous fraction is a function of the transport processes only.

The thermodynamic database ThermoChimie [7] was used for all the simulations. With respect to the aqueous species, molecular hydrogen $\text{H}_2(\text{aq})$ produced by the anoxic corrosion of iron was fully decoupled (kinetic inhibition) from the redox reactions in the modelling, e.g. it could not reduce H_2O_2 or U(VI) in solution. The disproportionation of $\text{H}_2\text{O}_2(\text{aq})$ into H_2O and $\text{O}_2(\text{aq})$ was under kinetic control only. Based on the literature review, a subset of uranium and plutonium solids that could precipitate as secondary phases was taken from the ThermoChimie database or from the literature [8].

3 Modelling of $\text{U}_{0.73}\text{Pu}_{0.27}\text{O}_2$ alteration under self α -radiolysis

Modelling was first applied to experiments that were conducted in carbonate water to quantify the dissolution rates of the homogeneous MOX matrix, with an emphasis on the strong disproportionation of H_2O_2 at the surface of the Pu-enriched oxide. The experimental data and kinetic parameters [9] had not been acquired in the framework of the DisCo Project. However, further modelling of the experiments was done in the DisCo Project for the sake of developing a full reactive transport model of the WP4 experiment and its application for performance assessment of the spent MOX fuel package in a disposal cell.

3.1 Modelling of kinetic processes

Under alpha irradiation, the most important species to be considered regarding the dissolution of $\text{U}_{0.73}\text{Pu}_{0.27}\text{O}_2$ is H_2O_2 . Several experimental studies have calibrated the oxidative dissolution of UO_2 matrices with H_2O_2 . The main oxidative species in terms of concentrations is H_2O_2 according to CHEMSIMUL calculation. It is not sure that CHEMSIMUL has the full set of kinetic rate constants for all the radicals induced by radiolysis in the complex chemistry of the COx water at neutral pH. All these reactions are very sensitive to the chemistry and taking a semi-empirical calibration versus experiments where H_2O_2 is measured seems a reasonable approach within DisCo.

The $\alpha\beta\gamma$ -activities of the MOX fuel indicated that the α -irradiation field was the main source of H_2O_2 radiolytic production. The hydrogen peroxide production rate law by water radiolysis at the vicinity of the MOX pellet was

$$\frac{d[H_2O_2(aq)]}{dt} = (k^{prod}) A_v \quad \text{Eq. 2}$$

where A_v is the volumetric surface area of the pellet in $m^2 \cdot L^{-1}$. The constant k^{prod} normalized to the surface pellet was calculated to be around $10^{-8} \text{ mol} \cdot m^2 \cdot s^{-1}$ from alpha dose rate, alpha primary yield, and 40 μm penetration in water.

In carbonate water, strong uranyl carbonate complexes prevent the precipitation of secondary species and uranium can be used as a tracer of the alteration. The dissolution of U(VI) phases can also be considered relatively instantaneous. The uranium oxidation of the MOX surface is therefore directly linked to the uranium release rate and can be used to determine the H_2O_2 consumption rate by the uranium oxidation in the MOX. The oxidative dissolution rate law of the $U_{0.73}Pu_{0.27}O_2$ matrix was

$$\frac{d[U_{0.73}Pu_{0.27}O_2]}{dt} = (-k^{oxid} [H_2O_2(aq)]) A_v \quad \text{Eq. 3}$$

where A_v is again the volumetric surface area of the pellet in $m^2 \cdot L^{-1}$. Considering the maximal steady-state H_2O_2 concentration of $10^{-7} \text{ mol} \cdot L^{-1}$, the corresponding long-term steady-state rate constants k^{oxid} was fitted to about $10^{-3} \text{ mol} \cdot m^2 \cdot s^{-1}$. This rather low rate constant was probably linked to the formation of a Pu-enriched layer at the surface of the pellets, as proven by SEM-EDX [9].

The disproportionation reaction, $H_2O_2 \rightarrow H_2O + 0.5 O_2$, was also modelled with a first-order rate on H_2O_2

$$\frac{d[H_2O_2(aq)]}{dt} = (-k^{disprop} [H_2O_2(aq)]) A_v \quad \text{Eq. 4}$$

where A_v is also the same volumetric surface area of the MOX pellet in $m^2 \cdot L^{-1}$. The disproportionation rate constant $k^{disprop}$ was estimated to be around $10^{-1} \text{ L} \cdot m^2 \cdot s^{-1}$ for the steady-state regime.

Two additional mechanisms had not been considered: H_2O_2 disproportionation in pure water in the TiO_2 cell (that was very slow) and the precipitation of peroxide compounds at the surface of the pellets (not observed by [9]).

3.2 CHESS modelling of the experiments

Figure 1a shows the CHESS modelling results by introducing the kinetic laws introduced above at long-term range. In the model, the amorphous $Pu(OH)_4(am)$ phase was allowed to precipitate and the uranium concentration measured after 30 days was added to the calculated ones. The overall consistency of the kinetic rate constants obtained for the long-term leaching is clearly shown. The model is relatively robust for performance assessment. In both the experiment and the modelling, the pH of the solution was slightly alkaline and constantly buffered to 9.3 by HCO_3^- anions. The redox potential was around 0.350 V/SHE, which corresponds to mildly oxidizing conditions at this pH. The release of plutonium in solution was several orders of magnitude lower than uranium release during the whole experiment. The plutonium release was very low with a chemistry dominated by Pu(IV). The plutonium concentration in solution was almost constant, about $10^{-9} \text{ mol} \cdot L^{-1}$. This concentration was compatible with a thermodynamic control by an amorphous $Pu(OH)_4$ phase at pH 9 and Eh

around 0.35 - 0.40 V, the predominant species in solution being a carbonate complex $\text{Pu}(\text{CO}_3)_2(\text{OH})_2^{2-}$, as shown by the solubility diagram of plutonium (Figure 1b).

4 Modelling of $\text{U}_{0.73}\text{Pu}_{0.27}\text{O}_2$ alteration in synthetic clay water and the presence of metallic iron

In a second step, the reactive transport modelling dealt with leaching experiments of the same unirradiated $\text{U}_{0.73}\text{Pu}_{0.27}\text{O}_2$ cut pellets. Leaching was carried out in order to determine the effect of the near-field repository environment; that is to say synthetic COx clay water in contact with a coupon (foil) of metallic iron. This approach resulted from a tight collaboration between the experimental contribution (WP4) and modelling (WP5) on the dissolution of a homogenous $\text{U}_{1-x}\text{Pu}_x\text{O}_2$ within the DisCo project. The WP4 experiment is still in progress. Therefore, the modelling was only based on the data already available and will be improved in the final report. Again, emphasis was given on the development of a model useful for performance analysis of representative configuration of spent MOX fuel package in a disposal cell.

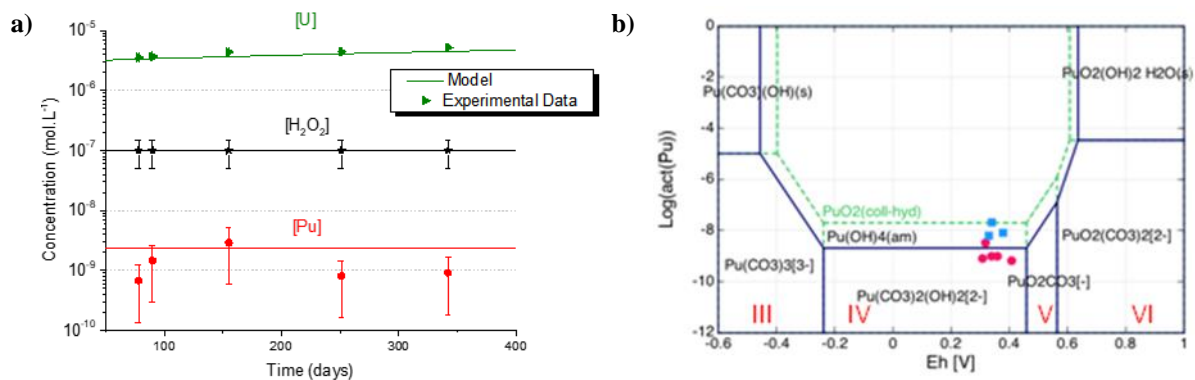


Figure 1: (a) CHESSE modelling of the long-term kinetic leaching of the homogeneous MOX pellet in carbonated water ($10^{-2} \text{ mol}\cdot\text{L}^{-1}$), (b) CHESSE solubility diagrams of plutonium as a function of redox potential (V/SHE) at pH 9 and 25°C.

4.1 Prerequisite on the kinetics of $\text{Fe}(\text{II})/\text{H}_2\text{O}_2$ reaction in solution

The experimental and modelling study of the effect of metallic iron on the oxidative dissolution of UO_2 doped with a radioactive alpha emitter [5] demonstrated that the redox reaction (Eq. 5) between dissolved ferrous iron (produced by iron corrosion) and hydrogen peroxide (produced by water radiolysis and enhancing UO_2 dissolution) was a key reaction in the present system. A kinetic control was investigated in the model based on a literature review [9]. Many studies dealt with the Fenton reaction under acidic to slightly acidic conditions, but at neutral pH $\text{Fe}(\text{III})$ is insoluble, precipitates, and, therefore, does not participate to such a reaction. This sensitivity analysis with HYTEC proved that the kinetics of the homogeneous reaction of Eq. 5 was very fast and could be modelled at thermodynamic equilibrium.



4.2 Kinetics of metallic iron corrosion

The chemical and reactive transport models considered the set of kinetics laws that had been validated on the leaching of $U_{0.73}Pu_{0.27}O_2$ in carbonate water (Section 3 of this contribution). In addition, the corrosion of metallic iron $Fe(0)$ in anoxic media can be written as Eq. 6.



A kinetic constraint was imposed on this corrosion process using the following law:

$$\frac{d[Fe(0)]}{dt} = -k^{corr} A_v \quad \text{Eq. 7}$$

where k^{corr} is the intrinsic kinetic rate constant of iron corrosion under anoxic conditions, A_v is the volumetric surface area of metallic iron ($m^2 \cdot L^{-1}$). The constant k_{anox} was taken from the literature, about $10^{-9} \text{ mol} \cdot m^{-2} \cdot s^{-1}$.

4.3 Uranium and plutonium releases and precipitation

CHESS modelling in batch mode was performed to get a first idea of the system evolution. Figure 2a shows that the release of uranium in the COx water/iron system was lowered by four orders of magnitude compared to carbonate water, both in the experiment and in modelling. The concentration quickly decreased close to the thermodynamic equilibrium with the amorphous U(IV) phase $UO_2 \cdot 2H_2O$. This dramatic effect of the environment is very similar to what had been obtained for Pu-doped UO_2 with an alpha activity corresponding to a spent UOX of 50 years old. Odorowski et al. [5] showed that the COx groundwater itself decreased the uranium concentration but that iron played the main role by fully scavenging H_2O_2 reactivity and the oxidative dissolution of UO_2 . The same process did occur with the present MOX fuel most probably.

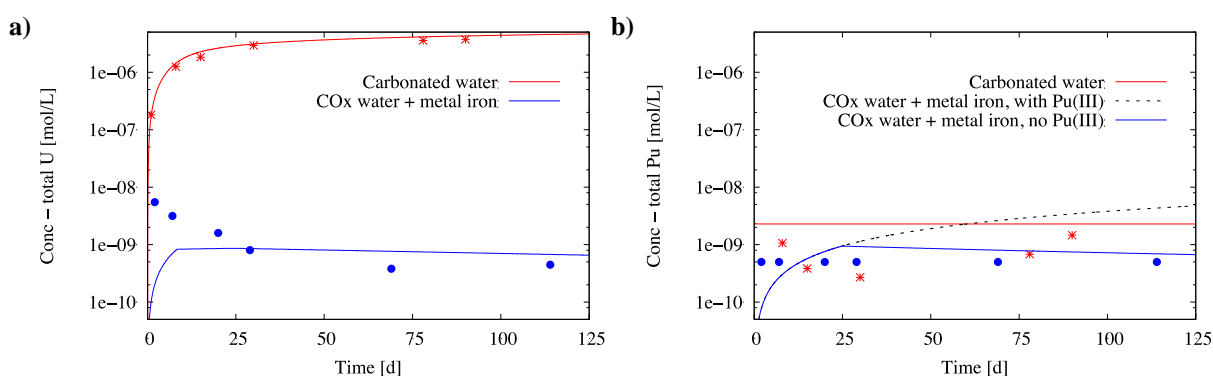


Figure 2. Experimental and CHESS modelling results of uranium (a) and plutonium (b) of the homogeneous MOX pellet in carbonate water and in synthetic COx groundwater in presence of a pre-corroded iron foil.

The experimental release of plutonium was not well captured by the chemical model when the whole redox states of the plutonium were taken into account (Figure 2b, dashed line). Once one decouples the Pu(III) species, the modelling, reproduced correctly the full set of experimental data. In the

modelling, the Pu(III) species predominate in solution over the Pu(IV) species since the redox condition were sufficiently reducing ($Eh \sim -200$ mV, $pH \sim 7.3$) due to the presence of Fe(II) in solution, to allow the reduction of Pu(IV) into Pu(III). The measured experimental Eh value was in the range -40 mV – 120 mV. This measure was semi quantitative only. However, this proved that the system was mildly reducing only. The global mechanism is not yet understood. The precipitation of amorphous $Pu(OH)_3$ could be a possibility.

4.4 Corrosion of the iron foil

In this experimental set-up without stirring, the transport of species was driven by diffusion within the solution, especially between the MOX pellets and the iron foil separated by just a few centimetres. A diffusion coefficient of 10^{-9} $m^2 \cdot s^{-1}$ was considered in the calculations. Figure 3a shows the simulation grid of the cylindrical leaching cell used for the HYTEC calculations. Furthermore, the mass transport over space plays an important role. The hydrogen peroxide generated within the alpha-track is initially very close to the fuel surface (tens of μm), while the ferrous iron generated through corrosion of metallic iron lies usually much longer from the fuel surface (cm scale).

The HYTEC modelling of the corrosion of the iron foil (Eq. 6 and Eq. 7) releases ferrous iron ions into the synthetic CO_x solution, and slightly increases the local pH around the iron foil (Figure 3b). A fraction of them precipitate as the carbonated corrosion product siderite (Figure 3c), the remaining fraction diffuses from the foil throughout the cell solution.

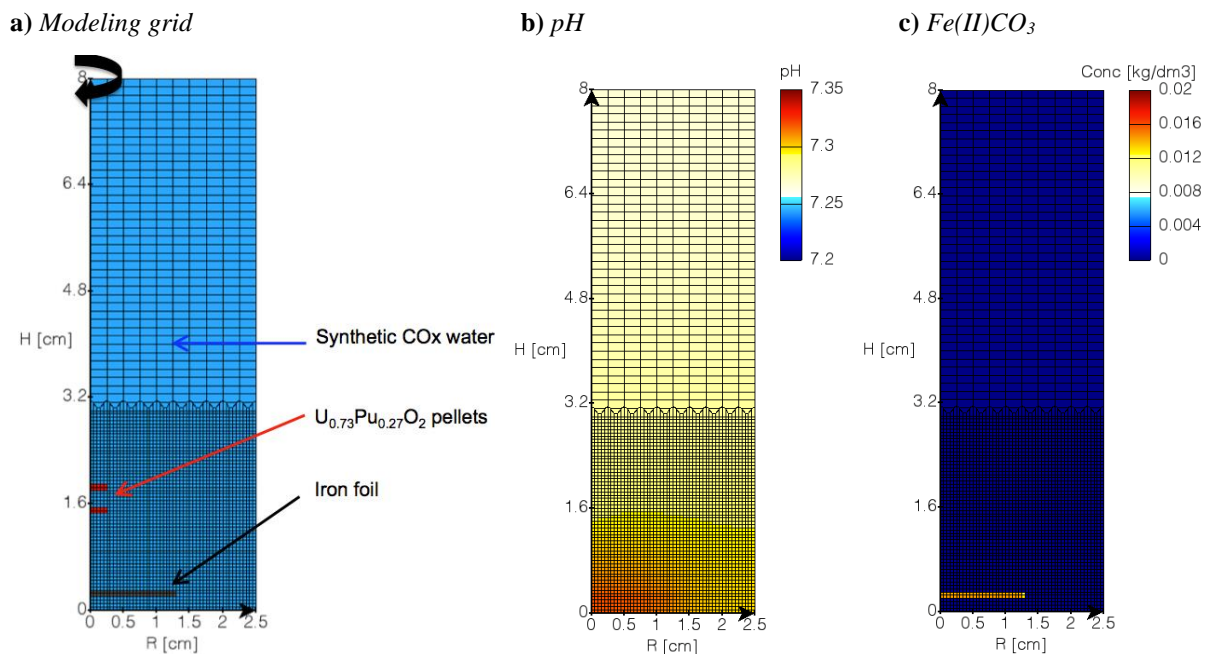
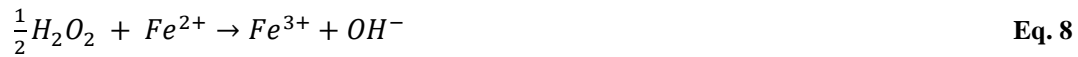


Figure 3: HYTEC modelling of the iron foil corrosion in synthetic CO_x water.

4.5 Scavenging effect of Fe(II) versus the H_2O_2 plume

The complete consumption of hydrogen peroxide by aqueous ferrous iron can be schematized by the following mass balance equation (Eq. 8).



The fact that this reaction prevents any oxidative dissolution of $U_{0.73}Pu_{0.27}O_2$ in the modelling is supported by three modelling results. First, the lack of hydrogen peroxide in solution (Figure 4b) that could raise the potential towards more oxidizing values. Then, the (slight) decrease of Fe(II) concentration in the solution in contact with the MOX pellets (Figure 4a); as Fe(II) induced by iron corrosion, diffuses from the iron foil towards the MOX pellet's surface. Eventually, the precipitation of Fe(III)-(oxy)hydroxide on the pellet surface (Figure 4c) from the Fe(III) species produced by Eq. 8; which is consistent with the precipitation of akaganeite (FeOOH) observed in the experiments of Odoroswki et al. [5].

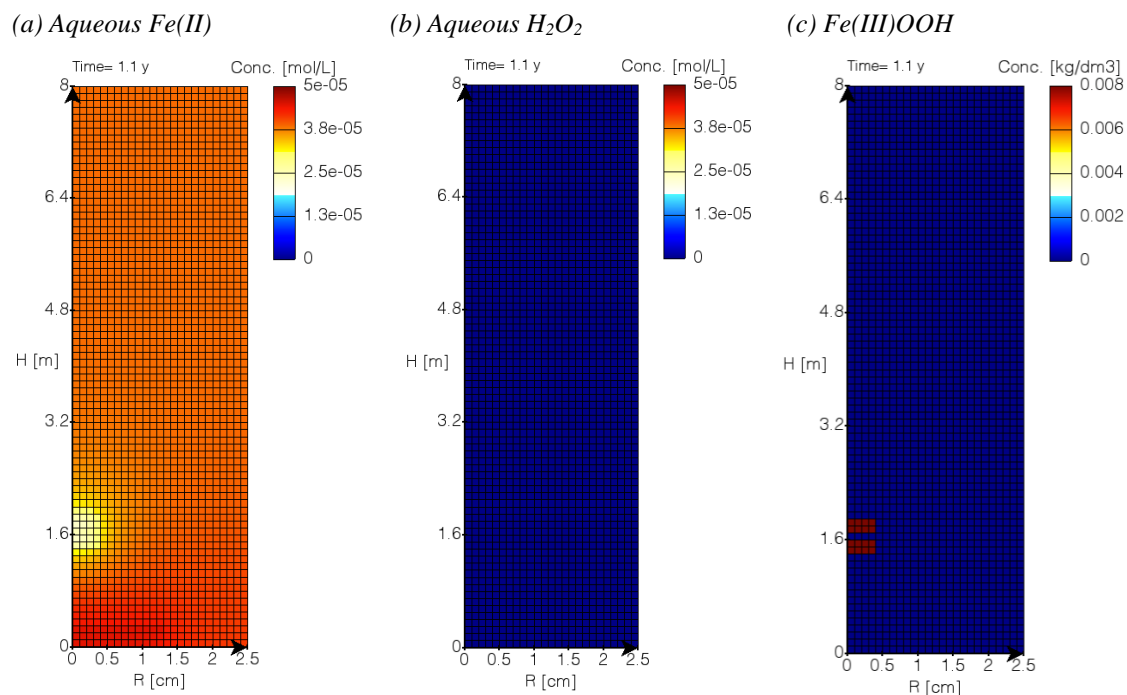


Figure 4: HYTEC modelling of the production of a Fe(II) plume in solution by iron corrosion depletes the H_2O_2 in solution, which leads to the precipitation of goethite on the MOX pellets.

5 Intermediate conclusion and perspectives

This modelling study has brought some insights into the two main objectives of the DisCo project: to assess whether novel types of fuel (MOX here) behave like the more well studied conventional ones (UOX here), and to enhance the understanding of spent fuel matrix dissolution under conditions representative of failed containers (carbon steel here) in reducing repository environments. In the first experiment, the overall consistency of the kinetic processes (H_2O_2 production and disproportionation, oxidative dissolution) obtained from leaching of the unirradiated homogeneous $U_{0.73}Pu_{0.27}O_2$ pellet in carbonate water has been shown. The release of uranium, the concentration of plutonium controlled by the precipitation of an amorphous $Pu(OH)_4$ altered layer have also been correctly modelled. The plutonium content seems to make $U_{0.73}Pu_{0.27}O_2$ more resistant than UO_2 towards leaching.

The release of uranium in groundwater in the presence of metallic iron became very significantly lowered compared to carbonate water conditions. This is very similar to what have been obtained on

alpha-doped UO₂ pellet [5]. In the modelling, iron corrosion has been identified to be a key parameter because Fe(II) released in solution by the iron foil anoxic corrosion consumes H₂O₂ produced by alpha-radiolysis of water. This redox reaction occurs where radiolytic H₂O₂ is produced, i.e. on the surface of the MOX pellets. The CHESS/HYTEC model developed as part of this work led to results in agreement with the preliminary solution analysis, but should be further validated by mass balance (dissolved, colloidal and sorbed fractions for U and Pu) as well as the observation and analysis of the solid phases at the end of the leaching tests.

The knowledge gained from such reactive transport modelling at laboratory scales can then serve as a basis for simulations at larger scales and longer durations to better assess and constrain the long-term evolution of a disposal cell of spent MOX fuel. In the second half of the DisCo project, the reactive transport model will be applied to a disposal package and disposal cell developed on the basis of the present French vitrified waste concept. One single MOX assembly will be inserted in carbon steel overpack. The overpack will directly be placed in a carbon steel liner within the Cox host rock. For the sake of simplicity, the MOX complexity will be reduced to the unirradiated homogeneous solid solution; possibly extended to the heterogeneous microstructure of unirradiated heterogeneous MOX fuel. Several types of corrosion products of the steel container and, therefore, various concentration limits of dissolved Fe(II) could be considered in the modelling, i.e. corresponding to different corrosion products of steel (chukanovite, siderite, magnetite...).

Acknowledgement

The careful and relevant reviews by Pierre De Cannière and Robert Winsley are greatly acknowledged.

The research leading to these results has received funding from the European Commission Horizon 2020 Research and Training Programme of the European Atomic Energy Community (EURATOM) (H2020-NFRP-2016-2017-1) under grant agreement n° 755443 (DisCo project).

References

- [1] Odorowski, M., Jégou, C., De Windt, L., Broudic, V., Peugeot, S., Magnin, M., Tribet, M., Martin, C. (2016). Oxidative dissolution of unirradiated Mimas MOX fuel (U/Pu oxides) in carbonate water under oxic and anoxic conditions. *Journal of Nuclear Materials*, 468, 17-25.
- [2] De Windt, L. and Spycher, N. (2019). Reactive transport modeling: A key performance assessment tool for the geologic disposal of nuclear waste. *Elements*, 15, 99-102.
- [3] Spahiu, K., Cui, D.Q., Lundstrom, M. (2004). The fate of radiolytic oxidants during spent fuel leaching in the presence of dissolved near field hydrogen. *Radiochimica Acta*, 92, 625-629.
- [4] Amme, M., Pehrman, R., Deutsch, R., Roth, O., Jonsson, M. (2012). Combined effects of Fe(II) and oxidizing radiolysis products on UO₂ and PuO₂ dissolution in a system containing solid UO₂ and PuO₂. *Journal of Nuclear Materials*, 430, 1-5.
- [5] Odorowski, M., Jégou, C., De Windt, L., Broudic, V., Jouan, G., Peugeot, S., Martin, C. (2017). Effect of metallic iron on the oxidative dissolution of UO₂ doped with a radioactive alpha emitter. *Geochimica et Cosmochimica Acta*, 219, 1-21.
- [6] van der Lee, J., De Windt, L., Lagneau, V., Goblet, P. (2003). Module-oriented modeling of reactive transport with HYTEC. *Computational Geosciences*, 29, 265-275.

-
- [7] Giffaut, E., Grive, M., Blanc, P., Vieillard, P., Colas, E., Gailhanou, H., Gaboreau, S., Marty, N., Made, B., Duro, L. (2014). Andra thermodynamic database for performance assessment: ThermoChimie. *Applied Geochemistry*, 49, 225-236.
- [8] De Windt, L., Kerleguer, V., Jégou, C., Goblet, P., Martin, C. (2018). Modelling of the oxidative leaching of in synthetic groundwater with metallic iron – first results. 1st Annual DisCo Meeting, 15-16 May, Sheffield (UK).
- [9] Kerleguer, V., Jégou, C., De Windt, L., Broudic, V., Jouan, G., Miro, S., Tocino, F., Martin, C. (*in prep*) The mechanisms of alteration of a homogeneous $U_{0.73}Pu_{0.27}O_2$ MOx fuel under alpha radiolysis. In preparation for *Journal of Nuclear Materials*.

Development and application of a solid solution model for Cr-doped UO₂ fuel

Curti, E., Miron, G.D., Kulik D.A.

Paul Scherrer Institut, Laboratory for Waste Management (LES), Villigen (CH)

Abstract

In the framework of WP5, thermodynamic calculations are being carried out at PSI in order to assess the influence of Cr-doping on the fuel oxygen potential. This contribution summarizes the progress achieved during the last project year. After reviewing the defect chemistry literature on Cr(III), U(V) and O(-II) substitutions, we develop a ternary 3-sites solid solution model for Cr-doped hyperstoichiometric urania. The mixing parameters are calibrated against published experimental data on Cr-solubility in UO₂ and oxygen potentials of hyperstoichiometric UO_{2+y}. The model was implemented in the chemical equilibrium code GEM-Selektor and applied both to non-doped and Cr-doped model UO₂ fuel compositions. The results of our calculations do not indicate any significant effect of Cr-doping on the fuel oxygen potential. Nevertheless, further implementations of the fuel thermodynamic model are needed for conclusive results. In the next project year, we will expand the model by adding lanthanides, Pu and minor actinides as components to the Cr(III)-UO_{2+y} phase. Furthermore, solid solutions for metallic inclusions (ϵ -particles) and the oxide “grey” phase will be implemented. Finally, we will estimate the influence of oxidation at the internal cladding surface and of burnup progress.

1 Defect chemistry of Cr-doped uranium oxide

1.1 Structure of UO_{2+y} and Cr-coordination

Uranium (IV) dioxide crystallizes in the fluorite structure, typical for compounds having a cation/anion radius ratio close to unity and MX₂ stoichiometry. The crystal lattice can be described as cubic close-packed arrangement of U⁴⁺ cations (cationic sublattice) defining a face-centered primitive cell with all eight tetrahedral interstices occupied by O²⁻ anions (Figure 1, left). These inscribe a cube in the interior of the unit cell with a cation vacancy (v) in its center. The O²⁻ anions define an infinite 3-dimensional network of face-shared equally sized cubes, the anionic sublattice (Figure 1, right). In stoichiometric UO₂, half of these cubes host 8-fold coordinated U⁴⁺ cations belonging to the cationic sublattice, whereas the other half of the sites is vacant. These empty sites are named in the literature interstitial sites and define a third sublattice, which is termed here vacancy sublattice.

In contrast to compact structures like NaCl fluorite structures are relatively open, thus offering space for hosting a variety of foreign ions and facilitating ionic diffusion (see [1]). Specifically, molecular oxygen diffusion through the vacancy sublattice appears to be the main driving force for the formation of hyperstoichiometric urania (UO_{2+y}, $y > 0$) [2], leading to a strong dependence of the off-stoichiometry coefficient y on oxygen partial pressure. As oxygen diffuses into the UO₂ lattice, it

picks up electrons and is incorporated as O^{2-} in the interstitial sites, thereby oxidizing U^{4+} to U^{5+} [3-5]. At high y , interstitial oxygen forms defect complexes in off-centered positions called Willis defects [3, 6, 7].

According to the HSAB classification [8] chromium is a hard metal, thus Pauling's 1st rule for ionic crystals [9] can be applied. From application of these principles, it is clear that only Cr^{2+} or Cr^{3+} ions could be conceivably hosted in the UO_2 structure, occupying regular U^{4+} sites or interstitial sites with oxygen coordination numbers (CN) of VI, VII or VIII. Incorporation of metallic Cr can be excluded since it would require CN=XII, which is hardly feasible in the UO_2 structure, and Cr^{5+} or Cr^{6+} are too small to be stable in such a structure. For Cr^{2+} the ideal oxygen coordination number is VIII, which would make it suitable to be hosted in the cationic and interstitial sublattices of UO_2 . The usual coordination number of Cr(III) by oxygen is VI (e.g. in Cr_2O_3 , $CrOOH$, $FeCr_2O_4$). According to Pauling's 1st rule, CN=VII is also possible, however not CN=VIII. Therefore, incorporation of Cr^{3+} in the cationic sublattice of UO_2 requires a decrease in the number of first-shell coordinating oxygen ions. Cr^{3+} has the highest crystal-field stabilization energy (CFSE) of all d-series transition metals [10], i.e. the strongest tendency among transition metals to assume octahedral coordination. X-ray absorption spectroscopy data provide evidence that the dominant form of chromium dissolved in UO_2 is trivalent [11, 12]. However, the occurrence of Cr(II) cannot be excluded based on the quality of these data.

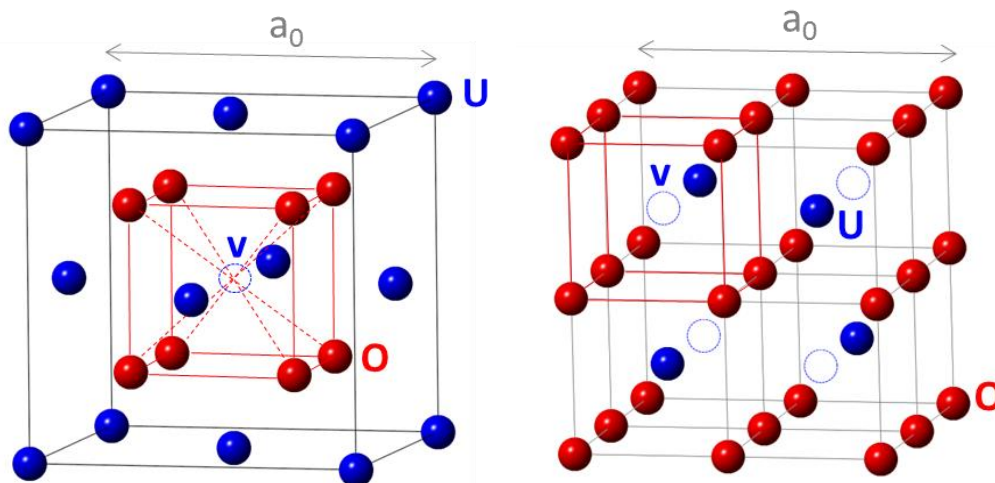
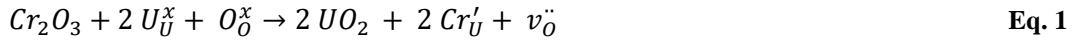


Figure 1: Visualization of the stoichiometric UO_2 crystal structure. *Left:* cationic sublattice (unit cell); *right:* anionic sublattice.

1.2 Substitution of Cr(III) in stoichiometric and hyperstoichiometric urania

When dealing with Cr(III) dissolution in stoichiometric UO_2 , one can take advantage of work performed on the well-studied ZrO_2 - Y_2O_3 system (yttria-stabilized zirconia). This system is to some extent a chemical analogue of Cr-doped stoichiometric UO_2 , since the dopant is a trivalent cation and tetravalent zirconium cannot be oxidized or reduced in oxides. Neutron diffraction data and *ab initio* calculations indicate that the charge-compensating mechanism upon substitution of trivalent Y in Zr_2O is the formation of oxygen vacancies in the regular anionic sublattice [13, 14]. We may therefore postulate, using the standard Kröger-Vink notation [1], the following defect formation reaction for Cr(III) in stoichiometric UO_2 :



Note that no free oxygen appears in reaction (Eq. 1), therefore the equilibrium Cr(III) concentration in stoichiometric UO_2 will be $p\text{O}_2$ -independent, if this is the only incorporation mechanism of Cr. We postulate, in agreement with Middleburgh et al. [15] that reaction (2.1) is indeed the governing mechanism during the fabrication of Cr-doped fuel. The incorporation mechanisms discussed below for hyperstoichiometric urania must need not to be considered, since sintering of Cr-doped UO_2 fuels is carried out under strictly reducing conditions (H_2/CO_2 atmosphere) [16].

The substitution expressed by reaction (Eq. 1) is shown schematically in Figure 2. This arrangement is analogous to the "fixed configuration" identified by Guo et al. [17] to be the energetically most favourable. Note that this substitution involves a decrease in the oxygen coordination number of Cr, as predicted by simple crystal chemistry rules.

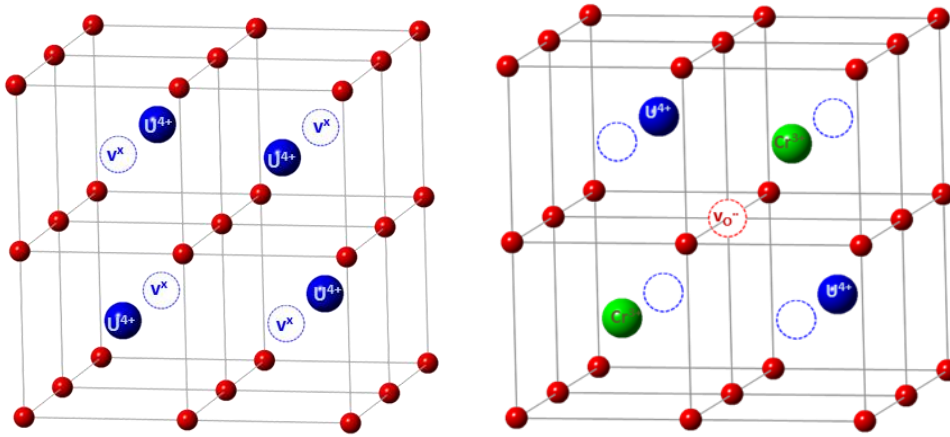
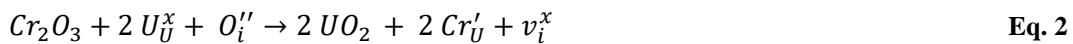


Figure 2: Substitution mechanism of Cr(III) in stoichiometric UO_2 . The *left* side shows the undisturbed UO_2 anionic sublattice; the *right* side shows the same (unrelaxed) lattice region after the substitution.

For hyperstoichiometric urania, Middleburgh et al. [15] postulate the following two Cr-substitution reactions:

(A) Replacement of 2 U^{4+} by 2 Cr^{3+} , charge-balanced by eliminating one interstitial O^{2-} :



(B) Replacement of 3 U^{4+} ions and 1 U^{4+} vacancy by 4 Cr^{3+} ions:

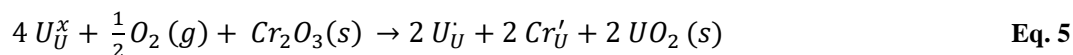


Based on their atomistic calculations, Middleburgh et al. [15] determined reaction (2.2) (Eq. 11 in [15]) to be energetically favoured compared to reaction (Eq. 3). U^{4+} vacancy formation in UO_2 is hindered by the low thermal diffusivity of uranium compared to oxygen. Therefore, reaction (Eq. 3) will be disregarded, and we postulate reaction (Eq. 2) to be the dominant mechanism of Cr(III) incorporation in hyperstoichiometric urania. Contrary to the case of incorporation in stoichiometric UO_2 , we expect a $p\text{O}_2$ dependency for incorporation in UO_{2+y} .

In order to couple reaction (Eq. 2) with the oxygen partial pressure, one has to consider the equilibria leading to formation of interstitial oxygen in hyperstoichiometric urania. The dominant mechanism at low hyperstoichiometry is the formation of mono-interstitials (see Eq. 8 in reference [18]):



Combining reactions (2.2) and (2.4) results in the following pO_2 -dependent equilibrium:



The substitution reaction (Eq. 2) is illustrated in Figure 3. Locally, the incorporated Cr^{3+} ions are charge-balanced by adjacent pentavalent uranium ions. For each two Cr^{3+} ions incorporated, 1 interstitial O^{2-} is annihilated.

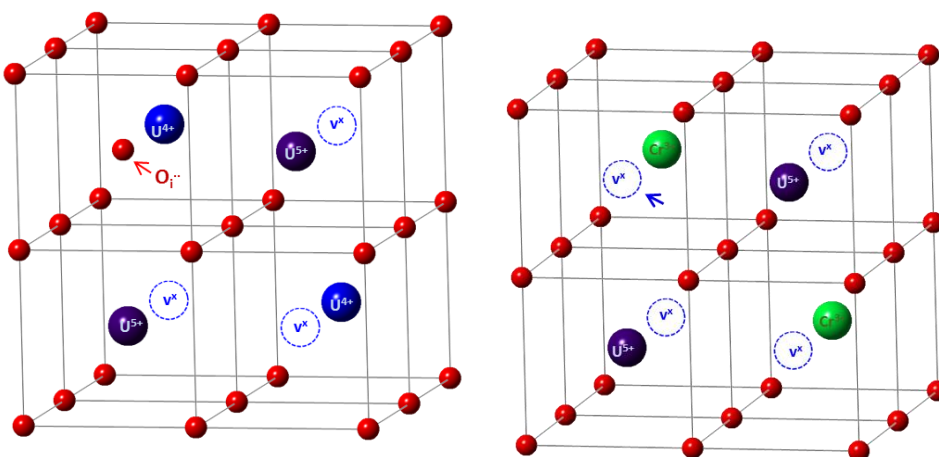


Figure 3: Schematic substitution mechanism of Cr(III) in hyperstoichiometric urania. The *left* side shows the UO_{2+y} anionic sublattice with 2 U^{5+} cations, charge-balanced by 1 interstitial O^{2-} anion (see arrow). The *right* side shows the same sublattice after substitution of 2 U^{4+} by 2 Cr^{3+} .

The defect chemistry of UO_2 has been widely studied. Equilibrium models based on defect reactions have been developed that can accurately predict hyperstoichiometry as a function of pO_2 and other properties [18-20]. In principle, it is possible to combine such equilibrium models with reactions (Eq. 2 to Eq. 5) and obtain a model including Cr-doping. The model could be calibrated with the help of the enthalpy data derived atomistically in reference [15] and of available experimental data on Cr-solubility in urania [14]. This equilibrium model for the U-O-Cr system would however not be sufficient for our purpose, since we intend to make predictions applicable to chemically much more complex systems such as irradiated fuels. To this aim, the method of choice is classical thermodynamics.

We will thus make use of the advanced chemical equilibrium code GEM-Selektor [21] (<http://gems.web.psi.ch/>) applying the in-house database HERACLES (<https://www.psi.ch/heracles/>), which provides the necessary thermodynamic data. The code is based on the principle of non-linear Gibbs energy minimization and allows for a complete and accurate description of complex chemical

systems with multiphase solid solutions. The knowledge on Cr defects formation in urania is merely used here as a help to identify appropriate end-members of solid solutions.

2 Development of a thermodynamic solid solution model for the Cr-U-O system

In the first reporting year (see D1.10), preliminary oxygen potential calculations for a model fuel composition were carried out based on an *ideal* solid solution defined with Cr(III)O_{3/2}, U(IV)O₂ and U(V)O_{2.5} end-members. Incorporation of Cr(III) in UO₂ is expected however to have a large positive enthalpy of mixing, due to the different charge and ionic size of Cr³⁺ and U⁴⁺. Therefore, Cr(III) should form with UO₂ a non-ideal solid solution with large positive mixing parameters for Cr/U interactions. The low measured solubility of Cr in UO₂ [11] reinforces this expectation. In this section, we first define the end-members of the ternary Cr-U-O solid solution consistently with the postulated substitution mechanisms, and then we derive interaction parameters for a Berman-type solid solution, by calibrating them with published data on Cr-solubility in UO₂ and on hyperstoichiometry data (pO₂ vs. O/U ratios). Finally, in Section 4, the so derived solid solution is applied to calculate chemical equilibrium with a model fuel composition.

Figure 4 shows the compositional space of the Cr-U(IV)-U(V)-O system. The selected end-member stoichiometries of the ternary solid solution are defined by the red triangle, besides alternative stoichiometries for the U(V) end-member that have been discarded. Both bulk (bold) and site stoichiometries (enclosed in square brackets) are given. UO_{2.5}, the end-member used in the preliminary calculations presented in last years' proceedings, was discarded since the thermodynamic data (and even the structure) of this phase are highly uncertain. UCrO₄, which crystallizes in the orthorhombic system, would be an adequate end-member, but thermodynamic standard properties are largely unknown. As a consequence, the mixed U(IV)/U(V) compound U₄O₉ was selected due to its well-known thermodynamic properties [22, 23] and the fact that the structures of α - and β -U₄O₉ are closely related to the fluorite-type UO₂ lattice [24, 25].

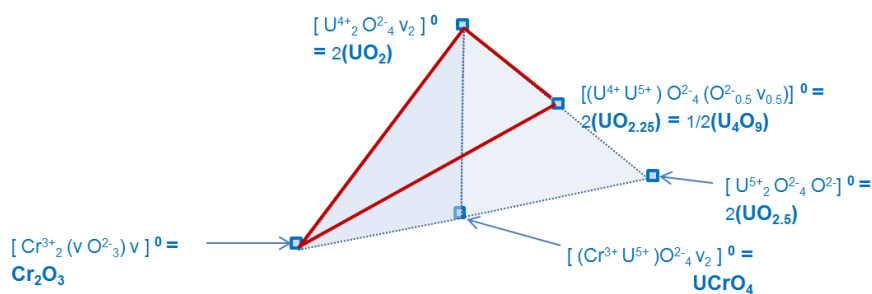


Figure 4: Compositional diagram of the U-Cr-O system showing the selected end-member stoichiometries (red triangle). The blue triangles indicate discarded alternatives (see text).

Site stoichiometries in square brackets show the occupancies of the three sites in the various end-members (the symbol 'v' denotes vacancies). For instance, the U(V) end-member with bulk stoichiometry $\frac{1}{2}$ (U₄O₉) (equivalent to 2(UO_{2.25}) or U₂O_{4.5}) has a site formula in which the cationic sublattice is half occupied by U⁴⁺ and half by U⁵⁺ cations, the anionic sublattice is fully filled by O²⁻ ions and the vacancy sublattice half-filled with O²⁻ ions, the remaining half being vacant.

This notation is consistent with the mixing model of Berman and Brown [26], adopted here to formulate the Cr(III)-U(IV)-U(V)O_{2+y} solid solution in GEM-Selektor. This model, originally developed to describe solid solutions and melts, is flexible as it allows treating vacancies as well as partially occupied end-members. For the latter reason, it is preferred to the more rigorous Compound Energy Formalism (CEF) [27]. For instance, it would not be possible to define U₄O₉ as end-member with the CEF model because the cationic sublattice is occupied by two mutually mixing species (U⁴⁺ and U⁵⁺). CEF requires each site to be fully occupied by a single species. The optimized interaction parameter table of the Berman-type non-ideal Cr-UO_{2+y} solid solution formulated in GEM-Selektor is shown in Figure 5. Eleven pseudo-ternary interaction parameters were defined, each allowing for three coefficients. It turned out that three non-zero parameters are sufficient to fit the experimental data used for model calibration (see later).

| | ipic1 | ipxT | ipxT | ipxT | ipxT | ph cf[0] | ph cf[1] | ph cf[2] |
|----|--------------|------|------|------|------|----------|----------|----------|
| 0 | W_Cr_Cr_U4 | 0 | 5 | 5 | 1 | 0 | 0 | 0 |
| 1 | W_Cr_Cr_U5 | 0 | 5 | 5 | 0 | 0 | 0 | 0 |
| 2 | W_Cr_U4_U4 | 0 | 5 | 1 | 1 | 255000 | 0 | 0 |
| 3 | W_Cr_U5_U5 | 0 | 5 | 0 | 0 | 0 | 0 | 0 |
| 4 | W_U4_U5_U5 | 0 | 1 | 0 | 0 | 100000 | 0 | 0 |
| 5 | W_U4_U4_U5 | 0 | 1 | 1 | 0 | 100000 | 0 | 0 |
| 6 | W_Cr_U4_U5 | 0 | 5 | 1 | 0 | 0 | 0 | 0 |
| 7 | W_O1_O1_Va1 | 1 | 2 | 2 | 6 | 0 | 0 | 0 |
| 8 | W_O1_Va1_Va1 | 1 | 2 | 6 | 6 | 0 | 0 | 0 |
| 9 | W_Va2_Va2_O2 | 2 | 3 | 3 | 4 | 0 | 0 | 0 |
| 10 | W_Va2_O2_O2 | 2 | 3 | 4 | 4 | 0 | 0 | 0 |
| | | | | | | w1 | w2 | w3 |

Figure 5: Screenshot from GEM-Selektor showing the interaction parameter table for the non-ideal Cr-UO_{2+y} solid solution.

In order to determine the parameter (W_Cr_U4_U4) describing interaction between trace amounts of Cr and UO₂, we used the Cr-solubility data compiled in Riglet-Martial et al. [11]. These data were obtained in the temperature range 1500 - 1760°C. They are shown in Figure 6 as mole fractions of Cr in UO₂ as a function of the measured equilibrium pO_2 . Corresponding best fit calculations are shown as lines with colours corresponding to the data for a specific temperature. Each line is obtained from a series of GEM-Selektor calculations (typically 50) in which the amount of O₂ in a closed system containing 1 mole of UO₂ and a small excess of metallic Cr is progressively increased. The lines define the log pO_2 - Cr mole fraction values for the solid solution in equilibrium either with metallic Cr (to the left of the sharp kink) or with pure Cr₂O₃ (to the right of the kink).

The optimized W_Cr_U4_U4 values in J·mol⁻¹ are indicated in the legend of Figure 6. It is evident that high positive parameters are required to fit the very low measured Cr-solubilities in UO₂ (between 0.1 and 1 mol%). The ideal solid solution model predicts equilibrium mole fractions of Cr in UO₂ that are greatly in excess of the experimental data. The fitted W_Cr_U4_U4 – values are remarkably independent of temperature, as indicated by the low standard deviation of the calculated average

($261.8 \pm 6.6 \text{ kJ}\cdot\text{mol}^{-1}$). Taking into account a possible slight increase at $T \geq 1700^\circ\text{C}$, we decided to adopt the value of $255 \text{ kJ}\cdot\text{mol}^{-1}$ obtained at 1500°C , which is comparable to central pellet temperatures during irradiation in commercial LWRs.

In order to determine the goodness of fit, we calculated R-squared also known as coefficient of determination (see e.g. Dodge, 2008, The concise encyclopedia of statistics, Springer). For the data at $T = 1740^\circ\text{C}$ and 1700°C , we obtained $R^2 = 0.893$ (good fit) and $R^2 = 0.613$ (acceptable fit), respectively. This test is not significant at other temperatures, since data are limited either to a single point or to a single cluster with almost identical (x, y) values.

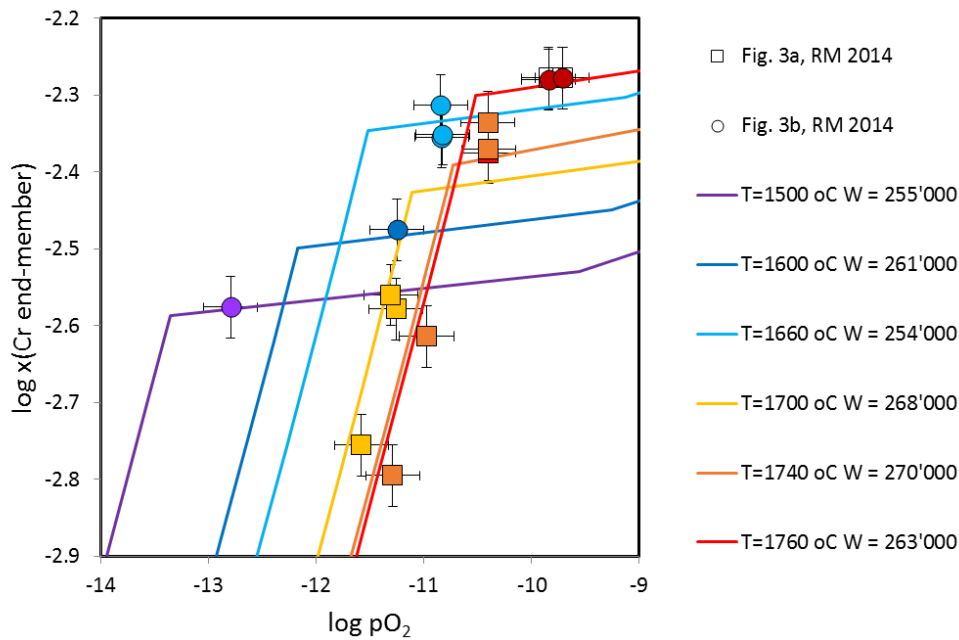


Figure 6: Determination of $W_{Cr_U4_U4}$ mixing parameter: Cr-solubility data from Riglet-Martial et al. [11] are fitted by trial and error GEM-Selektor calculations. The sharp kinks in the model curves correspond to the transition of Cr metal to Cr_2O_3 stability field for the specific temperature.

Nakamura and Fujino [20] measured and compiled from other studies the oxygen equilibrium partial pressures over a wide temperature range ($500 - 1100^\circ\text{C}$) as a function of the hyperstoichiometry coefficient y in UO_{2+y} . These measurements constitute an important data set for calibrating the $(\text{UO}_2)_2$ - $(\text{UO}_{2.25})_2$ binary of our solid solution model. We attempted a global fitting by varying simultaneously several interaction parameter combinations using GEMSFIT [28]. This is a specialized software, which runs systematically GEM equilibria calculations and seeks for optimized values of predefined parameter sets. In our case, up to four interaction parameters, to which results proved to be sensitive, were varied simultaneously. After a large number of attempts, it turned out that it is not possible to find a single combination of interaction parameters capable of fitting the whole ensemble of the data. We however succeeded in finding two distinct combinations, one fitting satisfactorily the low-hyperstoichiometry data, the other fitting the high hyperstoichiometry region. Because we are only interested in the very low-hyperstoichiometry region (off-stoichiometry of irradiated UO_2 fuels are a few permils at most), this outcome is acceptable. We finally end up with a simple combination ($W_{U4_U5_U5} = W_{U4_U5_U5} = 100 \text{ kJ}\cdot\text{mol}^{-1}$) that reproduces all data at $y < 0.02$ reasonably well (Figure 7).

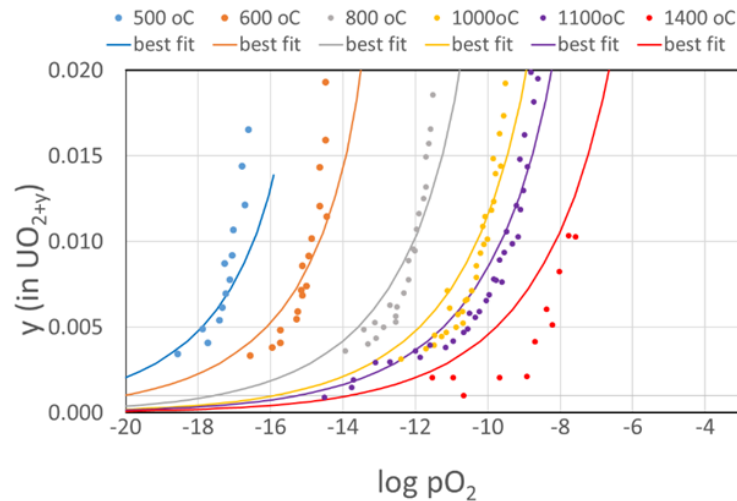


Figure 7: Determination of interaction parameters for the low hyperstoichiometry region of the $(\text{UO}_2)_2$ - $(\text{UO}_{2.25})_2$ binary by fitting published experimental data [20]. The calculated R^2 values (goodness of fit) are: 0.41 (800°C), 0.60 (600°C), 0.77 (800°C), 0.79 (1000°C), 0.89 (1100°C), 0.18 (1400°C).

3 Fuel oxygen potential calculations

The calibrated non-ideal solid solution for Cr-doped UO_{2+y} was applied to predict the oxygen potentials of a non-doped UO_2 fuel and of a doped fuel of equivalent composition (1 mol% Cr). The model fuel composition was derived from the inventories specified for a $60 \text{ GWd} \cdot \text{t}_{\text{HM}}^{-1}$ LWR fuel in Ferry et al. (Table XV, 2 years post-irradiation) [29]. Some simplifications were required since the HERACLES thermodynamic database does not include all the listed elements. For instance, the inventories of a number of lanthanides (Pm, Sm, Gd, Tb, Dy, Ho) were assigned in equal proportions to La and Nd. Figure 8 shows the results of two fuel oxygen potential calculations, both for the same Cr-doped model fuel. One is obtained using the optimized non-ideal Cr(III)- UO_{2+y} solid solution described in the previous section, the second assuming ideality (all interaction parameters set to zero).

The results yield very similar fuel potentials for both calculations, slightly more negative in the case of ideal mixing at high temperatures. The oxygen potential calculated assuming equilibrium with the non-ideal solid solution coincides with the pure Mo/ MoO_2 buffer line except at the highest temperatures, where it joins the ideal solid solution (idSS) model curve.

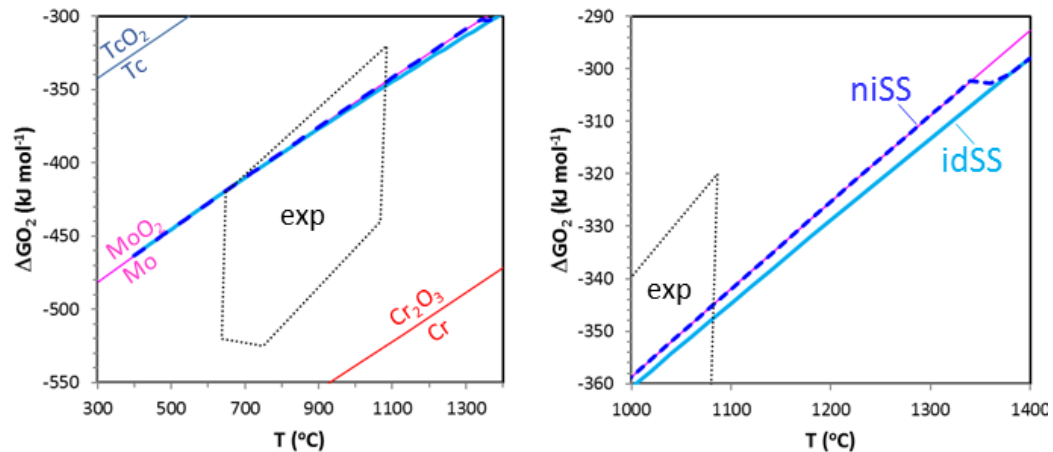


Figure 8: Calculated fuel potentials compared to equilibria of coexisting pure metal/oxide pairs (*left*: overview; *right*: detail). The area denoted ‘exp’ is the region of measured oxygen potentials for LWR fuels up to 58 GWd·t_{HM}⁻¹ [30]. The ‘niSS’ curve was calculated using optimized interaction parameters for the Cr(III)UO_{2+y} solid solution. The ‘idSS’ is the equivalent prediction assuming ideal mixing.

The lower potentials calculated for the ‘idSS’ model result from the higher oxygen content (and thus higher hyperstoichiometry) in the ideal Cr(III)-UO_{2+y} solid solution compared to the calculation with the non-ideal solid solution. Suppressing the strongly positive U(IV)/U(V) interaction parameters resulting from the calibration procedure implies that more oxygen can be stored in the ideal solid solution phase. The excess oxygen incorporated in the ideal Cr(III)-UO_{2+y} solid solution is not available to the redox species “outside”, destabilizing e.g. MoO₂ and thus leading to the breakdown of the Mo/MoO₂ buffer at comparatively low temperatures. As a result, lower fuel oxygen potentials are obtained compared to the more realistic calculation with optimized interaction parameters. The described effects are however minor, since both curves cross the field defined by ΔGO_2 measurements of LWR fuels by Matzke [30].

An equivalent calculation (not shown in Figure 8) for non-doped UO₂ fuel, using the optimized non-ideal Cr(III)-UO_{2+y} solid solution, yielded indistinguishable results, i.e. identical oxygen potentials were calculated for non-doped and Cr-doped UO₂ fuel. Because the assumed doping level (1 mol% Cr) ensured that chromium solubility in urania was reached at all temperatures (400 - 1400°C), these calculations suggest that Cr-doping should not affect significantly the oxygen potential of the fuel.

Therefore, the results obtained so far do not indicate any change in the redox behaviour of the fuel, neither under in-pile nor under geological disposal conditions. Specifically, there is no indication that dose-relevant nuclides (e.g. ⁹⁹Tc, ⁹³Mo, ¹⁰⁷Pd or ¹²⁶Sn) would be oxidized and become more soluble upon contact with aqueous solution in a repository. Also, the calculated oxygen potentials exclude formation of highly hyperstoichiometric matrix, which would facilitate fuel dissolution.

4 Outlook

The results presented here are not conclusive. Our thermodynamic model still needs improvements that we will implement and finalize in the next project year. Additional solid solution phases will be introduced, particularly for the metallic phase (ϵ -particles) and for the so-called oxide “grey phase”.

Furthermore, we will improve the thermodynamic description of the Cr(III)-UO_{2+y} solid solution by introducing lanthanides, Pu and the minor actinides as components. Finally, we plan to carry out calculations related to the oxygen potential evolution with increasing burnup and also taking into account oxidation of Zircaloy at the internal cladding surface.

Acknowledgement

The research leading to these results has received funding from the European Commission Horizon 2020 Research and Training Programme of the European Atomic Energy Community (EURATOM) (H2020-NFRP-2016-2017-1) under grant agreement n° 755443 (DisCo project).

References

- [1] Smyth, D.M. (2000). The defect chemistry of metal oxides. Oxford University Press, New York & Oxford, 294 p.
- [2] Yu, J., Bai, X-M., El-Azab, A., Allen, T.R. (2015). Oxygen transport in off-stoichiometric uranium dioxide mediated by defect clustering dynamics. *The Journal of Chemical Physics*, 142, 094705.
- [3] Wang, J., Ewing, R.C., Becker, U. (2014). Average structure and local configuration of excess oxygen in UO_{2+x}. *Scientific Reports*, 4, 4216.
- [4] Prieur, D., Martin, Ph., Lebreton, F., Delahaye, Th., Banerjee, D., Scheinost, A.C., Jankowiak, A. (2013). Accommodation of multivalent cations in fluorite-type solid solutions: Case of Am-bearing UO₂. *Journal of Nuclear Materials*, 434, 7-16.
- [5] Prieur, D., Martel, L., Vigier, J-F., Scheinost, A.C., Kvashnina, K.O., Somers, J., Martin, Ph. (2018). Aliovalent Cation Substitution in UO₂: Electronic and local structures of U_{1-y}La_yO_{2±x} Solid Solutions. *Inorganic Chemistry*, 57, 1535-1544.
- [6] Olander, D.R. (1976). Fundamental aspects of nuclear reactor fuel elements. National Technical Information Service, U. S. Department of Commerce, Springfield, Virginia 22161, 613 p.
- [7] Willis, B.T.M. (1978). The defect structure of hyperstoichiometric uranium dioxide. *Acta Crystallographica*, A34, 88-90.
- [8] Pearson, R.G. (1968). Hard and soft acids and bases, HSAB, part 1: Fundamental principles. *Journal of Chemical Education*, 1968 (45), 581-586.
- [9] Pauling, L. (1929). The principles determining the structure of complex ionic crystals. *Journal of the American Chemical Society*, 51(4), 1010-1026.
- [10] Stubican, V.S. and Greskovich, C. (1975). Trivalent and divalent chromium ions in spinels. *Geochimica et Cosmochimica Acta*, 39, 375-881.
- [11] Riglet-Martial, Ch., Martin, Ph., Testemale, D., Sabathier-Devals, C., Carlot, G., Matheron, P., Iltis, X., Pasquet, U., Valot, C., Delafoy, C., Largenton, R. (2014). Thermodynamics of chromium in UO₂ fuel: A solubility model. *Journal of Nuclear Materials*, 447, 63-72.
- [12] Mieszczynski, C., Kuri, G., Bertsch, J., Martin, M., Borca, C.N., Delafoy, Ch., Simoni, E. (2014). Microbeam x-ray absorption spectroscopy study of chromium in large-grain uranium dioxide fuel. *Journal of Physics: Condensed Matter*, 26, 355009.
- [13] Goff, J.P., Hull, S., Hutchings, M.T., Clausen, K.N. (1999). Defect structure of yttria-stabilized zirconia and its influence on the ionic conductivity at elevated temperatures. *Physical Review B: Condensed Matter*, 59(22), 14203-14219.

- [14] Parkes, M.A., Refson, K., d’Avezac, M., Offer, G.J., Brandon, N.P., Harrison, N.M. (2015). Chemical descriptors of yttria-stabilized zirconia at low defect concentration: An ab initio study. *Journal of Physical Chemistry A*, 119, 6412-6420.
- [15] Middleburgh, S.C., Parfitt, D.C., Grimes, R.W., Dorado, B., Bertolus, M., Blair, P.R. Hallstadius, L., Backman, K. (2012). Solution of trivalent cations into uranium dioxide. *Journal of Nuclear Materials*, 420, 258-261.
- [16] Arborelius, J., Backman, K., Hallstadius, L., Limbaeck, M., Nilsson, J., Rebensdorff, B., Zhou, G., Kitano, K., Loefstroem, R., Roennberg, G. (2006). Advanced doped UO₂ pellets in LWR applications. *Journal of Nuclear Science and Technology*, 43, 967-976.
- [17] Guo, Z., Ngayam-Happy, R., Krack, M., Pautz, A. (2017). Atomic-scale effects of chromium-doping on defect behaviour in uranium dioxide fuel. *Journal of Nuclear Materials*, 488, 160-172.
- [18] Garcia, Ph., Pizzi, E., Dorado, B., Andersson, D., Crocombette, J.-P., Martial, Ch., Baldinozzi, G., Siméone, D., Maillard, S., Martin, G. (2017). A defect model for UO_{2+x} based on electrical conductivity and deviation from stoichiometry measurements. *Journal of Nuclear Materials*, 494, 461-472.
- [19] Catlow, C.R.A. (1977). Point-defect and electronic properties of uranium-dioxide. *Philosophical Transactions of the Royal Society of London, Series A: Mathematical, Physical and Engineering Sciences*, 353, 533-561.
- [20] Nakamura, A. and Fujino, T. (1987). Thermodynamic study of UO_{2+x} by solid state EMF technique. *Journal of Nuclear Materials*, 149, 80-100.
- [21] Kulik, D.A., Wagner, T., Dmytrieva, S.V., Kosakowski, G., Hingerl, F.F., Chudnenko, K.V., Berner, U. (2013). GEM-Selektor geochemical modeling package: revised algorithm and GEMS3K numerical kernel for coupled simulation codes. *Computational Geosciences*, 17, 1-24.
- [22] Guillaumont, R., Fanghänel, T., Neck, V., Fuger, J., Palmer, D.A., Grenthe, I., Rand, M.H. (2003). Update on the Chemical Thermodynamics of Uranium, Neptunium, Plutonium, Americium and Technetium, F.J. Mompean et al. Eds., *Chemical Thermodynamics Vol. 5*, Nuclear Energy Agency, Elsevier, Amsterdam, 918 p.
- [23] Cordfunke, E.H.P. and Konings, R.J.M. (1990). *Thermochemical data for reactor materials and fission products*. North Holland, Amsterdam.
- [24] Desgranges, L., Baldinozzi, G., Siméone, D., Fischer, H.E. (2011). Refinement of the α -U₄O₉ crystalline structure: New insight into the U₄O₉ - U₃O₈ transformation. *Inorganic Chemistry*, 50, 6146-6151.
- [25] Bevan, D.J.M., Grey, I.E., Willis, B.T.M. (1986). The crystal structure of β -U₄O_{9-y}. *Journal of Solid State Chemistry*, 61, 1-7.
- [26] Berman, R.G. and Brown, T.H. (1984). A thermodynamic model for multicomponent melts, with application to the system CaO-Al₂O₃-SiO₂. *Geochimica et Cosmochimica Acta*, 48, 661-678.
- [27] Hillert, M. (2001). The compound energy formalism. *Journal of Alloys and Compounds*, 320, 161-176.
- [28] Miron, G.D., Kulik, D.A., Dmytrieva, S.V., Wagner, T. (2015). GEMSFITS: Code package for optimization of geochemical model parameters and inverse modeling. *Applied Geochemistry*, 55, 28-45.
- [29] Ferry, C., Poinssot, Ch., Broudic, V., Cappelaere, Ch., Desgranges, L., Garcia, Ph., Jégou, Ch., Lovera, P., Marimbeau, P., Piron, J.-P., Poulesquen, A., Roudil, D. (2004). Synthesis on the long term spent fuel evolution. Report CEA-R-6084.
- [30] Matzke, H. (1995). Oxygen potential measurements in high burnup LWR UO₂ fuel. *Journal of Nuclear Materials*, 223, 1-5.

EUG Feedback

Summary of Feedback from the End User Group

The members of the End User Group (EUG) had their second meeting during the last day of the second DisCo workshop in Cologne, in parallel with the individual Work Package (WP) sessions preceding the General Assembly. Present at the EUG meeting were representatives of the following WMO's: Andra (Christelle Martin), Enresa (Miguel Cuñado Peralta), Nagra (Nikitas Diomidis), RWM (Robert Winsley), Posiva (represented by Jani Huttunen from TVO) and SKB (Kastriot Spahiu). Furthermore, representatives of the following 5 regulators were also present at the EUG meeting: BfE (Christoph Borkel), CSN (Carlos Javier Diez), ENSI (Eduard Feldbaumer), FANC (Pierre De Cannière), and SSM (Jinsong Liu). The meeting was led by Roberto Gaggiano (Ondraf/Niras), who is the EUG representative and was also present at the ExCom meeting on the first day of the workshop.

The two tasks of the EUG are (i) to review the ongoing scientific work within the project and to advise the participants of the project, and (ii) to see if the needs and expectations of the EUG are achieved/satisfied. The interaction with the EUG allows checking whether the project provides the answers to the questions/needs of the EUG and makes sure that the work remains within the initially set scope of the project.

The review of the scientific work entails on the one hand reviewing the Scientific & Technical (S&T) contributions that are written by the beneficiaries and on the other hand attending the annual workshops. Only the EUG representative (Roberto Gaggiano, Ondraf/Niras) is present at the ExCom meeting and reports on the ExCom meeting to the other members of the EUG at the EUG meeting. The EUG members do not participate at the General Assembly, which is restricted to the project beneficiaries only.

The 2nd annual meeting, hosted in Cologne by FZ Jülich, was well organized and efficient. The ExCom considered the EUG feedback from the first annual meeting (in Sheffield), when more time was requested for each lecture and further discussion. For this second annual meeting, the EUG expectations were taken into account and sufficient time was foreseen in the programme to allow for the discussion of the results. Moreover, this year, parallel sessions were organised for WP3, WP4, and WP5, where technical issues and progress were discussed. This allowed for a good interaction between the different work packages. Sufficient time was also foreseen for the EUG discussion.

The S&T contributions were sent to the EUG members in advance of the workshop. The S&T contributions are a description of the current status of the project. However, according to the EUG, it is sometimes difficult to relate the contribution with the overall context of the work, the previous work already performed and the future perspectives. Therefore, for the third annual meeting of the DisCo project (which will be held in May 2020 in Karlsruhe), the EUG would like to anticipate the deadline for the submission of the contributions. The EUG will provide a first feedback based on the contributions 1-2 weeks before the annual meeting. This will allow the authors/speakers to optionally orient their presentations taking the EUG feedback into account. The final EUG feedback will be then provided during the last day of the workshop, as usual. By next year the EUG expects that the obtained experimental data will also be explained and contextualized as a function of the available knowledge

The DisCo project is progressing well. Most of the scientific contributions are on track. In the second year of the project quite a number of experiments and results are already available, which is a major achievement of the DisCo project. However, some issues and delays are identified within the project:

- Issues concerning WP2 (sample preparation and characterisation): alpha-doped UO_2 and some $(\text{U}_{1-x}, \text{Th}_x)\text{O}_2$ samples are still being prepared,
- Some delays in WP3 (spent fuel experiments), due to issues concerning hot cells and/or autoclaves.

These delays are due to issues at facilities and/or experimental setup rather than to the experiments already ongoing (the most of which are being carried out without problems). The EUG is worried that the delayed tests cannot be achieved if specific actions are not taken in order to get back on schedule. The expectation of the EUG is that the WP sub-task leader and the particular beneficiary involved should clearly explain/justify the delay and put in place a credible plan of action to try and recover the task as well as possible in order to achieve the goals of the project.

A potential interest was raised within the EUG in a continuation of the DisCo project after 2021 if some of the questions are not answered within the project. Any support for a phase II of the DisCo project would have to be taken in line with other priority R&D needs. It would also have to be coordinated with the IGD-TP and the EURAD WMO college and, if supported by them, be proposed at an EURAD General Assembly meeting as possible future scope. The EUG encourages the DisCo participants to discuss and prepare a next call for EU projects or other initiatives and try to coordinate with the IGD-TP to further support.

The entire EUG looks forward to the next annual meeting in Karlsruhe (in May 2020) and wishes to thank the ExCom and all the beneficiaries for their excellent work done so far. The EUG is also grateful to all the team in charge of the perfect organization of the workshop and to FZJ for his hospitality.